

Syntheses of polyethers and biodegradable polyesters utilizing aluminium-based catalysts

Fei Zhang



A thesis submitted to Cardiff University in accordance with the requirements for the degree of Doctor of Philosophy

School of Chemistry

Cardiff University

United Kingdom

March 2021

ACKNOWLEDGEMENTS

To begin with, I want to give my most sincere gratitude to Dr. Benjamin Ward who has always been a terrific supervisor with steadfast academic excellence, brilliant personality and devoted concern during my 4 years of postgraduate research. This thesis and works related to it are only made possible with his numerous guidance and researching experiences.

Secondly, I want to appreciate everyone (Mark Sullivan, Sahar Al Fayez, Owaen Guppy, Matthew Shaw, Robert Amesbury, Ibitisam Mousa, Halimah Alahmari, Alysia Draper) in the Ward group who has worked together with me for their constant help, encouragement and amiability. I would like to also thank all the technical staffs in School of Chemistry of Cardiff University, especially Dr. Benson Kariuki for his support regarding the X-ray crystallography and Thomas Williams for his help about mass spectrometry. Special thanks to Claire Mitchell and Dr. Sankar Meenakshisundaram for their help with operating of high-pressure reacting vessels.

I want to express my deepest love and gratefulness to my loving parents, for their unconditional support, advices and caring throughout my Ph.D. years, there is no words that can describe how much I thank my father and mother. I want to also appreciate my grandmother and my aunt for their support. Although my paternal grandfather and my maternal grandparents have passed away, I can always feel their support and love, and they will always be with me in my heart.

Abstract

Four aluminium-based complexes have been synthesized, of which one is previously reported complex but with different crystal structure and not tested with catalysis, and three are complexes have not seen published records yet. These aluminium-based complexes are tested as catalysts for ring-opening copolymerization between cyclic anhydrides and epoxides, and for self-polymerization of epoxides.

This thesis consists of six chapters listed below:

Chapter 1 is a general introduction about the syntheses of polyesters via ring-opening copolymerization, syntheses of polyether through homopolymerization of epoxides and their mechanistic illustrations when metal-based catalysts were used. Several previously reported examples of metal-based catalyst for biodegradable polyester syntheses were given. Discussions about why bio-degradable polyesters are needed, why aluminium was chosen as the central metal ion for desired catalysts are also included.

Chapter 2 contains details of ligand synthesis, complex synthesis of $[(\text{CpHO})_2\text{Al}_2\text{Me}_4]$ (complex **1**) and its characterizations via NMR and single crystal X-Ray diffraction (SCXRD).

Chapter 3 provides information regarding polyester syntheses through epoxide/anhydride Ring-Opening Co-Polymerization (ROCOP) catalyzed by complex **1**.

Chapter 4 contains information of catalytic performances of complexes **1** for epoxide homopolymerization and discussion around the results. .

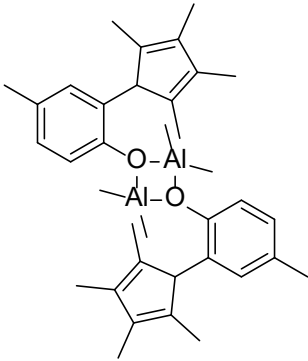
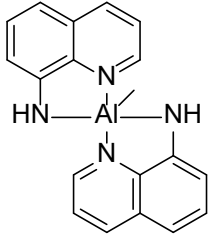
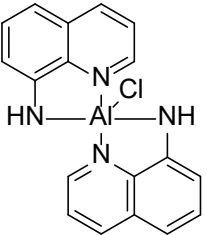
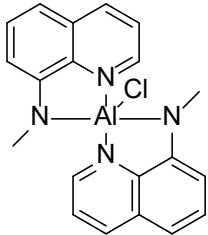
Chapter 5 provides catalytic performances of complex **1** for ϵ -caprolactone homopolymerization and the discussions about the results.

Chapter 6 provides details of syntheses of aminoquinoline-aluminium complexes [(AQ)₂AlMe] (complex **2**), [(AQ)₂AlCl] (complex **3**), and [(AQMe)₂AlCl] (complex **4**). Their catalytic performances in cyclic anhydride / epoxide Ring-Opening Co-Polymerization (ROCOP) were included. Mechanistic elucidations and discussions were included.

Chapter 7 contains full experimental records and full characterizations of all ligands and complexes, as well as the experimental methods for catalyzed polymer syntheses and polymer isolation/purification.

Chapter 8 briefly summarizes all the works, research and conclusions of this thesis.

Structures and assigned codes of aluminium-based complexes

	
$[(\text{CpHO})_2\text{Al}_2\text{Me}_4]$ (1)	$[(\text{AQ})_2\text{AlMe}]$ (2)
	
$[(\text{AQ})_2\text{AlCl}]$ (3)	$[(\text{AQMe})_2\text{AlCl}]$ (4)

Abbreviations

General

Bn	Benzyl
Et	Ethyl
H	Hour(s)
Me	Methyl
min	Minute(s)
NBO	Natural Bonding Orbital
Py	Pyridyl
salen	Bis(salicylaldimine)
salph	Bis(salicylphenylenediamine)
salpy	Bis(salicylpyridyliminophenolate)

THF	Tetrahydrofuran
vs.	Versus
<i>i</i> Pr	iso-propyl
<i>t</i> Bu	tert-butyl
Å	Angstrom
ε-CL	Epsilon-Caprolactone
°C	Degrees Celsius

Spectroscopy

app.	Apparent (coupling pattern or coupling constant)
d	Doublet
dd	Double doublet
EI	Electron Impact
HSQC	Heteronuclear Single Quantum Coherence
Hz	Hertz
J	Coupling constant
M	Multiplet
MHz	Megahertz
NMR	Nuclear Magnetic Resonance
ppm	Parts per million
s	Singlet
t	Triplet
δ	Chemical shift in ppm

Polymerization

CHO	Cyclohexene Oxide
ECH	Epichlorohydrin

GA	Glutaric Anhydride
GPC	Gel-Permeation Chromatography
IO	Isobutylene Oxide
MA	Maleic Anhydride
MALDI-ToF	Matrix-assisted laser desorption- ionization time of flight
M_n	Number-average molecular weight
M_w	Weight-average molecular weight
OR	Alkoxy group
PA	Phthalic Anhydride
PCL	Poly(ϵ -Caprolactone)
PLA	Poly(lactide)
PO	Propylene Oxide
ROCOP	Ring-opening Co-polymerization
ROP	Ring-opening Polymerization
SA	Succinic Anhydride
SO	Styrene Oxide
TBPA	Tetrabromophthalic Anhydride
TCPA	Tetrachlorophthalic Anhydride
ϵ -CL	ϵ -Caprolactone

Contents

Chapter 1: General Introduction.....	1
1.1. Introduction	1
1.2. Biodegradable polyesters.....	6
1.2.1. Step-growth polymerization	8
1.2.2. Chain-growth polymerization.....	9
1.3. Ring-opening polymerization of cyclic esters and epoxides	10
1.3.1. Cationic ROP	14
1.3.2. Anionic ROP	15
1.3.3. Coordination-insertion ROP	15
1.3.4. Radical ROP	20
1.4. Ring-opening copolymerization	21
1.4.1. General ROCOP mechanism.....	22
1.4.2. Catalysts for the ROCOP of epoxides with anhydrides.....	25
1.4.3. ROCOP of epoxides with carbon dioxide	32
1.5. References.....	36
Chapter 2: Synthesis, characterization, X-Ray crystal structure of CpHOH ligand and [(CpHO) ₂ Al ₂ Me ₄] complex	42
2.1. Introduction	42

2.2.	Synthesis and characterization of CpHOH ligand	49
2.2.1.	Synthesis of CpHOH ligand	49
2.2.2.	Characterization of ligand CpHOH	50
2.3.	Synthesis and characterization of $[(\text{CpHO})_2\text{Al}_2\text{Me}_4]$ (1).....	52
2.3.1.	Synthesis of $[(\text{CpHO})_2\text{Al}_2\text{Me}_4]$ (1).....	52
2.3.2.	Characterization of $[(\text{CpHO})_2\text{Al}_2\text{Me}_4]$ (1)	53
2.4.	References	63
Chapter 3: Catalytic performance of $[(\text{CpHO})_2\text{Al}_2\text{Me}_4]$ for ROCOP of epoxides / anhydrides		66
3.1.	Introduction	66
3.2.	Epoxide / anhydride monomers and co-catalysts for ring-opening copolymerization with $[(\text{CpHO})_2\text{Al}_2\text{Me}_4]$ (1).....	68
3.3.	General procedure for ROCOP of epoxides and anhydrides	72
3.4.	Gel-Permeation Chromatography (GPC) data	81
3.5.	Results and discussion	81
3.6.	References	92
Chapter 4: Ring-opening polymerization of epoxides with $[(\text{CpHO})_2\text{Al}_2\text{Me}_4]$ (1)....		96
4.1.	Introduction	96
4.2.	$[(\text{CpHO})_2\text{Al}_2\text{Me}_4]$ (1) catalyzed epoxide ROP	98
4.2.1.	Epoxide monomers	98

4.2.2. General procedure for epoxide ROP	100
4.2.3. [(CpHO) ₂ Al ₂ Me ₄] (1) catalyzed epoxide ROP results	102
4.2.4. [(CpHO) ₂ Al ₂ Me ₄] (1) catalyzed VCHO ROP reaction kinetics	106
4.3. Conclusions.....	124
4.4. References.....	124
Chapter 5: Ring-opening polymerization of ε-Caprolactone with [(CpHO) ₂ Al ₂ Me ₄] (1)	127
5.1. Introduction	127
5.2. General procedure for ε-caprolactone ring-opening polymerization .	128
5.2.1. General procedure for PCL film preparation	129
5.2.2. Characterization and evaluation of the obtained polymer	130
5.2.3. ε-caprolactone polymerization results	132
5.3. Mechanism and additional discussion	152
5.4. Conclusions.....	158
5.5. References.....	160
Chapter 6: Synthesis, characterization, X-Ray crystal structure of aminoquinoline- aluminium complexes and the ROCOP performance of the complexes	163
6.1. Introduction	163
6.2. Synthesis and characterization of complexes	164
6.2.1. Synthesis and characterization of [(AQ) ₂ AlMe] (2).....	164

6.2.2. Synthesis and characterization of [(AQ) ₂ AlCl] (3)	171
6.2.3. Synthesis and characterization of [(AQMe) ₂ AlCl] (4).....	180
6.3. ROCOP of anhydrides / epoxides with aminoquinoline – aluminium complexes as catalysts	185
6.3.1. ROCOP of anhydrides / epoxides with [(AQ) ₂ AlMe] (2) as catalyst	186
6.3.2. ROCOP of anhydrides / epoxides with [(AQ) ₂ AlCl] (3) and [(AQMe) ₂ AlCl] (4) as catalysts	188
6.3.3. MALDI-MS data of polymer samples	200
6.3.4. Gel-Permeation Chromatography (GPC) data of polymer sample	215
6.3.5. Density Functional Theory (DFT) calculations and mechanistic interpretations.....	226
6.4. Conclusion	232
6.5. References.....	234
Chapter 7: Experimental	237
7.1. General Methods and Instrumentation	237
7.2. Ligand Synthesis.....	238
7.2.1. Synthesis of CpHOH ligand	238
7.3. Metal complex synthesis	240
7.3.1. Synthesis of [(CpHO) ₂ Al ₂ Me ₄], (1).....	240

7.3.2. Synthesis of [(AQ) ₂ AlMe], (2).....	242
7.3.3. Synthesis of [(AQ) ₂ AlCl], (3).....	243
7.3.4. Synthesis of [(AQMe) ₂ AlCl], (4).....	244
7.4. Syntheses and isolation of polymers.....	246
7.4.1. Syntheses of polyethers with chosen metal complexes as catalysts 246	
7.4.2. Syntheses of polyesters via ring-opening copolymerization of anhydrides and epoxides with chosen catalysts	246
7.4.3. Syntheses of poly-caprolactones via ring-opening polymerization with [(CpHO) ₂ Al ₂ Me ₄] (1) as catalyst.....	247
7.4.4. Isolation of polymers from reaction mixture	248
7.5. References.....	249
Chapter 8: Conclusions.....	250
Appendices: X-ray crystal structure data	252

Chapter 1: General Introduction

1.1. Introduction

As one of the most important and common categories of materials exploited by human beings, polymers have found roles in daily life since the earliest days of humans. For examples, silk which can be fabricated into clothes is protein fibre (biological polymer); paper is made from cellulose (derived from plants). Along with the development of society and science, synthetic polymers came into the sights of people in mid-19th century, enjoying booming evolution and advancement through the efforts of inventors, researchers, etc.,^{1,2} as demonstrated in Figure 1.1.

Since the advent of synthetic polymers, these materials have found their use in every corner of the world. As a result of their extensive applications, consumption has increased; a plot of plastics production has seen a steep increase over the past decades, as can be seen from Figure 1.2, from 2010 to 2015, the production of plastics has grown by about 180 million tonnes (~200 million tonnes in 2010, ~380 million tonnes in 2015).

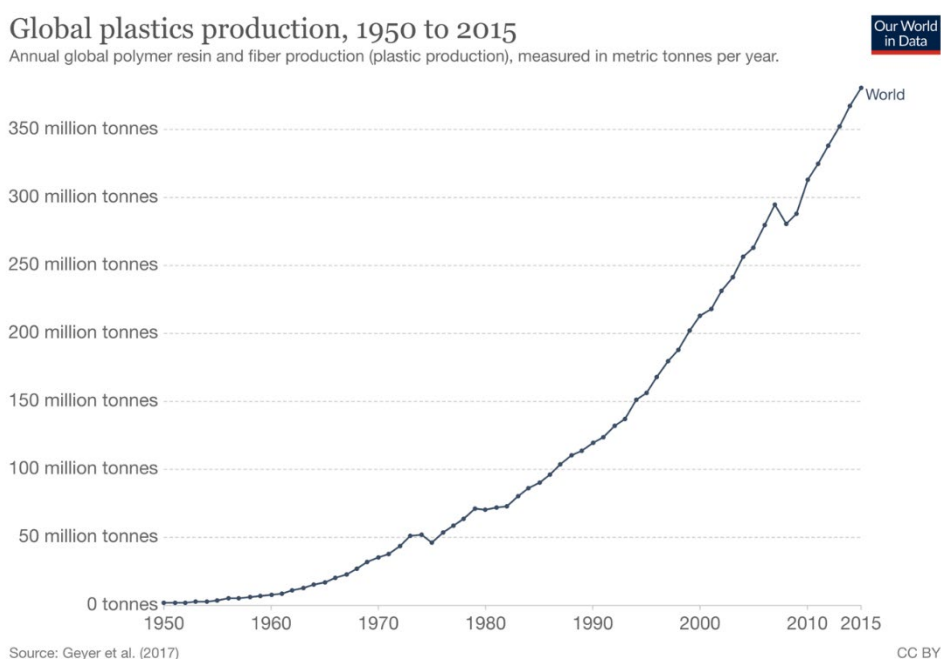


Figure 1.2 Global plastics production from 1950 to 2015.^{3,4}

However, once-unimaginable conveniences and advantages are not the only things synthetic polymers have brought to us. The non-biodegradable nature of many synthetic polymers has posted an extreme challenge to the environment of our planet. Although research has shown that in the foreseeable future, the recycling rate of plastics would see a steady increase based on the past trends (Figure 1.3),^{3,4} for now, most of the synthetic polymers produced are discarded rather than incinerated or recycled. Moreover, the non-biodegradability of many synthetic polymers means they stay in the soil, water, or other environments for hundreds or even thousands of years, which will bring various long-lasting negative effects to the environment and biosystems, such as marine organism entanglement (which severely damages the health or even kills marine life);⁵ ingestion of synthetic polymers and subsequent accumulation of toxic compounds in animals^{5,6} and soil pollution (accumulation of microplastic in the soil leads to health issues of animals in the soil, transfer of toxic compounds through food chain, etc.).⁷⁻⁹ To avoid these undesired impacts towards the ecosystem, recycling of polymers has become more and more important.

Milestones in Polymer History

Date	Polymer	Pioneers	Date	Polymer	Pioneers
1841	Vulcanized rubber	Goodyear, Hancock	1944	Polyethylene terephthalate	Winfield/Dickson
1870	Cellulose nitrate	Hyatt	1946	ABS resins	
1909	Phenolics	Baekeland	1947	Epoxies	Castan/Greenlee
1919	Cellulose acetate	C. & H. Dreyfus	1950	Polyurethanes	Bayer
	Staudinger's macromolecular hypothesis		1956	Linear polyethylene	Ziegler/Hogan
1927	Acrylics	Rohm	1957	Polypropylene	Natta
	Alkyds	Koenle	1959	Polyacetals	Staudinger/McDonald
1929	Thiokol rubber	Patrick	1959	Polycarbonates	Schnell/Fox
1930	Polystyrene	Staudinger	1963	Ionomers	Rees
	Styrene-butadiene rubber	Tschunkur		Polyimides	Siroo
1931	Polyvinyl chloride	Klatte/Semon	1966	Polyphenylene oxide	Hay
	Polychloroprene	Carothers		Aramid Fibers	Morgan
1939	Melamines	Henkel		Polysulfones	Farnham/Johnson/Rose
	Branched polyethylene	Fawcett/Gibson	1967	Macromonomers	Milkovich
	Nylon 6,6	Carothers	1974	Liquid crystalline polymers	Jackson/Economy/Jaffe
1941	Polytetrafluoroethylene	Plunkett	1985	Dendrimers	Vögtle/Tomalia/Newcome/Fréchet
1943	Butyl rubber	Sparks/Thomas	1978 - 1989	Olefin Metallocene catalysts	Kaminsky and others
	Nylon 6	Schlack			
	Silicones	Rochow, Hyde Andrianov			

Figure 1.1: Outstanding milestones in history of synthetic polymers.^{1,2}

Currently, the general synthetic polymer recycling process can be divided into two main types: mechanical recycling (or reprocessing) and chemical recycling. For mechanical recycling, the polymers are separated and sorted based on shape, density, size, colour and chemical composition, then washed (to remove contaminants), ground and melted to reform new products.¹⁰ Despite seeming an easy process, most polymers can only go through this mechanical recycling for about one to three times, before the loss in desired properties makes it necessary to confine them to landfill. In chemical recycling, polymers are depolymerized, forming the original monomers, which then go through polymerization to produce new synthetic polymers which are identical in every way to the original materials.¹⁰ To drive the recycling of synthetic polymers forward and minimize the environmentally unfriendly waste disposal, making polymers bio-degradable or recyclable via depolymerization (chemical recycling as mentioned above) is a good solution. Biodegradable polymers are those polymers which can be converted to simpler, smaller molecular weight compounds by living organisms (usually microorganisms) and redistributed through the biosphere. Another factor that needs to be taken into account is the non-renewable nature of the resources that most common plastics are manufactured from. For instance, polystyrene (PS), polyethylene (PE) and polyvinyl chloride (PVC) are produced from crude oil. As one of the main fossil fuels, crude oil is well known for its wide range of derived materials and products including plastics; limited reserves and massive consumption make crude oil dependent plastics non-sustainable unless a circular economy of plastics can be developed.

The topics of environmental friendliness and sustainability are emphasized more and more as society marches forward. As pivotal measures to cut down the negative effects applied to the environment by synthetic polymers, decreasing the amount of waste plastics which can only be landfilled or left in the surrounding environment can be realized through either manufacturing biodegradable polymers as

replacements for conventional non-biodegradable ones, or increasing the ratio of incinerated wasted plastics for energy recovering.³

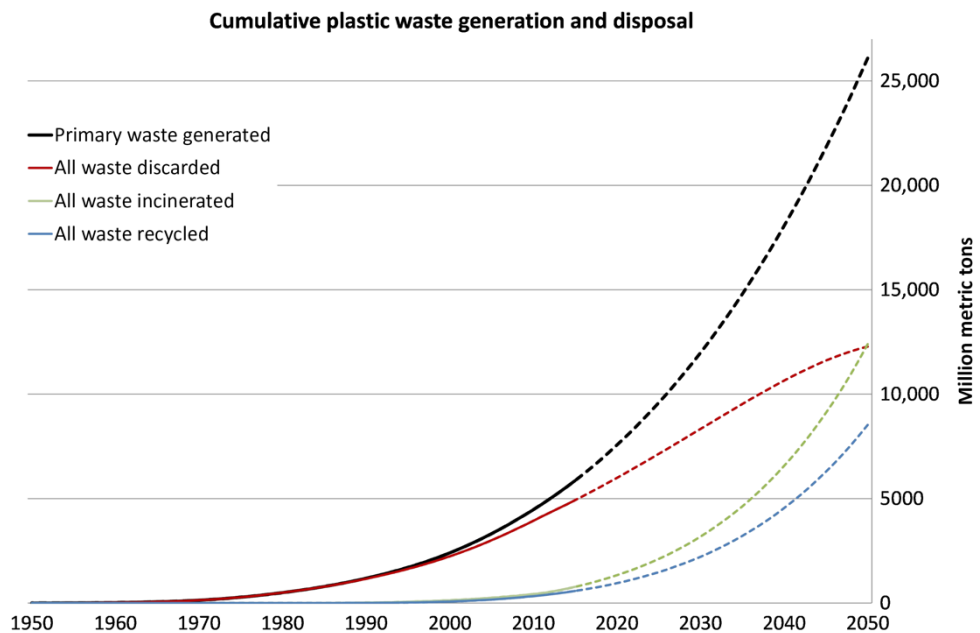
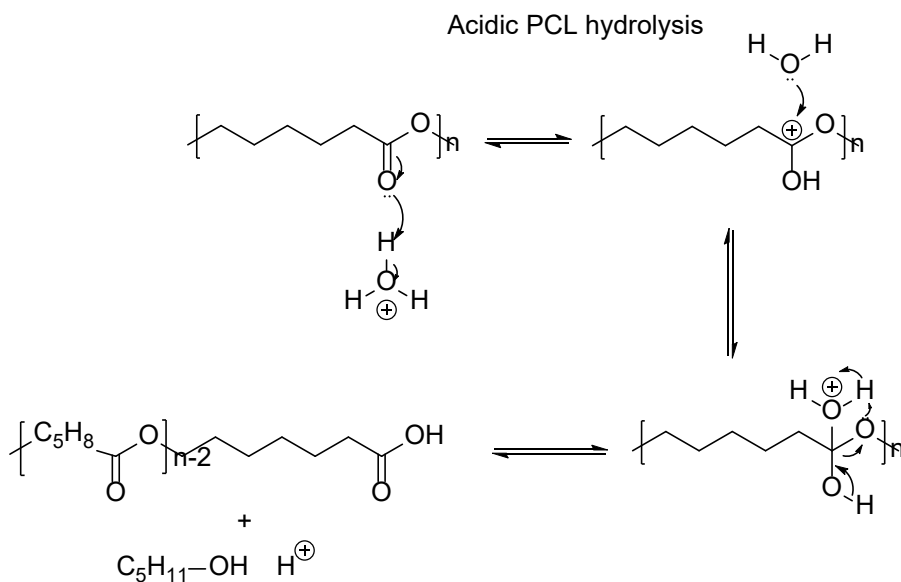


Figure 1.3: Cumulative plastic waste generation and disposal and estimated trends for the future.^{3,4}

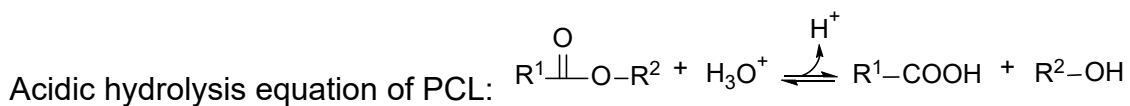
In order to realize the goal of replacing most conventional polymers with biodegradable ones, the newly developed biodegradable polymers not only have to possess comparable properties (e.g., hardness, density and other mechanical properties) / materials performance (acid / base resistance, tearing-resistance, fire-proof, fluorescence, phosphorescence) compared to traditional polymers, but also must be economically viable. Although in recent years better environmental awareness combined with a stronger environmental voice have made the compromise towards slightly lower performance, higher manufacturing costs and eventually higher consumer-end prices in exchange for biodegradability, the extent to which the industries and consumers can accept is still limited. Thus, a biodegradable polymer would still be disqualified as the next generation replacement for current non-biodegradable synthetic polymers if their overall costs and performance are not convincing enough.

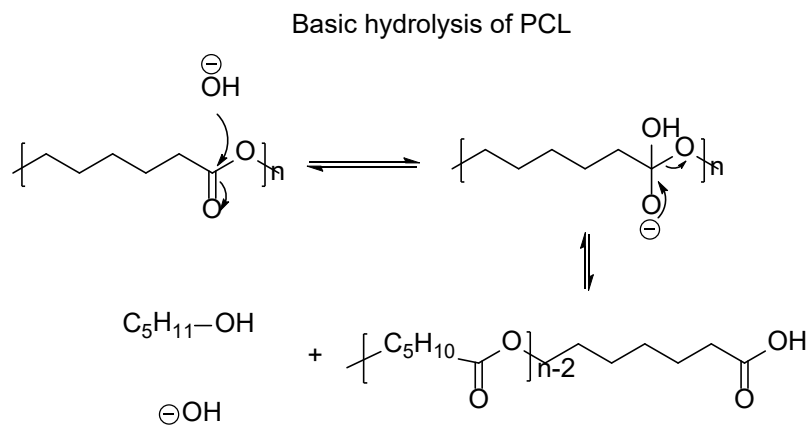
1.2. Biodegradable polyesters

Polyesters are a good example of synthetic polymers with excellent performance and versatility, and which find applications in fields like biomedical,¹¹ fabrics,^{12,13} etc. In theory all polyesters are biodegradable, as esterification is a reversible process. Realistically, as hydrolytically degradable polymers, aliphatic polyesters with relatively short distance between ester bonds are most easily degraded through hydrolysis.¹⁴ For an instance, polycaprolactone (PCL) can be degraded through hydrolysis as can be seen in scheme 1.1 (acidic hydrolysis) and scheme 1.2 (basic hydrolysis).

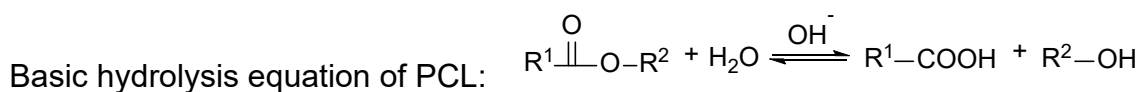


Scheme 1.1: Acidic hydrolysis of polycaprolactone.

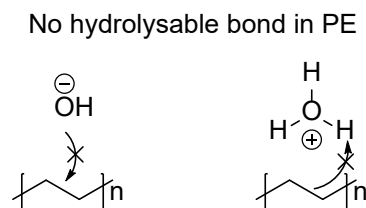




Scheme 1.2: Basic hydrolysis of polycaprolactone



On the other hand, non-biodegradable polymers like polyethylene (PE), have no hydrolysable bonds hence cannot be degraded back to monomers via hydrolysis (Scheme 1.3).

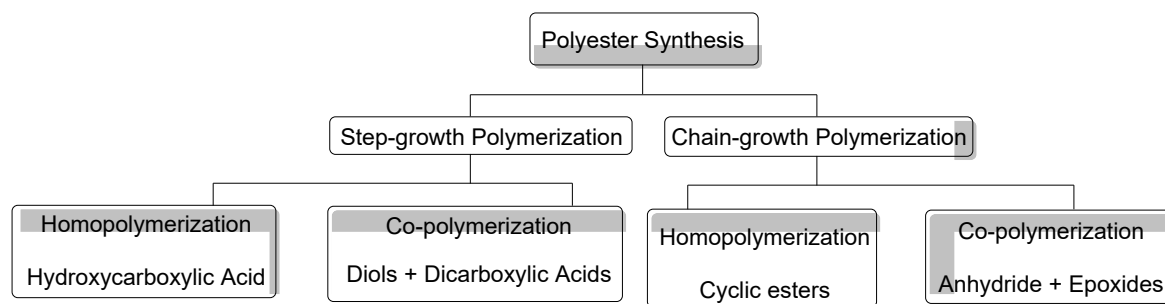


Scheme 1.3: Non-hydrolysable polyethylene.

Therefore, in this thesis, most of the research will be focus on biodegradable polyesters synthesized from simple, small molecule monomers. Apart from their biodegradability, polyesters can be synthesized from renewable, sustainable monomers as well. For an example, lactide, which can homopolymerize into poly(lactic acid), can be obtained from renewable bio-sources.

Synthetic polyesters can be obtained from two general classes of polymerization: step-growth polymerization and chain-growth polymerization, as shown in Scheme 1.4. Step growth polymerization can be either homo-polymerization of hydroxycarboxylic acid or co-polymerization between diols and dicarboxylic acids.

On the other hand, chain-growth polymerization can be either homo-polymerization of cyclic esters or co-polymerization between anhydrides and epoxides.



Scheme 1.4: General polyester synthetic methods

1.2.1. Step-growth polymerization

Step-growth polymerization is where one specific reaction is responsible for the formation of the whole polymer chain.¹⁵ In a step-growth polymerization, monomers are usually bifunctional and both of their ends are polymerizable, thus any two molecular species can react together to form longer oligomers, with two reactive ends which can further react to afford longer oligomers, and eventually polymers, this leads to random chain growth, e.g. two dimers can react to form a tetramer, and tetramers can again react to form oligomers. Due to the random reacting nature, every chain is capable of linking with another chain, and the resulting polymer chains will have very high molecular weights. In other words, step-growth method tends to give a broad, relatively uncontrolled range of molecular weights.¹⁵ Step-growth polymerization also requires high degree of monomer purity to maintain the internal balance of the monomer in order to yield high molecular weight polymers. However, for step-growth polymerizations, such as condensation polymerizations, the inherent existence of by-product like water is a formidable obstacle when it comes to reaction condition optimization, product purification and energy consumption.

1.2.2. Chain-growth polymerization

Chain-growth polymerization is the polymerization in which unsaturated monomers add to the active site of a growing chain one at a time.¹⁵ Unlike step-growth polymerization which has a universal reaction for the formation of the whole polymer chain, chain-growth polymerization has different reactions, mechanisms and reaction rates for initiation, propagation and termination. With the requirement for monomers to add to a certain active site to induce the chain growth, the chain must grow by one monomer unit at a time. With this growing manner, the resultant polymer chains of chain-growth polymerization usually have better molecular weight control (narrow molecular weight distribution range) and fewer growing chains.

There is also research that suggests that with a catalyst, chain-growth polymerizations will give better polymer microstructure control and better polymer molecular weight control.^{15,16,17} For an instance, Diccio *et al.*¹⁶ have shown that the catalyst **1.1** (Figure 1.4) exhibits outstanding regioselectivity when catalysing the ROCOP between propylene oxide and maleic anhydride, with the production of semi-crystalline, stereo-regular polyesters made possible. The resulting polymer has exclusive tail-to-head (tail and head referring to propylene oxide) connection between propylene oxide and maleic anhydride).

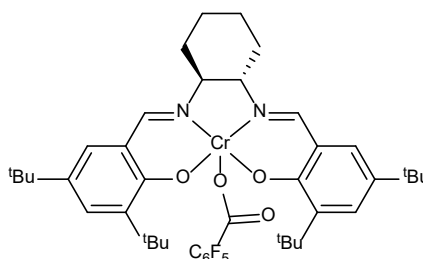


Figure 1.4: Structure of catalyst **1.1**¹⁶.

Another good example of higher polymer microstructure control via chain-growth polymerization is given by Kumhari and co-workers in 2018 (**1.2a**, **1.2b**, Figure 1.5).¹⁷ Unlike most of catalysts included in this thesis, **1.2a** and **1.2b** are a Lewis

acid / base pair, which are metal-free. This Lewis pair can produce polyester with regioselectivity of more than 85% (head-to-tail).

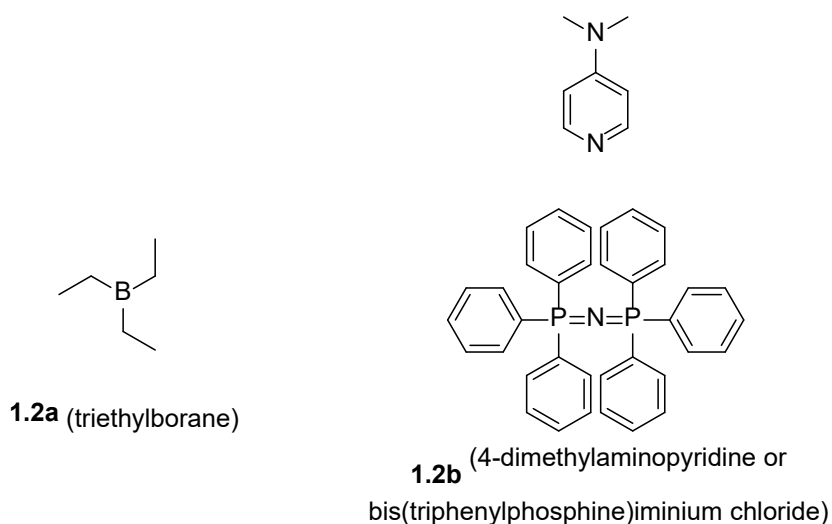
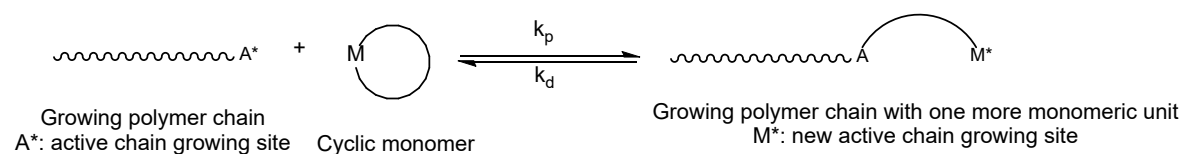


Figure 1.5: Structure of Lewis pair catalyst **1.2a** and **1.2b**¹⁷.

As such, in recent years, great efforts have been put into chain-growth polymerization which has no by-product during polymerization reactions, and has great potential of superior regioselectivity, dispersity control, etc.

1.3. Ring-opening polymerization of cyclic esters and epoxides

By the IUPAC (International Union of Pure and Applied Chemistry) definition, a ring-opening polymerization (ROP) is a process during which a cyclic monomer yields a monomeric unit which is acyclic or contains fewer cycles than the monomer,¹⁸ as demonstrated in Scheme 1.5. If the monomer is polycyclic, opening of any single ring in the monomer still qualifies it as ROP.



Scheme 1.5: Ring-opening polymerization

For a ROP reaction to be viable, it must be allowed both thermodynamically and kinetically.¹⁹ In practice this means a ROP must have its equilibrium shifted to the side where polymer lies, and an appropriate mechanism must exist. Different from the common polymerizations of unsaturated monomers, the ROP of cyclic monomers often exhibits a relatively high unreacted monomer concentration at equilibrium, due to the reversibility of the propagation step (k_p vs. k_d in Scheme 1.5), e.g., the thermodynamics for ROP of cyclic monomers is generally less favourable compared to the polymerization of unsaturated monomers. The thermodynamic terms for ROP of cyclic polymers can be described by the classic Gibbs energy equation (Equation 1)

$$\Delta G(xy) = \Delta H(xy) - T\Delta S(xy) \quad (\text{Equation 1})$$

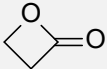
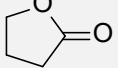
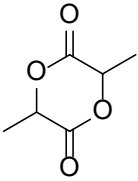
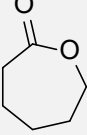
Where x and y represent the state of monomer and polymer respectively (e.g., solid state, liquid state and gas state), ΔG is the Gibbs energy, ΔH is the enthalpy change of ROP reaction, ΔS is the entropy change of ROP reaction. Utilizing Flory's assumption (reactivity of active site on a long enough polymer chain does not depend on the polymerization degree DP_i) and assuming the reaction is at equilibrium (i.e., $\Delta G = 0$), we can obtain:

$$\Delta G = \Delta H - T(\Delta S + R \ln[M]_{\text{eq}}) = 0 \quad (\text{Equation 2})$$

$$[M]_{\text{eq}} = \exp(\Delta H/RT - \Delta S/R) \quad (\text{Equation 3})$$

Where $[M]_{\text{eq}}$ is the concentration of monomer at equilibrium. As we can see from Equation 3, $[M]_{\text{eq}}$ depends on ΔH and ΔS of the reaction.¹⁹ Some common cyclic monomers with their ΔH and ΔS for ROP are summarized in Table 1.1.

Table 1.1: $[M]_{eq}$, ΔH and ΔS for ROP of common cyclic monomers¹⁹

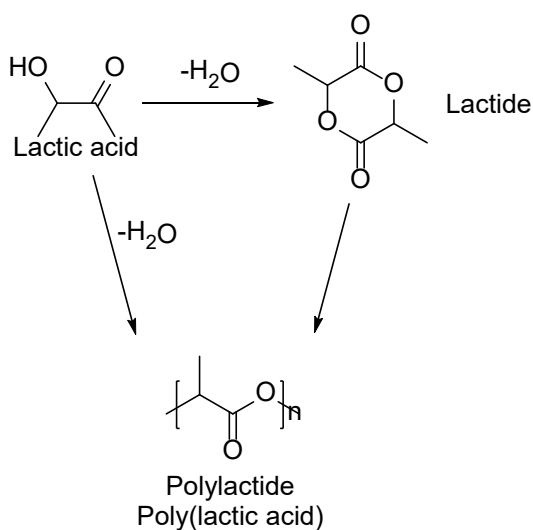
Monomer	Ring size	$\Delta H/\text{kJ mol}^{-1}$	$\Delta S/\text{J mol}^{-1} \text{K}^{-1}$	$[M]_{eq}/\text{mol L}^{-1}$
	3	-140	-174	7.9×10^{-15}
	4	-82.3	-74	3×10^{-15}
	5	-19.1	-74 ^a	3.3
	5	5.1	-29.9	3.3×10^3
	6	-22.9	-41.1 ^b	1.2×10^{-2}
	7	-28.8	-53.9	5.1×10^{-4}

All measured at 298 K. ^a: Measured at 1 M in monomer / polymer melt. ^b: Measured in 1,4 - dioxane solution, otherwise 10 M in liquid monomer.

As can be seen from Table 1.1, the release of ring strain affects $[M]_{eq}$ heavily. The relief from high ring strain of 3- and 4-membered rings leads to almost negligible $[M]_{eq}$, while the 5-membered ring monomers have a much bigger $[M]_{eq}$ number since they are far less strained. These results indicate that inherently, 5-membered ring monomers are not as suitable for ROP comparing to other bigger / smaller rings. For 6-membered ring monomer (lactide), ring strain is minimal. However, the sp^2 hybridized carbonyl carbons force a planar conformation around it rather than a proper 6-membered ring chair conformation, therefore leading to ring strain. For 7-membered rings (caprolactone), the same principle applies: little ring strain, forced planar conformation of carbonyl groups. Any larger ring (e.g., 14-, 16-membered rings) becomes entropy-driven in ROP, as the entropy difference between monomer and polymer is much smaller when rings gets larger, hence leading to smaller polymerization energy barrier thus favours Gibbs energy change.¹⁹

Among the enormous number of cyclic esters which can be exploited as monomers for ROP, lactide (LA) and ϵ -Caprolactone (ϵ -CL) are the two that have received the most attention.

The most obvious reason for the popularity of poly(lactic acid) (PLA) is that it is obtained from a renewable source. Lactide, with the formula $C_6H_8O_4$, is commercially produced by fermentation of plant starch (Scheme 1.6), which usually comes from corn, sugar cane, etc. Structurally, the lactide monomer has two stereogenic centres, which means lactide can exist as D-lactide, L-lactide and meso lactide (Figure 1.6). If the racemic mixture of lactide were polymerized without stereoselectivity, the resultant polymer is usually a chain of random tacticity thus amorphous. However, if the ROP of lactide was catalysed by a stereoselective catalyst, production of PLA with specific tacticity and crystallinity can be induced.



Scheme 1.6: Lactide synthesis from lactic acid and synthesis of PLA.

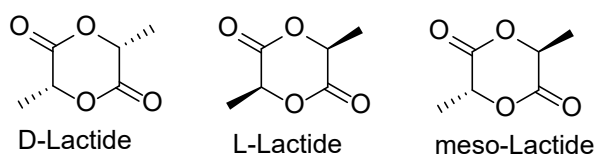
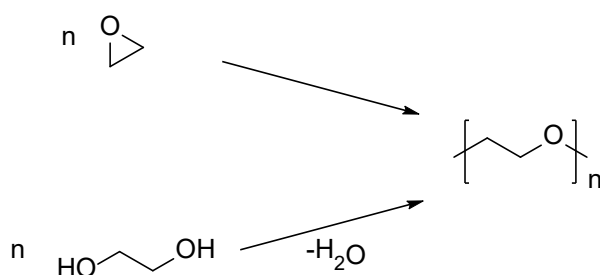


Figure 1.6: stereoisomers of lactide.

As a vital cyclic ester monomer, ϵ -caprolactone (ϵ -CL) can be polymerized, via ring-opening polymerization, into poly(ϵ -caprolactone) (PCL) which exhibits high biocompatibility, good bio-degradability, and can have a renewable source.^{20–25}

Polyethers are also very important in the commercial and industrial sectors. They can be manufactured into foams, surfactants, elastomers, biomedical materials, etc.²⁶ Conventionally, polyethers can be synthesized through the polymerization of diols and the ROP of epoxides (Scheme 1.7).



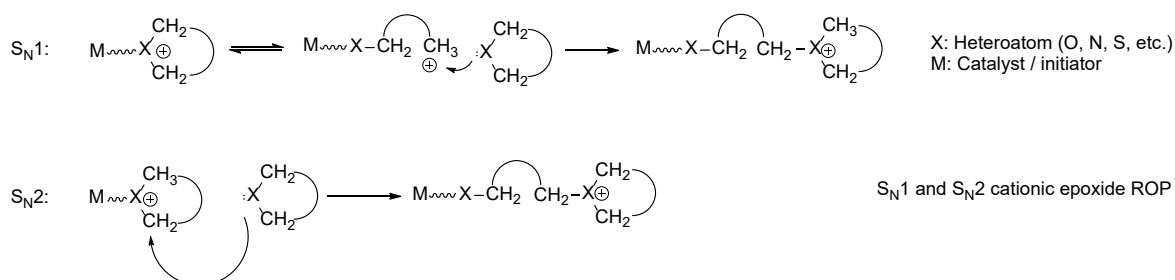
Scheme 1.7: Synthesis of polyethylene glycol from ethylene oxide and ethylene glycol

Mechanistically, ROP can be divided into five different categories: cationic ROP; anionic ROP, coordination-insertion ROP, enzymatic ROP and radical ROP (enzymatic is not quite relevant to the contents of this thesis and so will not be discussed). The general reaction mechanisms of cationic, anionic, coordination insertion and radical ROP reactions will be discussed in the following sections.

1.3.1. Cationic ROP

Cationic ROP (CROP) is identified by the existence of cationic initiators and cationic intermediates. Examples of some important industrial polymers obtained via CROP are: polyacetals, polytetrahydrofurans and copolymers of tetrahydrofuran and oxiran.²⁷ CROP can proceed through two different routes, S_N1 and S_N2 . In the case of S_N1 , the cationic centre is at the end of the growing chain, which will subsequently attack the heteroatom on another cyclic monomer to induce the chain growth.

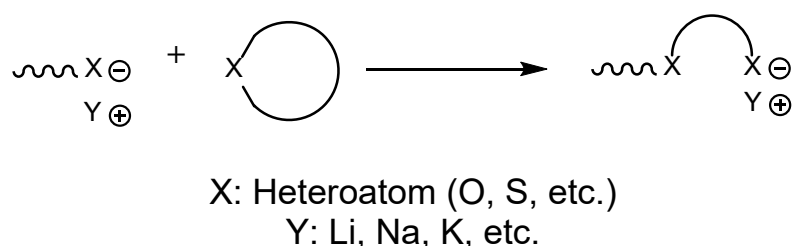
Conversely for the S_N2 route, the cationic centre is on the heteroatom of the growing chain which will then be attacked by another heteroatom of a cyclic monomer in a nucleophilic manner.²⁷ The schematic illustrations of both routes are in Scheme 1.8.



Scheme 1.8: Mechanisms of S_N1 and S_N2 CROP.

1.3.2. Anionic ROP

Anionic ROP (AROP) proceeds via the nucleophilic attack of an anionic heteroatom on the growing polymer chain end to a free monomer, as shown in Scheme 1.9.²⁷



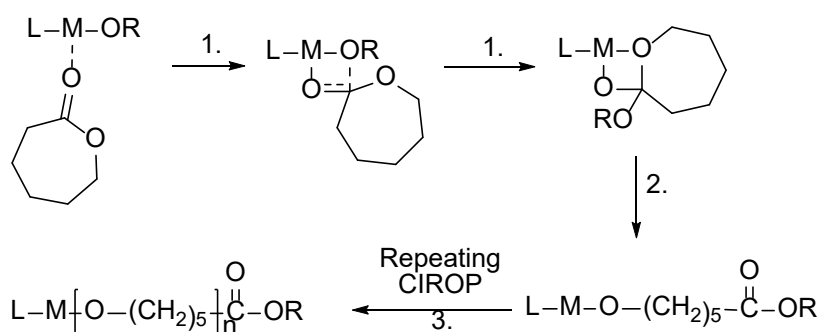
Scheme 1.9: Mechanism of AROP

Monomers that can be polymerized via AROP include but are not limited to: ethylene oxide; ethylene sulfide; trimethylene sulfide, 3,6-dimethyl-1,4-dioxane-2,5-dione and ϵ -caprolactam.²⁷

1.3.3. Coordination-insertion ROP

Coordination-insertion ROP (CIROP) is one of the ROP mechanisms that is usually responsible for the formation of polymer when a coordination complex catalyst is used. Generally speaking, CIROP consists of three main steps: 1. Monomer is

coordinated onto the metal catalyst, then metal alkoxide is inserted onto the carbonyl carbon. 2. The ring of the monomer opens through acyl-oxygen bond cleavage. 3. Formation of the new M-O-R structure with the original OR group at the end of the chain, and the polymer chain is ready for the next turn of polymer chain growth, as shown in Scheme 1.10 (using ϵ -caprolactone as a monomer example).



Scheme 1.10: Mechanism for ϵ -caprolactone CIROP.

The earliest investigations about the CIROP were carried out by researchers such as Kricheldorf and co-workers,²⁸ Jacobs and co-workers.²⁹ The caprolactone CIROP mechanism is well documented by many researchers including Kricheldorf *et al.*³⁰ and Abraham *et al.*³¹ Several examples of modern catalysts with CIROP mechanism are discussed below.

In 2015, Armitage and co-workers reported a series of aluminium complexes **1.3** which can be utilized as ϵ -CL ROP catalyst.³² The structure of it is as shown below in Figure 1.7.

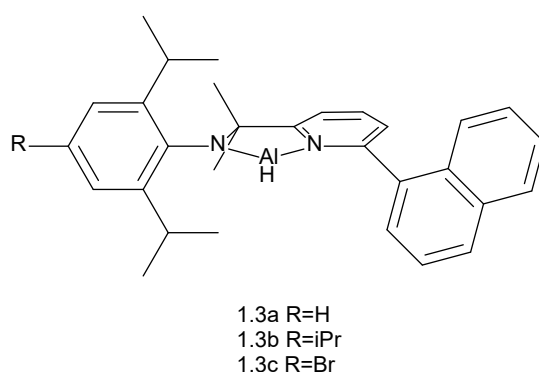


Figure 1.7: Structure of **1.3** series catalysts³²

Unlike many other complexes, **1.3** has two unequal halves around the aluminium central ion. The catalytic performances of **1.3** for ϵ -CL ROP were summarized in Table 1.2.

Entry	Catalyst	Conversion	M _n (SEC)	M _n (Calcd)	Đ
1	1.3a	59%	19010	16920	1.38
2	1.3b	80%	20790	22910	1.39
3	1.3c	38%	10810	10940	1.24

All reactions were done with cat:co-cat: ϵ -CL=1:1:250; co-catalyst is PhCH₂OH; reaction temperature 30°C; 120 minutes; toluene as solvent. SEC: size exclusion chromatography. Calcd: calculated. Đ: dispersity of polymer

It can be seen from the table that Đ is only slightly affected by the R group, while conversion experiences a much greater effect. An electron donating *i*Pr group gave the highest conversion, an electron-withdrawing Br group gave lowest conversion. Armitage and co-workers proposed that the overall ROP rate depends on a combination of different factors, with the Lewis acidity of the metal centre and the alkoxide nucleophilicity as the two most effective factors. Generally speaking, the more electron-donating R group leads to better reaction rate, thus better catalyst. **1.3b** yielded 80% conversion at 30°C, 120 minutes with a narrow 1.39 Đ, justifying itself to be an efficient catalyst.

In 2020, Fuchs and co-workers³³ reported a series of zinc Schiff base complexes **1.4** which can serve as catalysts for CIROP of lactide, structure shown in Figure 1.8.

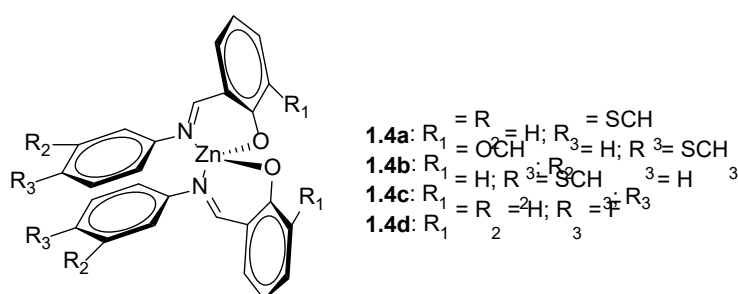


Figure 1.8: Structure of **1.4** series catalysts³³

The catalytic performances of **1.4** series catalysts are summarized in Table 1.3.

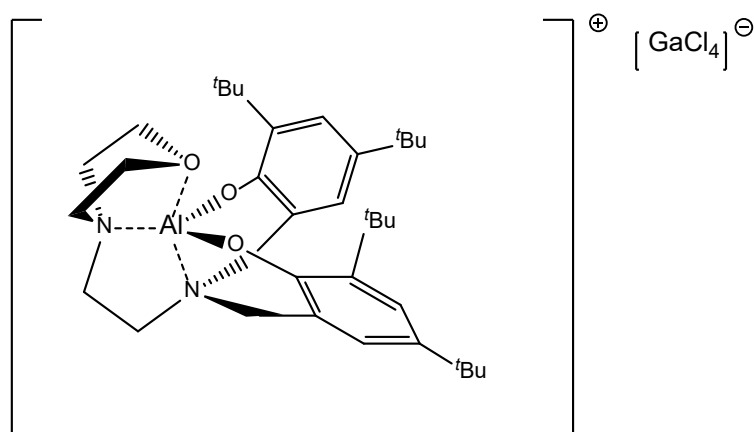
Table 1.3: Catalysis results of **1.4a-d** for L-lactide ROP³³

Entry	Catalyst	Conversion	$M_{n, \text{calc}}$ (g mol ⁻¹)	M_n (g mol ⁻¹)	\bar{D}
1	1.4a	66%	95000	48000	1.6
2	1.4b	56%	80600	35000	1.7
3	1.4c	60%	86000	58000	1.3
4	1.4d	54%	77700	64000	1.3

Reaction conditions: recrystallized L-lactide as monomer, [cat] : [lactide] = 1 : 1000, 150°C, 1-hour reaction time.

As can be seen from the table, the dispersity control is mediocre, but conversion is satisfactory for 1-hour reaction time, although the 150°C temperature can be hardly regarded as mild. However, polylactides are usually made as commodity plastics, which do not have any strict requirement for specific control over dispersity or exceptional mechanical properties, thus the dispersity control is not an extremely important factor when considering the performance of the catalyst. For industrial applications, reaction conditions and conversions should be the main focus, if the goal is mass production of commodity grade PLA.

In 2019, Kerton and co-workers reported an aluminium complex **1.5** which can be used as catalyst for CIROP of ϵ -CL,³⁴ structure shown in Figure 1.9.



1.5

Figure 1.9: Structure of catalyst **1.5**³⁴

The intriguing point of **1.5** is that it contains a gallium tetrachloride anion to balance the aluminium cation. In most metal complex catalysts, the anion is a halide (e.g., Cl⁻, **1.9**) or ordinary acidic groups (e.g., NO₃⁻, **1.10**). The catalysis results of **1.5** are summarized in Table 1.4. $M_{n,calc}$: calculated molecular mass of the polymer, calculated by: $[CL]/[cocat] \times 114.14 \times Conv.$ + molecular weight of co-catalyst. M_n measured by triple detection GPC in THF.

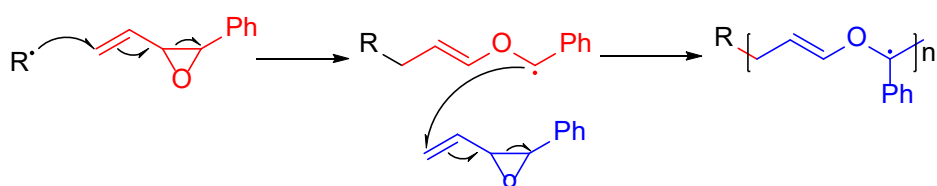
Table 1.4: ϵ -CL ROP catalysis results of 1.5 ³⁴								
Entry	Co-cat	[CL]:[cat]:[cocat]	T/°C	Time/h	$M_{n,calc}$	M_n	\bar{D}	Conv.
1	^t BuOH	200:1:1	70	2	3950	45600	1.01	17%
2	EtOH	200:1:1	70	2	22900	2790	1.03	>99%
3	EtOH	200:1:2	70	2	22600	26800	1.05	>99%
4	Glycidol	200:1:2	20	20	10200	44400	1.01	89%
5	Glycidol	200:1:1	20	20	22900	164000	1.46	>99%

As found for many other metal complex catalysts, **1.5** performed poorly when no co-catalyst was included. With EtOH as co-catalyst, at 70°C and 2 hours reaction time, C9 achieved more than 99% conversion and $\bar{D} = 1.03$ (entry 2), which are excellent performance indicators. However, the M_n is rather poor, only 2790. With 2 equivalents of EtOH (entry 3), the M_n saw a drastic increase to 26800, almost ten-fold of the number with one equivalent of EtOH, with \bar{D} and conversion left essentially unchanged, which is a curious observation. When glycidol was applied as co-catalyst, **1.5** also showed good results. As found from entries 4 and 5 above, 2 equivalents of glycidol as co-catalyst leads to much lower M_n , 10% drop in conversion, but greatly improved the dispersity control comparing to 1 equivalent of glycidol. As for the reaction temperature, glycidol co-catalyst enables **1.5** to catalyze the ROP of ϵ -CL at room temperature, which will be a big advantage for industrial

applications, although the reaction time is at a slightly long, 20 hours with 89% conversion.

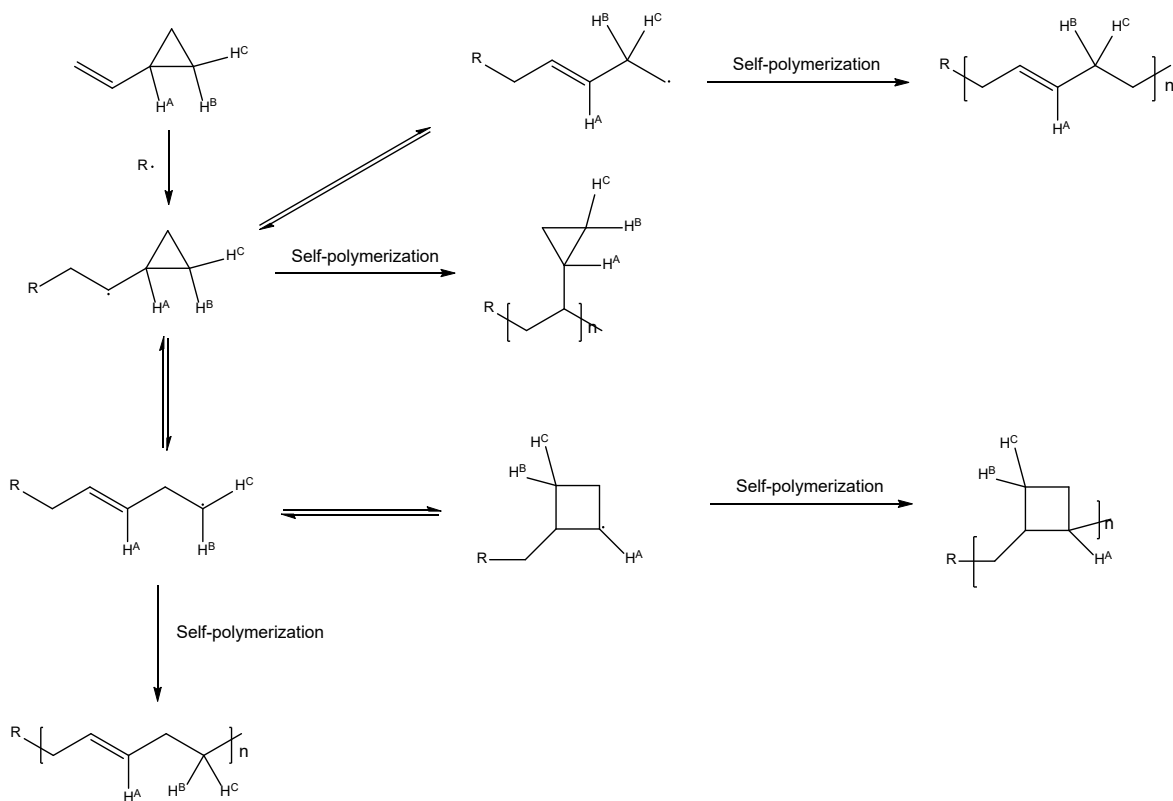
1.3.4. Radical ROP

Radical ROP (RROP), is the ring-opening polymerization in a radical manner, which is initiated using a radical initiator and has three basic steps including initiation, propagation and termination.¹⁸ For instance, the RROP mechanism of phenyl vinyl oxirane is illustrated in Scheme 1.11.^{27,35}



Scheme 1.11: RROP mechanism of phenyl vinyl oxirane.

For some other monomers such as vinyl cyclopropane, however, the propagation may have multiple pathways, depending on the rearrangement of the radical and thus resulting in several different polymers,^{36–39} as shown in Scheme 1.12.



Scheme 1.12: RROP mechanism of vinyl cyclopropane

Generally speaking, for synthetic polymers, RROP is a method with higher uncertainty comparing to other methods like CROP and AROP, as a result of the rearrangements coming from the radical nature of the intermediates. Because of this, radical ROP is industrially less favourable for syntheses of synthetic polymers where more certainty is required over the reaction products.

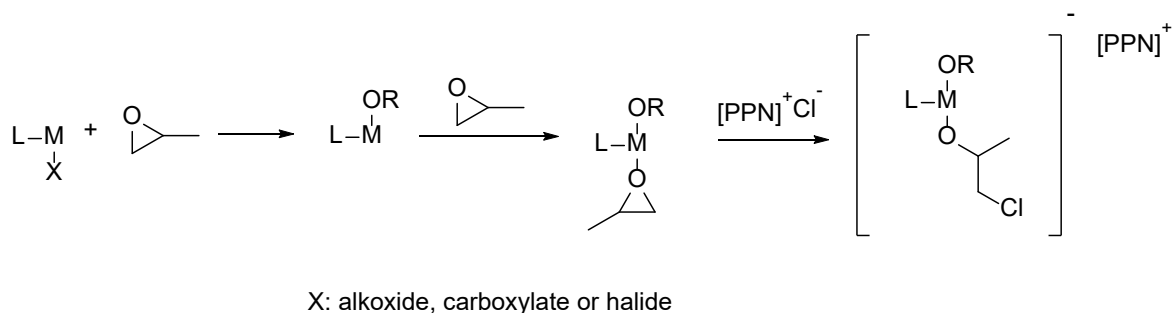
1.4. Ring-opening copolymerization

As stated in section 1.2, the chain-growth method is an effective and promising way to obtain functional synthetic polymers. In this class of polymerization reactions, ring-opening co-polymerization (ROCOP) between anhydrides and epoxides is an especially advantageous method. For co-polymers, fine tuning of properties of resultant polymers can be achieved easily by changing either one of the two monomers;^{40,41} the inclusion of aromatic ring-containing monomers as the backbone (which would improve thermal and mechanical properties) is made possible,^{40,42–45} and most importantly, the wider range of monomer choices means many of them

can be obtained easily with low cost, or from renewable sources. Huge numbers of potentially available monomers combined with the bio-degradable attribute of polyesters provides a high-hope solution for next-generation synthetic polymers.

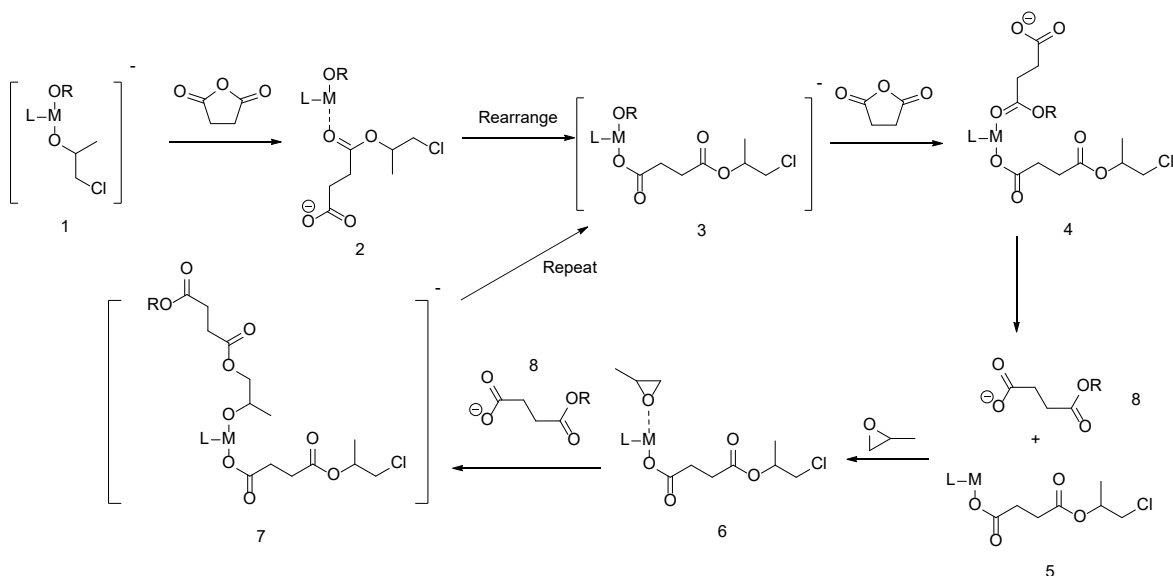
1.4.1. General ROCOP mechanism

Although a small number of metal complex catalysts do not need a co-catalyst to perform the catalysis smoothly (e.g., report from Diccio and Coates⁴⁵), most metal complex catalysts do need a co-catalyst to either work properly or have their performance improved to acceptable levels. The most commonly-used co-catalyst for ROCOP is bis(triphenylphosphine)iminium chloride, abbreviated as PPNCl. Coates and co-workers⁴⁶ has reported the initiation steps of ROCOP with the present of PPNCl, as illustrated in Scheme 1.13. The main advantage PPNCl brings to the ROCOP reaction is that PPNCl facilitates the ring-opening of the epoxide through the nucleophilic attack of chloride ion towards the epoxide, thus accelerates the initiation step of the ROCOP reaction.



Scheme 1.13: The initiation of ROCOP with presence of PPNCl.⁴⁶

The general mechanism of epoxide / anhydride ROCOP with metal complex and co-catalyst is well researched and investigated,^{19,40,46-48} as illustrated in Scheme 1.14.



Scheme 1.14: Epoxide / anhydride ROCOP mechanism. M: central metal ion; OR: opened epoxide unit with initiating group (e.g., Cl) / growing polymer chain; L: ancillary ligand.

As we can see from Scheme 1.14, after initiation with PPNCI, the catalyst will have two alkoxides on the central metal ion formed from epoxide units attached to it (Scheme 1.14, 1). The alkoxide oxygen will then attack at the carbonyl carbon on an anhydride unit to obtain intermediate 2. After rearrangement, intermediate 2 will become intermediate 3 (with the carboxylate-terminated polymer chain bound to the metal ion in intermediate 2). Since anhydride ring-opening is faster than epoxide ring-opening, the remaining OR group attacks another unit of anhydride in the similar way that 1 converts to 2, and intermediate 4 will be obtained. The carboxylate-terminated polymer chain (intermediate 8) then detaches from central metal ion to allow binding of an epoxide unit to metal ion, allowing for the non-coordinate carboxylate-terminated polymer chain to externally attack the epoxide in 6, opening the ring to regenerate an alkoxide and completing the catalytic cycle with growth of the polymer chain. Intermediate 7 will serve as the new intermediate 3, and the polymer chain growth will be done through this cycle. According to the density function theory (DFT) calculations reported by Coates *et al.*,⁴⁶ at 333 K, the relative Gibbs free energy change for ring-opening of epoxide was lowered by 3.5

kcal/mol with the presence of PPNCI (catalyst used in the calculation is [(salph)AlCl], structure in Figure 1.10). A mechanistic explanation was proposed that without PPNCI, the initiation step (ring opening of epoxide) would need the chloride ligand on the neutral aluminium catalyst to dissociate so that it may serve as a nucleophile. Also, a carboxylate-terminated chain (intermediate 8) cannot easily dissociate from the metal ion without the presence of PPN⁺ ions. Another theory is that there is a possible bimetallic activation route for catalyst without PPNCI presence, but so far there is no solid evidence to determine which one is correct.

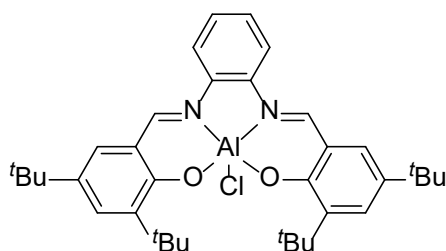
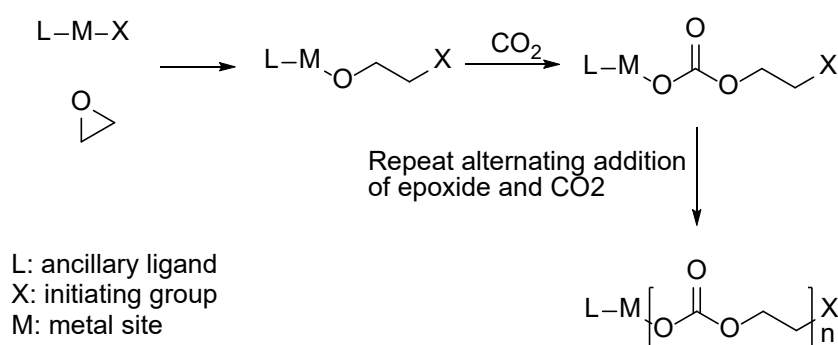


Figure 1.10: Structure of [(salph)AlCl]

Surely, this alternating addition of epoxide and anhydride is not necessarily perfect, in some cases the sequential addition of several epoxides could occur to yield polyether blocks in the polymer chain. What percentage of the polymer is alternating polyester is how the selectivity (i.e., the percentage of polyester compared to polyether) of the catalyst is defined. The main driving force for a high selectivity is the lower energy barrier for the reaction between epoxide and anhydride comparing to epoxide homopolymerization, and therefore the two processes are under kinetic control. However, as the ROCOP reaction usually requires heating (although in many cases mild heating), the two processes can often be seen to operate in parallel. The higher the temperature is, the higher the possibility that homopolymerization could become a significant side reaction, which would result in a worsening of the reaction selectivity. To avoid this, ROCOP reactions are usually optimized to the lowest temperature possible whilst allowing the ROCOP reaction to proceed. Lower reaction temperature also means better applicability as well as lower costs when it comes to the industrial application, which is the ultimate goal for ROCOP catalysts.

The ROCOP of CO₂ / epoxide follows a similar mechanism as the epoxide / anhydride ROCOP, with the CO₂ taking anhydride's place. CO₂ / epoxide ROCOP initiates with the formation of metal alkoxide between epoxide and metal followed by the addition of CO₂, as shown in Scheme 1.15.



Scheme 1.15: Mechanism of catalysed CO₂ / epoxide ROCOP

Alternating polyester selectivity issue exists for CO₂ / epoxide ROCOP as well, and the selectivity is influenced by the catalyst, co-catalyst and temperature as for anhydride / epoxide ROCOP. The discussions for the selectivity kinetic control of epoxide / anhydride ROCOP generally also apply to CO₂ / epoxide ROCOP.

1.4.2. Catalysts for the ROCOP of epoxides with anhydrides

Initiators for anhydride/epoxide ROCOP are commonly in the form 'LMX', of which L is an ancillary ligand, M is the central metal ion, and X is the initiating group (usually halide, carboxylate or alkoxide).⁴⁰ Previously reported metal-based catalysts have utilized metal ions including (but not limited to) aluminium (III),^{45,49–53} manganese (III),^{49–51} cobalt (II, III),^{45,49–51,54,55} zinc (II),^{45,49,54–58} iron (III),⁴⁹ chromium (III),^{45,50,51,55,59,60} and nickel (II).⁵⁶ There are also a handful of reports about metal-free catalysts for epoxide / anhydride ROCOP.^{17,61,62} Also, in many cases, a co-catalyst is also required for the catalytic ROCOP to be carried out smoothly and efficiently. Common co-catalyst choices are (but not limited to):

bis(triphenylphosphoranylidene)ammonium chloride (PPNCl), tetraphenylphosphonium chloride (PPh₄Cl) and tetrabutylammonium chloride (nBu₄NCl). Most co-catalysts have a general feature: a bulky, stable, inert cation and a halide anion which serves as an initiating nucleophile. Most of the ligand systems are also planar with 4 donors, for an example, salph system has 2 nitrogen donors and 2 oxygen donors; porphyrin system has 4 nitrogen donors.

In 2011, DiCiccio and Coates reported a chromium salen catalyst **1.6** (Figure 1.11) capable of catalysing the ROCOP of maleic anhydride with epoxides.⁴⁵

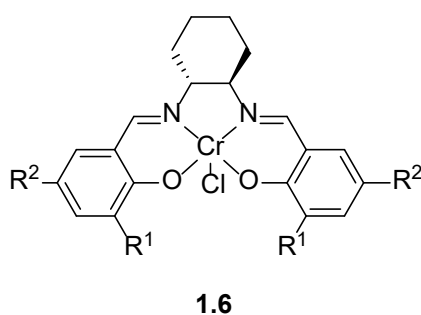
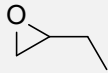
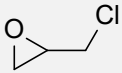
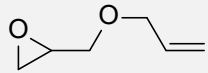
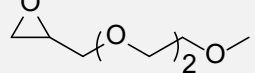
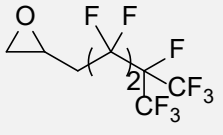
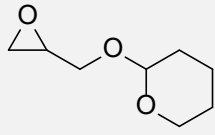
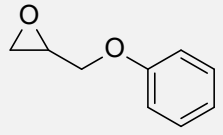


Figure 1.11: Structure of catalyst **1.6**⁴⁵

The catalytic performance of **1.6** (maleic anhydride with various epoxides) were summarized in Table 1.5 below.

Table 1.5: **1.6** Catalysis results for ROCOP between maleic anhydride and epoxides⁴⁵

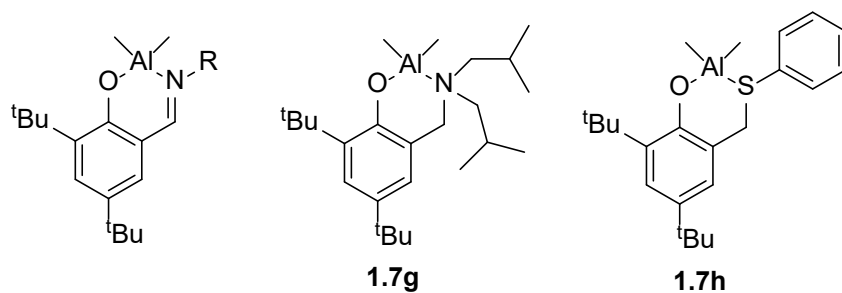
						
BO	ECH	AGE	EPO			
						
FHPO	CEPO	BPO				
Entry	Epoxide	Time/hours	conversion	Selectivity	M _n /Da	Đ
1	BO	14	90	>99%	21000	1.5
2	ECH	6	99	>99%	25000	1.7
3	AGE	15	98	>99%	25000	1.3
4	EPO	4	99	>99%	33000	1.1
5	FHPO	16	90	>99%	25000	1.7
6	CEPO	15	99	>99%	21000	1.4
7	BPO	12	99	>99%	31000	1.4

Conditions: temperature = 45°C; [MA]:[epoxide]:[cat] = 200 : 200 : 1; [MA] = [epoxide] = 4 mmol in 1 mL of hexanes; solvent: hexanes.

Generally speaking, **1.6** requires a relatively long reaction time with mild reaction temperature (only 45°C), giving excellent selectivity, high M_n but slightly poor dispersity.

Of course, metal complexes with smaller, simpler ligands can also serve as catalysts for epoxide/anhydride ROCOP; some examples are listed below.

In 2019, a tetracoordinate aluminium-based catalyst **1.7a-h** for ROCOP was reported by Isnard and co-workers.⁶³ Figure 1.12 illustrates their structures.



- 1.7a:** R = n-propyl
1.7b: R = Ph
1.7c: R = 2,6-diisopropylphenyl
1.7d: R = 2,6-dimethylphenyl
1.7e: R = 4-methoxyphenyl
1.7f: R = C₆F₅

Figure 1.12: Structure of catalyst **1.7a-h**⁶³

The catalysis data of **1.7a-h** catalysing ROCOP between cyclohexene oxide (CHO) and succinic anhydride (SA) are listed in Table 1.6.

Table 1.6: Catalysis result of **1.7a-h** in ROCOP between CHO and SA⁶³

Entry	Catalyst	Conversion	Selectivity	M _n /Da	Đ
1	1.7a	94%	>99%	1570	1.17
2	1.7b	91%	>99%	1910	1.20
3	1.7c	87%	94%	1810	1.22
4	1.7d	87%	95%	1820	1.26
5	1.7e	100%	>99%	1850	1.23
6	1.7f	62%	>99%	3750	1.12
7	1.7g	85%	90%	1970	1.27
8	1.7h	86%	87%	1520	1.15

Conditions: reaction time: 5 hours; catalyst = 2.0×10^{-5} mol, [cat]:[DMAP]:[SA]:[CHO] = 1 : 1 : 125 : 125; temperature = 110°C; solvent: 1 mL toluene.

As we can see from the table, **1.7a**, **1.7b** and **1.7e** gave good conversions and selectivities with slightly poor dispersity control, while other **1.7** catalysts gave slightly dissatisfactory conversions, selectivities and dispersity.

1.8a-c are a series of gallium-based catalysts with a distinct feature of having 4 gallium ions per molecule, reported by Ghosh and co-workers.⁶⁴ Most of the catalysts are either mononuclear or binuclear, which means this tetranuclear catalyst is unique in its structure. Also, as this structure sees higher flexibility (i.e., the four donors around each Ga are not in the same rigid planar structure), its reaction mechanisms and kinetics could be vastly different from the mono- or binuclear catalysts. The structure of it is depicted in Figure 1.13, and this series of catalysts require benzyl alcohol (BnOH) as co-catalyst.

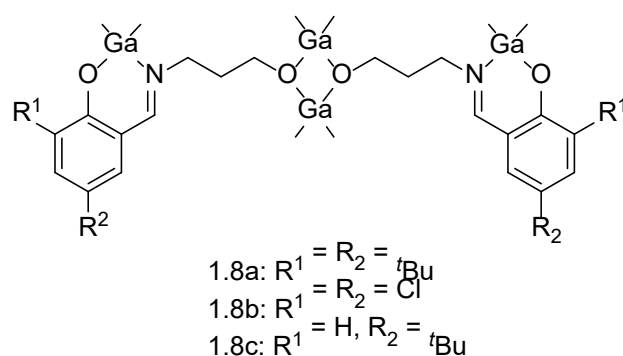


Figure 1.13: Structure of catalyst **1.8a-c**⁶⁴

Table 1.7 summarizes the catalytic performance of **1.8a-c** for ROCOP of cyclohexene oxide (CHO) with succinic anhydride (SA) or maleic anhydride (MA).

Table 1.7: 1.8a-c catalysis results for ROCOP of CHO with SA/MA							
Entry	Anhydride	catalyst	Time/h	Conversion	M _n /Da	Đ	Selectivity
1	SA	1.8a	12	95%	11200	1.3	>99%
2	SA	1.8b	20	80%	10300	1.4	>99%
3	SA	1.8c	15	92%	12800	1.4	>99%
4	MA	1.8a	12	99%	13200	1.3	>99%
5	MA	1.8b	20	85%	10700	1.3	>99%
6	MA	1.8c	15	93%	11500	1.5	>99%

Conditions: catalyst = 25.5 μmol; [cat]:[co-cat]:[CHO]:[anhydride] = 1:4:200:200; reaction temperature: 100°C; solvent: toluene.

Figure 1.14: Structure of **1.9**⁴⁹

The co-catalyst tris(methylcyclohexylamino)cyclopropenium chloride was bonded covalently to the salen ligand. This structure was claimed to enable easier steric and electronic perturbations, thus leading to better catalytic activity. Table 1.8 summarizes the reported catalytic performances of **1.9**.

Table 1.8: ROCOP catalysis results for **1.9**⁴⁹

Entry	Epoxide	Anhydride	conversion	M _n /Da	Đ
1	PO	PA	> 100%	22100	1.14
2	PO	DMPA	88%	21900	1.08
3	PO	CPMA	95%	23400	1.14
4	BO	CPMA	53%	16000	1.12
5	CHO	CPMA	51%	8200	1.24
6	EPB	CPMA	42%	9200	1.11
7	^t BGE	CPMA	19%	5500	1.18
8	AGE	CPMA	54%	12700	1.16

Conditions: reaction time: 4 hours (6 hours for entry 5); [cat]:[anhydride]:[epoxide]=1:400:2000; temperature: 60°C, neat. PO: propylene oxide; BO: butylene oxide; CHO: cyclohexene oxide; EPB: (2,3-epoxypropyl)benzene; ^tBGE: ^tbutyl glycidyl ether; AGE: allyl glycidyl ether; PA: phthalic anhydride; CPMA: carbic anhydride; DMPA: 3,6-Dimethylphthalic anhydride.

Table 1.8 suggests that **1.9** have rather poor conversion at the given reaction times (4 hours / 6 hours), large M_n when epoxide is propylene oxide and good Đ control. In **1.9**'s case, although the built-in co-catalyst simplifies reaction processes (e.g., no need to weight out co-catalyst, no stoichiometry troubles), the overall catalytic performance is not improved, which could be one of the potential reasons why this kind of built-in co-catalyst structure is not commonly seen for ROCOP catalysts.

1.4.3. ROCOP of epoxides with carbon dioxide

For ROCOP with epoxides as one of the co-monomers, the partner of epoxides does not have to be anhydride. As have been mentioned before, one of the advantages of ROCOP is a huge selection of monomers and many of them being renewable. Carbon dioxide, the major component of the greenhouse gases that modern human society eagerly wants to get rid of, contributed 81% of all the greenhouse gases emitted in 2018, as shown in Figure 1.15.⁶⁵ If large-scale exploitation of CO₂ as industrial raw material is made possible, we will not only benefit from cheap, seemingly endless resource supply and low costs, more importantly, the reduction of greenhouse effect caused by free CO₂ in the atmosphere will be an added benefit. Fortunately, carbon dioxide is a potential candidate for co-monomer of ROCOP with epoxides, and many catalysts have already been developed to actualize this goal.

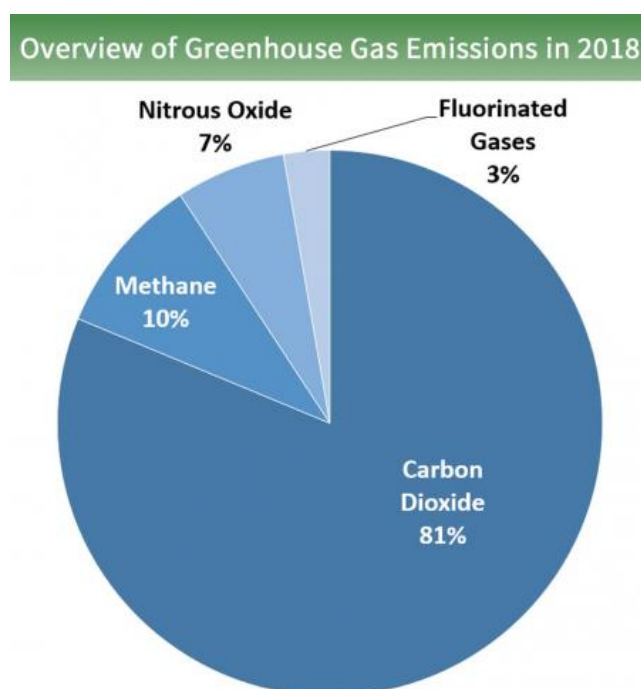


Figure 1.15: Greenhouse gases emitted in 2018⁶⁵

In 2012, Lee *et al.*⁶⁶ reported a salen-based cobalt catalyst **1.10**, as shown in Figure 1.16. This catalyst is used for synthesis of low molecular weight and subsequent *in*

situ synthesis of polyurethane with feeding of diisocyanates. Chain transfer agents (CTAs) are used in order to obtain low molecular weight polypropylene carbonate with OH groups at both ends. The subsequent *in situ* reaction with diisocyanates (which acts as chain-transfer agent) would give thermoplastic polyurethanes (PU). At 30 bar CO₂ pressure, [1.10] : [PO] = 1 : 500, 70°C, , 1 hour, 1.10 showed conversions (conversion to PU) at about 20% to 30%, with PU selectivities (% of polycarbonate converted to PU) all above 90%, but with poor \bar{D} (even over 4.0), as summarized in Table 1.9.

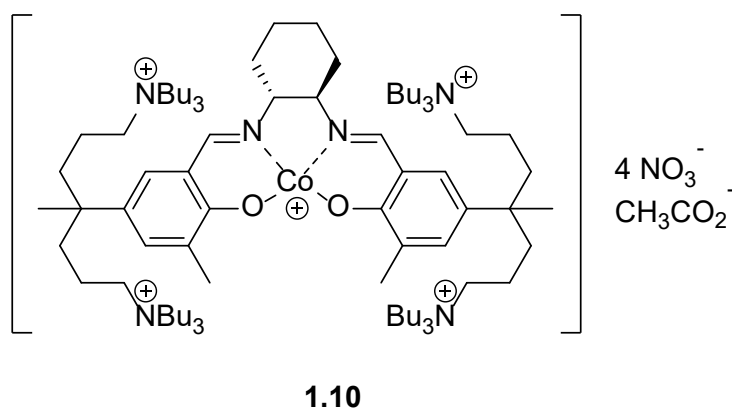


Figure 1.16: Structure of catalyst 1.10⁶⁶

Table 1.9: CO₂ / propylene oxide ROCOP results for **1.10**⁶⁶

Entry	CTA	Diisocyanate	[CTA]:[1.10]	Conversion	Selectivity	M _n /Da	Đ
1	PDO	N/A	400	21%	94%	4100	1.05
2	PDO	DPMD	400	20%	95%	37800	4.25
3	PDO	DPMD	450	18%	96%	23200	3.68
4	PDO	PD	400	22%	93%	28900	4.07
5	TPA	TD	400	27%	92%	23700	4.67
6	TPA	DPMD	400	27%	97%	48800	3.51
7	TPA	PD	400	22%	95%	20600	3.48
8	TPA	TD	400	24%	94%	20700	3.91

CTA: chain-transfer agent.

This is a good example of post-functionalization of CO₂ / epoxide co-polymer. The low conversion can be rationalized since this is a two-step polymerization, which will intrinsically have lower conversion. The use of chain transfer agent, which stops polymer chains from propagating at low molecular weight stage, put uncertainties onto the dispersity control thereby giving lower control over the polymer molecular weight. The key catalytic performance, selectivity, is generally good for **1.10**, which proves it to be a highly active catalyst. Structural wise, ion pairs are not common for metal complex catalysts. But the anions which come together with the catalysts could potentially facilitate the leaving of carboxylate-terminated chains from the central metal ion, which may increase the reaction speed.

In 2020, Andrea and co-workers⁶⁷ reported two catalysts **1.11a** and **1.11b** capable of catalyzing CO₂ / epoxide ROCOP as well (Figure 1.17). **1.11a** and **1.11b** are based on indium, which is not a common metal for ROCOP catalysis. The catalysis

performance of them catalysing ROCOP between CO₂ and cyclohexene oxide (CHO) are summarized in Table 1.10.

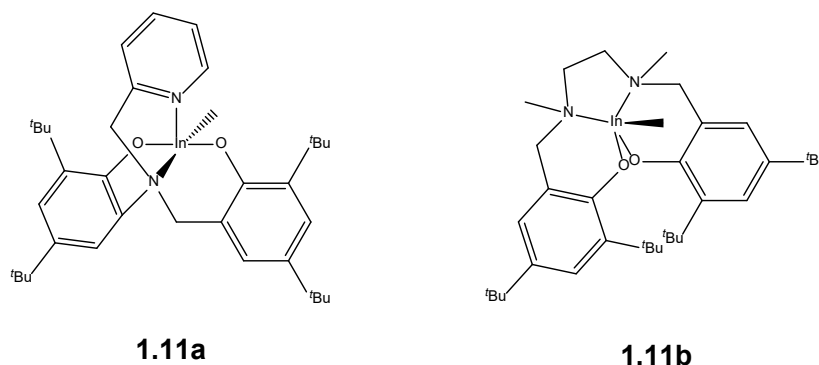


Figure 1.17: Structure of catalyst **1.11a** and **1.11b**⁶⁷

Table 1.10: **1.11a** and **1.11b** catalysis results of ROCOP between CO₂ and CHO⁶⁷

Entry	Catalyst	Conversion	Selectivity	M _n	Đ
1	1.11a	73%	>99%	5260	1.08
2	1.11b	71%	>99%	7640	1.09

Conditions: [cat] : [CHO] = 1 : 200, 40 bar CO₂ pressure, 60°C, 24 hours.

In general, **1.11** exhibit good selectivity and dispersity control, but requires a rather long reaction time at elevated temperature. The ancillary ligand is again substituted salen ligand, indicating the popularity of salen-system within this area of catalysis.

From the information and data provided in this section, over one decade of development, catalysts nowadays exhibit much better dispersity control with high selectivity and much better conversion, although requiring longer reaction time. However, the majority of metal complexes are still based on salph, porphyrin or modified systems of them. Although steric, electronic and other critical properties can be tuned to some extent for these kinds of rigid, planar 4-donor ligand systems, the level of freedom is much less if the ligand system is still salph / porphyrin type, comparing to a brand-new ligand environment. I therefore proposed a hypothesis

that ligand systems with flexible, twistable structure can possibly provide lower energy transition states in catalytic cycle by conformational changes (in chapter 6, more investigations into this hypothesis were done with DFT calculations). As such, the development of new ancillary ligands are urgently needed for the advancement of the ROCOP catalysis field. To provide some progress in this area, I hereby provide research into two new ligand environments in the remainder of this thesis.

1.5. References

- 1 D. Barton, Introduction to the Types and Classes of Polymeric Materials, 2020.
- 2 D. Feldman, *Des. Monomers Polym.*, 2008, **11**, 1–15.
- 3 R. Geyer, J. R. Jambeck and K. L. Law, *Sci. Adv.*, 2017, **3**, e1700782.
- 4 Plastic Pollution, <https://ourworldindata.org/plastic-pollution>, (accessed 13 October 2020).
- 5 M. R. Gregory, *Philos. Trans. R. Soc. B Biol. Sci.*, 2009, **364**, 2013–2025.
- 6 M. Eriksen, L. C. M. Lebreton, H. S. Carson, M. Thiel, C. J. Moore, J. C. Borerro, F. Galgani, P. G. Ryan and J. Reisser, *PLoS ONE*, 2014, **9**, e111913.
- 7 Y. Chae and Y.-J. An, *Environ. Pollut.*, 2018, **240**, 387–395.
- 8 E. Huerta Lwanga, J. Mendoza Vega, V. Ku Quej, J. de los A. Chi, L. Sanchez del Cid, C. Chi, G. Escalona Segura, H. Gertsen, T. Salánki, M. van der Ploeg, A. A. Koelmans and V. Geissen, *Sci. Rep.*, 2017, **7**, 14071.
- 9 M. O. Gaylor, E. Harvey and R. C. Hale, *Environ. Sci. Technol.*, 2013, **47**, 13831–13839.
- 10 K. Ragaert, L. Delva and K. Van Geem, *Waste Manag.*, 2017, **69**, 24–58.

- 11 L. S. Nair and C. T. Laurencin, *Prog. Polym. Sci.*, 2007, **32**, 762–798.
- 12 E. S. Abdel-Halim, F. A. Abdel-Mohdy, S. S. Al-Deyab and M. H. El-Newehy, *Carbohydr. Polym.*, 2010, **82**, 202–208.
- 13 W. Xu and X. Liu, *Eur. Polym. J.*, 2003, **39**, 199–202.
- 14 R. Chandra and R. Rustgi, *Prog. Polym. Sci.*, 1998, **23**, 1273–1335.
- 15 J.K. Stille, *J. Chem. Educ.*, 1981, **58**, 5.
- 16 A. M. DiCiccio, J. M. Longo, G. G. Rodríguez-Calero and G. W. Coates, *J. Am. Chem. Soc.*, 2016, **138**, 7107–7113.
- 17 A. Kummari, S. Pappuru and D. Chakraborty, *Polym. Chem.*, 2018, **9**, 4052–4062.
- 18 M. Nič, J. Jirát, B. Košata, A. Jenkins and A. McNaught, Eds., in *IUPAC Compendium of Chemical Terminology*, IUPAC, Research Triangle Park, NC, 2.1.0., 2009.
- 19 L. Fontaine, *Angew. Chem. Int. Ed.*, 2009, **48**, 9780–9780.
- 20 V. R. Sinha, K. Bansal, R. Kaushik, R. Kumria and A. Trehan, *Int. J. Pharm.*, 2004, **278**, 1–23.
- 21 P. B. Messersmith and E. P. Giannelis, *J. Polym. Sci. Part Polym. Chem.*, 1995, **33**, 1047–1057.
- 22 L. Ghasemi-Mobarakeh, M. P. Prabhakaran, M. Morshed, M.-H. Nasr-Esfahani and S. Ramakrishna, *Biomaterials*, 2008, **29**, 4532–4539.
- 23 T. K. Dash and V. B. Konkimalla, *J. Controlled Release*, 2012, **158**, 15–33.
- 24 R. A. Gross, *Science*, 2002, **297**, 803–807.

- 25 J. K. Oh, D. I. Lee and J. M. Park, *Prog. Polym. Sci.*, 2009, **34**, 1261–1282.
- 26 R. M. Thomas, P. C. B. Widger, S. M. Ahmed, R. C. Jeske, W. Hirahata, E. B. Lobkovsky and G. W. Coates, *J. Am. Chem. Soc.*, 2010, **132**, 16520–16525.
- 27 O. Nuyken and S. Pask, *Polymers*, 2013, **5**, 361–403.
- 28 H. R. Kricheldorf, M. Berl and N. Scharnagl, *Macromolecules*, 1988, **21**, 286–293.
- 29 P. Dubois, C. Jacobs, R. Jerome and P. Teyssie, *Macromolecules*, 1991, **24**, 2266–2270.
- 30 H. R. Kricheldorf and I. Kreiser-Saunders, *Polymer*, 2000, **41**, 3957–3963.
- 31 G. A. Abraham, A. Gallardo, A. E. Lozano and J. S. Roman, *J. Polym. Sci., Part A: Polym. Chem.* 2000, **38**, 1355–1365.
- 32 A. Armitage, O. Boyron, Y. Champouret, M. Patel, K. Singh and G. Solan, *Catalysts*, 2015, **5**, 1425–1444.
- 33 M. Fuchs, S. Schmitz, P. M. Schäfer, T. Secker, A. Metz, A. N. Ksiazkiewicz, A. Pich, P. Kögerler, K. Yu. Monakhov and S. Herres-Pawlis, *Eur. Polym. J.*, 2020, **122**, 109302.
- 34 H. Plommer, J. N. Murphy, L. N. Dawe and F. M. Kerton, *Inorg. Chem.*, 2019, **58**, 5253–5264.
- 35 B. Ochiai and T. Endo, *J. Polym. Sci. Part Polym. Chem.*, 2007, **45**, 2827–2834.
- 36 P. Sarker, J. R. Ebdon and S. Rimmer, *Macromol. Rapid Commun.*, 2006, **27**, 2007–2013.
- 37 N. K. Singha, A. Kavitha, P. Sarker and S. Rimmer, *Chem. Commun.*, 2008, 3049.

- 38 F. Sanda and T. Endo, *J. Polym. Sci.*, 2001, **39**, 265–276.
- 39 N. Moszner, F. Zeuner, T. Volkel and V. Rheinberger, *Macromol. Chem. Phys.*, 1999, **200**, 2173–2187.
- 40 S. Paul, Y. Zhu, C. Romain, R. Brooks, P. K. Saini and C. K. Williams, *Chem. Commun.*, 2015, **51**, 6459–6479.
- 41 M. R. Kember, A. Buchard and C. K. Williams, *Chem Commun.*, 2011, **47**, 141–163.
- 42 E. Hosseini Nejad, C. G. W. van Melis, T. J. Vermeer, C. E. Koning and R. Duchateau, *Macromolecules*, 2012, **45**, 1770–1776.
- 43 T. Stößer, C. Li, J. Unruangsri, P. K. Saini, R. J. Sablong, M. A. R. Meier, C. K. Williams and C. Koning, *Polym. Chem.*, 2017, **8**, 6099–6105.
- 44 D. J. Darensbourg and S. J. Wilson, *Macromolecules*, 2013, **46**, 5929–5934.
- 45 A. M. DiCiccio and G. W. Coates, *J. Am. Chem. Soc.*, 2011, **133**, 10724–10727.
- 46 M. E. Fieser, M. J. Sanford, L. A. Mitchell, C. R. Dunbar, M. Mandal, N. J. Van Zee, D. M. Urness, C. J. Cramer, G. W. Coates and W. B. Tolman, *J. Am. Chem. Soc.*, 2017, **139**, 15222–15231.
- 47 W. Kuran, *Prog. Polym. Sci.*, 1998, **23**, 919–992.
- 48 T. Aida, K. Sanuki and S. Inoue, *Macromolecules*, 1985, **18**, 1049–1055.
- 49 B. A. Abel, C. A. L. Lidston and G. W. Coates, *J. Am. Chem. Soc.*, 2019, **141**, 12760–12769.
- 50 E. H. Nejad, A. Paoniasari, C. G. W. van Melis, C. E. Koning and R. Duchateau, *Macromolecules*, 2013, **46**, 631–637.

- 51 E. Hosseini Nejad, A. Paoniasari, C. E. Koning and R. Duchateau, *Polym. Chem.*, 2012, **3**, 1308.
- 52 N. J. Van Zee, M. J. Sanford and G. W. Coates, *J. Am. Chem. Soc.*, 2016, **138**, 2755–2761.
- 53 A. Takasu, T. Bando, Y. Morimoto, Y. Shibata and T. Hirabayashi, *Biomacromolecules*, 2005, **6**, 1707–1712.
- 54 P. K. Saini, C. Romain, Y. Zhu and C. K. Williams, *Polym Chem*, 2014, **5**, 6068–6075.
- 55 M. Winkler, C. Romain, M. A. R. Meier and C. K. Williams, *Green Chem.*, 2015, **17**, 300–306.
- 56 C.-Y. Yu, H.-J. Chuang and B.-T. Ko, *Catal. Sci. Technol.*, 2016, **6**, 1779–1791.
- 57 D.-F. Liu, L.-Y. Wu, W.-X. Feng, X.-M. Zhang, J. Wu, L.-Q. Zhu, D.-D. Fan, X.-Q. Lü and Q. Shi, *J. Mol. Catal. Chem.*, 2014, **382**, 136–145.
- 58 Y. Zhu, C. Romain and C. K. Williams, *J. Am. Chem. Soc.*, 2015, **137**, 12179–12182.
- 59 D. J. Darensbourg, R. R. Poland and C. Escobedo, *Macromolecules*, 2012, **45**, 2242–2248.
- 60 J. Liu, Y.-Y. Bao, Y. Liu, W.-M. Ren and X.-B. Lu, *Polym. Chem.*, 2013, **4**, 1439–1444.
- 61 S. Pappuru and D. Chakraborty, *Eur. Polym. J.*, 2019, **121**, 109276.
- 62 P. K. Gupta, S. K. Tripathi, S. Pappuru, S. C. Chabattula, K. Govarathanan, S. Gupta, B. K. Biswal, D. Chakraborty and R. S. Verma, *Mater. Sci. Eng. C*, 2020, **107**, 110285.

- 63 F. Isnard, F. Santulli, M. Cozzolino, M. Lamberti, C. Pellicchia and M. Mazzeo, *Catal. Sci. Technol.*, 2019, **9**, 3090–3098.
- 64 S. Ghosh, E. Glöckler, C. Wölper, A. Tjaberings, A. H. Gröschel and S. Schulz, *Dalton Trans.*, 2020, 10.1039.D0DT02831B.
- 65 O. US EPA, Overview of Greenhouse Gases, <https://www.epa.gov/ghgemissions/overview-greenhouse-gases>, (accessed 26 November 2020).
- 66 S. H. Lee, A. Cyriac, J. Y. Jeon and B. Y. Lee, *Polym. Chem.*, 2012, **3**, 1215.
- 67 K. A. Andrea, A. R. Beckett, G. G. Briand, S. A. Martell, J. Masuda, K. M. Morrison and E. M. T. Yammine, *J. Organomet. Chem.*, 2020, **919**, 121307.

Chapter 2: Synthesis, characterization, X-Ray crystal structure of CpHOH ligand and [(CpHO)₂Al₂Me₄] complex

2.1. Introduction

During the history of developing catalysts for molecular transformations, most organometallic (homogeneous) catalysts contain transition metals, and the platinum group metals are dominant in this area (although for polymerization, platinum group metals are not as common as for other reactions). Despite good catalytic performance, the overuse of transition metals has given rise to many problems. Transition metals like palladium, rhodium and platinum are scarce resources coming with high price and limited supply. The average prices for palladium, rhodium and platinum are given in Table 2.1 below. In contrast, aluminium is inexpensive, being the most abundant metal in the earth's crust; its average price is included in Table 2.1 for comparison. The price charts of platinum group metals for 2020 are provided for price trend visualization (Figure 2.1, 2.2 and 2.3).

Table 2.1: Price ranges of common metals for catalyst in 2020

Metal	Price Range/U.S. Dollars per troy Ounce
Palladium ¹	1522 – 2370
Rhodium ²	5500 – 17000
Platinum ³	753.86 – 1028
Aluminium ⁴	4.56 – 6.27

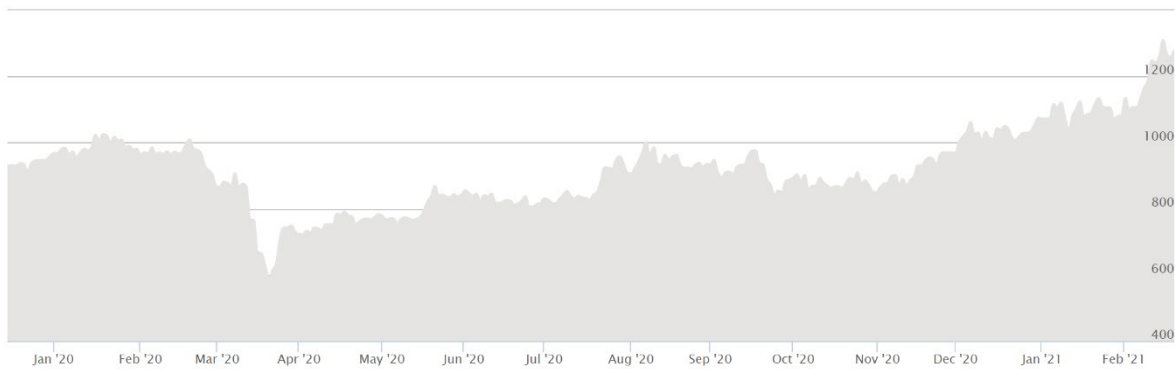


Figure 2.1: 2020 price chart of platinum, U.S. Dollars/troy Ounce⁵



Figure 2.2: 2020 price chart of palladium, U.S. Dollars/troy Ounce⁶

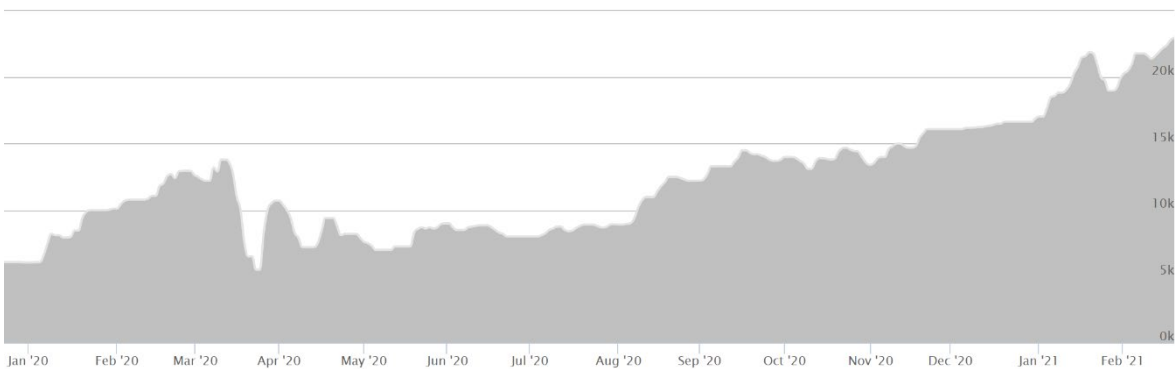


Figure 2.3: 2020 price chart of rhodium, U.S. Dollars/troy Ounce⁷

As can be seen from the figures above, the price of precious metals generally increased in 2020 (palladium price fluctuating), while aluminium's price was almost negligible compared to the precious metals. The high cost of using precious metals for catalysts inevitably requires good recycling process so that the waste can be minimized. However, due to the nature of organometallic catalysts in polymerization,

the recycling processes are extremely expensive, time-consuming and difficult. The problem is intensified in polymerization catalysis, since the catalysts almost always remain trapped inside the polymers and cannot be extracted and re-used. Although platinum group metals are not as common in polymerization catalysis as for other catalysis, the pursuit for cheaper metal catalysts will nevertheless make cost control and catalyst supply much easier. On the other hand, the low cost of aluminium naturally allows it to be part of a realistic sacrificial catalyst for industrial applications, as losing the aluminium complexes would not incur enormous costs, especially when the ancillary ligands for the complexes are cheap and easily synthesized. Secondly, the mining and purification processes for precious metals are usually carried out with heavy-labour (which damage the workers' health (physically and by chemical / toxicological means), giving rise to ethical issues. Even those transition metals that are less scarce usually come with higher cost than aluminium. Aluminium, on the other hand, is of much higher abundance than any other metal in the earth's crust. With its contribution of 1.59% of Earth's total mass (7th most abundant among all elements),⁸ 8.23% of Earth crust (3rd most abundant after oxygen and silicon in Earth crust),⁹ aluminium comes with a seemingly infinite supply; the modern aluminium mining and purifying process provide this metal to society with low cost. Another critical issue for transition metal complexes is the toxicity. Most transition metals are toxic in their ionic forms, and the unavoidable immobilization of them inside the final polymer products brings about concerns of safety. Many daily polymer commodities get into close contact with the human body and are highly likely to be ingested, for example in food packaging. On the contrary, aluminium is much safer compared to many transition metals; no acute toxicity has been observed when ingested by human beings. Thus, if a highly efficient catalyst (for synthetic polymers) can be made out of aluminium rather than other transition metals, society would benefit greatly from it in ethical, commercial and environmental perspectives. Many previous reports regarding aluminium organometallic catalysts / co-catalysts for olefin polymerization,^{10,11} ring-opening copolymerization (ROCOP),^{12,13} lactide homopolymerization,¹⁴⁻¹⁶ ϵ -caprolactone

polymerization¹⁷ and many more have been found in the chemical literature, as scientists seek to realize these benefits.

For several decades, many metal complexes have been developed to serve as the catalysts for ring-opening co-polymerization (ROCOP) of epoxides and anhydrides. Despite their decades of history, it is only in recent years that epoxide/anhydride ROCOP has attracted appreciable amount of attention and become a substantial topic of research. However, the vast majority of catalysts are based on ancillary ligands that are planar and have donor atoms consisting of 4 nitrogens (e.g., porphyrin-type), 2 nitrogens and 2 oxygens (e.g., salen-type), or derivatives of these systems; examples are given in Figure 2.4.

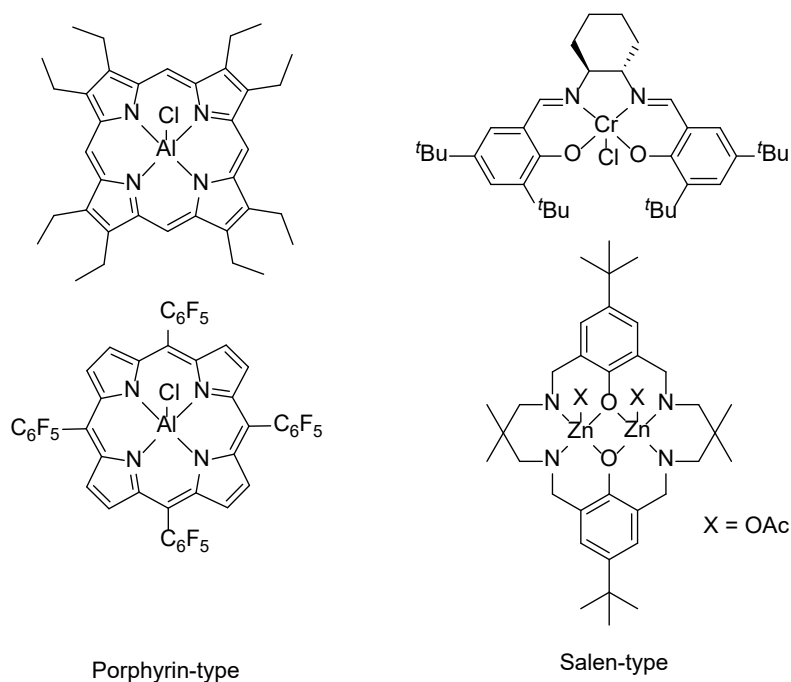


Figure 2.4: Examples of conventional ROCOP catalysts^{18,19}

Despite the fact that many salen-type and porphyrin-type catalysts are highly active and exhibit high ROCOP catalytic performance, reports that utilize radically different ligands are comparatively rare. The repetitive using of porphyrin / salen type ligands for ROCOP catalysts obviously provides research space for other ligand systems which can be exploited to give equal or better catalytic results than the existing ones, and can be targeted to expand the scope of possible substrates (existing ligand

systems do not always perform well with every possible substrate), or easier, lower-cost catalyst synthetic protocols. Previously in the BDW group, Mark Sullivan has undertaken comprehensive research around complexes with TACN-type ligand, as shown in Figure 2.5.

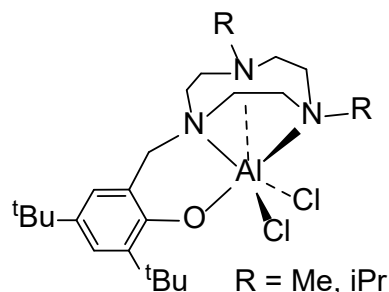


Figure 2.5: TACN-type complex developed by Mark Sullivan in BDW group

This complex gave a number of excellent results for ROCOP catalysis, which in turn sparked an idea about whether the TACN could be exchanged with something isoelectronic (e.g., 6-electron donor) and still obtain an active ROCOP catalyst; an additional negative charge would give only one chloride remaining on the metal ion, possibly allowing more space and a corresponding increase in activity. A fairly common anionic 6-electron ligand is the cyclopentadienyl (Cp) ligand. Literature searches on Cp-based complexes and ROCOP catalysis was therefore been conducted. During the literature search, an interesting Cp-ring containing ligand which stood out as a Cp analogue of the ligand is illustrated in Figure 2.6.

The original idea of choosing 2-(tetramethylcyclopentadienyl)-4-methylphenol (CpHOH, structure in Figure 2.6) as the ligand came from a paper by Chen *et al.*²⁰ In this paper, CpHOH was reported as a ligand capable of forming “constrained geometry complex” (CGC). The CGCs Chen and co-workers developed with CpHOH were [CpOTi(CH₂Ph)₂] and [(CpO)₂Zr], with structures shown in Figure 2.6.

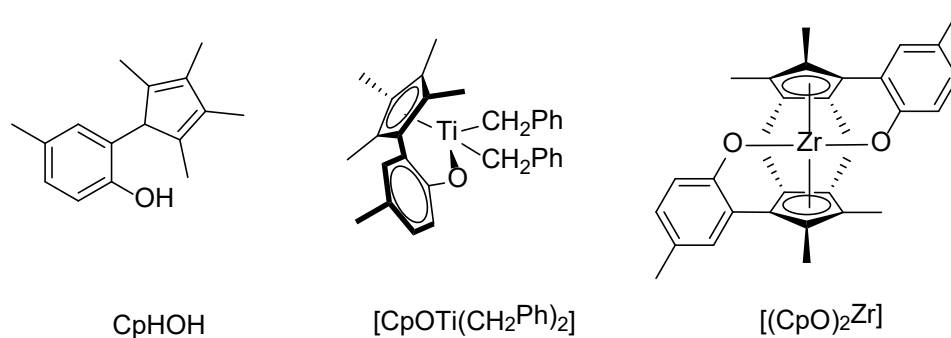


Figure 2.6: Structures of CpHOH, $[\text{CpOTi}(\text{CH}_2\text{Ph})_2]$ and $[(\text{CpO})_2\text{Zr}]$ ²⁰

According to further tests carried out by Chen *et al.*, both $[\text{CpOTi}(\text{CH}_2\text{Ph})_2]$ and $[(\text{CpO})_2\text{Zr}]$ are capable of catalyzing the α -olefin polymerizations. Although there were no experiments regarding ROCOP of epoxides/anhydrides; it is possible that this type of constrained-geometry complex could have potential to be effective ROCOP catalysts.

The first “constrained geometry complex” (CGC) was reported by Shapiro and co-workers²¹ in 1990. The CGC they reported, $[\text{Sc}(\text{Cg})\text{H}]_2$ (Cg = Cp-amide ligand) has two scandium ions per molecule with two bridging hydrides, and one Cg ligand per scandium, as shown in Figure 2.7. This complex was developed to serve as a catalyst for α -olefin polymerization.

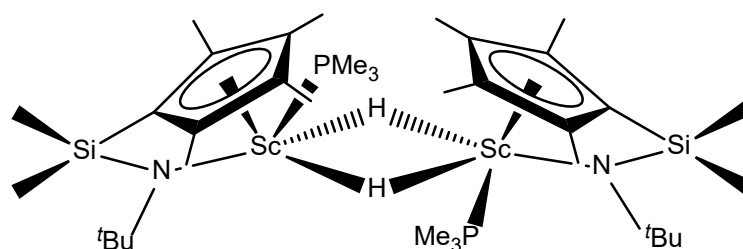


Figure 2.7: Structure of the first CGC, $[\text{Sc}(\text{Cg})\text{H}]_2$ ²¹

The main feature of the CGCs is that the Cp ring on the ligand and the secondary donor adopt a bite angle smaller than they would comparing to the equivalent complex with the Cp ring and secondary donor non-linked, thus called “constrained geometry complex”, as shown in Figure 2.8.

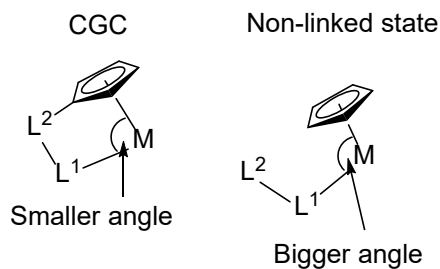


Figure 2.8: Constrained geometry illustration

The majority of the CGCs are Cp-amide complexes, such as the $[\text{Sc}(\text{Cp})\text{H}]_2$ in Figure 2.7. Apart from Cp-amide complexes, another commonly-seen class of metal complexes which have their bond angles constrained are the ansa-metallocene complexes (example of ansa-metallocene complex in Figure 2.9).²²

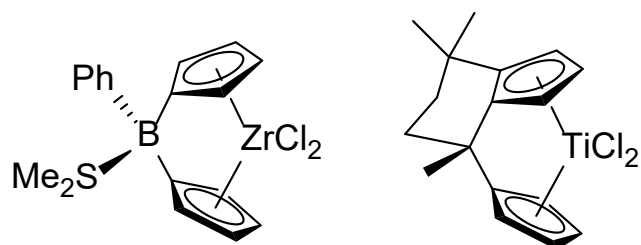


Figure 2.9: Examples of ansa-metallocene type complexes²²

The bond angles in ansa-metallocene systems can be affected by many factors including the identity of the bridging group, the central metal ion, other ligands binding to the central metal site, etc. In terms of reactivity, the key differences between the ansa-metallocene system and the CGC system is the greatly reduced steric hinderance around central metal site in the CGC and the lower valence electron count due to the half-sandwich structure instead of double-sandwich structure. These fundamental differences not only make the metal site in CGC much easier to approach for substrates, but also greatly increased the Lewis acidity of the metal ions. Therefore theoretically, CGCs could be more catalytically active compared to their counterparts in the double-sandwich structure of ansa-metallocene systems, as the substrates are activated by binding to the metal centre. The first CGC, developed by Shapiro *et al.*,²¹ actually showed much higher catalytic

activity for α -olefin polymerization than the ansa-metallocene scandium congener, again proving the critical role of developing CGC as catalysts.

CGCs are generally developed as catalysts for olefin polymerization reactions,^{23–25} and some other reactions such as hydroamination / cyclization.²⁶ However, there are no reports of CGCs catalyzing the copolymerization of CO₂ / epoxides or epoxides / anhydrides, thus illustrating a unique opportunity for a new avenue of research into ROCOP catalysis with radically different ligand environments to the current state of the art. In the paper of Chen *et al.*,²⁰ CpHOH successfully formed CGCs with titanium and zirconium, but no attempt with aluminium was made.

With all these factors in mind, the attempt to make a CGC based on aluminium and the CpHOH ligand was undertaken. However, although a complex was successfully obtained, it was not the expected structure. Nevertheless, the complex thus produced was probed for its efficacy in the ROCOP of epoxides and cyclic anhydrides.

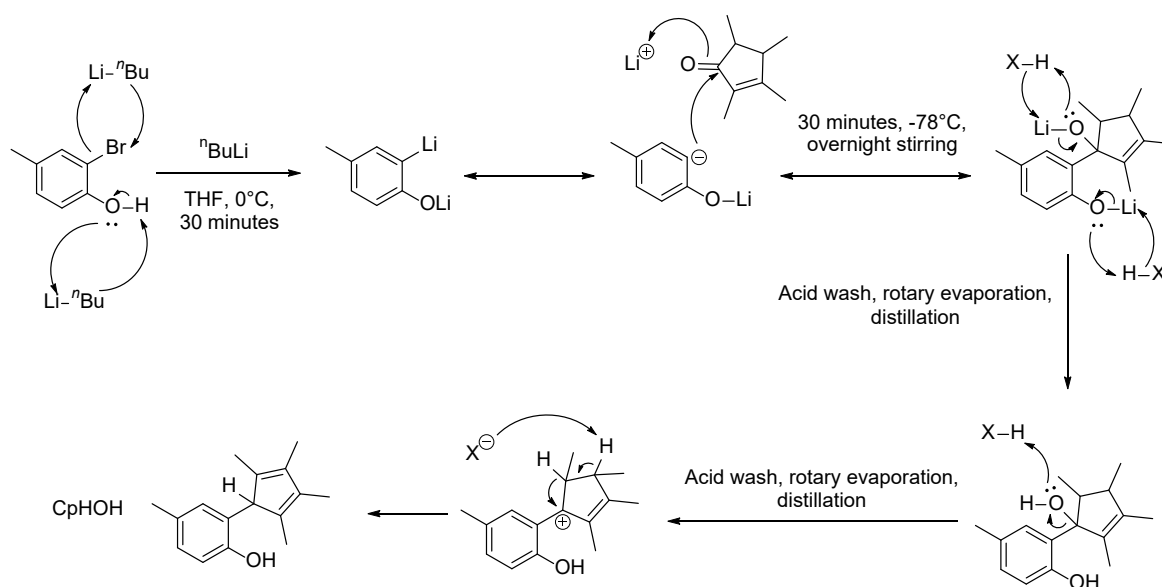
2.2. Synthesis and characterization of CpHOH ligand

2.2.1. Synthesis of CpHOH ligand

The pro-ligand CpHOH was prepared according to the method reported by Chen and co-workers²⁷ in 1997, which is described as followed.

2-(Tetramethylcyclopentadienyl)-4-methylphenol (CpHOH) was obtained via a two-step synthesis (Scheme 2.1). In the first step, 2-bromo-4-methylphenol was dissolved in THF and reacted with 2 equivalents of ⁿBuLi solution to deprotonate the hydroxyl group and substitute the bromide with lithium. Since the proton of the hydroxy group competes with bromide when reacting with ⁿBuLi, simply adding one equivalent of ⁿBuLi will not remove bromide. As such, 2 equivalents of ⁿBuLi was used to not only remove bromide, but deprotonate hydroxy group as well. In the second step, 2,3,4,5-tetramethyl-2-cyclopentenone was added dropwise over 30

minutes at -78°C to the reaction mixture. After stirring overnight, the reaction mixture was washed with distilled water and concentrated hydrochloric acid. The purpose of the acid wash is to reprotonate the hydroxy group thus we have CpHOH at the end of the reaction. The volatiles then removed under reduced pressure, leaving an oily residue with yellow-brownish colour. The residue was then distilled under reduced pressure, giving CpHOH as a yellow crystalline solid.



Scheme 2.1: Synthetic route of CpHOH

2.2.2. Characterization of ligand CpHOH

Since the ligand CpHOH is a known ligand that has been reported before, characterization was done by comparing the NMR data of the sample with the reported NMR data in the paper (original paper used deuterated benzene as solvent but the synthesized CpHOH in this thesis was identified in deuterated chloroform; the general pattern is the same but with some small differences in chemical shift). Figure 2.10 contains the 400MHz ^1H NMR spectrum of the CpHOH sample obtained from the reported synthetic route.

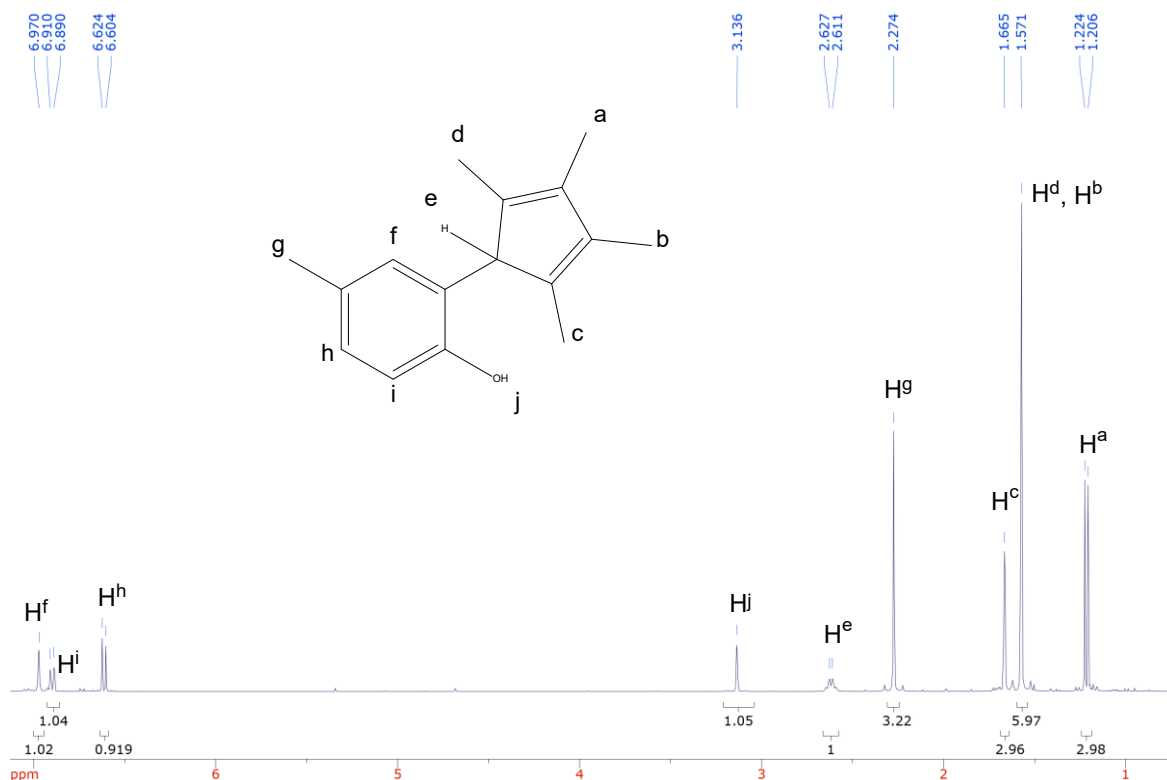


Figure 2.10: $^1\text{H-NMR}$ (400 MHz, CDCl_3 , 293 K) of ligand CpHOH

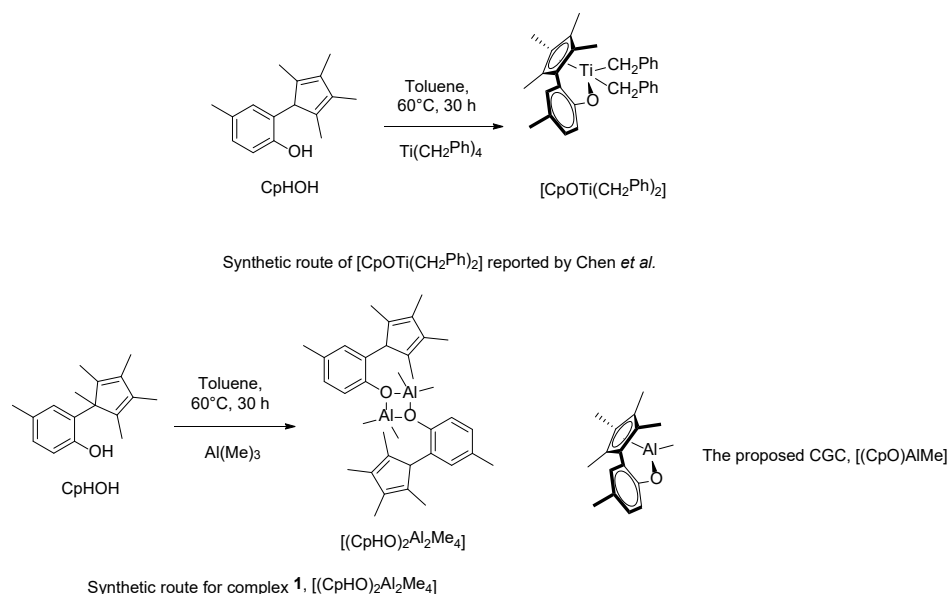
The most upfield signal at 1.22 ppm is attributed to H^a . It has an integration of 3H, consistent with a methyl signal, and was observed as an app. doublet with app. $^3J_{\text{H-H}}=7.2$ Hz. Since no symmetry exists for the Cp ring, the four methyl groups will theoretically give four signals (although in the spectrum H^d and H^b were coincident). The signal at 1.571 ppm is attributed to H^d and H^b . It has an integration of 6H, consistent with signal of two methyl groups and observed as a singlet. The other two Cp methyl groups were observed as a doublet at 1.22 ppm (reported above) and singlet at 1.67 ppm respectively, all with 3H integration as expected. The signal at 2.27 ppm is attributed to tolyl proton H^g , appeared as an app. singlet, and integrates to 3H as it should be. Signal at 2.63 ppm is attributed to H^e , the Cp proton. It has an integration of 1H, and was observed as an app. quartet $^3J_{\text{H-H}}=6.4$. This signal at 2.63 ppm is expected to be lost after deprotonation of the Cp ring in the proposed synthesis for CGC (which persist after reaction). Singlet at 3.14 ppm is assigned to hydroxyl proton H^j , which is expected to be lost after reaction. Aromatic protons H^h , H^i and H^f were observed as two app. doublets (H^i and H^h) and one app. singlet (H^f) at 6.62, 6.91 and 6.97 ppm respectively, all in the expected region. App.

singlet is assigned to H^f since no adjacent proton exist for strong coupling, and the other two couples with each other to split into doublets. The whole spectrum closely resembles the NMR pattern reported by Chen and co-workers,²⁵ but with different chemical shifts since different NMR solvent was used to prepare the NMR sample.

2.3. Synthesis and characterization of [(CpHO)₂Al₂Me₄] (1)

2.3.1. Synthesis of [(CpHO)₂Al₂Me₄] (1)

As the originally proposed plan was to make an aluminium CGC, reaction was carried out with the same procedures as given by Chen *et al.* in their report but using Al(Me)₃ instead of Ti(CH₂Ph)₄.²⁰ The reported reaction scheme is for the CGC of titanium with CpHOH, as shown in Scheme 2.2. The synthetic route of [(CpHO)₂Al₂Me₄] is also given in parallel in Scheme 2.2 for comparison.

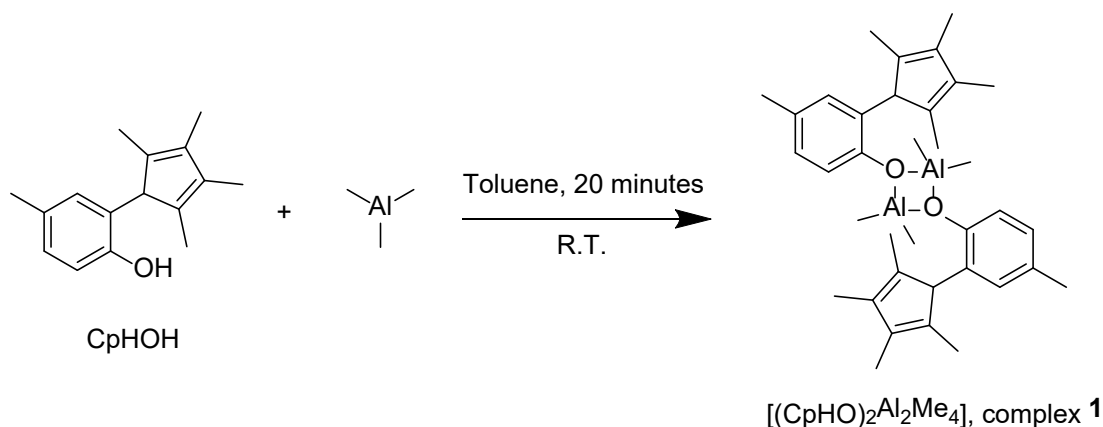


Scheme 2.2: Synthetic route of [CpOTi(CH₂Ph)₂] and [(CpHO)₂Al₂Me₄] (1)

As can be seen from the scheme, complex **1** was synthesized in exactly the same way as [CpOTi(CH₂Ph)₂], but the resultant complex is not a CGC, which became evident via analysis of the NMR and single crystal X-Ray diffraction data (more details in the following section). The ¹H NMR spectrum of **1** still contains the characteristic Cp proton signal around 2.1 ppm, indicating that the cyclopentadiene

ring has not been deprotonated by trimethyl aluminium. X-Ray data revealed that the structure of **1** is actually dimeric; the synthesis of the proposed CGC [(CpO)AlMe] was therefore not as expected. However, since this experimental procedure yielded complex **1** in a rapid and facile manner, it was still used with some minor modifications for an improved synthesis of **1** before pursuing further reactivity studies in the ring-opening co-polymerization (ROCOP) of epoxide/anhydride, epoxide ring-opening polymerization and ϵ -caprolactone ring-opening polymerization.

General synthetic route for [(CpHO)₂Al₂Me₄] (**1**): The synthesis of **1** is executed by directly reacting CpHOH with trimethyl aluminium (TMA) under an argon atmosphere, reaction scheme is shown in Scheme 2.3. One equivalent of CpHOH was dissolved in toluene and stirred until fully dissolved, before 1 equivalent of TMA (in solution) was added dropwise into the mixture. The mixture then allowed to stir and react before volatiles were removed under reduced pressure to afford complex **1** as a cream-coloured powder.



Scheme 2.3: Synthesis of [(CpHO)₂Al₂Me₄] (**1**)

2.3.2. Characterization of [(CpHO)₂Al₂Me₄] (**1**)

Upon obtaining complex **1**, the confusing NMR signal that justified the survival of Cp proton immediately pointed to the fact that the desired CGC has not been successfully made. For structural clarification, single crystals of [(CpHO)₂Al₂Me₄] (**1**)

were grown by cooling a saturated toluene solution to -40°C . Diffraction data were collected by the EPSRC National Crystallography Service hosted by the University of Southampton, and the structure solved by Dr. Benjamin Ward. The molecular structure of complex **1** is illustrated in Figure 2.11, and the principal bond lengths and bond angles are listed in Tables 2.2 and 2.3.

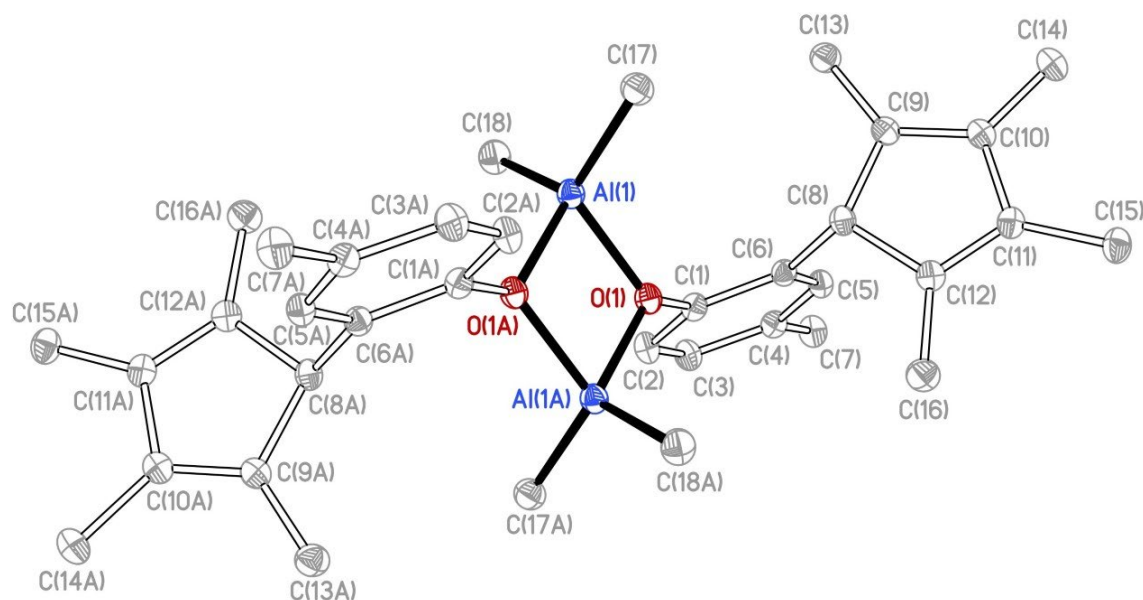


Figure 2.11: Molecular structure of $[(\text{CpHO})_2\text{Al}_2\text{Me}_4]$ (**1**). Ellipsoids drawn at 30% probability and H atoms omitted for clarity

Table 2.2: Principal bond lengths in **1**

Bond	Bond length/Å
Al(1)-O(1A)	1.8630(10)
Al(1)-O(1)	1.8642(10)
Al(1)-C(18)	1.9446(15)
Al(1)-C(17)	1.9509(15)
Al(1)-Al(1A) distance	2.8539(8)
O(1)-Al(1A)	1.8629(10)

Table 2.3: Principal bond angles in **1**

Bond	Bond angle/°
O(1A)-Al(1)-O(1)	80.06(4)
O(1A)-Al(1)-C(18)	114.58(6)
O(1)-Al(1)-C(18)	109.70(6)
O(1A)-Al(1)-C(17)	112.73(6)
O(1)-Al(1)-C(17)	115.22(5)
C(18)-Al(1)-C(17)	118.47(7)
O(1A)-Al(1)-Al(1A)	40.05(3)
O(1)-Al(1)-Al(1A)	40.01(3)
C(18)-Al(1)-Al(1A)	119.46(5)
C(17)-Al(1)-Al(1A)	122.04(5)
C(1)-O(1)-Al(1A)	128.06(8)
C(1)-O(1)-Al(1)	125.83(8)
Al(1A)-O(1)-Al(1)	99.94(4)
C(1)-C(6)-C(8)	123.57(12)
C(6)-C(1)-O(1)	120.19(11)

It is immediately clear upon initial inspection of the structure, that the cyclopentadienyl ring has not been deprotonated, which is evidenced by the tetrahedral carbon atom on the Cp ring and is consistent with the NMR data; and that as a consequence the structure contains a single phenoxide donor. The complex adopts a dimeric structure with the phenoxides bridging two aluminium centres, rather than the anticipated CGC structure. Complex **1** crystallizes in the space group $P2_1/n$. The two aluminium ions in **1** adopts a distorted tetrahedral geometry. An ideal tetrahedron would have a bond angle of 109.5° . In complex **1**, the bond angles around aluminium centres are: 80.06° , 114.58° , 109.70° , 112.73° , 115.22° and 118.47° . These are expected results as the groups around aluminium centres are not equal to each other both in terms of electronic and steric interactions,

thus the tetrahedron around the aluminium centres will not be ideal. According to the Cambridge Structural Database (CSD),²⁸ bond lengths of similar structures (recorded structures that contains Al-O, Al-O bridging and Al-C bonds) were listed below.

Table 2.4: Principal bond lengths and bond angles of similar structures of [(CpHO)₂Al₂Me₄] from CSD

Bond	Min. Length/Å	Max. Length/Å	Average Length/Å
Al-O	1.638	2.736	1.819
Al-O (bridging)	1.638	2.353	1.891
Al-C	1.629	2.458	1.993

In **1**, the bond length Al-O is around 1.86 Å, which is in between the average bond lengths of Al-O and Al-O (bridging), and closer to the Al-O (bridging) value. This is as expected, as the Al-O bonds in **1** serve as bridges. For the Al-C bond, the ~1.95 Å bond length is slightly shorter than the average 1.99 from CSD database, indicating slightly stronger Al-C bonds in **1** comparing to average Al-C in reported crystal structures.

With the crystal structure discussed above, the once-confusing NMR spectra of **1** now become easy to interpret. The ¹H NMR spectrum of complex **1** is shown in Figure 2.12. The NMR sample of **1** was prepared with C₆D₆ due to the existence of metal-Me groups which may react with CDCl₃.

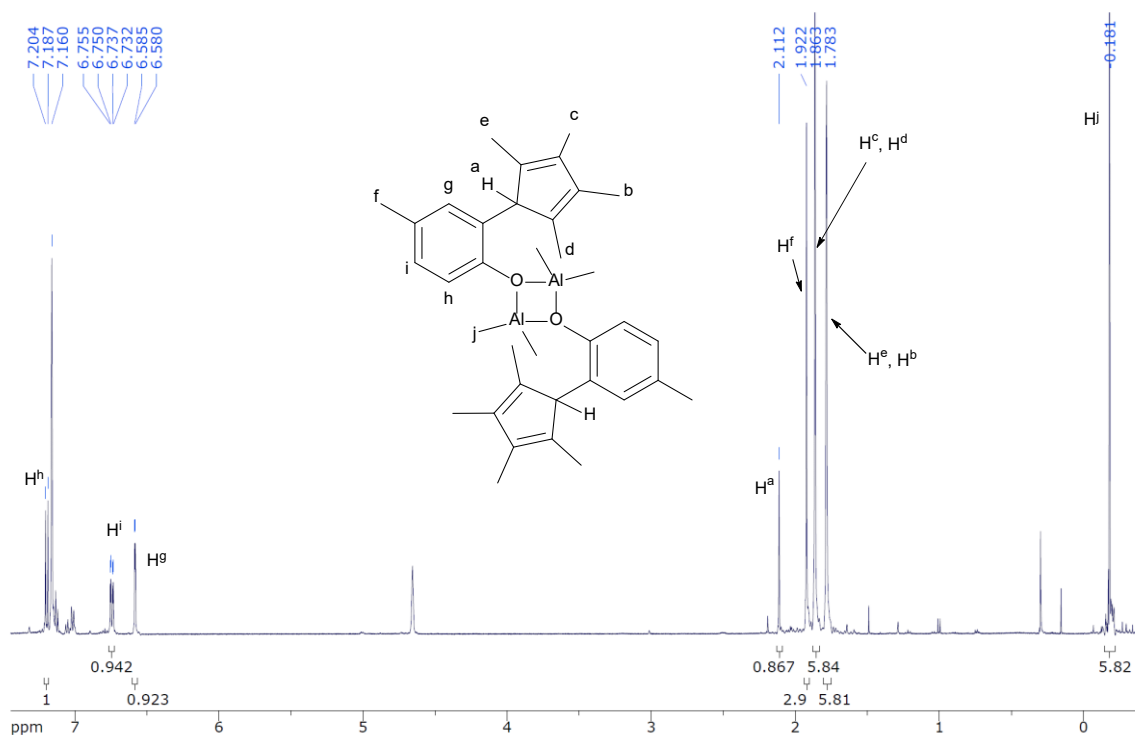


Figure 2.12: ¹H NMR spectrum (500 MHz, C₆D₆, 293 K) of [(CpHO)₂Al₂Me₄] (**1**)

Since the structure of **1** is rotational symmetric, the protons of each half of the dimer should share same chemical environment with their counterpart. The singlet at -0.18 ppm integrates to 12H and is assigned to the Al-Me protons Hⁱ; this chemical shift is comparable to the region where Al-Me signals are typically seen, for examples, Imhoff and co-workers²⁹ reported Al-Me protons at -0.37 ppm, Armitage and co-workers reported Al-Me protons at -0.25 ppm,³⁰ Slaughter *et al.* reported Al-Me protons at -0.47 ppm.³¹ The multiplet at 1.78 ppm integrates to 12H and is assigned to the Cp-Me protons H^e and H^b; this chemical shift is comparable to the region where Cp-Me signals are commonly found, e.g., the original report of CpHOH by Chen *et al.*²⁰ assigned the Cp ring methyl protons to 1.63, 1.48, 1.28 and 1.00 ppm respectively, while in the [(CpO)Ti(CH₂Ph)₂] complex the Cp ring methyl protons were assigned to 1.90 and 1.44 ppm respectively. The multiplet at 1.86 ppm integrates to 12 H and is assigned to Cp-Me protons H^c and H^d; this chemical shift is comparable to the reported Cp-Me proton chemical shifts from Chen *et al.*²⁰ as well, which are 1.90 and 1.44 ppm in Ti complex or 1.63, 1.48, 1.28 and 1.00 ppm

in pro ligand. It is also worth mentioning that although the Cp methyl groups do not share same chemical environment, they are assigned to two singlets in the literature, which is observed in the ^1H spectrum of $[(\text{CpHO})_2\text{Al}_2\text{Me}_4]$ as well. The app. singlet at 1.92 ppm integrates to 6H and is assigned to the phenyl protons H^f ; this chemical shift is in the same region as the original report of Chen *et al.*, in which the phenyl protons are assigned to signal at 2.18 ppm (pro ligand) or 2.11 ppm (Ti complex). The multiplet at 2.11 ppm integrates to 2H and is assigned to H^a , which is the key and fundamental difference between the real structure of $[(\text{CpHO})_2\text{Al}_2\text{Me}_4]$ and what we initially proposed CGC. Chen's report²⁰ of CpHOH assigned the signal at 2.50 ppm to the Cp-H in the pro ligand. Also, the signals with 2H integrations could only be the aromatic protons or Cp-H, but 2.11 ppm is too upfield for aromatic protons. The app. doublet with app. $^4J_{\text{H-H}}=2.5$ Hz at 6.59 ppm integrates to 2H and is assigned to the aromatic proton H^g ; the chemical shift is comparable to Chen's original report's²⁰ aromatic protons at 6.88, 6.78 ppm for pro ligand; the 4-bond coupling with H^i explains the doublet with small coupling constant, which is common for 4-bond coupling between protons. The app. double doublet with app. $^3J_{\text{H-H}}=8.5$ Hz, app. $^4J_{\text{H-H}}=2.5$ Hz at 6.75 ppm integrates to 2H and is assigned to the aromatic proton H^i ; this chemical shift is comparable to the chemical shift of Ar-H in the original report from Chen *et al.*,²⁰ which is at 6.88 and 6.78 ppm. The 3-bond coupling constant 9 Hz due to coupling with H^h is comparable to reported substituted benzene proton coupling constants by Martin *et al.*³² (8.1 to 9.0 Hz); the 4-bond coupling constant 2.5 Hz is comparable to Martin *et al.*'s report³² (2.1 to 3.1 Hz) as well. The app. doublet at 7.204 ppm integrates to 2H and is assigned to aromatic proton H^h ; the chemical shift is comparable to report by Shapiro *et al.*³³ regarding substituted aromatic ring protons (6.8 to 7.4 Hz); the app. coupling constant 8.5 Hz is within the range from report of Martin *et al.*³² as well. The baseline is a little bit noisy probably due to existence of minor impurities or side products. The NMR sample was prepared with crystals which were from the same batch with the X-Ray diffraction crystals, yet impurities still persisted, and multiple times of repetitions cannot eliminate the minor signals. Moreover, the minor signals were at basically

the same chemical shifts and in same patterns, indicating a high chance of existence of aggregated / rearranged complexes in solution. Ideally, the VT-NMR (variable-temperature NMR) and Van't Hoff plot drawn from it would show that the complexes are interchanging, however, as the outbreak of Covid-19 happened, the lab closure prevented experiment from happening. 4-coordinate aluminium is common for alkyl, but alkoxides tend to be 5- or 6-coordinate for aluminium with two alkoxide ligands. Therefore, redistribution of ligand in solution is possible, although the signals from redistribution is against the NMR characterization. In BDW group, an example of 5-coordinate complex $[Al_2(Salpy)_2Me_2]$ (structure in Figure 2.13) has seen this situation, which means redistribution of ligands for a 4-coordinate complex like **1** is possible. The aggregation of complex has also been seen for $[(AQMe)_2AlCl]$ (**4**), which is discussed in section 6.2.3.

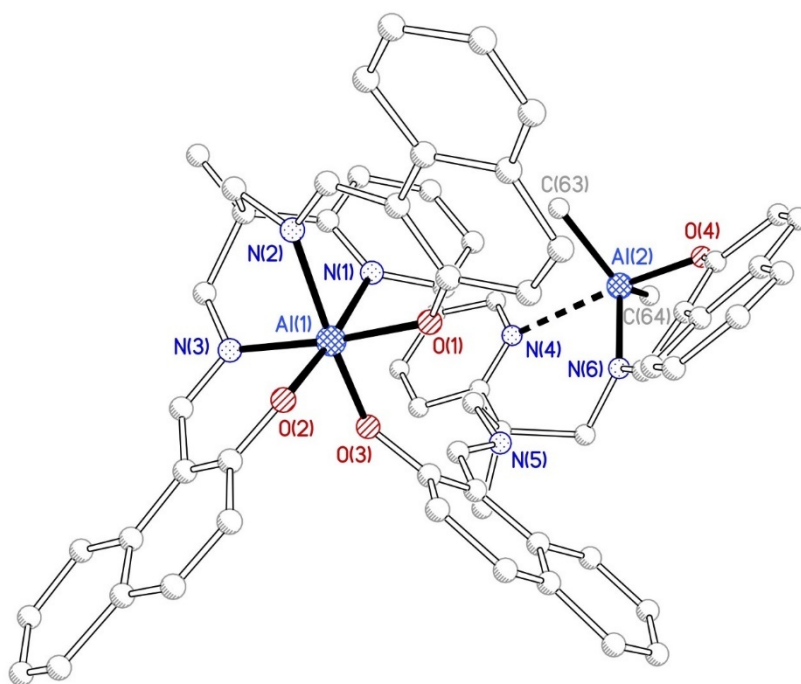


Figure 2.13: Structure of $[Al_2(Salpy)_2Me_2]$

The hydrogen on the Cp ring of CpHOH ligand remains and is not absent (as expected for a deprotonated Cp ring), which was demonstrated by the resonance at chemical shift ~ 2.11 ppm, indicating the existence of it and the failed deprotonation of Cp ring by trimethyl aluminium. Without the deprotonation, the Cp ring is not bonded to the central metal ion as an η^5 ligand moiety, thus formation of

CGC is impossible. Other than the 2.11 ppm signal for Cp-H, the general pattern of proton NMR for **1** closely resembles the complex [(CpO)Ti(CH₂Ph)₂]; and if taking Cp-H into account, closely resembles the pro ligand CpHOH from Chen and co-workers' report.²⁵

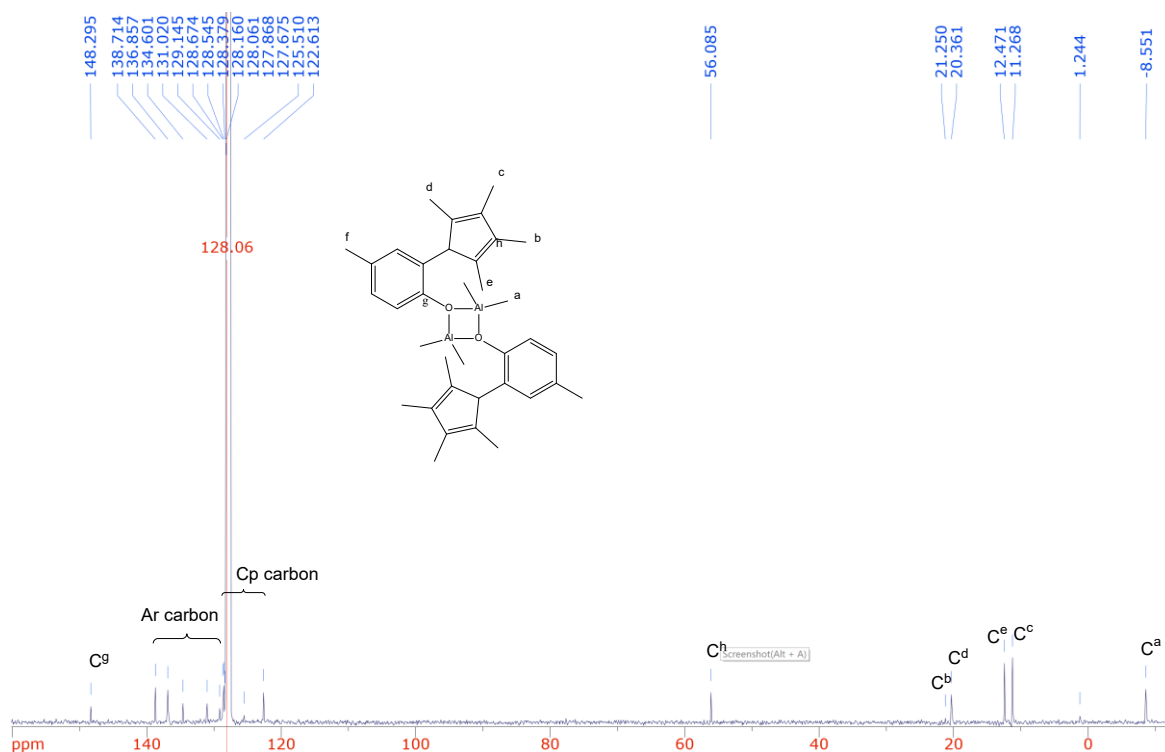
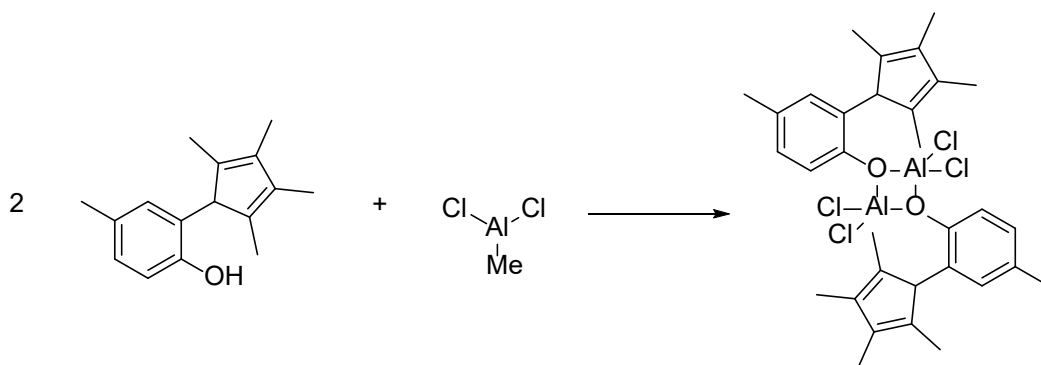


Figure 2.14: ¹³C NMR spectrum (125MHz, C₆D₆, 293 K) of [(CpHO)₂Al₂Me₄] (**1**)

Similar to ¹H spectrum, the rotational symmetric structure of **1** makes the carbons of each half of the dimer share same chemical environment with their counterpart. The signal at -8.6 ppm is assigned to aluminium-methyl carbons C^a; this chemical shift is comparable to the typical Al-Me values from the paper by Tritto *et al.*³⁴, which is -8.0 ppm. The signal pairs at 11.3/12.5 ppm and 20.4/21.3 ppm are assigned to Cp-methyl carbons C^c/C^e and C^d/C^b respectively; these two pairs of chemical shifts are comparable to the original report of CpHOH from Chen *et al.*,²⁰ which assigned 21.0/20.5 ppm and 12.3/9.7 ppm signal pairs to Cp-methyl carbons. Since there is no symmetry for the Cp ring, the Cp-methyls should have 4 different signals, which is in agreement with the spectrum obtained. The signal at 56.1 ppm is assigned to C^h on Cp ring; and the chemical shift is comparable to Chen *et al.*'s original CpHOH

report²⁰ at 51.40 ppm. Signals at 122.6, 125.5, 128.2 and 128.4 ppm are assigned to be the Cp carbons; which are comparable to the range from Chen *et al.*'s report, ranging from 123.0 to 114.0 ppm. The most downfield signal at 148.3 is assigned to aromatic carbon C⁹; this chemical shift is comparable to original report of CpHOH at 157.11 ppm. The signals at 138.7, 136.9, 134.6, 131.0 and 129.1 ppm are assigned to the rest aromatic carbons; these chemical shifts are comparable to the original report, ranging from 138.6 to 125.4 ppm. Similar to the Cp ring, no symmetry for aromatic ring means all six aromatic carbons should have different signals. Generally, the ¹³C NMR pattern of [(CpHO)₂Al₂Me₄] resembles that of the pro-ligand, except the existence of Al-Me signals.

Attempts to make the chloride version of complex **1**, which is [(CpHO)₂Al₂Cl₄] (essentially the analogue of complex **1** with all methyl groups swapped with chloride), has been made, as shown in Scheme 2.4. 2 equivalents of CpHOH was reacted with 1 equivalent of AlMeCl₂, other conditions were kept the same as synthesis of complex **1**.



Scheme 2.4: Proposed synthetic route of [(CpHO)₂Al₂Cl₄]

All reaction conditions being the same as the synthetic route of (TCP)₂Al₂Me₄. The resulting product appears to be a purple powder, different from the cream-coloured complex **1**, indicating existence of different compound. However, despite the vastly different colour, NMR spectrum of the product is quite messy, with non-identifiable peaks over the whole spectrum, as illustrated in Figure 2.15.

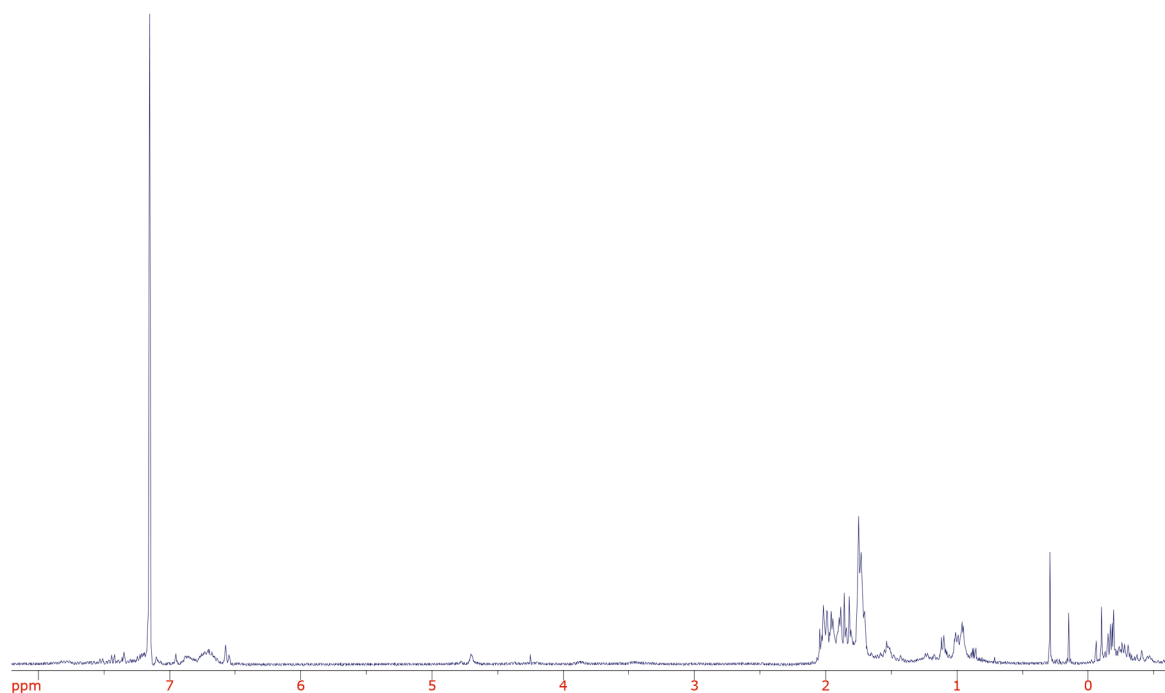


Figure 2.15: ^1H spectrum (400 MHz, C_6D_6 , 293 K) of $[(\text{CpHO})_2\text{Al}_2\text{Cl}_4]$

Subsequent attempts of repeating reaction and recrystallization of the product did not succeed either, without reliable evidence about its structure, the idea of synthesizing $[(\text{CpHO})_2\text{Al}_2\text{Cl}_4]$ and utilizing it as a catalyst cannot proceed further.

The fact **1** is not a CGC may makes it much easier for monomers to approach due to less steric hinderance since no actual bond exists between central metal sites and the Cp rings. Also, the dimeric structure of **1** opens up the possibilities for bimetallic mechanisms for polymerization reactions. Thus, despite not meeting our initial goal of making aluminium-CGC, **1** may still be capable of catalyzing some polymerization reactions. The catalytic performance of **1** for epoxide/anhydride ROCOP, epoxide polymerization and ϵ -caprolactone polymerization were therefore investigated and reported in the following chapters.

2.4. References

- 1 Palladium Outlook 2021 | INN, <https://investingnews.com/daily/resource-investing/precious-metals-investing/palladium-investing/palladium-outlook/>, (accessed 9 February 2021).
- 2 RHODIUM | 2012-2021 Data | 2022-2023 Forecast | Price | Quote | Chart | Historical, <https://tradingeconomics.com/commodity/rhodium>, (accessed 9 February 2021).
- 3 Platinum Price, https://ycharts.com/indicators/platinum_price, (accessed 9 February 2021).
- 4 Aluminum Price, https://ycharts.com/indicators/aluminum_price, (accessed 10 February 2021).
- 5 Live Platinum Price Charts | Platinum Price Per Ounce, <https://www.apmex.com/platinum-price>, (accessed 23 March 2021).
- 6 Live USD Palladium Price Charts & Historical Data, <https://www.apmex.com/palladium-price>, (accessed 23 March 2021).
- 7 Rhodium Spot Prices Per Ounce Today, Live Bullion Price Chart USD, <https://www.moneymetals.com/precious-metals-charts/rhodium-price>, (accessed 19 February 2021).
- 8 W. F. McDonough, in *The composition of the Earth*, Harvard University.
- 9 Cardarelli and François, in *Materials handbook: a concise desktop reference (2nd ed.)*, London: Springer, 2008.
- 10 L. Negureanu, R. W. Hall, L. G. Butler and L. A. Simeral, *J. Am. Chem. Soc.*, 2006, **128**, 16816–16826.

- 11 L. Resconi, S. Bossi and L. Abis, *Macromolecules*, 1990, **23**, 4489–4491.
- 12 Y. Rios Yepes, C. Quintero, D. Osorio Meléndez, C. G. Daniliuc, J. Martínez and R. S. Rojas, *Organometallics*, 2019, **38**, 469–478.
- 13 D. Osorio Meléndez, J. A. Castro-Osma, A. Lara-Sánchez, R. S. Rojas and A. Otero, *J. Polym. Sci. Part A: Polym. Chem.*, 2017, **55**, 2397–2407.
- 14 N. Nomura, R. Ishii, Y. Yamamoto and T. Kondo, *Chem. Eur. J.*, 2007, **13**, 4433–4451.
- 15 A. Kowalski, A. Duda and S. Penczek, *Macromolecules*, 1998, **31**, 2114–2122.
- 16 P. Hormnirun, E. L. Marshall, V. C. Gibson, A. J. P. White and D. J. Williams, *J. Am. Chem. Soc.*, 2004, **126**, 2688–2689.
- 17 R.-C. Yu, C.-H. Hung, J.-H. Huang, H.-Y. Lee and J.-T. Chen, *Inorg. Chem.*, 2002, **41**, 6450–6455.
- 18 S. Paul, Y. Zhu, C. Romain, R. Brooks, P. K. Saini and C. K. Williams, *Chem. Commun.*, 2015, **51**, 6459–6479.
- 19 D. J. Darensbourg, R. R. Poland and C. Escobedo, *Macromolecules*, 2012, **45**, 2242–2248.
- 20 Y.-X. Chen, P.-F. Fu, C. L. Stern and T. J. Marks, *Organometallics*, 1997, **16**, 5958–5963.
- 21 P. J. Shapiro, E. Bunel, W. P. Schaefer and J. E. Bercaw, *Organometallics*, 1990, **9**, 867–869.
- 22 B. Wang, *Coordination Chemistry Reviews*, 2006, **250**, 242–258.
- 23 J. Klosin, P. P. Fontaine and R. Figueroa, *Acc. Chem. Res.*, 2015, **48**, 2004–2016.

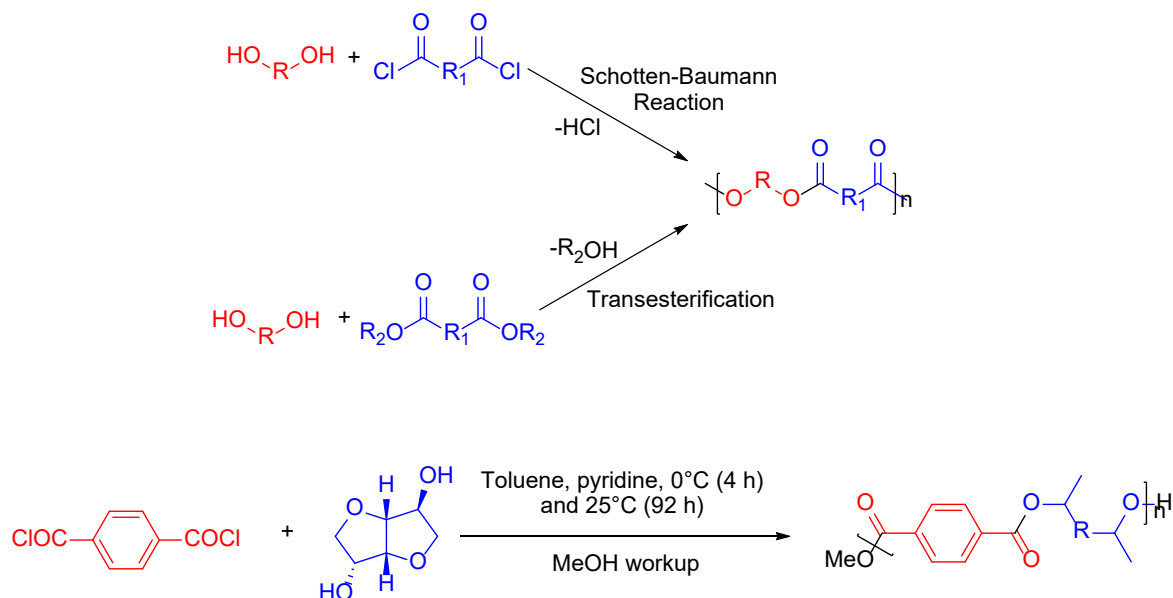
- 24 Y. Liang, G. P. A. Yap, A. L. Rheingold and K. H. Theopold, *Organometallics*, 1996, **15**, 5284–5286.
- 25 Y.-X. Chen, P.-F. Fu, C. L. Stern and T. J. Marks, *Organometallics*, 1997, **16**, 5958–5963.
- 26 A. M. Seyam, B. D. Stubbert, T. R. Jensen, J. J. O'Donnell, C. L. Stern and T. J. Marks, *Inorganica Chimica Acta*, 2004, **357**, 4029–4035.
- 27 Y.-X. Chen, P.-F. Fu, C. L. Stern and T. J. Marks, 6.
- 28 C. R. Groom, I. J. Bruno, M. P. Lightfoot and S. C. Ward, *Acta Crystallogr B Struct Sci Cryst Eng Mater*, 2016, **72**, 171–179.
- 29 D. W. Imhoff, L. S. Simeral, S. A. Sangokoya and J. H. Peel, *Organometallics*, 1998, **17**, 1941–1945.
- 30 A. Armitage, O. Boyron, Y. Champouret, M. Patel, K. Singh and G. Solan, *Catalysts*, 2015, **5**, 1425–1444.
- 31 J. Slaughter, A. J. Peel and A. E. H. Wheatley, *Chem. Eur. J.*, 2017, **23**, 167–175.
- 32 J. Martin and B. P. Dailey, *The Journal of Chemical Physics*, 1962, **37**, 2594–2602.
- 33 B. L. Shapiro and L. E. Mohrmann, *Journal of Physical and Chemical Reference Data*, 1977, **6**, 919–992.
- 34 I. Tritto, M. C. Sacchi, P. Locatelli and S. X. Li, *Macromol. Chem. Phys.*, 1996, **197**, 1537–1544.

Chapter 3: Catalytic performance of $[(\text{CpHO})_2\text{Al}_2\text{Me}_4]$ for ROCOP of epoxides / anhydrides

To verify the viability of $[(\text{CpHO})_2\text{Al}_2\text{Me}_4]$ (**1**) to act as a ring-opening co-polymerization (ROCO) catalyst, a series of epoxide/anhydride ROCOP reactions were performed. The data thereby acquired suggests that complex **1** is a viable catalyst for the ROCOP of epoxides and cyclic anhydrides.

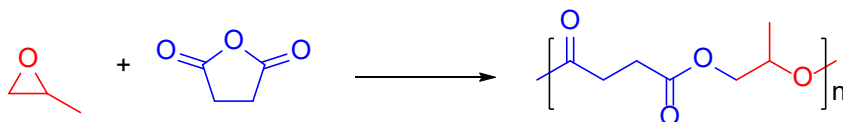
3.1. Introduction

In modern synthetic polymer industries, condensation polymerization is widely used for the synthesis of polyesters, invariably in the co-polymerization of diesters or diacids with diols.¹ By far, polyester is the most extensively used fibre.² With a global production of 57.7 million tonnes in 2019, polyesters comprise about 52% of global fibre production.² In contrary to their vast, simple applications, polyesters made from condensation polymerization usually require high temperature and reaction times, leading to energy consumption problems. Condensation polymerization is a step-growth polymerization process during which any monomer / reactive growing chain have both of their ends available for polymerization (examples in Scheme 3.1^{3,4}), thus condensation polymerization usually yields polymers with relatively uncontrolled, broad molecular weight distribution.¹ Also, to produce high molecular weight polyesters, the by-product that naturally comes with condensation polymerization need to be removed from the reaction to maintain a high degree of monomer purity, which again causes complications for industrial applications.³



Scheme 3.1: Examples of step-growth condensation polymerization

Condensation polymerization is not the only way through which polyesters can be made, another method is the ring-opening co-polymerization (ROCOP) between epoxides and anhydrides (ROP of cyclic esters like ϵ -CL and ROCOP of epoxide / CO_2 are also very popular for polyester production; the former was discussed in Chapter 5). As a chain-growth polymerization reaction, each growing chain in the ROCOP process has only one reactive site, which will react with one monomer to expand the polymer chain, a single monomer at a time. Compared to the step-growth method, with suitable catalysts and co-catalysts, chain-growth polymerization can easily achieve higher molecular weight polymers, with a high degree of control over the molecular weight distribution.³ In recent years, there has been significant development of catalysts that allow precise control over the tacticity of resultant polymer, e.g., the relative stereochemistry of the synthetic polymer can be controlled.^{4,5} Thus in recent years, chain-growth polymerization has attracted much research interest. An example of chain-growth polymerization between propylene oxide (PO) and succinic anhydride (SA)^{4,6,7} is demonstrated in Scheme 3.2.



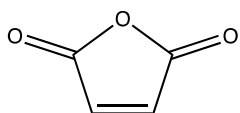
Scheme 3.2: Chain-growth polymerization via the ring-opening co-polymerization of epoxides and anhydrides

3.2. Epoxide / anhydride monomers and co-catalysts for ring-opening co-polymerization with $[(\text{CpHO})_2\text{Al}_2\text{Me}_4]$

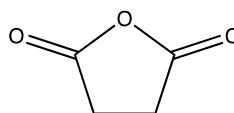
(1)

One of the advantages of ring-opening co-polymerization (ROCOP) is the ease of property tuning, via the incorporation of different monomers;^{8,9} the large number of monomers available means the properties of the resulting polymer (polyester in this case) can be easily tuned to match specific applications, such as the degree of hydrophilicity, inclusion of interconnecting functional groups, etc. For the ROCOP catalyzed by **1**, small molecule, liquid (at room temperature) epoxides and cyclic anhydrides were used as monomers. The anhydride and epoxide monomers used are listed in Table 3.1 and Table 3.2 below.

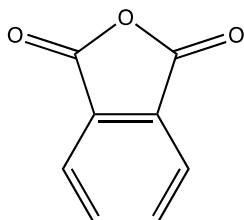
Table 3.1: Anhydride monomers



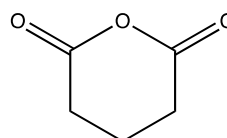
Maleic anhydride (MA)



Succinic anhydride (SA)

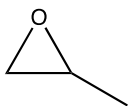


Phthalic anhydride (PA)

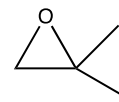


Glutaric anhydride (GA)

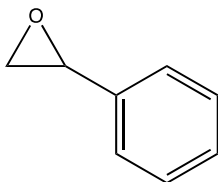
Table 3.2: Epoxide monomers



Propylene oxide (PO)



Isobutylene oxide (IO)



Styrene oxide (SO)



Cyclohexene oxide (CHO)

MA, SA, GA and PA are in the sequence of increasing steric bulkiness to check how the anhydride monomers' steric sizes would affect the ROCOP outcome. As a monomer, succinic anhydride usually gives flexible co-polymers with low glass transition temperatures.^{10,11} The CH₂ backbone also causes co-polymers of SA to be highly hydrophobic. Moreover, comparing to succinic anhydride, the existence of unsaturated bond on MA makes it possible for further post-functionalization via C=C double bond oxidation, thus enabling more property adjustments and application directions. For example, double bonds enable cross-linking with bisazides as cross-linkers¹² (Figure 3.1); functionalization by thiol-ene click reactions¹³ (Figure 3.2) and many more.

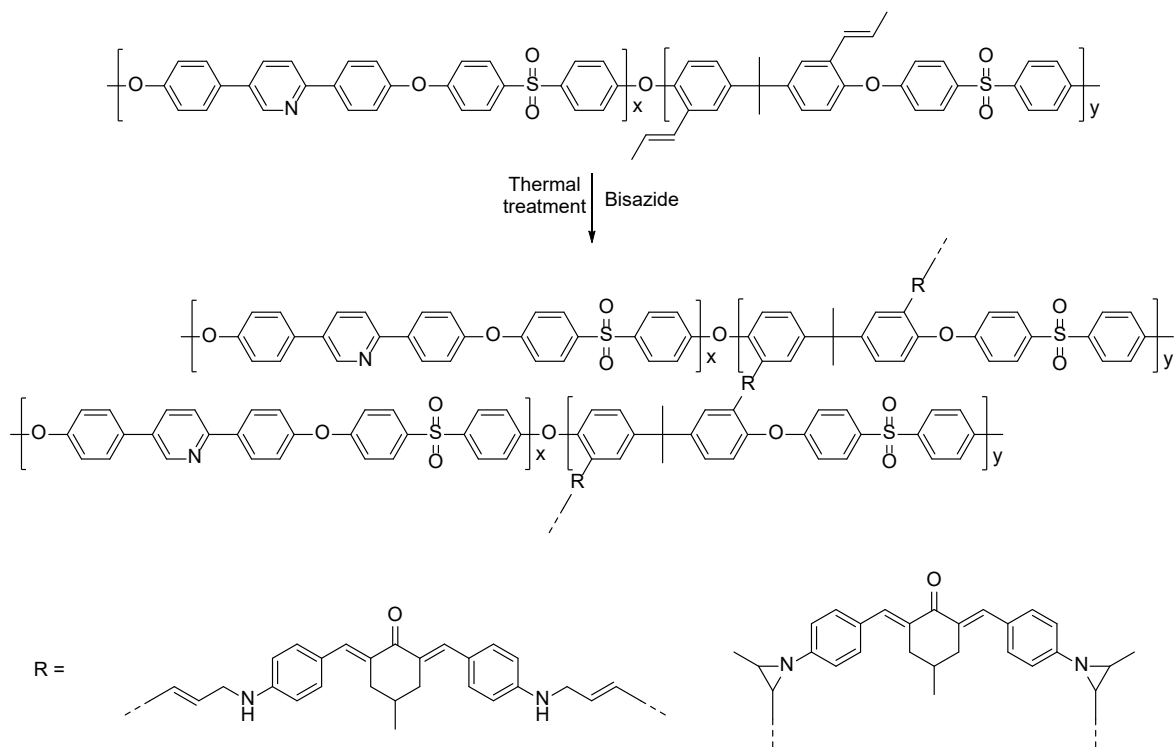


Figure 3.1: Unsaturated polymer crosslinking using bisazides as cross-linkers¹²

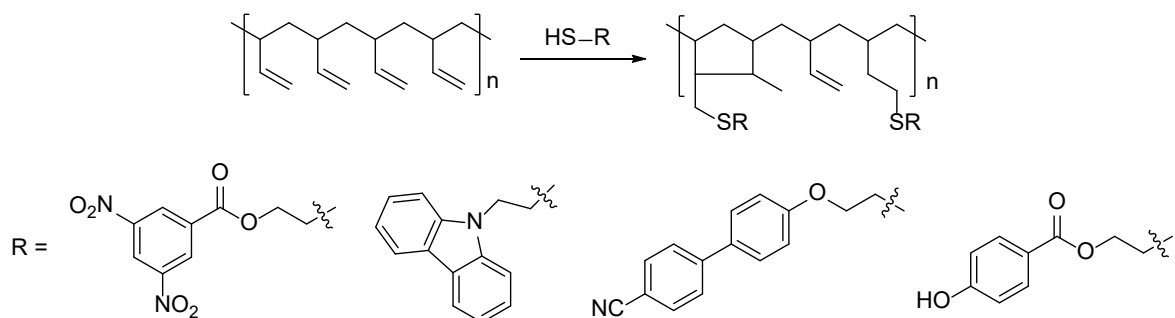


Figure 3.2: Thiol-ene functionalization of unsaturated polymer¹³

Post-functionalization brings the possibilities of fine-tuning of properties^{12,14} (mechanical properties, thermal properties, optical properties, etc.) beyond the choice of monomers, which again expands the scope of applications of these polymers.

Compared to SA, how the electronic environment changes on including the double bond of MA would affect the ROCOP reaction and the resultant polymer properties, can also be investigated. Also, as the ROCOP involves ring-opening of both the hetero rings on anhydride and epoxide, the release of ring strain will be one of the

thermodynamic driving forces for the reaction. By including GA, which has a 6-membered ring, the contrast between 5-membered ring and 6-membered rings in ROCOP can be illustrated. Since 6-membered rings have less ring strain, the ring-opening process is naturally less thermodynamically favoured than the 5-membered ring, thus using 6-membered ring anhydride as a substrate for ROCOP will pose a bigger challenge for the catalysts. Nevertheless, the inclusion of more challenging monomers is still essential for pushing the monomer scope for ROCOP. Even if the experiment failed, the data should still provide important insight for future catalyst development. Phthalic anhydride, on the other hand, serves as a great handle for ^1H NMR analysis. Its aromatic protons have signals near 8.0 ppm, the polymerized PA protons can be easily distinguished from the monomer PA protons, and they are not overlapping with other signals. Thus, PA working as a more reliable integration calibrant than any other anhydride monomer. Other previous works in BDW group have proved the effectiveness of PA, to the extent that PA has become the standard anhydride for preliminary testing and catalyst optimization.

PO, IO, CHO and SO were selected for comparisons between monomers with different steric bulkiness, as discussed for anhydride monomers. CHO, as a common, standard monomer for ROCOP, is known for its reliability, and is included in the tests as a calibrant. CHO usually affords polymers with high glass transition temperatures. PO usually give copolymers with lower glass transition temperature compared to other epoxides; SO is more sterically demanding than all other epoxide monomers, thus a challenging substrate for ROCOP, and is included in the comparison based on the same reason as GA as discussed before.

The co-catalysts used for ROCOP with complex **1** are bis(triphenylphosphine)iminium chloride (PPNCI) and benzyl alcohol (BnOH), with structures illustrated as below.

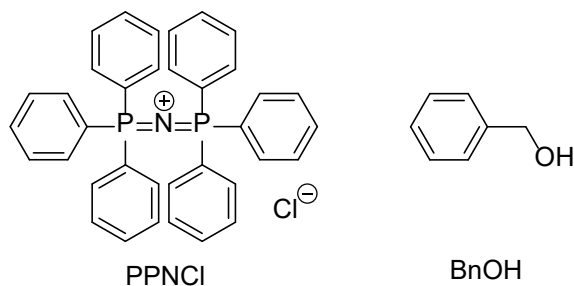


Figure 3.3: Structures of PPNCI and BnOH

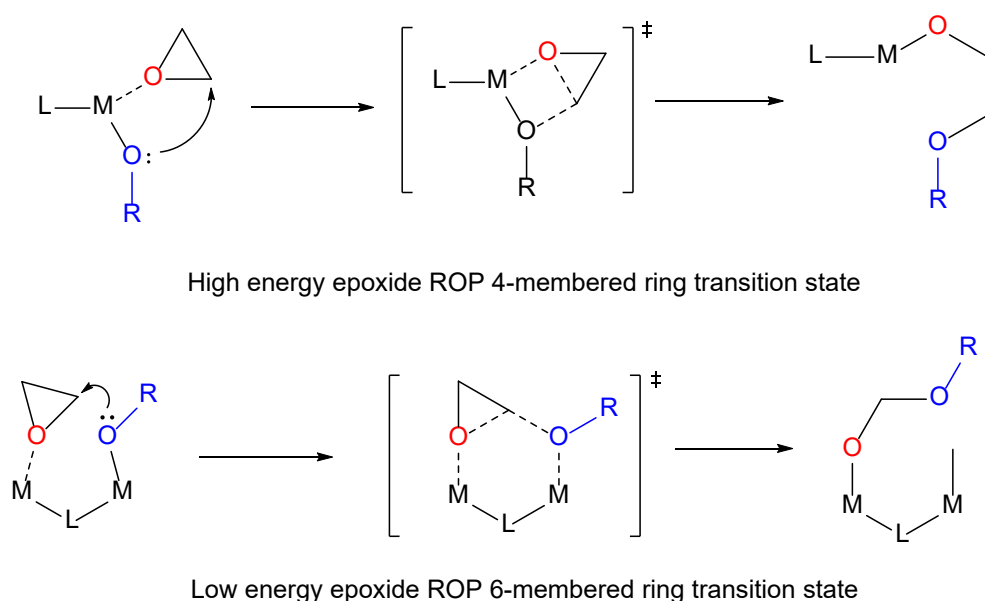
Co-catalysts usually serve as initiators which facilitate the formation of an alkoxide via nucleophilic attack on the first epoxide monomer. In the case of PPNCI, the subsequent propagation of polymer chains is also assisted by the PPN^+ ions which form ion pairs with carboxylate to de-coordinate, a necessary step in the catalytic cycle.¹⁵ On the other hand, BnOH forms metal alkoxide with metal complexes thus initiating the polymerization reaction. Due to this fundamental difference, these two co-catalysts were used to investigate the differences they would bring to the ROCOP reactions.

3.3. General procedure for ROCOP of epoxides and anhydrides

In glove box, $[(\text{CpHO})_2\text{Al}_2\text{Me}_4]$ (**1**) (10 mg, 1.76×10^{-5} mol) and co-catalyst (PPNCI or BnOH) were added into an oven-dried screw-cap vial. Anhydride (200 equivalents to aluminium central ions, 400 equivalents to complex **1** as **1** is bimetallic) was then added into the vial, followed by the addition of epoxide (200 equivalents to aluminium central ions, 400 equivalents to **1**). The vial was then sealed, taken out of the glove box and transferred onto a pre-heated aluminium heating block that has been adjusted to the desire temperature. The reaction mixture then stirred under designated temperature for a certain time. Upon finishing, methanol was injected into the reaction mixture to quench the reaction. A small aliquot of reaction mixture was taken and dissolved in deuterated chloroform for NMR purposes. The remaining reaction mixture was then washed into a beaker with methanol. Methanol was then

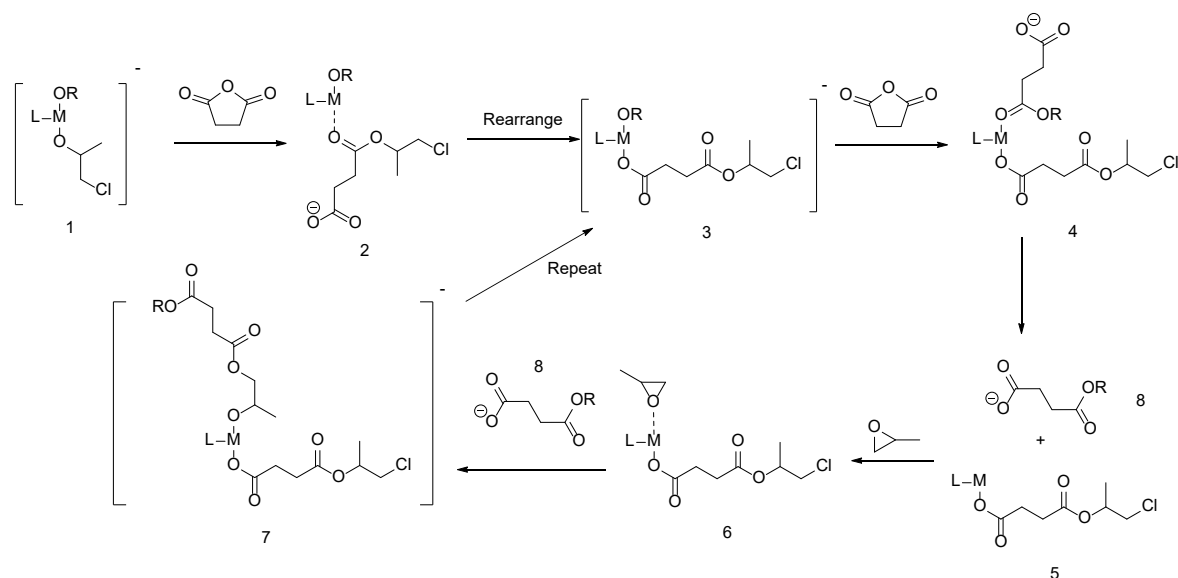
added into the beaker to precipitate the polymer. The mixture was stirred and followed by gravitational filtration to isolate the precipitated polymer. Wet polymer sample was air-dried and dried under reduced pressure until it appeared to be a free-flowing powder.

With different combinations of monomers, various reaction conditions (temperature, reaction time, solvent) and inclusion / exclusion of co-catalysts, a series of ROCOP tests were undertaken with **1**. In most cases, the catalyzed ROCOP of epoxide/anhydride is in competition with the homopolymerization (ROP) of the epoxide monomer. This competition decides the selectivity of the resultant polymer. The energy of the transition states are different and largely depend on the nature of the catalyst. Normally, ROCOP has lower activation energy since the epoxide ROP requires alkoxide intermediates to form a 4-membered transition state which is high in energy (unless a bimetallic mechanism can be followed), and alkoxides do not de-coordinate from the metal site during the catalytic cycle, which means a high energy intramolecular attack is needed. This also means if the catalyst provides a possible lower energy transition state (such as bimetallic mechanism in Scheme 3.3), the epoxide ROP will be more kinetically favoured, thus resulting in lower selectivity (Scheme 3.3).



Scheme 3.3: High and low energy transition states for epoxide ROP¹⁶

On the contrary, ROCOP involves de-coordination of carboxylate which is lower in energy (4 to 7 in Scheme 3.4, where the alkoxide de-coordinate from the metal site first then attack on the coordinated epoxide) due to the delocalization of charges that facilitates external attack of epoxide. This difference in activation energy determines the selectivity in the way of kinetic control (Scheme 3.4).



Scheme 3.4: Epoxide / anhydride ROCOP mechanism

For an ideal ROCOP-targeted catalyst, the transition state energy for ROCOP should be lower than the transition state energy of epoxide ROP. By Boltzmann distribution, higher temperature will lead to increased ratio of particles beyond a certain energy threshold. Therefore, increasing the temperature usually causes a decrease in selectivity as more epoxide monomers will have sufficient energy to cross the energy barrier for epoxide ROP. Another factor comes into play for selectivity is the co-catalysts. Co-catalysts alter the reaction mechanisms, hence change the transition state energy which ultimately causes the change of selectivity. Since co-catalyst plays a vital role in the initiation and propagation steps, increasing the amount of co-catalyst will theoretically increase the number of activated polymer chains (by chloride in PPNCI), thus resulting in lower M_n . The number of activated chains should be equal to the number of chlorides in the reaction mixture. But since **1** does not contain any chloride itself, the number of activated chains should be the

same as the number of PPNCI (thus chloride from it) in the reaction. To check how the catalytic performance of complex **1** is affected by different amount of co-catalyst, co-catalyst has been used in 0, 1 or 2 equivalents. From several literature reports in the ROCOP/ROP field, it can be seen that metal complexes with planar ligands tend to be good catalysts for the epoxide homopolymerization,^{16–19} thus may not be ideal catalysts for ROCOP, as the transition state energy for epoxide ROP is too low for that of ROCOP to actually compete with (although some planar ligand systems have proven themselves to be capable of catalyzing the ROCOP, non-planar ligand systems could still be better in terms of selectivity control as they intrinsically disfavour epoxide ROP). And as can be spotted from the experimental results, this hypothesis proved to be correct. Figure 3.4 is an example of sample (Entry 3, Table 3.3) with high ester selectivity. Due to the structural differences (thus chemical environment differences) between polyester and polyether, the proton signals of polymerised PO are different in polyester and polyether. Polyether PO signals should be about the same as the pure polyether signals obtained from PO homopolymerization, as they are in comparable chemical environments. As we can see from the ¹H NMR spectrum, the resultant solution of Entry 3 has very obvious peaks for CH and CH₂ protons of PO in polyester (integration 1 and 2.01 respectively), while CH and CH₂ protons of PO in polyether are very weak (integration 0.291). As we are integrating the signals of the proton that at the similar positions on the monomer, the ratio of the integration values of polyester and polyether protons therefore represents the relative ratios of polyester and polyether in the resultant polymer. Selectivity is defined by the percentage of polyester in the resultant polymer. Thus selectivity = (1 + 2.01) / (1 + 2.01 + 0.291) = 91.18% ≈ 91%. 91% selectivity makes a selective alternating copolymer.

Selectivity is calculated by the formula:

$$\text{Selectivity} = \frac{[\text{integration of chosen proton peak of epoxide units in polyester}]}{[\text{sum of integrations of chosen proton peaks of epoxide units in both polyester and polyether region}]}$$

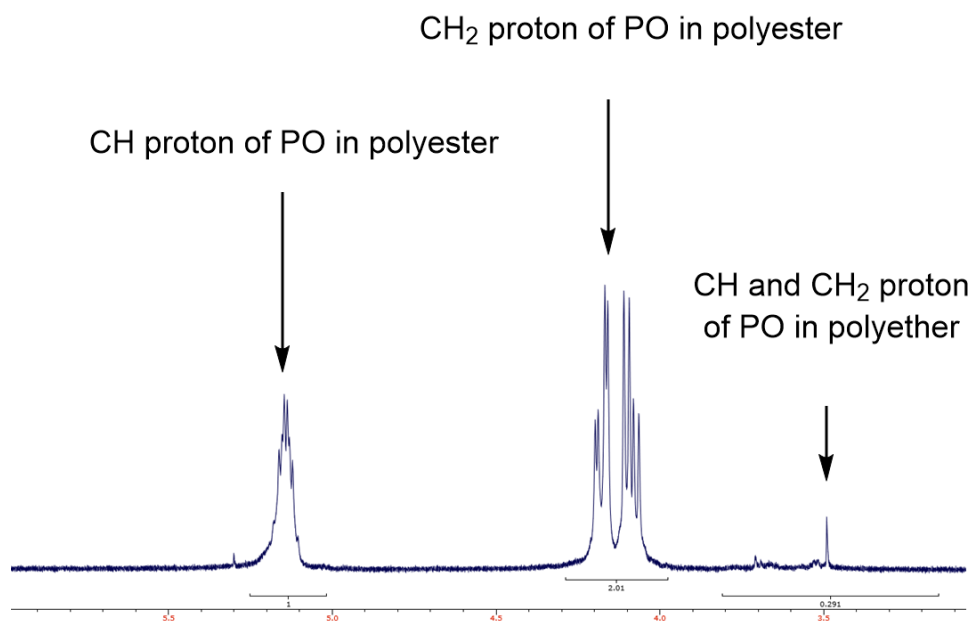


Figure 3.4: Part of ¹H NMR spectrum (400 MHz, CDCl₃, 293 K) of Entry 3 (SA / PO, Table 3.3)

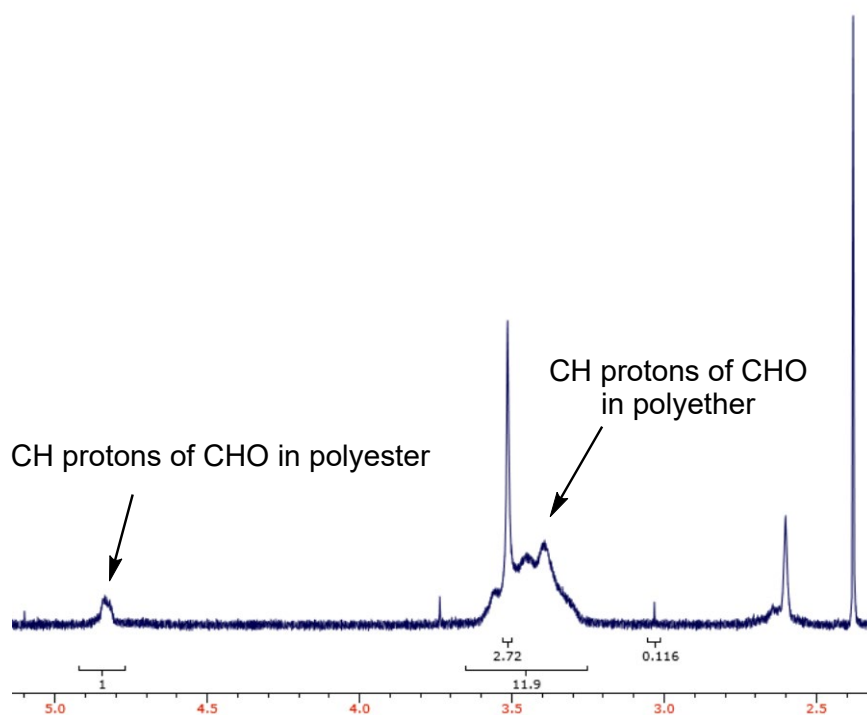


Figure 3.5: Part of ¹H NMR spectrum (400 MHz, CDCl₃, 293 K) of Entry 6 (SA / CHO, Table 3.3)

The ^1H NMR spectrum in Figure 3.5, however, is an example of low ester selectivity. The signal for ester CH protons of CHO is rather small compared to the one for ether CH protons. One thing worth noticing is the prominent sharp peak with integration 2.72 within the polyether range. After checking all the proton chemical shifts for all the chemical identities in the mixture, there is no other signal in this range, so the 11.9 integration for polyether is considered to be real. A previously reported NMR spectrum states that poly-CHO gives proton signals in this range, consistent with the spectrum in Figure 3.5.²⁰

It is also critical to monitor the conversion. For neat ROCOP reactions (much faster compared to reactions in solvents such as toluene) which use excess epoxide as solvent as well as substrate, running the reaction for too long will inevitably lead to full depletion of anhydride monomer, and the catalyst will start to catalyze the ROP of epoxide. This will lead to formation of polyether that decreases the selectivity. Thus for neat reactions, quenching the reaction as close as possible to 100% conversion is critical for selectivity control. In this chapter, all reactions were undertaken with organic solvent, while in Chapter 6 most of the reactions were conducted neat.

Conversion is calculated by the formula:

$$\text{Conversion} = \frac{[\text{integration of chosen proton peak of epoxide unit in polyester}]}{[\text{sum of integrations of chosen proton peaks in epoxide monomers, polyester and polyether}]}$$

An example of ^1H spectrum used for conversion calculation is as below.

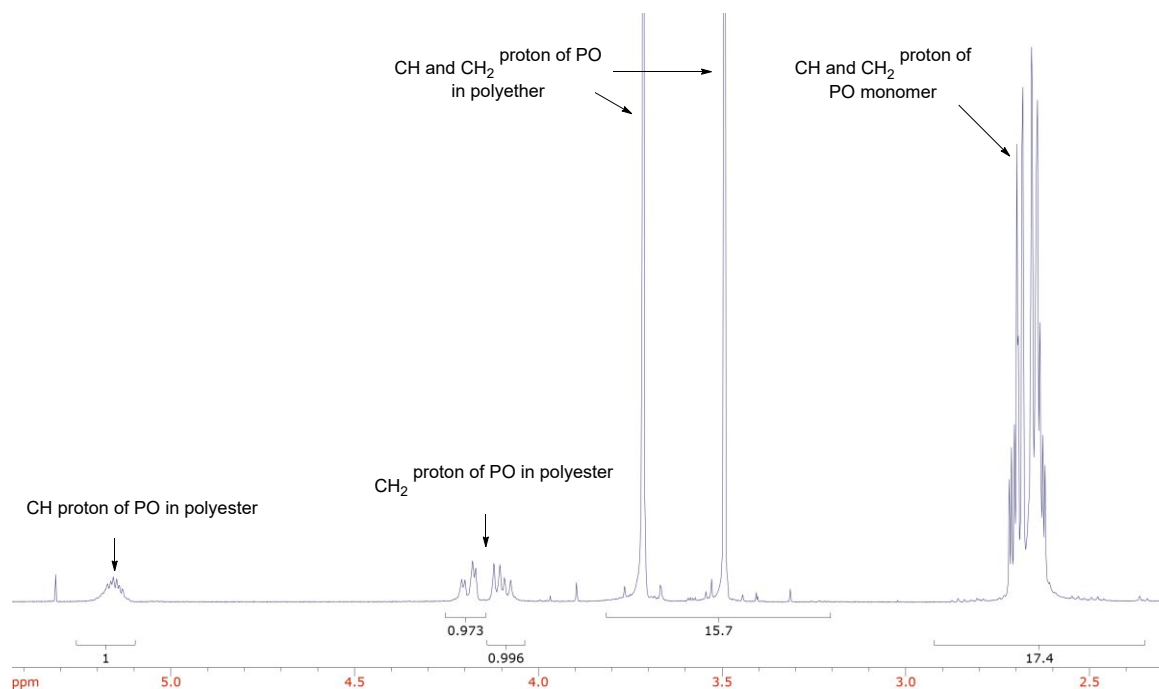


Figure 3.6: Part of ¹H NMR spectrum (400 MHz, CDCl₃, 293 K) of Entry 9 (SA / PO, Table 3.3)

This ¹H NMR spectrum (Figure 3.6) is a perfect example where all three different type of PO unit can be seen (PO in polyester, PO in polyether, unreacted PO monomer). According to the conversion formula, we can calculate the conversion to be: $\text{conversion} = (1 + 0.973 + 0.996 + 15.7) / (1 + 0.973 + 0.996 + 15.7 + 17.4) = 51.76\% \approx 52\%$. This spectrum illustrates that at 70°C, the reaction is rather slow, gives only 52% conversion at 72 hours. Also, as we can easily see from the spectrum, the epoxide homopolymerization is highly favoured over co-polymerization.

When phthalic anhydride (PA) is used as the anhydride monomer, the conversion is much easier to determine, since the anhydride signals in the monomer and polymer are easily distinguishable. The conversion can therefore be calculated by:

$$\text{Conversion} = \frac{[\text{integration of PA aromatic protons in copolymer}]}{[\text{sum of integration of PA aromatic protons in copolymer and monomer}]}$$

An example of ¹H spectrum used for PA conversion calculation is as below.

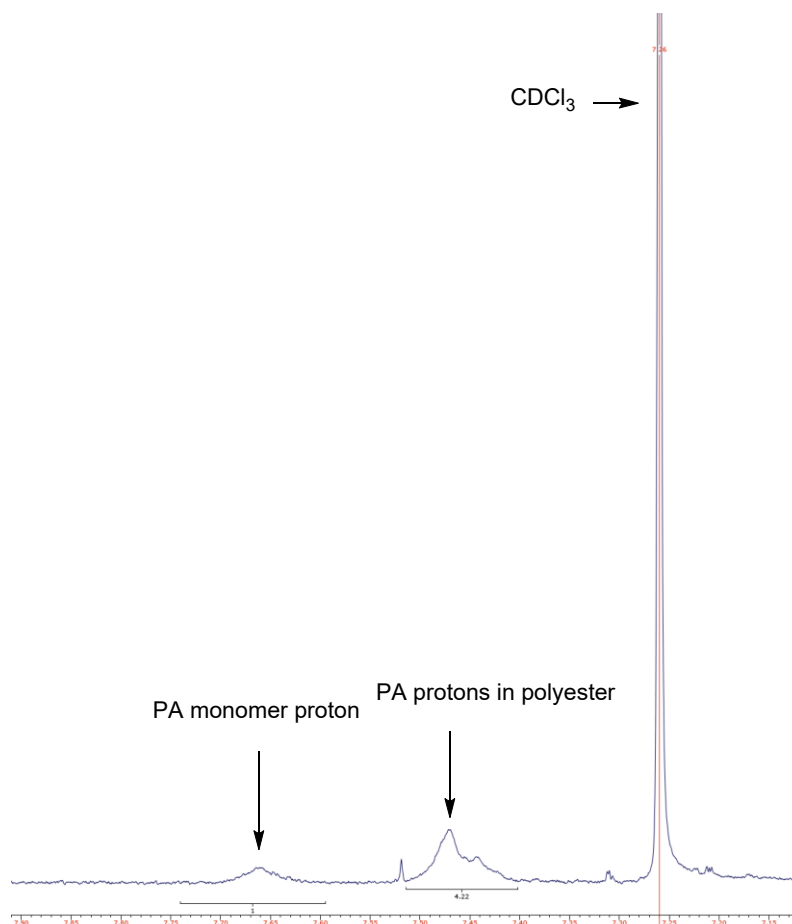


Figure 3.7: Part of ^1H NMR spectrum (400 MHz, CDCl_3 , 293 K) of Entry 18 (PA / PO, Table 3.3)

The reason why PA serves as a superior analyzing handle for conversion is because that the PA monomer proton signals appears further downfield compared to their counterparts in the polyester, thus not overlapping with any other signals, and both sets of signals sitting close to the CDCl_3 signal, further downfield of all other signals, thus unobscured. The extraction of conversion data thus becomes straightforward. The conversion from this spectrum, according to the formula, can be calculated by: $\text{Conversion} = 4.22 / (4.22 + 1) = 80.84\% \approx 81\%$. For other anhydrides, the proton signals either merge with other signals (e.g., reaction solvent, NMR solvent) or are too messy to be clearly identified (monomer and polyester peaks too close to each other), thus the anhydride integration method cannot be used. The most advantageous point about using anhydride signals to calculate conversion is that we can judge whether the reaction time is beyond the time needed for total

consumption of the anhydride and start to consume epoxide anyway, which will lead to a drop in selectivity. If the epoxide and anhydride are used in equal amount, this might not occur. But if excess epoxide was used as both monomer for ROCOP and as reaction solvent, accurate reaction quenching right at the time when anhydride is fully consumed becomes critical. Thus, in Chapter 6 where all ROCOP reactions were done with excess epoxide as solvent, we use this phthalic anhydride analysis method to obtain conversions. Also, since the ring-opening of epoxide is rate-determining,¹⁵ the reaction time for all anhydrides with the same epoxide should be approximately the same. Therefore theoretically, PA can be used to determine the reaction time for a certain epoxide and extrapolated to other anhydrides.

The results of ROCOP with [(CpHO)₂Al₂Me₄] (**1**) are summarized in Table 3.3. Abbreviations used in Table 3.3 are listed in Table 3.1 and Table 3.2 above.

The chemical shifts of relevant polyesters and polyethers were obtained from literature reports.^{21–26} ¹H NMR data were obtained from aliquots extracted from quenched polymerization mixtures. All percentages were rounded to the nearest integers due to possible inaccuracy that may incur during NMR signal integration. All entries with 0% selectivity by default have 0% conversion as well, since the goal is to obtain alternating polyester rather than polyether. All the ratios in the table use 1 unit of metal central ion as ratio 1, thus 1 unit of catalyst actually counts as 2 unit of metal central ion. For an example, 1 : 200 ratio in the table is 1 : 400 complex : monomer.

3.4. Gel-Permeation Chromatography (GPC) data

Following the ROCOP reactions, some of the polymer samples were then submitted for molecular weight determination by Gel-Permeation Chromatography (GPC) analysis. The GPC data of the samples are also summarized in Table 3.3 together with catalysis results. GPC was used as triple detection, which includes refractive index, multi-angle light scattering and viscometry. Triple detection means the molecular weights obtained from GPC analyses are real values instead of relative values that need further conversion.²⁷ For some of the samples, due to non-isolable product or too little amount of isolated product, GPC was not possible and in these cases no data are reported. Some of the samples were poorly soluble thus the GPC results might be affected. To compare with the GPC results, the theoretical Mn is also included, which is calculated by the formula:

$$\text{Theoretical Mn} = 200 \times (\text{molecular weight of epoxide monomer} + \text{molecular weight of anhydride monomer}) \times \text{conversion} / \text{No. of co-catalyst equivalents}$$

Number of co-catalyst equivalents is the same as number of chloride equivalents, as no chloride is present in the complex itself.

As discussed before, chlorides in the co-catalysts initiate the reaction, thus the number of equivalents of co-catalyst should be equal to the number of polymer chains. When no co-catalyst is used, number of polymer chain per metal centre is assumed to be one.

3.5. Results and discussion

All ROCOP results and GPC data are summarized in Table 3.3.

Table 3.3: ROCOP conditions and results with complex **1** as catalyst

Entry	Anh/Ratio	Epo/Ratio	Co-cat/Ratio	Solvent	T/ °C	t/h	Conv.	Select./%	Mn/Da	Đ	Theo Mn/Da
1	SA/200	PO/200	N/A	Toluene	80	40	28%	21%	6199	3.85	8857
2	MA/200	PO/200	N/A	Toluene	80	40	77%	26%	N/A	N/A	24046
3	SA/200	PO/200	PPNCI/1	Toluene	70	72	40%	91%	1889	1.07	12652
4	SA/200	IO/200	PPNCI/1	Toluene	70	72	68%	64%	2065	2.02	23416
5	SA/200	SO/200	PPNCI/1	Toluene	70	72	91%	92%	4538	1.34	40080
6	SA/200	CHO/200	N/A	Toluene	70	24	99%	8%	22571	2.40	39246
7	SA/200	CHO/200	PPNCI/1	Toluene	70	24	0%	0%	N/A	N/A	0
8	SA/200	CHO/200	BnOH/1	Toluene	70	24	96%	10%	16438	2.20	38057
9	SA/200	PO/200	PPNCI/1	Toluene	70	72	52%	16%	3758	2.13	16448
10	SA/200	PO/200	PPNCI/1	Toluene	70	24	66%	36%	N/A	N/A	20876
11	SA/200	PO/200	PPNCI/1	THF	70	24	50%	20%	N/A	N/A	15815
12	SA/200	PO/200	PPNCI/1	THF	70	24	47%	12%	2696	16.29	14866
13	SA/200	IO/200	PPNCI/1	THF	70	24	64%	54%	660	1.022	22039
14	SA/200	SO/200	PPNCI/1	THF	70	24	47%	10%	1111	2.22	20701

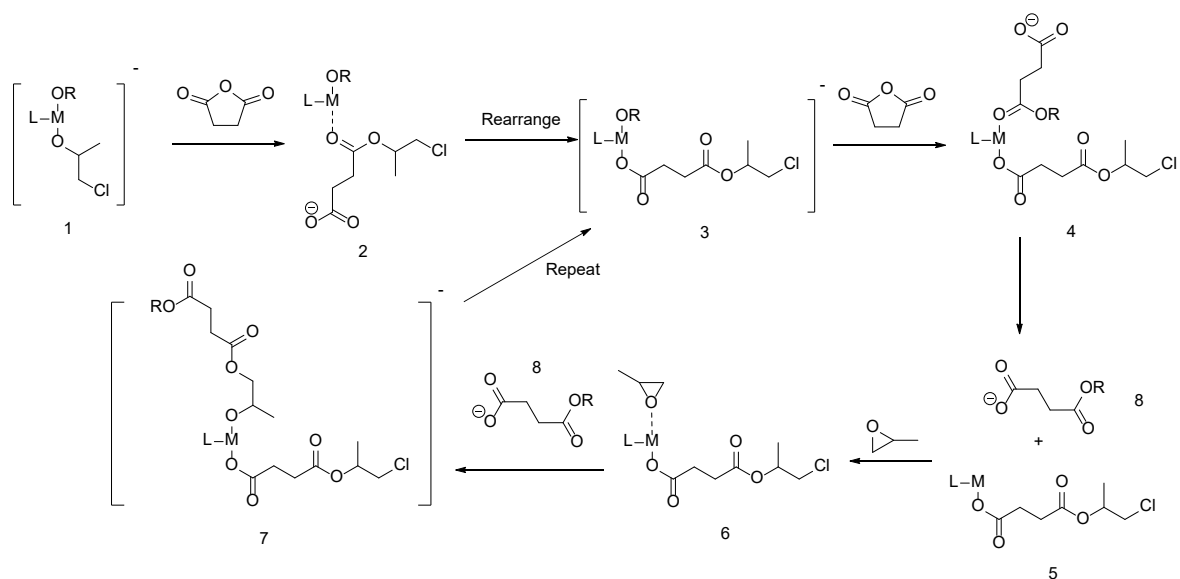
15	SA/200	PO/200	PPNCI/2	THF	70	24	45%	11%	10652	1.79	7117
16	SA/200	IO/200	PPNCI/2	THF	70	24	59%	50%	4669	3.204	10159
17	SA/200	SO/200	PPNCI/2	THF	70	24	42%	17%	N/A	N/A	9249
18	PA/200	PO/200	PPNCI/1	THF	70	24	81%	37%	N/A	N/A	33401
19	GA/200	PO/200	PPNCI/1	THF	70	24	93%	1%	1583	3.86	32025
20	GA/200	CHO/200	PPNCI/1	THF	70	24	0%	0%	N/A	N/A	0
21	GA/200	SO/200	PPNCI/1	THF	70	24	0%	0%	N/A	N/A	0
22	SA/200	PO/200	N/A	Toluene	70	72	33%	24%	N/A	N/A	10438
23	MA/200	PO/200	PPNCI/1	Toluene	70	24	48%	76%	N/A	N/A	14989

Anh : anhydride; Epo : epoxide; Co-cat: co-catalyst; T : reaction temperature; t : reaction time; Conv. : conversion; Select. : selectivity; Đ: dispersity; Theo Mn: theoretical Mn.

Complex **1** was used with various combinations of epoxides and anhydrides under a range of different reaction conditions, to test its viability as a ROCOP catalyst. Several general conclusions can be drawn from Table 3.3.

Upon analyzing the data for polymerization experiments conducted with and without co-catalyst, it is apparent that complex **1** requires PPNCI as a co-catalyst to function effectively as a catalyst for the ROCOP of epoxides and anhydrides. As can be seen from Entry 22 (SA + PO, no co-catalyst, 72 hours, 70°C) has a low selectivity of 24% and a conversion of 33%, which are common for no co-catalyst reactions. On the other hand, Entry 3, which was performed under the same conditions except using PPNCI as a co-catalyst gave a much higher 91% selectivity, as well as slightly higher conversion at 40%. The improvement in both selectivity and conversion means that PPNCI does provide a more kinetically favoured reaction route for ROCOP, comparing to the situation where PPNCI is not included. Entry 6, 7 and 8 (SA + CHO, 70 °C, 24 hours) were also done under same conditions, but Entry 6 involved no catalyst, Entry 7 used PPNCI as co-catalyst and Entry 8 used BnOH as co-catalyst. In this case, PPNCI actually made the selectivity and conversion (which is defined as zero when selectivity is zero, as the polymer without alternating monomer is meaningless) go down to zero from 8% when no co-catalyst was used. This indicates that PPNCI is actually creating a reaction mechanism which is kinetically more plausible for CHO homopolymerization rather than for ROCOP, thus causing the selectivity to decrease. When BnOH is used as co-catalyst, the selectivity went up slightly to 10%, indicating a slightly more kinetically favoured transition state for ROCOP, but the difference is tiny. All the discussions above are based on the assumption that NMR integrations are accurate. However, in reality the baseline noise and integration inaccuracy could result in an error as high as 10%. Since most of the differences in percentage discussed above is below 10%, there is a high chance that all these different percentages are caused by errors rather than the actual mechanistic or kinetic differences. Still, based on the Entry 22 vs. Entry 3, we can draw the conclusion that PPNCI improved the catalytic performance (especially

the selectivity) by a significant amount, thus should follow a mechanism similar to the one reported by Coates *et al.*¹⁵, as shown in Scheme 3.5.



Scheme 3.5: Epoxide / anhydride ROCOP mechanism. M: central metal ion; OR: opened epoxide unit with initiating group (Cl^- from PPNCI) / growing polymer chain; L: ancillary ligand.¹⁵

Generally, **1** does not exhibit satisfactory catalytic performance for epoxide / anhydride ROCOP when conversion, selectivity, reaction time and temperature are all taken into consideration; as ideally a good ROCOP catalyst should give good selectivity and conversion in a rather short time and low temperature (like complex **3** and **4** reported in Chapter 6) The combination SA / PO (Entry 3, 91% selectivity) and SA / SO (Entry 5, 92% selectivity) are the only exceptions. However, the relatively low conversion of Entry 3, which is only 40% at 72 hours under 70°C , still cannot justify complex **1** to be an efficient catalyst. Despite the seemingly nice results at the first glance, repeating the same experiment yielded various different selectivities and conversions for unknown reasons. Several other group members in BDW research group also encountered the same problem when conducting repeating ROCOP reactions with succinic anhydride (SA), which could suggest a general lack of compatibility of this substrate with ROCOP catalysts. One possible explanation is that the $\alpha\text{-CH}_2$ hydrogen next to the carbonyl being relatively reactive

(for example, consider the reactivity of such positions in the context of tautomerism and Aldol reactions), which could potentially lead to unwanted side reactions that ultimately causes the reaction results to be inconsistent, particularly in the presence of highly basic Al-Me ligands. For maleic anhydride (MA) reactions (Entry 2 and 23) and SA / CHO reaction (Entry 6, 7, 8), unidentifiable black solids appeared on completion of the reactions, and the reaction mixture (solution) became dark yellow (same observation made by other BDW group members when conducting MA / epoxide ROCOP as well), which strongly suggests the existence of side reactions, which may also apply to SA cases.

Changing the solvent system from toluene to THF caused both selectivity and conversion to decrease. Comparing Entries 10, 11 and 12 we can see that while keeping all other factors constant, changing solvent from toluene to THF resulted in the drop of conversion from 66% to 50% or 47%. This can be potentially explained by the competitive coordination of THF and monomers to the catalyst, as THF contains an oxygen atom which has an available lone pair electron which could possibly make THF molecule coordinate to the aluminium ion. This will cause the monomers to have less chance to coordinate to the aluminium ion thus lower conversion is observed. The selectivity also dropped from 36% to 20% or 12% (non-stable results due to the possible side reactions discussed above). A potential cause of this phenomenon could be the polarity change of the solvent system, as THF is more polar than toluene, and the ROCOP mechanism involves an ion pair step when the polymer chain de-coordinates and attacks the epoxide externally. The change in solvent polarity therefore significantly affects the energy of the transition state. Though the effects brought by the solvent polarity change is hard to predict, they will surely change the kinetics of the ROCOP reactions. Same observation can be obtained by comparing Entry 4 and 13. Although Entry 4 has a shorter reaction time (temperature is the same at 70°C), it still gave higher conversion and selectivity than Entry 13, because Entry 13 was performed in THF solution and Entry 4 was carried out in toluene solution. In previous literature from Ryu *et al.*²⁸, their 1,9-naphthalic

anhydride/CHO ROCOP reaction with chromium complex saw a conversion drop from 29% to < 1% when solvent is changed from toluene to THF as well. A report from Buchaca and co-workers²⁹ also stated that their ROCOP of CHO + SA saw decreases in conversion (100% to 81%) and selectivity (91% to 89%) when the solvent is changed from toluene to THF.

The stoichiometry of PPNCI co-catalyst (1 : 1 or 1 : 2, metal central ion : co-catalyst) has no prominent effect on conversion or selectivity. Entry 12 and Entry 15 showed a 1 – 2% change in both conversion and selectivity with change in PPNCI ratio, which is within experimental error. Entry 13 vs. 16 saw a 4 – 5% selectivity and conversion drop accompany the increase in PPNCI ratio, which based on the uncertainties in the complex **1** ROCOP reactions, can be considered as in the same level. A previous report from Ryu *et al.* showed that when 5 equivalents of PPNCI is used instead of 1 equivalent, conversion saw a 3% increase while selectivity saw a 4% decrease (Table 3.4). Entry 14 vs. 17, a 4% drop in conversion was observed but a 7% increase in selectivity was observed after increasing ratio of PPNCI. Conversely, the unremarkable changes in selectivity and conversion when increasing usage of PPNCI from 1 : 1 to 1 : 2 were accompanied by significant changes in Mn, Mw and Đ (polymer dispersity index). From Table 3.3 we can see that comparing to Entry 12, Entry 15 saw a big increase in Mn, and a huge reduction in Mw, which made the Đ for Entry 15 = 1.79, indicating a much better polymer dispersity control than Entry 12's extremely high 16.29 Đ value. However, theoretically more co-catalysts should result in more polymer chains thus lower Mn, which contradicts the observation here. This is possibly due to poor initiation of catalyst with 1 equiv. PPNCI which makes polymer chain lengths distributed randomly, thus a high dispersity. When more PPNCI is used, the dispersity control is much better and overall Mn rises because the proper initiation causes chain lengths to be more uniform. For Entry 13 and Entry 16, the story is different. A tremendous increase in Mn was observed, which is similar to the Entry 12 / 15 case. The Mw, on the other hand, saw a surge in its value together with Mn rather than

decrease. These changes in Mn and Mw resulted in a much higher Đ value of 3.204, comparing to 1.02 Đ of Entry 13 (Table 3.3). Ryu and co-workers reported their chromium-based catalyst's catalytic performances with different ratio of PPNCI as co-catalyst,²⁸ the results are listed as below in Table 3.4.

Table 3.4: Catalyst performances with different co-catalyst ratio reported by Ryu and co-workers²⁸

Monomers/Ratio	Co-catalyst/Ratio	Conversion	Selectivity	Mn/Da
PA+CHO/800:1600	DMAP/5	95%	>99%	19300
PA+CHO/800:1600	DMAP/1	3%	41%	/
PA+CHO/800:1600	DMAP/2.4	92%	91%	43800
PA+CHO/800:1600	PPNCI/5	95%	93%	15900
PA+CHO/800:1600	PPNCI/1	92%	97%	17400

Ratios are relative to catalyst = 1. DMAP refers to 4-dimethylaminopyridine.

As can be seen from Table 3.4, increasing in DMAP ratio gave increased conversion and selectivity, especially when the ratio is increased from 1 to 2.4. For PPNCI, however, although increase in ratio from 1 to 5 gave a 3% conversion rise, the selectivity dropped from 97% to 93%, which is comparable to Entry 13 and 16 case in Table 3.3. In terms of the molecular weight, the Mn value of the polyesters decreased when the co-catalyst ratio was increased for both PPNCI and DMAP. This observation is in accordance with the theory that Cl⁻ ion serves as a leaving group which initiates the chain growth (as does DMAP), thus more PPNCI (or DMAP) means that there are a greater number of chains, which in turn leads to lower molecular weight for each chain. However, my GPC data is contrary of this theory for some reasons (Entry 12 and 15, Table 3.3). This could be due to the incomplete, poorly initiated catalysts with only 1 equivalent of Cl⁻ which causes poor control over polymer chain length that results in existence of all different polymer chain lengths thus high Đ. This means that there is an optimum co-catalyst equivalent for complex 1, which should be 2 equivalents as the 2 equivalent PPNCI reactions (Entries 15 and 16) showed much higher Mn in comparison to the 1 equivalent PPNCI reactions

(Entries 12 and 13). In another paper discussing ROCOP mechanism which was prepared by Coates *et al.*,¹⁵ plots regarding co-catalyst stoichiometry was drawn, as shown below.

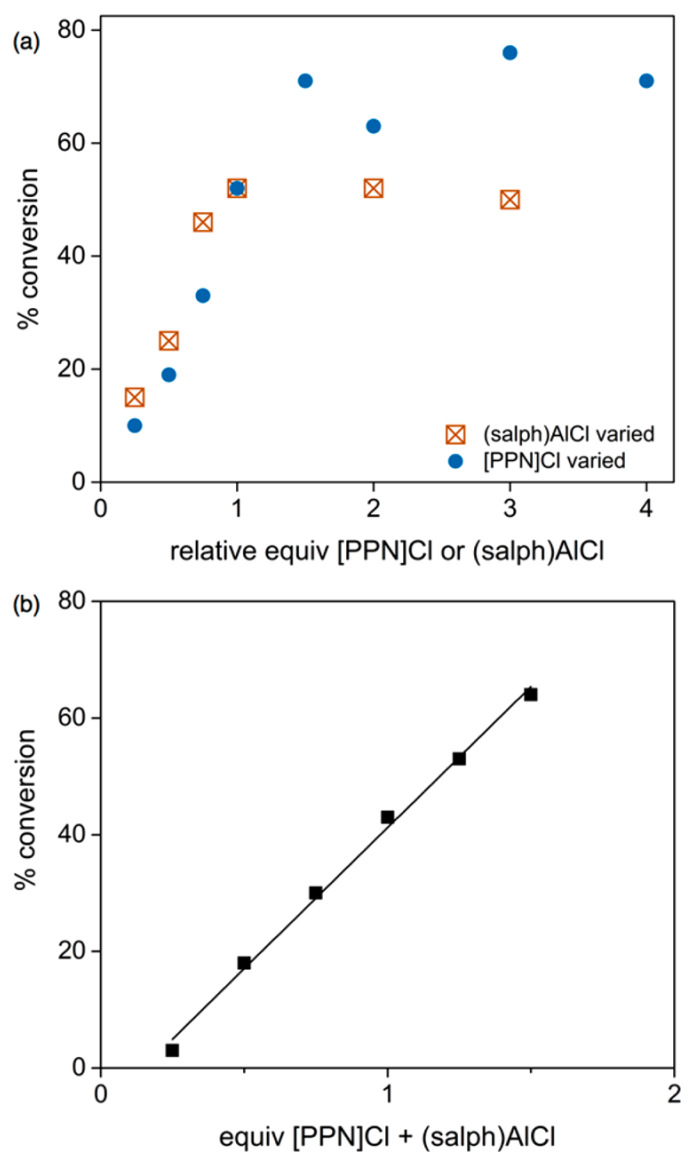


Figure 3.8: Conversion vs. PPNCI ratio plot by Fieser *et al.*¹⁵ (a) The ratio of catalyst [(salph)AlCl] was kept constant at 1 while ratio of PPNCI changing (data points represented by blue dots). (b) Ratio of catalyst and PPNCI varied concurrently and equal to each other (from 0.25:0.25 to 1.5:1.5).

As can be seen from Figure 3.8 (a), when the ratio of catalyst is kept constant and ratio of PPNCI varied, the conversion first showed step increase till 1.5 equiv. of PPNCI, then a trough at 2 to 2.5 equiv, followed by rising and oscillations around

~75%. This investigation showed that PPNCI, when serving as a co-catalyst, provides prominent catalytic performance enhancement at around 1 to 1.5 equivalents, while at 2 to 2.5, it actually suppresses the reactivity of catalyst. This conversion suppression effect of PPNCI could be happening to Entry 13/16 and Entry 14/17. Coates and co-workers also provided a comprehensive paper including research into the co-catalyst behaviour,³⁰ the data are listed below.

Table 3.5: Catalyst performances with different co-catalyst ratio reported by Coates and co-workers³⁰

PPNCI ratio to catalyst	Reaction time/min	Conversion	Mn/kDa	Đ
0.5	25	15%	N/A	N/A
0.9	25	39%	3.5	1.16
1.1	25	44%	3.7	1.18
0.5	300	>99%	8.1	1.46
0.9	180	>99%	7.5	1.66
1.1	180	>99%	9.8	1.64

This set of conversions are generally in agreement with the data from Fieser *et al.*,¹⁵ increases can be seen when PPNCI ratio increases from 0.5 to 1.9, relative to catalyst complex. However, the Mn saw a decrease from 8.1 to 7.5 then rise again to 9.8, and Đ is higher for 0.9 than 0.5 and 1.1 ratio of PPNCI. These trends, observed when using PPNCI as cocatalyst, are not yet fully resolved and many questions remain in the field of ROCOP. Several hypotheses could be : 1. Different epoxide/anhydride combination cope with PPNCI/catalyst in different ways thus there is no general trend which is suitable for all. 2. Different catalysts form different active species with PPNCI, hence the reaction mechanisms and reaction kinetics are not the same, and this ultimately causes unequal trends. 3. Unstable side reactions disturbing the catalytic cycle, and the side reactions are related to PPNCI.

Overall, it was proposed that for the complex [(CpHO)₂Al₂Me₄] (**1**), metal ion : PPNCI should be kept at 1 : 2 for the best catalytic performance. Although minor decreases

in conversion and selectivity could occur, the better control over molecular weight is achieved, which is more important.

During workup of the polymerization reactions, it was found that for the majority of the entries, there was very little polymer precipitated upon addition of antisolvent. It is possible that this may be due to the relatively low molecular weights of the polymers affording fine dispersions of polymer in the solvent mixture, which therefore pass through the filter paper during isolation.

An overall assessment of the efficacy of $[(\text{CpHO})_2\text{Al}_2\text{Me}_4]$ (**1**) in epoxide / anhydride ROCOP catalysis is not as favourable as other catalyst complexes reported in the literature, especially in terms of ester selectivity. One possible reason for this is the bimetallic nature of the complex. Whilst there are bimetallic complexes that have been shown to be highly effective in this type of catalysis, those complexes are in a more rigid supporting environment and may offer a greater degree of control over the bimetallic ring-opening polymerization of epoxide. This conclusion suggests an alternative proposition: $[(\text{CpHO})_2\text{Al}_2\text{Me}_4]$ (**1**) could be an excellent catalyst for epoxide polymerization rather than for ROCOP. The epoxide homopolymerization experiments (discussed in chapter 4) will show that this suggestion is correct. One thing worth mentioning about the temperature control of the ROCOP reactions is that during investigation of epoxide homopolymerization with complex **1**, the reactions were found to be highly exothermic, causing surge of reaction mixture temperature once the epoxides were added into the vial. The intense temperature change can even be felt through the glove box rubber gloves. The same situation may also apply to the ROCOP reactions with complex **1**, as epoxides were also included in the reactions, and the low selectivities are the evidence that complex **1** was preferably catalyzing the epoxide homopolymerization. This observation could potentially be the explanation of the low selectivities exhibited by complex **1** for ROCOP, as the non-uniform internal temperature of reaction mixture would cause the reaction rates of different parts of the reaction mixture to be different, ultimately leading to inconsistent selectivities and conversions when same reaction is

repeated, and generally poorer molecular weight control. Moreover, during the complex **1**-catalyzed epoxide homopolymerization (Chapter 4), it was found that a fast epoxide homopolymerization sometimes results in the solidification in parts of the reaction mixture. The coagulated polyether around catalyst could possibly seal the catalyst molecules inside thus preventing them from any further reactions, either epoxide homopolymerization or epoxide / anhydride ROCOP. Also, as we have discussed before in this section, the kinetic control of ROP/ROCOP reactions means higher temperature could result in more polyether formation. Combining with the observation that complex **1** catalyzed epoxide ROP is highly exothermic, it is thermodynamically favoured as well. This means heat spots within the reaction mixture again increases the chance of epoxide homopolymerization, deteriorating the selectivity (more about the heat spots in chapter 4). With the evidence from chapter 4 and this chapter, it can be proposed that complex **1** serves as an epoxide homopolymerization catalyst and this disqualifies it as an efficacious epoxide / anhydride ROCOP catalyst. Also, from Chapter 4 and 5, it can be seen that complex **1** provides efficient mechanistic routes for ring-opening polymerization (ROP) for both ϵ -caprolactone as well as epoxides, thus complex **1** might be intrinsically more suitable for ROP catalysis rather than ROCOP. The two following chapters regarding epoxide homopolymerization and ϵ -caprolactone homopolymerization with complex **1** will provide more details about this conclusion.

3.6. References

- 1 G. G. Odian, in *Principles of polymerization*, Wiley-Interscience, Hoboken, N.J, 4th ed., 2004.
- 2 Preferred Fiber & Materials Market Report 2020, <https://textileexchange.org/2020-preferred-fiber-and-materials-market-report-pfmr-released/>, (accessed 17 October 2020).
- 3 J. K. Stille, *J. Chem. Educ.*, 1981, **58**, 862–866.

- 4 J. M. Longo, M. J. Sanford and G. W. Coates, *Chem. Rev.*, 2016, 116, 15167–15197.
- 5 A. Kummari, S. Pappuru and D. Chakraborty, *Polym. Chem.*, 2018, 9, 4052–4062.
- 6 S. Paul, Y. Zhu, C. Romain, R. Brooks, P. K. Saini and C. K. Williams, *Chem. Commun.*, 2015, **51**, 6459–6479.
- 7 L.-F. Hu, D.-J. Chen, J.-L. Yang and X.-H. Zhang, *Molecules*, 2020, **25**, 253.
- 8 E. Hosseini Nejad, C. G. W. van Melis, T. J. Vermeer, C. E. Koning and R. Duchateau, *Macromolecules*, 2012, **45**, 1770–1776.
- 9 T. Stößer, C. Li, J. Unruangsri, P. K. Saini, R. J. Sablong, M. A. R. Meier, C. K. Williams and C. Koning, *Polym. Chem.*, 2017, **8**, 6099–6105.
- 10 Y. Maeda, A. Nakayama, N. Kawasaki, K. Hayashi, S. Aiba and N. Yamamoto, *Polymer*, 1997, **38**, 4719–4725.
- 11 Y. Maeda, T. Maeda, K. Yamaguchi, S. Kubota, A. Nakayama, N. Kawasaki, N. Yamamoto and S. Aiba, *J. Polym. Sci., Part A: Polym. Chem.*, 2000, **38**, 4478–4489.
- 12 K. D. Papadimitriou, F. Paloukis, S. G. Neophytides and J. K. Kallitsis, *Macromolecules*, 2011, **44**, 4942–4951.
- 13 M. J. Kade, D. J. Burke and C. J. Hawker, *J. Polym. Sci. A Polym. Chem.*, 2010, **48**, 743–750.
- 14 V. Giménez, J. A. Reina, A. Mantecón and V. Cádiz, *Polymer*, 1999, **40**, 2759–2767.

- 15 M. E. Fieser, M. J. Sanford, L. A. Mitchell, C. R. Dunbar, M. Mandal, N. J. Van Zee, D. M. Urness, C. J. Cramer, G. W. Coates and W. B. Tolman, *J. Am. Chem. Soc.*, 2017, **139**, 15222–15231.
- 16 M. I. Childers, J. M. Longo, N. J. Van Zee, A. M. LaPointe and G. W. Coates, *Chem. Rev.*, 2014, **114**, 8129–8152.
- 17 C. G. Rodriguez, M. Chwatko, J. Park, C. L. Bentley, B. D. Freeman and N. A. Lynd, *Macromolecules*, 2020, **53**, 1191–1198.
- 18 R. C. Ferrier, J. Imbrogno, C. G. Rodriguez, M. Chwatko, P. W. Meyer and N. A. Lynd, *Polym. Chem.*, 2017, **8**, 4503–4511.
- 19 R. C. Ferrier, S. Pakhira, S. E. Palmon, C. G. Rodriguez, D. J. Goldfeld, O. O. Iyiola, M. Chwatko, J. L. Mendoza-Cortes and N. A. Lynd, *Macromolecules*, 2018, **51**, 1777–1786.
- 20 A. Yahiaoui, M. Belbachir, J. C. Soutif and L. Fontaine, *Materials Letters*, 2005, **59**, 759–767.
- 21 B. Han, L. Zhang, B. Liu, X. Dong, I. Kim, Z. Duan and P. Theato, *Macromolecules*, 2015, **48**, 3431–3437.
- 22 N. J. Van Zee and G. W. Coates, *Angew. Chem. Int. Ed.*, 2015, **54**, 2665–2668.
- 23 A. M. DiCiccio and G. W. Coates, *J. Am. Chem. Soc.*, 2011, **133**, 10724–10727.
- 24 R.-J. Wei, Y.-Y. Zhang, X.-H. Zhang, B.-Y. Du and Z.-Q. Fan, *RSC Adv.*, 2014, **4**, 21765–21771.
- 25 D. J. Darensbourg, R. R. Poland and C. Escobedo, *Macromolecules*, 2012, **45**, 2242–2248.
- 26 A. Kayan, *Des. Monomers. Polym.*, 2015, **18:6**, 545–549.

- 27 A guide to multi-detector gel permeation chromatography, <https://www.agilent.com/cs/library/primers/Public/5990-7196EN.pdf>, (accessed October 2020).
- 28 H. K. Ryu, D. Y. Bae, H. Lim, E. Lee and K. Son, *Polym. Chem.*, 2020, **11**, 3756–3761.
- 29 M. Martínez de Sarasa Buchaca, F. de la Cruz-Martínez, J. Martínez, C. Alonso-Moreno, J. Fernández-Baeza, J. Tejada, E. Niza, J. A. Castro-Osma, A. Otero and A. Lara-Sánchez, *ACS Omega*, 2018, **3**, 17581–17589.
- 30 N. J. Van Zee, M. J. Sanford and G. W. Coates, *J. Am. Chem. Soc.*, 2016, **138**, 2755–2761.

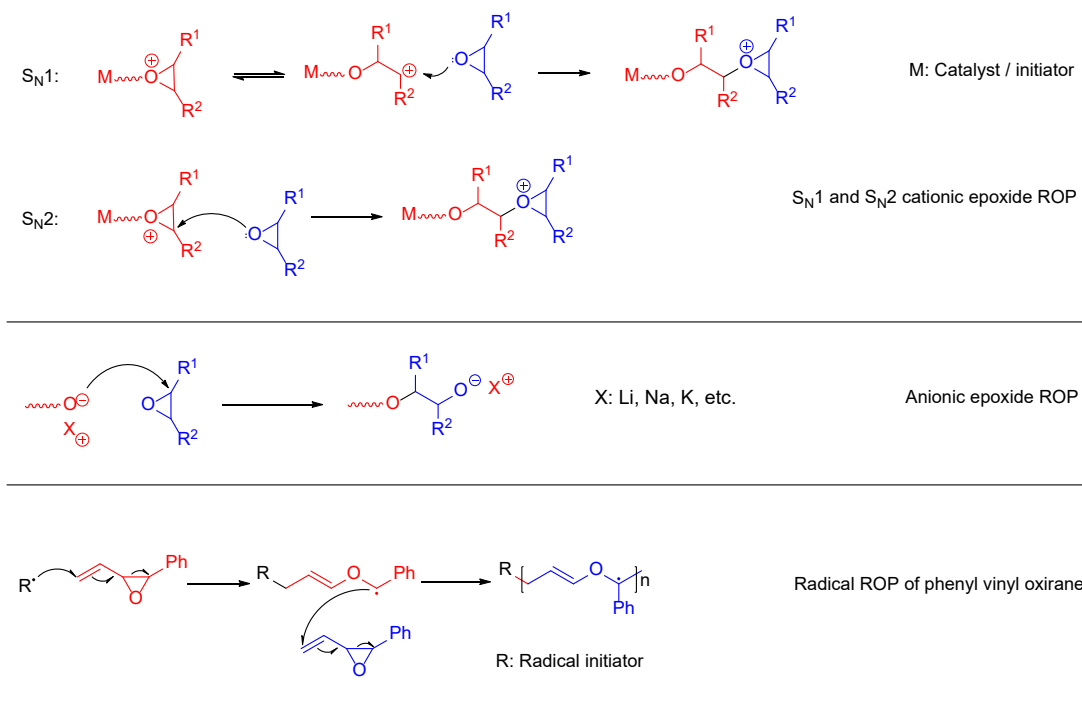
Chapter 4: Ring-opening polymerization of epoxides with $[(\text{CpHO})_2\text{Al}_2\text{Me}_4]$ (1)

4.1. Introduction

An epoxide is an ether containing a three-membered ring consisting of one oxygen and two carbons. This group of organic compounds are produced in large quantities for various industrial applications. For instance, glycidol can be used as stabilizer for natural oils / vinyl polymer as well as dye-levelling agent;¹ ethylene glycol can be used to produce ethylene glycol, ethoxylates and ethanol amines.²

Apart from the vast applications of epoxides themselves, polyethers that are synthesized from epoxide ring-opening polymerization also play an important part in the polymer industry. The most widely known example being polyethylene oxide, which is more commonly referred to as polyethylene glycol, finds its applications in a variety of scenarios including as an anti-foaming agent for food and drinks;³ dispersant in toothpastes;⁴ crowding agent in *in vitro* assays to mimic highly crowded cellular conditions,⁵ and many more. Another example of a polyether that is used widely is polypropylene oxide, which commonly named as polypropylene glycol. Polypropylene oxide can be applied as a component for polyurethane;⁶ non-ionic surfactant;⁷ etc.

Featuring three-membered hetero rings with one oxygen and two carbons, epoxides are subject to significant ring strain and are therefore highly reactive towards ring-opening. Some common polyether syntheses^{8,9} are given in Scheme 4.1.



Scheme 4.1: Examples of common polyether syntheses routes^{8,9}

Due to the existence of the ring strain, epoxides face low energy barriers towards ring-opening reactions, thus can be polymerized via ring-opening polymerization (ROP) easily.^{10–13} However, the intramolecular attack will have a high energy 4-membered transition state thus most ligands allow an intermolecular attack as well. For an example, bimolecular mechanism with the polymer on one metal attacking an epoxide coordinated to another metal central ion, which involves bimetallic mechanism that will be discussed in section 4.2). Methods for the catalyzed ROP of epoxides are well documented through works by various researchers such as Sarazin *et al.*¹⁰ and Brocas *et al.*¹¹ Catalyst wise, the metal-based catalysts for ROP of epoxides usually include planar ligand systems which can facilitate bimolecular reaction pathway, such as salen-type ligand^{14,15} or porphyrin-type ligand,^{14,16} with some examples illustrated in Figure 4.1.

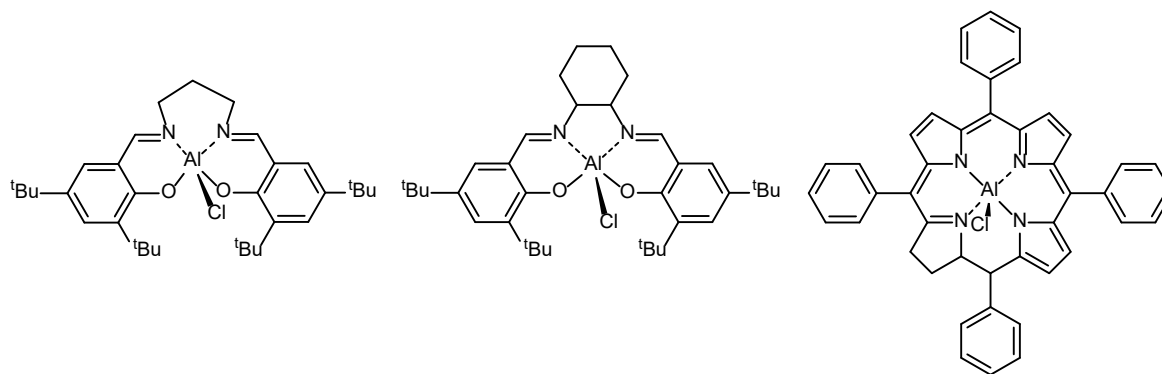


Figure 4.1: Examples of salen / porphyrin-type ligand aluminium-based catalysts for ROP of epoxides.^{14,15}

As shown in Figure 4.1, aluminium has been a popular choice for the central metal ion for catalysts of epoxide ROP. With the non-ideal epoxide / anhydride ring-opening co-polymerization (ROCOP) selectivity and the interpretation that $[(\text{CpHO})_2\text{Al}_2\text{Me}_4]$ (**1**) might be more catalytically active for epoxide ROP that have been made in Chapter 3, the catalytic performance of **1** for epoxide ROP was therefore investigated in this chapter.

4.2. $[(\text{CpHO})_2\text{Al}_2\text{Me}_4]$ (**1**) catalyzed epoxide ROP

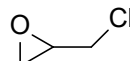
4.2.1. Epoxide monomers

The epoxides used for ROP catalysis tests with **1** are listed in Table 4.1 as below.

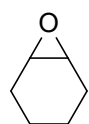
Table 4.1: Epoxide monomers used in epoxide homopolymerization



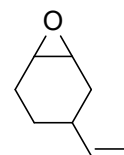
Propylene Oxide (PO)



Epichlorohydrin (ECH)

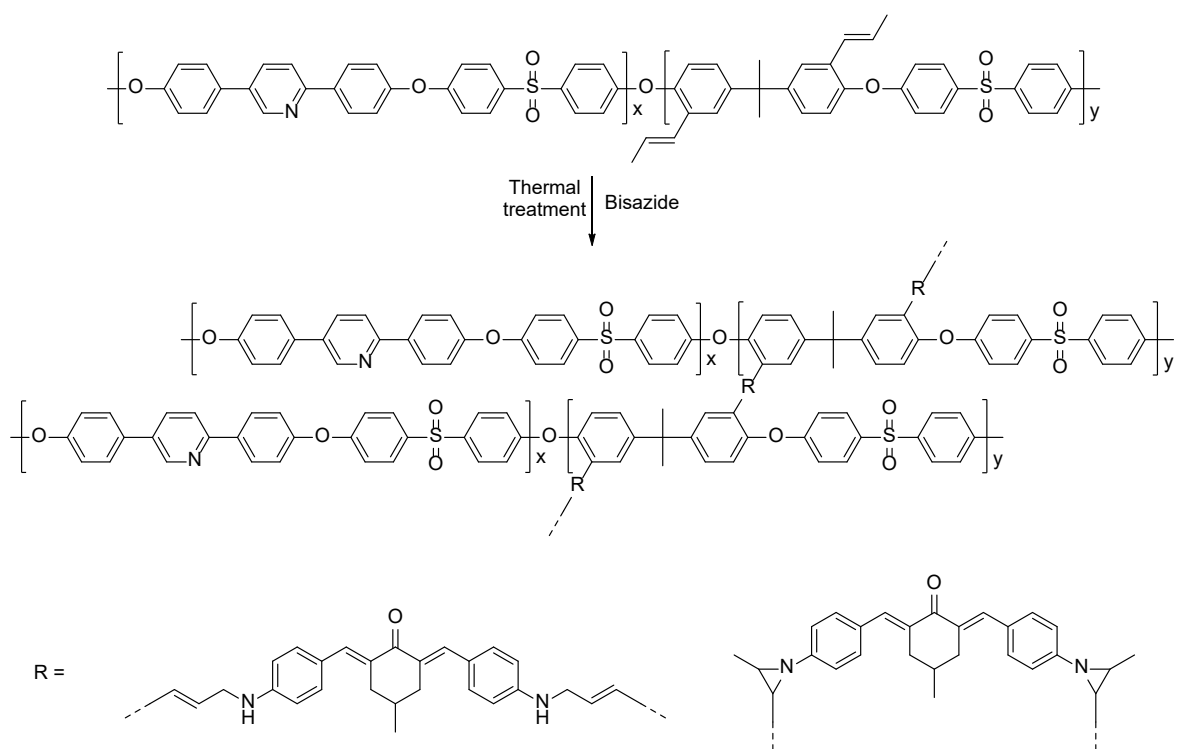


Cyclohexene Oxide (CHO)



4-Vinyl-1-cyclohexene 1,2-epoxide (VCHO)

Propylene oxide was chosen due to the enormous applications of its polymer, as have discussed in section 4.1. Epichlorohydrin (ECH), which is propylene oxide with one of its methyl hydrogens replaced by chlorine, was included as well to investigate the differences between PO ROP and ECH ROP that have been brought by the chlorine. Cyclohexene oxide (CHO) was chosen to check the capability of **1** to initiate the polymerization of epoxides larger (in terms of molecular weight and steric demand) than PO. 4-Vinyl-1-cyclohexene 1,2-epoxide (VCHO) was included to compare with CHO test results due to their closely-related structure. The unsaturated double bond on VCHO also grants its polymer more possibilities of cross-linking and side chain functionalization thus immense competency of applications in various fields. Some previous reported unsaturated side group cross-linking and functionalization examples are given in Scheme 4.2 and Scheme 4.3.



Scheme 4.2: Unsaturation polymer crosslinking using bisazides as cross-linkers¹⁷

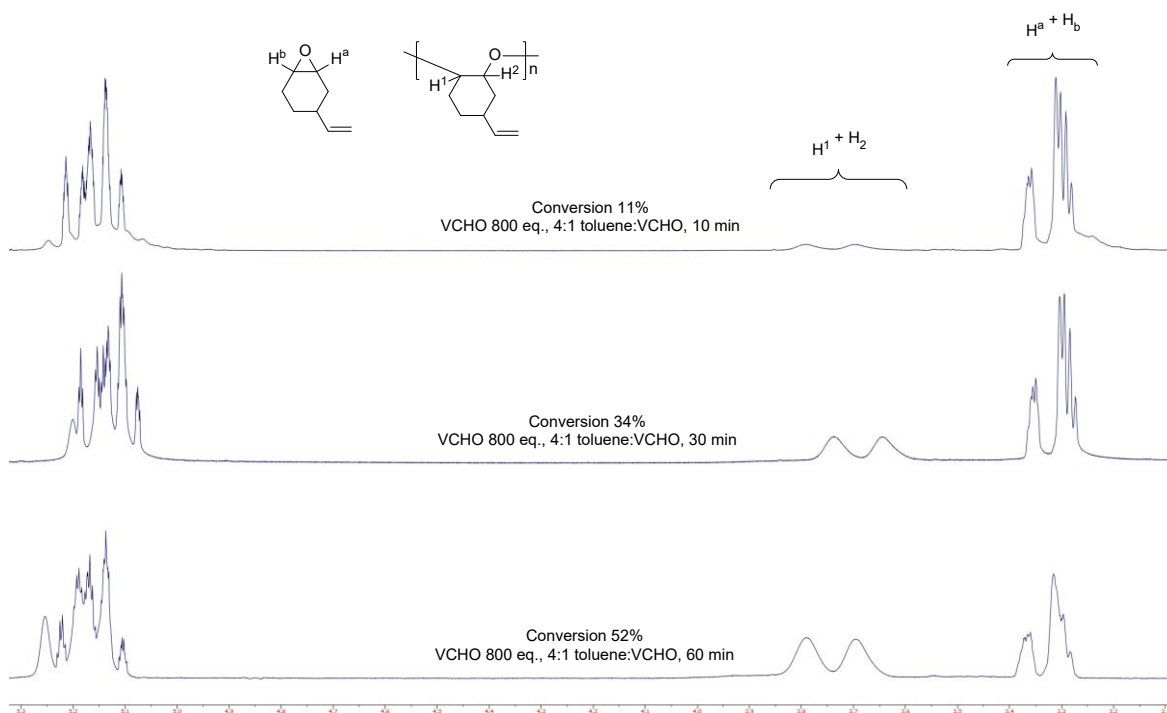


Figure 4.2: Stacked ^1H NMR (400 MHz, CDCl_3 , 293 K) spectra of polyether samples with different conversions (conversion 11% — entry 5; 34% — entry 7; 52% — entry 10; all from Table 4.4)

As shown in figure 4.2, the signals from the ether α protons are used to monitor the conversion. The ether α protons in both polymer and monomer do not overlap with any other proton signals (e.g., from the side chains), thus should be an easy and accurate way to assess the conversions. The relative integration ratio of the monomer ether α proton signals ($\text{H}^a + \text{H}^b$) will gradually decrease accompanying the depletion of monomers, while the relative ratio of the ether α protons in the polyether will increase with the formation of the polymer. Therefore, the conversion of the samples is calculated by the formula:

$$\text{Conversion} = \frac{\text{(integration of polyether ether } \alpha \text{ protons)}}{\text{(integration of polyether ether } \alpha \text{ protons and epoxide monomer ether } \alpha \text{ protons)}}$$

4.2.3. [(CpHO)₂Al₂Me₄] (**1**) catalyzed epoxide ROP results

The solvent-free epoxide ROP results are summarized in Table 4.2 as below.

Entry	Monomer/Ratio	Temperature/°C	Time/min	Conversion/%
1	PO/400	100	25	10
2	ECH/400	100	25	61
3	CHO/400	100	10	68
4	VCHO/400	100	10	76
5	VCHO/400	20	55	64
5	CHO/800	60	25	75
6	CHO/800	60	50	79
7	CHO/800	60	75	85
8	CHO/800	60	100	87
9	CHO/800	60	125	87
10	CHO/800	30	10	67
11	CHO/800	30	20	80
12	CHO/800	30	30	79
13	CHO/800	30	40	61
14	CHO/800	30	50	54
15	CHO/800	30	60	78

The ratio of aluminium centre is set to be 1 (equals to 0.5 equivalents of complex **1**)

The initial 100°C ROP reactions of ECH, CHO and VCHO (Entry 2-4, Table 4.2) are too fast for an accurate conversion vs. time plot to be drawn, and PO seemed not to polymerize in any valuable rate with complex **1** as catalyst, thus PO was omitted from subsequent ROP tests. Another phenomenon spotted was that for ECH, CHO and VCHO, the reaction mixture would quickly aggregate and solidify around several random positions in the mixture, possibly because the catalyst is of slightly higher concentration at these spots, or the random entanglement of the polymer chains, therefore there was not enough time for them to diffuse and form a uniform

solution before polymers formed around catalyst aggregate, solidify and seal the catalyst inside, which prevented further reactions from happening since no access to the catalyst metal site is available. This could be the reason why CHO showed inconsistent conversions over different temperatures and times, without any predictable trends (entries 6 to 15). To solve the aggregation problem and slow down the reaction to the level that data gathering can be done with acceptable precision, toluene was used as a solvent to dilute the reaction mixture. The results of toluene-diluted CHO ROP reactions with complex 1 are listed in Table 4.3 below.

Table 4.3: CHO ROP results

Entry	Monomer/Ratio	Solvent Ratio	Time/min	Conversion/%
1	CHO/800	4 : 1	10	5
2	CHO/800	4 : 1	20	5
3	CHO/800	4 : 1	30	8
4	CHO/800	4 : 1	40	10
5	CHO/800	4 : 1	50	11
6	CHO/800	4 : 1	60	8

Solvent ratio refers to volume (toluene) : volume (CHO); reaction temperature: 20°C.

From Table 4.3, it can be seen that after dilution with toluene, the reaction rate in terms of conversion saw a huge decrease; but the non-reliable random conversions persisted. Thus, VCHO was then tested with similar reaction conditions, and the results are listed in Table 4.4.

Table 4.4: VCHO catalysis results with complex 1

Entry	Catalyst Ratio	Monomer/ Ratio	Solvent Ratio	Time/min	Conversion /%
1	1	VCHO/800	1 : 1	4	75
2	1	VCHO/800	1 : 1	8	77
3	1	VCHO/800	1 : 1	12	78
4	1	VCHO/800	1 : 1	120	85
5	1	VCHO/800	4 : 1	10	11
6	1	VCHO/800	4 : 1	20	20
7	1	VCHO/800	4 : 1	30	34
8	1	VCHO/800	4 : 1	40	38
9	1	VCHO/800	4 : 1	50	46
10	1	VCHO/800	4 : 1	60	52
11	1.25	VCHO/800	4 : 1	10	25
12	1.25	VCHO/800	4 : 1	20	32
13	1.25	VCHO/800	4 : 1	30	38
14	1.25	VCHO/800	4 : 1	40	42
15	1.25	VCHO/800	4 : 1	60	51
16	1.5	VCHO/800	4 : 1	10	24
17	1.5	VCHO/800	4 : 1	20	35
18	1.5	VCHO/800	4 : 1	30	42
19	1.5	VCHO/800	4 : 1	40	45
20	1.5	VCHO/800	4 : 1	50	50
21	1.5	VCHO/800	4 : 1	60	54
22	1.75	VCHO/800	4 : 1	10	22
23	1.75	VCHO/800	4 : 1	20	34
24	1.75	VCHO/800	4 : 1	30	40
25	1.75	VCHO/800	4 : 1	40	45
26	1.75	VCHO/800	4 : 1	50	51
27	1.75	VCHO/800	4 : 1	60	53
28	2	VCHO/800	4 : 1	10	28
29	2	VCHO/800	4 : 1	20	37
30	2	VCHO/800	4 : 1	30	45

31	2	VCHO/800	4 : 1	40	50
32	2	VCHO/800	4 : 1	50	52
33	2	VCHO/800	4 : 1	60	56

Solvent ratio is volume (toluene) : volume (VCHO). All reactions are with toluene as solvent. Reaction temperature 20°C.

From Table 4.4 it can be interfered that when 1 : 1 solvent ratio was applied, the reaction is still too quick for precise data recording, and the conversions for entry 1 to 4 all stopped at around 80%, indicating a possible aggregation around catalyst which prohibited further polymerization reaction access to the central metal site, although the aggregation is not as quick as the solvent free reactions. Another possibility being the thermal decomposition of catalyst due to the exothermic nature of the polymerization reaction; the temperature rise accompanying the ROP may exceed the temperature tolerance of the catalyst and deactivate it. However, the retrieving of homogeneous catalyst from resultant reaction mixture is almost impossible since the quenching of the reaction is done by addition of methanol which will destroy any active catalysts left nonetheless. Therefore, no NMR (or other) data could be obtained to confirm whether thermal decomposition has affected the final conversion rate. Also, since there is no good way to track the temperature inside the reaction mixture in real time manner with common laboratory equipment, the temperature vs. time curve of the reaction mixture cannot be obtained, hence doing independent thermal decomposition test (e.g., dissolve complex **1** in C₆D₆ and heat it to certain temperature for a certain amount of time and NMR) would not give any useful information about whether thermal decomposition has affected the reaction. Subsequently, 4 : 1 solvent ratio was applied to further dilute the reaction mixture, which hopefully eliminate some of the problems mentioned above.

As can be seen in Table 4, entries 5 to 10 were undertaken with 4 : 1 solvent ratio, and the conversion in this series saw a steady increasing trend, which may allow the plot of a graph to determine the reaction kinetics of VCHO ROP with complex **1**

as catalyst. In light of this, different amount of complex **1** was used in a series of following reactions to compare their reaction rates (entries 5 to 33).

4.2.4. [(CpHO)₂Al₂Me₄] (**1**) catalyzed VCHO ROP reaction kinetics

With data from Table 4.4, plots of product concentration vs. reaction time were drawn, and exponential fittings were done to obtain the mathematical relations between product concentration and reaction time. Product concentration (unit: M) was calculated by:

Number of moles of monomer converted to polymer (mol) / total volume of reaction mixture (litre)

Reaction times are in seconds.

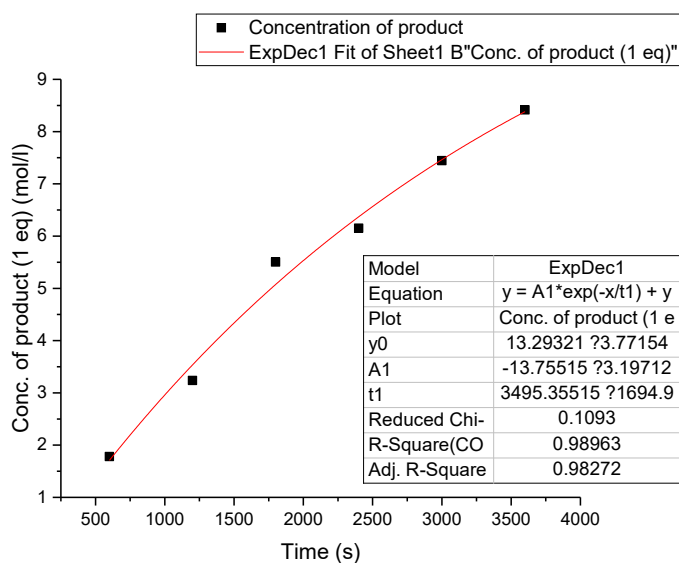


Figure 4.3: Conc. vs. Time plot for VCHO ROP, 1 equivalent of complex **1**

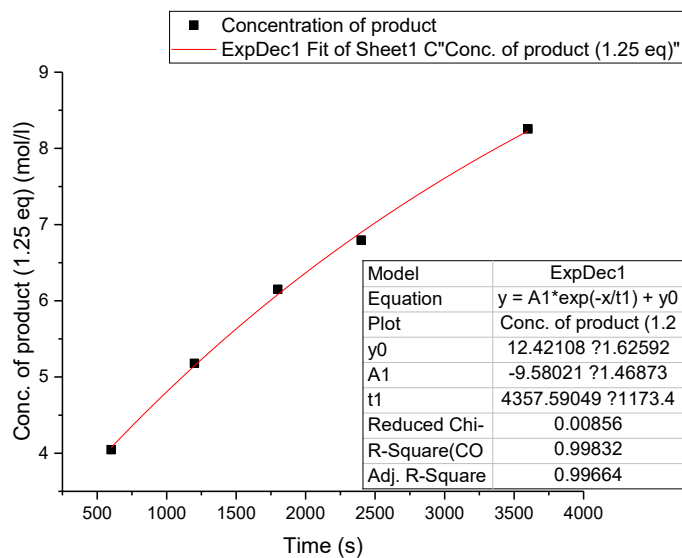


Figure 4.4: Conc. vs. Time plot for VCHO ROP, 1.25 equivalents of complex 1

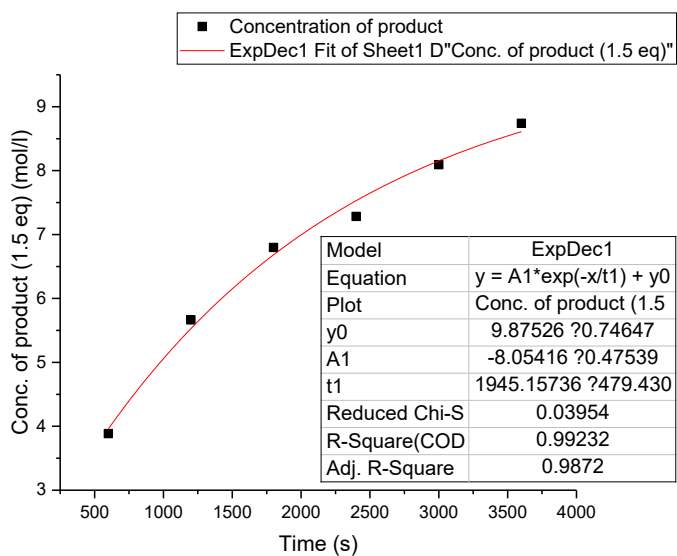


Figure 4.5: Conc. vs. Time plot for VCHO ROP, 1.5 equivalents of complex 1

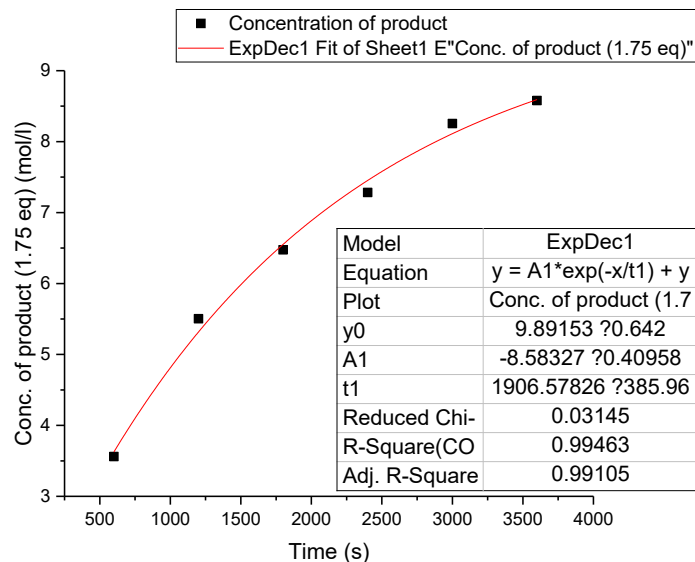


Figure 4.6: Conc. vs. Time plot for VCHO ROP, 1.75 equivalents of complex 1

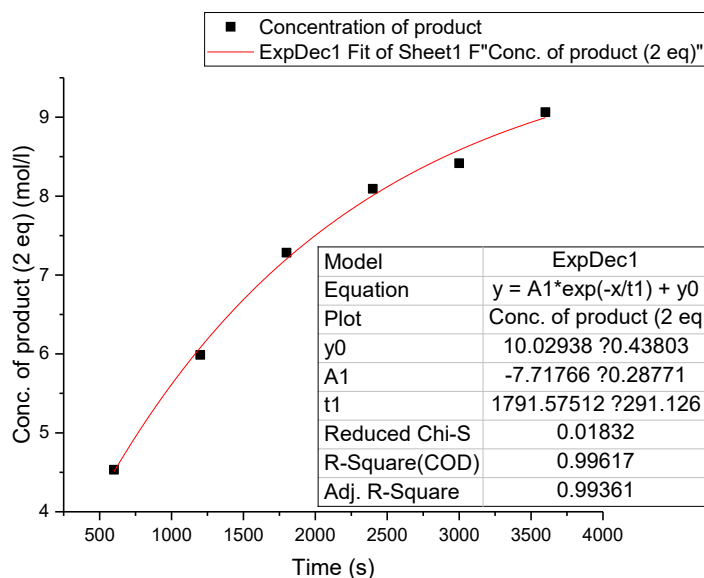


Figure 4.7: Conc. vs. Time plot for VCHO ROP, 2.0 equivalents of complex 1

For these exponentially fitted curves, the initial reaction rate, which is the gradient of the curve at Time = 0 s, can be calculated by differentiating the equation of the curve and let $x = 0$. The general equation for an exponential fitting is:

$$y = A_1 \text{Exp}(-x/t_1) + y_0$$

Where y is conc. of product, x is reaction time, A_1 , t_1 and y_0 are constants determined from the plot. After differentiation, the equation becomes:

$$\text{Gradient} = -(A_1 / t_1) \times \text{Exp}(-x/t_1)$$

For the initial reaction rate, $x = 0$, thus gradient is $-A_1 / t_1$.

Theoretically, the order of reaction in catalyst can be determined by plotting $\ln(\text{initial reaction rate})$ vs. $\ln(\text{complex 1 concentration})$. The calculated values are summarized in Table 4.5 below.

Equivalent of complex 1	Initial Rate	$\ln(\text{complex concentration})$	$\ln(\text{initial rate})$
1	3.94×10^{-3}	-6.20	-5.54
1.25	2.20×10^{-3}	-5.98	-6.12
1.5	4.14×10^{-3}	-5.80	-5.49
1.75	4.50×10^{-3}	-5.64	-5.40
2.0	4.31×10^{-3}	-5.51	-5.45

With the data in Table 4.5, the resultant plot of $\ln(\text{initial rate})$ vs. $\ln(\text{complex 1 concentration})$ is illustrated in Figure 4.8.

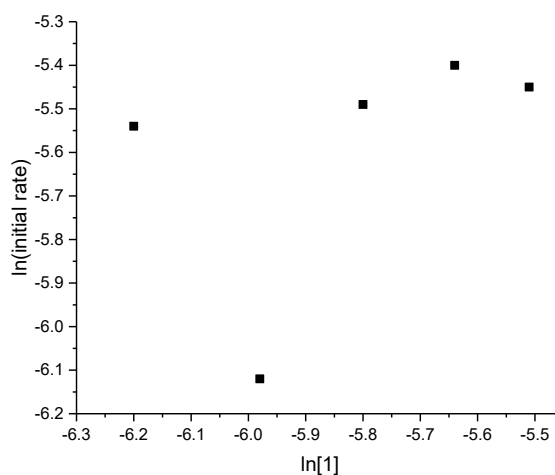


Figure 4.8: $\ln(\text{initial rate})$ vs. $\ln(\text{complex 1 concentration})$ plot

The five data points in Figure 4.8 do not fall near any common straight line. This means with respect to **1**, the reaction kinetics are complex, for examples, complex initiation kinetics or poor ROP initiation. With complex kinetics or poor initiation (not all catalysts are actively performing the catalysis due to incomplete initiation), the catalyst concentration that is actually working for the ROP will not be the same as the overall concentration of catalyst that present in the solution, therefore resulting in random initial reaction rate.

To investigate whether the epoxide ROP is 1st order with respect to monomer concentration, a series of semi-logarithmic plots was drawn with every different catalyst equivalent from Table 4.4. As conversion is the percentage of monomer that has polymerized, (1-conversion) is the percentage of free monomers, if the reaction is 1st order, its logarithmic plot will follow the equation:

$$\ln([M_0]/[M_t]) = kt$$

Where $[M_0]$ is the starting concentration of monomer, $[M_t]$ is the concentration of monomer at time t , t is time, k is rate constant. $[M_0]/[M_t] = 1/(1-\text{conversion})$. Should the reaction be 1st order, the semi-logarithmic plot will be a straight line with slope k .

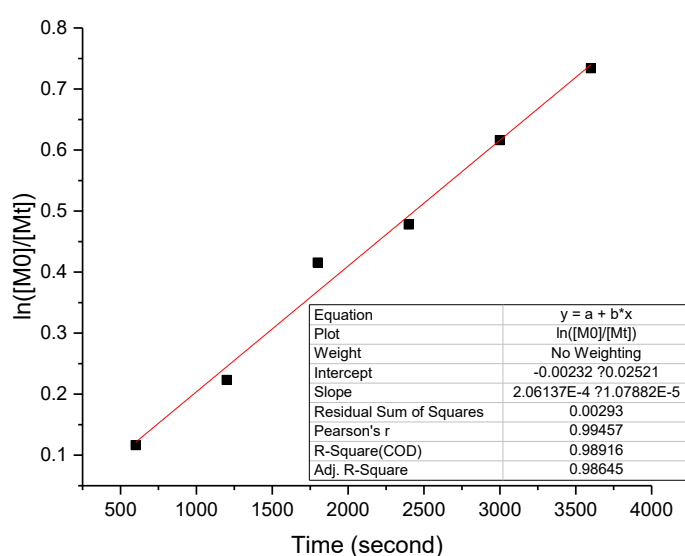


Figure 4.9: Semi-logarithmic plot for catalyst ratio = 1

The $R^2 = 0.989$ indicating a statistically satisfactory authenticity for the data points to follow a linear trend, based on the number of data points in the graph. The rate constant (slope of the straight line) $k = 2.06 \times 10^{-4}$.

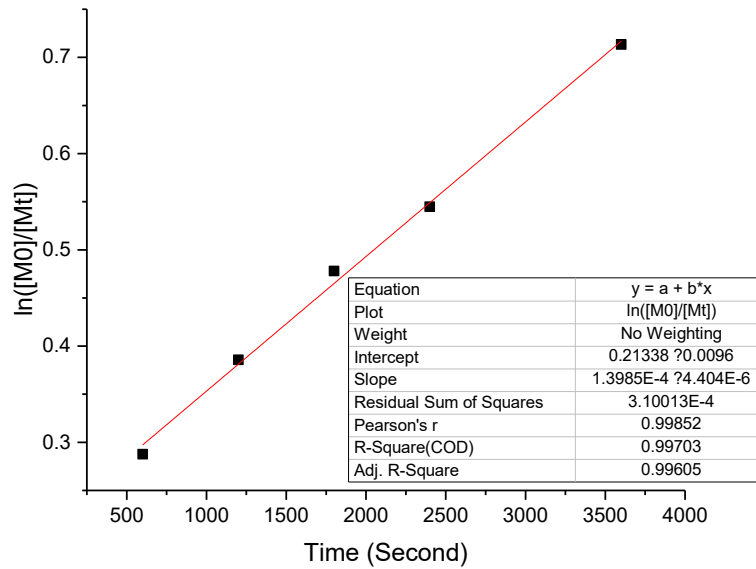


Figure 4.10: Semi-logarithmic plot for catalyst ratio = 1.25

The $R^2 = 0.997$ indicating a very good linear trend for 1.25 equivalent of catalyst, and the rate constant (slope of the straight line) $k = 1.40 \times 10^{-4}$.

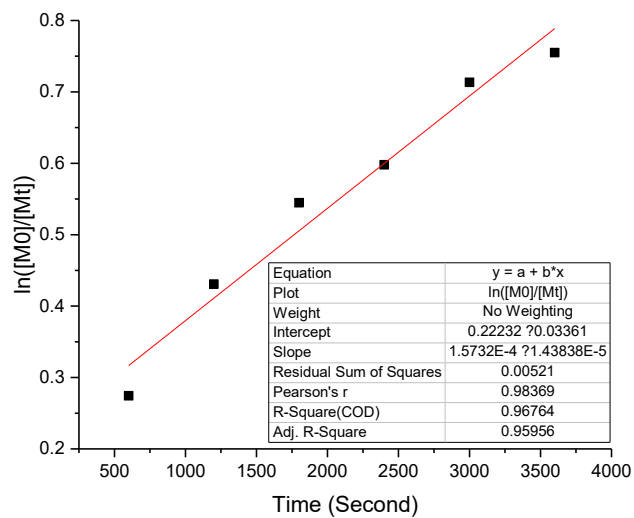


Figure 4.11: Semi-logarithmic plot for catalyst ratio = 1.5

$R^2 = 0.968$ means this set of data is less satisfactory than the previous two for a straight trend line. The rate constant for this graph is $k = 1.57 \times 10^{-4}$.

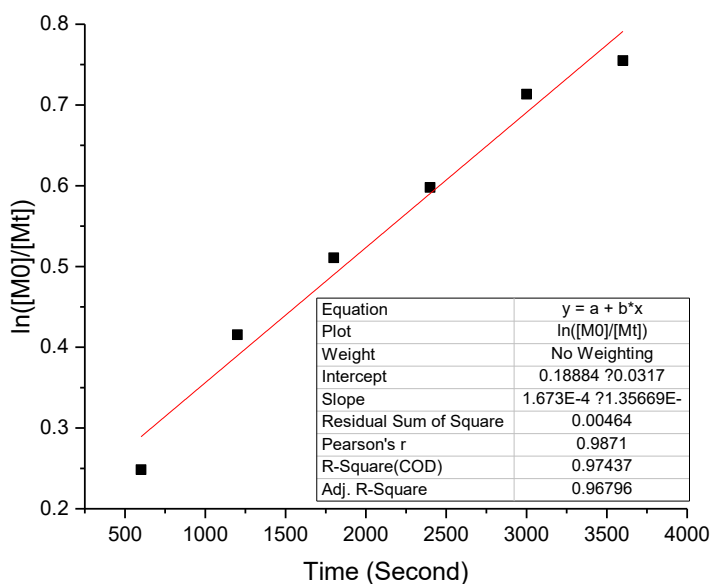


Figure 4.12: Semi-logarithmic plot for catalyst ratio = 1.75

$R^2 = 0.974$ with rate constant $k = 1.67 \times 10^{-4}$ for catalyst ratio = 1.75.

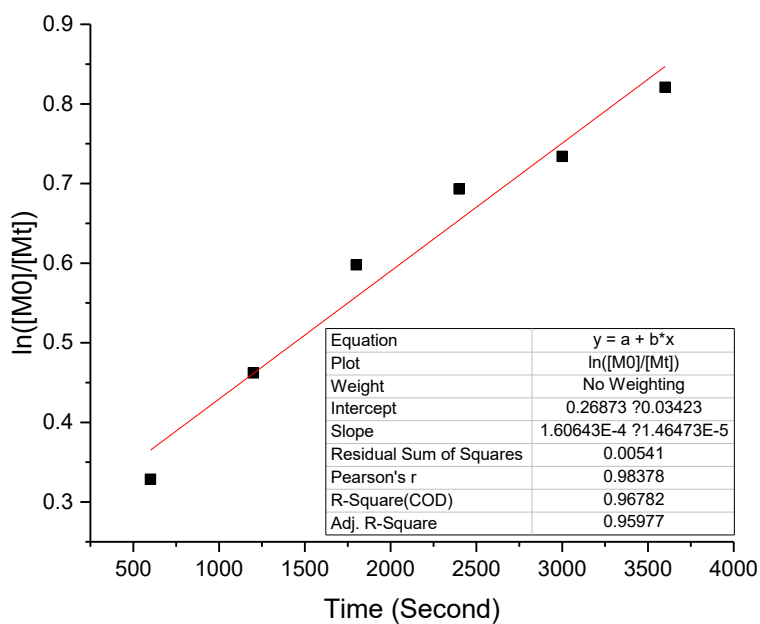


Figure 4.13: Semi-logarithmic plot for catalyst ratio = 2.0

$R^2 = 0.968$ with rate constant $k = 1.61 \times 10^{-4}$ for catalyst ratio = 2.0.

R^2 perspective, the fitting of the data points into a 1st order is satisfactory, as all R^2 values are above 0.95, ranging from 0.968 to 0.997. This indicates a good statistical authenticity of 1st order kinetics on epoxide monomer perspective.

The rate constants for all the semi-logarithmic plots are summarized in Table 4.6.

Cat. Ratio	1.0	1.25	1.5	1.75	2.0
k	2.06×10^{-4}	1.40×10^{-4}	1.57×10^{-4}	1.67×10^{-4}	1.61×10^{-4}

Cat. Ratio: catalyst ratio; k: rate constant.

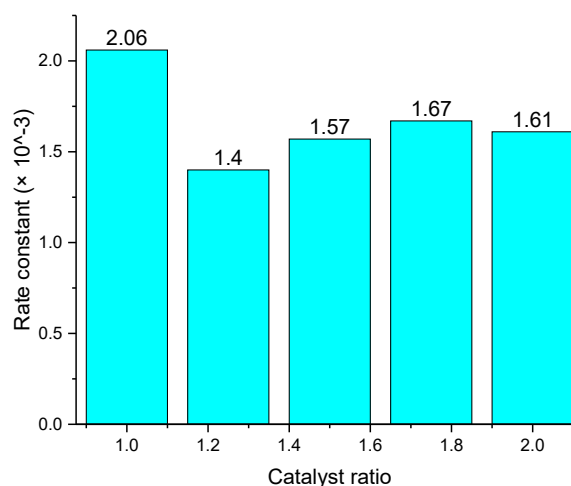


Figure 4.14: Rate constants of VCHO ROP with different catalyst ratio

From Figure 4.14 it can be seen that the rate constant is not greatly affected by the change of catalyst ratio, suggesting that they should theoretically be the same. To confirm how the errors during experimentation and NMR integration would affect the final determination of rate constant k , line of worst fit is done by drawing straight lines with maximum and minimum possible gradient within the error bars, for all 5 sets of data. For NMR integration, the error is usually within the range 0 to 10% conversion (absolute value, e.g., a 20% conversion could actually fall in the range

10 to 30% conversion). For the calculation here, the conversion error is set to be 5%, the middle point of 0% and 10%. The conversions of all the entries are generally in the range 10 to 60%, leading to a general $\{1/(1-\text{conversion})\}$ error of 7 to 11%, which will be averaged to 9%. Since $\ln([M_0]/[M_t]) = \ln \{1/(1-\text{conversion})\}$, by log rules, we therefore have:

$$\text{Maximum error of } \ln([M_0]/[M_t]) = \ln\{(1 \pm 0.09)([M_0]/[M_t])\} = \ln(1 \pm 0.09) + \ln([M_0]/[M_t])$$

$\ln(1.09) = 0.086$, and $\ln(0.91) = -0.094$, the y-axis average error is thus ± 0.09 .

The timing of reaction was done by electronic stopwatch, and theoretically have an error of ± 1 second, which will be neglected here since reactions times are generally hundreds to thousands to seconds, ± 1 second would make little difference and not worthy to be involved in error estimation.

The lines of worst fit are therefore drawn according to the assumptions made above, the rate constant k and their differences between line of best fit k (which are the errors) obtained from the line of worst fit plots are listed in Table 4.7.

Table 4.7: Line of worst fit rate constants and errors

Cat. ratio	1.00	1.25	1.50	1.75	2.00
Worst fit k (10^{-4})	1.46	0.82	1.00	1.09	1.04
Error (10^{-4})	± 0.6	± 0.58	± 0.57	± 0.58	± 0.57

Cat. Ratio: catalyst ratio.

The rate constants k vs. catalyst ratio plot was then drawn with error bars.

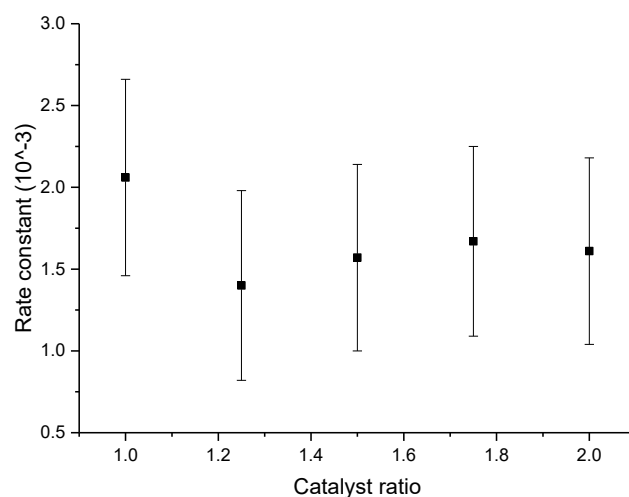


Figure 4.15: rate constant vs. catalyst ratio with error bar

As shown in Figure 4.15, a horizontal straight line can definitely be drawn across the error bars of all 5 data points, suggesting that changing catalyst ratio applies little effect on the reaction rate. This leads to the hypothesis that varying the amount of catalyst does not change the number of initiating aluminium centres, e.g., most of the catalysts are inactive, only a small and relatively unchanged amount of catalyst molecules are actually initiating the epoxide ROP.

To confirm whether these data sets lead to a 2nd order mechanism, the $1/[M_t] - 1/[M_0]$ vs. time plot is drawn for every different catalyst ratio from Table 4.4. For a second order reaction, the rate equation can be expressed by:

$$1/[M_t] - 1/[M_0] = kt$$

Where M_t is the concentration of monomer at any given time t , M_0 is the initial concentration of monomer, k is the rate constant and t is reaction time. $1/[M_t]$ can therefore be calculated by:

$$1/[M_t] = 1/\{[M_0] \times (1 - \text{conversion})\}$$

The $1/[M_t] - 1/[M_0]$ vs. t plots are drawn as followed.

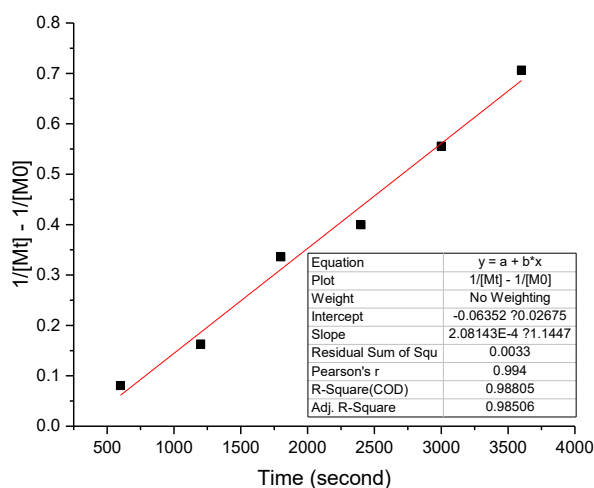


Figure 4.16: $1/[M_t] - 1/[M_0]$ vs. t plot for catalyst ratio = 1.0

The data point distributed almost evenly on both sides of the linear fitting line, with an $R^2 = 0.988$, slightly lower than the R^2 value of the semi-logarithmic plot for the same set of data. Rate constant $k = 2.08 \times 10^{-4}$.

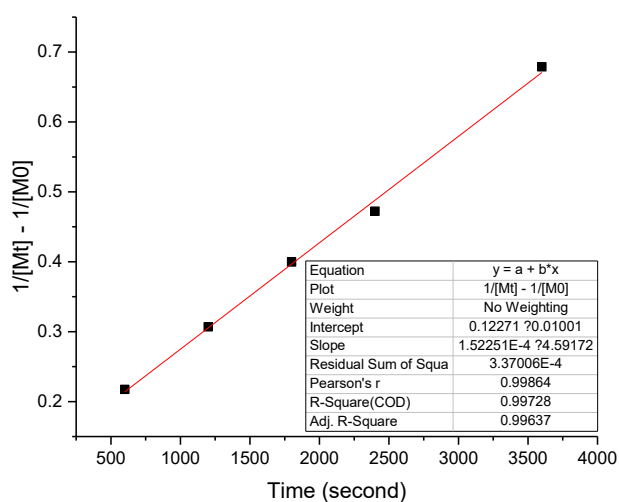


Figure 4.17: $1/[M_t] - 1/[M_0]$ vs. t plot for catalyst ratio = 1.25

This plot again has a good linear fitting line with $R^2 = 0.997$, about the same as the R^2 value of the semi-logarithmic plot for the same set of data. Rate constant $k = 1.52 \times 10^{-4}$.

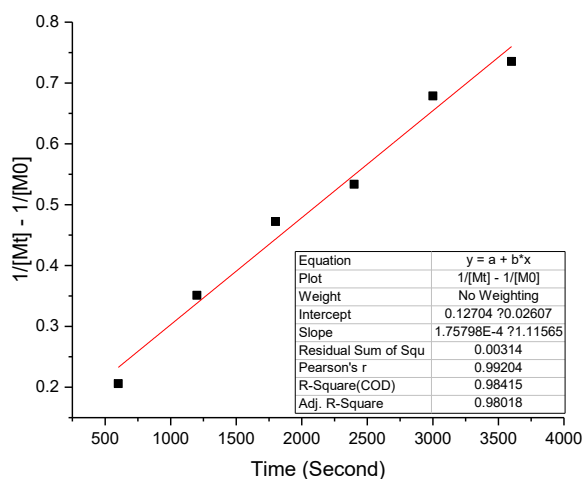


Figure 4.18: $1/[M_t] - 1/[M_0]$ vs. t plot for catalyst ratio = 1.50

Linear fitting line has an $R^2 = 0.984$, higher than R^2 for the semi-logarithmic plot (0.968) for the same set of data. Rate constant $k = 1.76 \times 10^{-4}$.

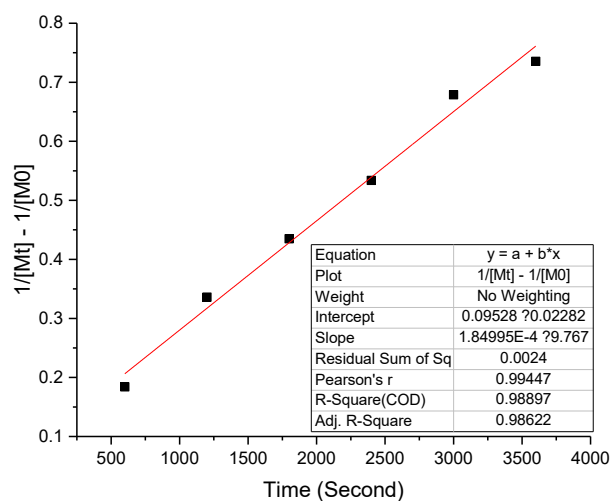


Figure 4.19: $1/[M_t] - 1/[M_0]$ vs. t plot for catalyst ratio = 1.75

The linear fitting line has an $R^2 = 0.989$, slightly higher than the 0.974 for semi-logarithmic plot. Rate constant $k = 1.85 \times 10^{-4}$.

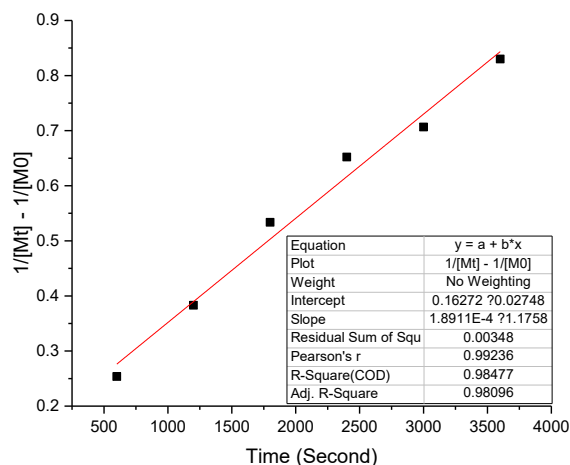


Figure 4.20: $1/[M]_t - 1/[M]_0$ vs. t plot for catalyst ratio = 2.00

The linear fitting line has an $R^2 = 0.985$, slightly higher than the 0.968 for semi-logarithmic plot of the same set of data. Rate constant $k = 1.89 \times 10^{-4}$.

The rate constant k from all 5 sets of data are summarized in Table 4.8.

Table 4.8: Rate constants of the 2nd order plot for VCHO ROP

Cat. Ratio	1.00	1.25	1.50	1.75	2.00
k	2.08×10^{-4}	1.52×10^{-4}	1.76×10^{-4}	1.85×10^{-4}	1.89×10^{-4}

Cat. Ratio: catalyst ratio; k : rate constant.

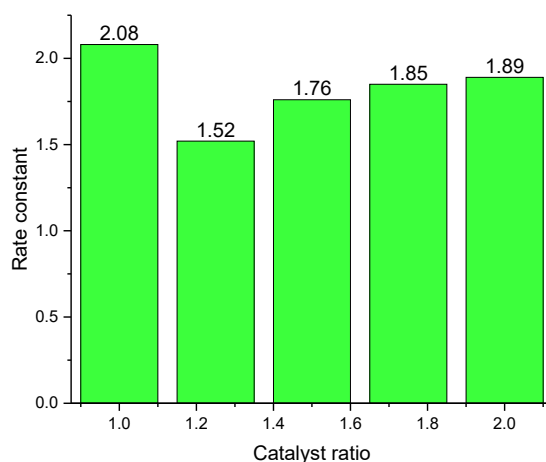


Figure 4.21: Rate constants of VCHO ROP with different catalyst ratio

Similar to the 1st order rate constants, the 1.0 equivalent data gave much higher k comparing to all other catalyst ratios. From 1.25 equivalent to 2 equivalents of catalysts the rate constant saw a general increase but with diminishing increase as the catalyst ratio gets higher. Same as 1st order rate constants, errors from line of worst fit are obtained and summarized in Table 4.9 and Figure 4.22 to evaluate whether these data are within error to each other. The average error from the conversion is set to 5% (absolute value) as well, and the errors in $1/[M_t] - 1/[M_0]$ is therefore calculated to be ± 0.135 .

Table 4.9: Rate constants and errors from the lines of worst fit

Cat. Ratio	1.00	1.25	1.50	1.75	2.00
Worst fit k (10^{-4})	1.19	0.64	0.87	0.94	1.02
Error (10^{-4})	± 0.89	± 0.88	± 0.89	± 0.91	± 0.98

Cat. Ratio: catalyst ratio.

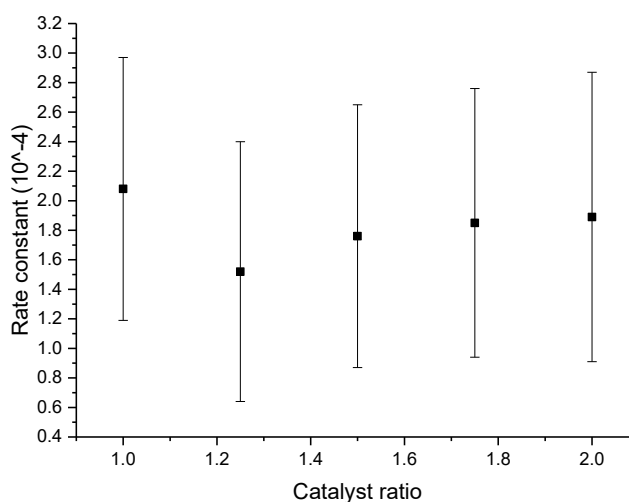
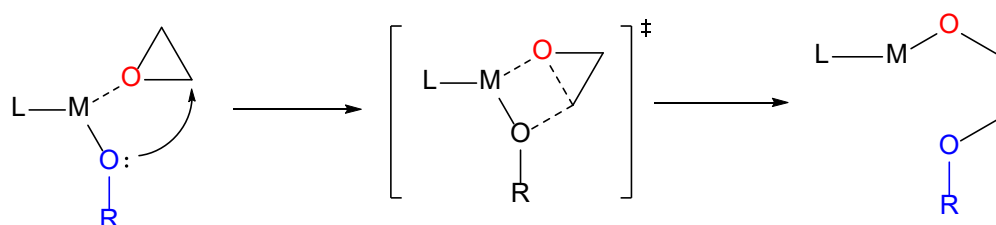


Figure 4.22: Rate constant vs. catalyst ratio plot with error bars

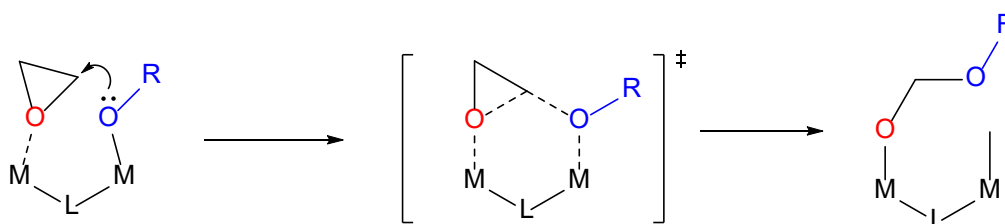
As shown in Figure 4.22, horizontal lines can definitely be drawn through the error bars of all five data points. Therefore, the same conclusion can be drawn from the 2nd order as well: the catalyst concentration does not affect the reaction rate constant. Thus, only a small and relatively unchanged amount of catalysts were

undertaking the catalysis while other catalyst molecules are not involved in the catalytic cycle (i.e., the extra catalyst molecules are not properly activated thus not performing the catalysis as they supposed to).

Many investigations of the ROP homopolymerization reactions with metal complexes reported their kinetics to be 1st order,^{19–21} even the bimetallic ones.^{22,23} However, very few papers have reported epoxide ROP with multi-nuclear complexes to be second order.²⁴ The reports regarding 1st order epoxide ROP with bimetallic complexes proposed that the ROP proceed via bimetallic cooperative mechanism, as shown in Scheme 4.4.



High energy monometallic epoxide ROP 4-membered ring transition state

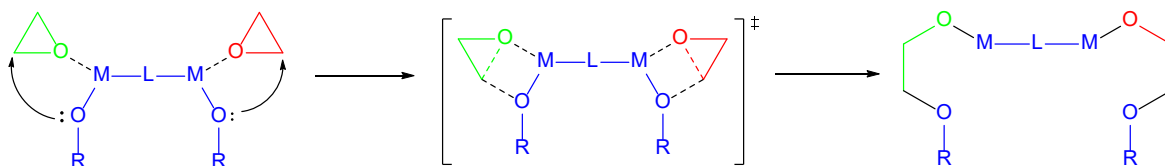


Low energy bimetallic cooperative epoxide ROP 6-membered ring transition state

Scheme 4.4: Comparison between monometallic and bimetallic epoxide ROP mechanism,²¹ 6-membered transition state is assuming then bridging ligand to be a single ion / atom

As shown in the scheme, in a bimetallic cooperative mechanism utilizing both metal centres: one binds to the propagation polymer chain, another accepts the incoming free monomer unit. The incoming epoxide monomer, polymer chain and metal complexes then form a 6-membered ring (or larger) transition state, which would reduce the ring strain thus decreasing the transition state energy and results in faster reaction / lower temperature requirement.

If the assumption is made that each metal centre in a bimetallic catalyst molecule has one polymer chain growing on them individually, the mechanism would be:



Scheme 4.5: Individual double chain growth for bimetallic catalyst

The mechanism in Scheme 4.5 has two individual chain growing on both metal site, but as the two polymer chains grow individually, the overall reaction is still 1st order with respect to epoxide monomer. Nevertheless, both suggested mechanisms should exhibit 1st order kinetics with respect to the catalyst, while the $\ln(\text{initial rate})$ vs. $\ln(\text{complex 1 concentration})$ plot failed to give any meaningful straight line. This is possibly because of the solidification of polyethers around several spots, thermal decomposition of catalyst, or complex / incomplete initiation as have mentioned before. Also, the double chain bimetallic mechanism means the chance of entanglement of the two chains on the same catalyst molecule and mutual steric hinderance effect of the two chains on each other would become much larger, again potentially causing unexpectedly slower reaction rates. It is possible that this phenomenon becomes more severe as the concentration of the catalyst goes up, which possibly explains why the 1.0 equivalent reaction has a higher rate constant, as higher catalyst concentration would result in higher extent of solidification and immobilization of catalysts, effectively reducing the number of active centres. For all the catalysis data in this chapter, it is assumed that the number of active catalyst molecules equals to the number of catalyst molecules present in the reaction and remains constant throughout the reaction. The failure to give any informative line of best fit for determining order of reaction with respect to the catalyst ratio (Figure 4.8) and the fact that for both 1st and 2nd order (with respect to substrate) calculation the rate of reaction is virtually not affected by the ratio of catalyst indicated that most of the catalyst molecules are inactive. Thus, the order of reaction with respect to the catalyst remain undetermined, as has been discussed above.

Performance wise, the room temperature catalytic performance can be regarded as good. Several previous samples of aluminium-based epoxide ROP catalysts are listed in Figure 4.23, with their performances summarized in Table 4.10.

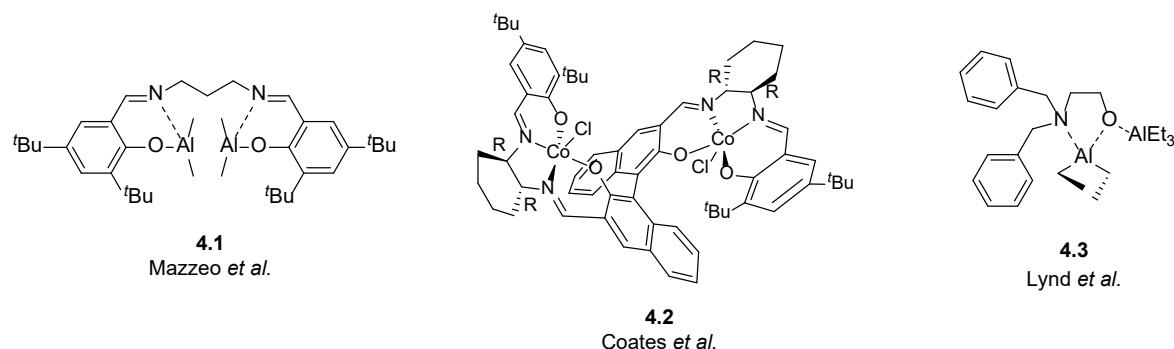


Figure 4.23: Structures of examples of reported aluminium-based epoxide ROP catalysts^{22,25,26}

Table 4.10: Performances of several aluminium-based catalysts

Cat.	Co-cat.	Epoxide	Ratio	Sol.	Temp./°C	Time/min	Conv./%
1	N/A	ECH	1:0:400	N/A	100	25	61
1	N/A	CHO	1:0:800	N/A	30	10	67
1	N/A	PO	1:0:400	N/A	100	25	10
1	N/A	VCHO	1:0:800	Tol. ^a	20	4	75
4.1	<i>i</i> PrOH	CHO	1:4:750	N/A	70	15	85
4.1	N/A	CHO	1:0:250	N/A	20	20	40
4.2	4.4	PO	1:1:4000	DME ^b	0	30	44
4.2	KOAc	PO	1:1:4000	DME ^b	20	1440	<1
4.3	N/A	ECH	1:0:430	N/A	80	2880	99
4.3	N/A	BO	1:0:350	N/A	70	5760	90

^a: 1 : 1 solvent : epoxide volume ratio; ^b: 12 : 1 solvent : epoxide volume ratio; Cat.: catalyst; Co-cat.: co-catalyst; Ratio: [Cat]:[Co-cat]:[Monomer]; Sol.: solvent; Temp.: temperature; Conv.: conversion; *i*PrOH: isopropyl alcohol; KOAc: potassium acetate; BO: butylene oxide; Tol.: toluene; DME: dimethoxyethane; 4.4: [(PPh₃)₂N]⁺[MeCO₂]⁻.

As shown in the table, ECH (epichlorohydrin) ROP with **1** is much faster compared to **4.3**, although **1** operates at a temperature 20°C higher than that of **4.3**, the much shorter reaction time with acceptable conversion justified the activity of **1**.

CHO (cyclohexene) wise, **1** and **4.1** exhibit comparable conversions, but **4.1** requires 4 equivalents of co-catalyst and operates at 70°C. For ROP catalyzed by **4.1**, Mazzeo *et al.* proposed a bimetallic cooperative mechanism as well, which is similar to the bimetallic mechanism in Scheme 4.4.

PO (propylene oxide) wise, as we have concluded before, complex **1** does not give any appreciable conversion even at 100°C, thus far outperformed by catalyst **4.2**. Noticeably, Coates and co-workers also proposed similar bimetallic cooperative mechanism for their catalyst. Generally, most bimetallic catalysts are considered to catalyze ROP reactions via bimetallic mechanism and having 1st order kinetics, which makes **1** a novel case. Also, from the performance comparisons that have been made above, the high-energy 4-membered ring transition state monometallic mechanism that is happening on both aluminium centre of **1** does not render it to be a low activity catalyst comparing to those that have low-energy 6-member ring transition states. It can be interfered that the concurrent double chain propagation on the same complex molecule compensates for the high-energy transition state and make the catalyst overall more efficient. To add up to the high activity, the fact that **1** does not require any co-catalyst to be catalytically active increases its industrial application potential as the cost of co-catalyst can be saved.

Although the examples of previously reported aluminium complexes do not provide data about VCHO ROP (which expected to be similar to CHO ROP theoretically), the room temperature swift catalysis of VCHO ROP with **1** can be regarded as above average performance as well.

4.3. Conclusions

In this chapter, the capability and performance of the $[(\text{CpHO})_2\text{Al}_2\text{Me}_4]$ (**1**) towards ring-opening polymerization of epoxides have been probed and discussed. Despite the fact that many previous aluminium-based catalysts are slow in epoxide ROP, **1** has shown high activity at room temperature, and even too active that dilution is needed for proper undertaking of ROP. Generally, $[(\text{CpHO})_2\text{Al}_2\text{Me}_4]$ (**1**) has proven itself to be an effective and efficient catalyst for ROP of CHO, VCHO and ECH. Although the reaction could be too fast and uncontrollable when epoxide monomers are of high concentrations, it can be controlled by adding solvents.

At all tested reaction temperatures, **1** does not require any co-catalyst for epoxide ROP catalysis to be successfully performed. This fact is consistent with the low epoxide / anhydride ring-opening co-polymerization selectivity that have been seen in Chapter 3, again proving **1** to be highly active towards epoxide ROP. Therefore, the hypothesis made in Chapter 3 that **1** is more suitable for epoxide ROP has been justified.

4.4. References

- 1 GLYCIDOL (2,3-EPOXY-1-PROPANOL), <http://www.chemicaland21.com/specialtychem/finechem/GLYCIDOL.htm>, (accessed 15 December 2020).
- 2 International Agency for Research on Cancer, Ed., *IARC monographs on the evaluation of carcinogenic risks to humans, volume 97, 1,3-Butadiene, ethylene oxide and vinyl halides (vinyl fluoride, vinyl chloride and vinyl bromide): this publication represents the views and expert opinions of an IARC Working Group on the Evaluation of Carcinogenic Risks to Humans, which met in Lyon, 5 - 12 June 2007*, WHO, Lyon, 2008.

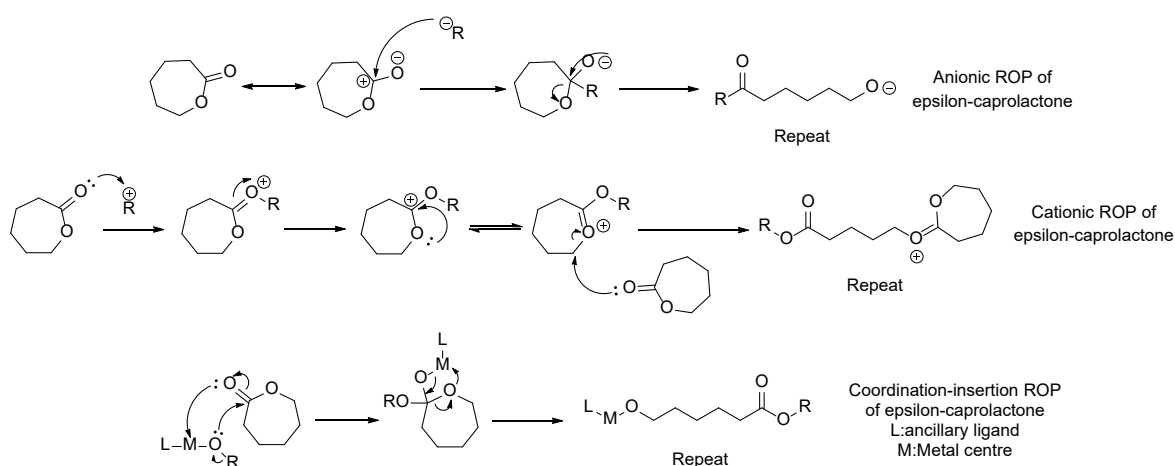
- 3 Food Additive Status List, <https://www.fda.gov/food/food-additives-petitions/food-additive-status-list>, (accessed 16 December 2020).
- 4 Chemical Hope, <https://www.sciencehistory.org/distillations/chemical-hope>, (accessed 16 December 2020).
- 5 M. Ganji, M. Docter, S. F.J. Le Grice, E. A. Abbondanzier, *Nucleic Acid Res.*, 2016, **44**, 8376–8384.
- 6 A. Prabhakar, D. K. Chattopadhyay, B. Jagadeesh and K. V. S. N. Raju, *J. Polym. Sci. A Polym. Chem.*, 2005, **43**, 1196–1209.
- 7 M. Kitis, C. D. Adams and G. T. Daigger, *Water Research*, 1999, **33**, 2561–2568.
- 8 O. Nuyken and S. Pask, *Polymers*, 2013, **5**, 361–403.
- 9 B. Ochiai and T. Endo, *J. Polym. Sci. A Polym. Chem.*, 2007, **45**, 2827–2834.
- 10 Y. Sarazin and J.-F. Carpentier, *Chem. Rev.*, 2015, **115**, 3564–3614.
- 11 A.-L. Brocas, C. Mantzaridis, D. Tunc and S. Carlotti, *Progress in Polymer Science*, 2013, **38**, 845–873.
- 12 Y. Watanabe, T. Yasuda, T. Aida and S. Inoue, *Macromolecules*, 1992, **25**, 1396–1400.
- 13 T. S. Anderson and C. M. Kozak, *European Polymer Journal*, 2019, **120**, 109237.
- 14 P. Chen, M. H. Chisholm, J. C. Gallucci, X. Zhang and Z. Zhou, *Inorg. Chem.*, 2005, **44**, 2588–2595.
- 15 M.-A. Munoz-Hernandez, M. L. McKee, T. S. Keizer, B. C. Yearwood and D. A. Atwood, *J. Chem. Soc., Dalton Trans.*, 2002, 410–414.

- 16 S. Asano, T. Aida and S. Inoue, *J. Chem. Soc. Chem. Commun.*, 1985, **442**, 1148–1149.
- 17 K. D. Papadimitriou, F. Paloukis, S. G. Neophytides and J. K. Kallitsis, *Macromolecules*, 2011, **44**, 4942–4951.
- 18 M. J. Kade, D. J. Burke and C. J. Hawker, *J. Polym. Sci. A Polym. Chem.*, 2010, **48**, 743–750.
- 19 J. Imbrogno, R. C. Ferrier, B. K. Wheatle, M. J. Rose and N. A. Lynd, *ACS Catal.*, 2018, **8**, 8796–8803.
- 20 J. E. Puskas, Y. Chen and M. Tomkins, *European Polymer Journal*, 2003, **39**, 2147–2153.
- 21 M. I. Childers, J. M. Longo, N. J. Van Zee, A. M. LaPointe and G. W. Coates, *Chem. Rev.*, 2014, **114**, 8129–8152.
- 22 F. Isnard, M. Lamberti, L. Lettieri, I. D'auria, K. Press, R. Troiano and M. Mazzeo, *Dalton Trans.*, 2016, **45**, 16001–16010.
- 23 R. C. Ferrier, S. Pakhira, S. E. Palmon, C. G. Rodriguez, D. J. Goldfeld, O. O. Iyiola, M. Chwatko, J. L. Mendoza-Cortes and N. A. Lynd, *Macromolecules*, 2018, **51**, 1777–1786.
- 24 L.-C. Wu, A.-F. Yu, M. Zhang, B.-H. Liu and L.-B. Chen, *J. Appl. Polym. Sci.*, 2004, **92**, 1302–1309.
- 25 A. M. DiCiccio and G. W. Coates, *J. Am. Chem. Soc.*, 2011, **133**, 10724–10727.
- 26 C. G. Rodriguez, R. C. Ferrier, A. Helenic and N. A. Lynd, *Macromolecules*, 2017, **50**, 3121–3130.

Chapter 5: Ring-opening polymerization of ϵ -Caprolactone with $[(\text{CpHO})_2\text{Al}_2\text{Me}_4]$ (1)

5.1. Introduction

To comply with more environmental concerns and requirements raised by governments and associations, biodegradable polymers are now taking more and more vital roles in the synthetic polymer related industries. Among all the biodegradable polymers, poly(ϵ -caprolactone) (PCL) is one of the polymers that has attracted lots of attentions due to its excellent biomedical and pharmaceutical applications.^{1,2} Typical PCL has a melting point around 59 to 64°C,¹ and its outstanding blend-compatibility / biocompatibility are the reasons for its extensive application in the biomedical area. Generally speaking, PCL can be synthesized via ring-opening polymerization (ROP) of ϵ -caprolactone (ϵ -CL) with various catalysts (anionic, cationic or coordination insertion mechanisms), or via free radical ring-opening polymerization of 2-methylene-1-3-dioxepane.¹ Some typical PCL synthetic routes are illustrated in Scheme 5.1.



Scheme 5.1: Typical PCL synthetic routes^{3,4}

To synthesize PCL with higher efficiency and lower costs, enormous efforts have been put into researching this field by scientist around the world. The extensive

research into this area has yielded lots of good papers and reviews; several most commonly used metals for catalysts are: aluminium,⁵⁻⁷ magnesium,⁸⁻¹⁰ titanium,¹¹⁻¹³ lanthanides¹⁴⁻¹⁶ and calcium.¹⁷⁻¹⁹ Among all the metal-based catalysts, aluminium-based catalysts have shown good efficiency but have a propensity to be rather slow. Some of the conversions of metal complex catalysts from previous reports are listed in Table 5.1. It can be seen from the table that the lanthanides generally give higher conversion with much lower temperature requirements.

Table 5.1: Catalytic results of some previous catalysts for PCL synthesis

Metal	[ϵ -CL]:[M]	Temp./ $^{\circ}$ C	Time/min	Conv./%
Al ²⁰	150:1	25	360	99
Al ²¹	100:1	70	15	99
Al ²²	100:1	80	10	94
Sm ¹⁴	135:1	21	5	84
Nd ¹⁵	100:1	30	60	88
La ¹⁶	1500:1	20	20	100

Metal: the central metal ion of the complex; Conv.: conversion; Temp.: temperature; [M]: concentration of metal complex.

In this chapter, the complex [(CpHO)₂Al₂Me₄] (**1**), which was reported in chapter 2 and chapter 3 in the context of ring-opening co-polymerization, has been used as a catalyst for the ring-opening polymerization of ϵ -caprolactone.

5.2. General procedure for ϵ -caprolactone ring-opening polymerization

In the glove box under a nitrogen atmosphere, [(CpHO)₂Al₂Me₄] (**1**) (12 mg, 2.11×10^{-5} mol, 0.5 equivalent, equals to 1.0 equivalent of aluminium metal centre as the complex is bimetallic) was added into an oven-dried screw-cap vial. ϵ -caprolactone (333.3 equivalents with respect to aluminium centre, [Al centre] : [ϵ -CL] = 1.2 : 400) was then added, followed by the addition of benzyl alcohol co-catalyst (1.0

equivalent with respect to aluminium centre). Toluene was then added into the vial as the solvent for the reaction. The vial was then sealed, taken out of the glove box and put into a pre-heated aluminium heating block (unless the reaction was undertaken at room temperature). The reaction mixture was then stirred at the designated temperature for a certain amount of time. Upon finishing, the vial was opened, and methanol was injected to quench the reaction. The remaining reaction mixture was washed into a beaker with n-hexane, and n-hexane was added into the beaker to precipitate the polymer. Mixture was then filtered by gravitational filtration, air-dried, then dried on rotary evaporator to a constant weight.

BnOH was used in 2 : 1 ratio to the catalyst since complex **1** is bimetallic, and each metal centre would theoretically need an equivalent of BnOH to serve as catalyst.

5.2.1. General procedure for PCL film preparation

After quenching the reaction mixture (as detailed above), the reaction mixture was directly transferred into a round bottom flask and put onto the rotary evaporator. The mixture was then dried under reduced pressure until appeared to be a clear film at the bottom of the round bottom flask. The round bottom flask was then heated with a heat gun until the film turned white. The film was then be scratched off the bottom, and the appearance is as illustrated in Figure 5.1 below.



Figure 5.1: Picture of prepared PCL film

5.2.2. Characterization and evaluation of the obtained polymer

The polymers prepared by the ring-opening polymerization of ϵ -caprolactone by $[(\text{CpHO})_2\text{Al}_2\text{Me}_4]$ (**1**) were analyzed by ^1H NMR spectroscopy, Gel Permeation Chromatography (GPC) and Matrix-Assisted Laser Desorption-Ionization Time of Fly Mass Spectrometry (MALDI-ToF MS).

To evaluate the conversion of the ϵ -caprolactone monomer to its polymer, ^1H NMR spectra were used. The stacked ^1H spectra of ϵ -caprolactone and PCL are provided in Figure 5.2.

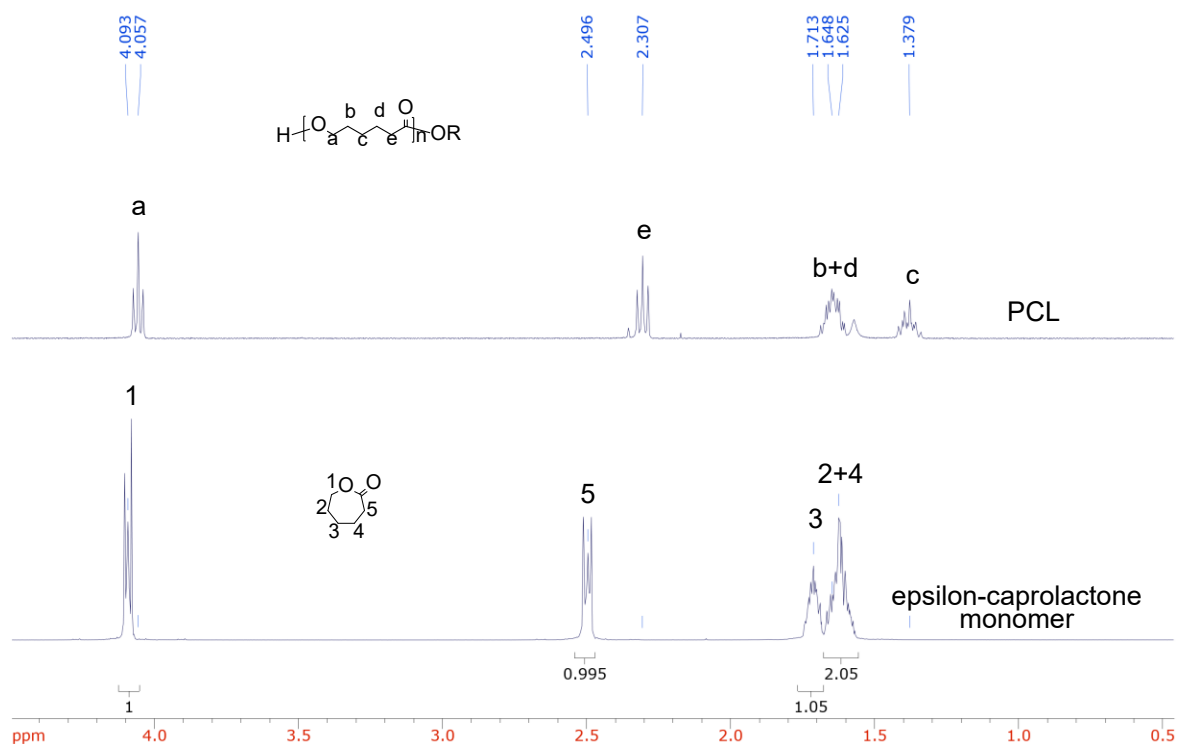


Figure 5.2: Stacked ^1H NMR spectra (400 MHz, CDCl_3 , 293 K) of ϵ -caprolactone monomer and PCL

As can be seen from Figure 5.2, the multiplet at 2.50 and 2.31 ppm, which correspond to the ester alpha protons in monomer and PCL respectively (H^5 for ϵ -caprolactone, H^a for PCL) showed a prominent change in chemical shift going from monomer to polymer. In monomer, H^5 has its peak positioned at 2.50 ppm. While in polymer, H^e has its peak positioned at 2.31 ppm, which is about 0.19 ppm away from the original monomer's ester α proton signal. This provides a pivotal handle for us to calculate the conversion of the monomer by comparing the integration of the peak corresponding to the monomer and the polymer. A series of stacked 1H NMR spectra with different conversions (Figure 5.3) is provided as below.

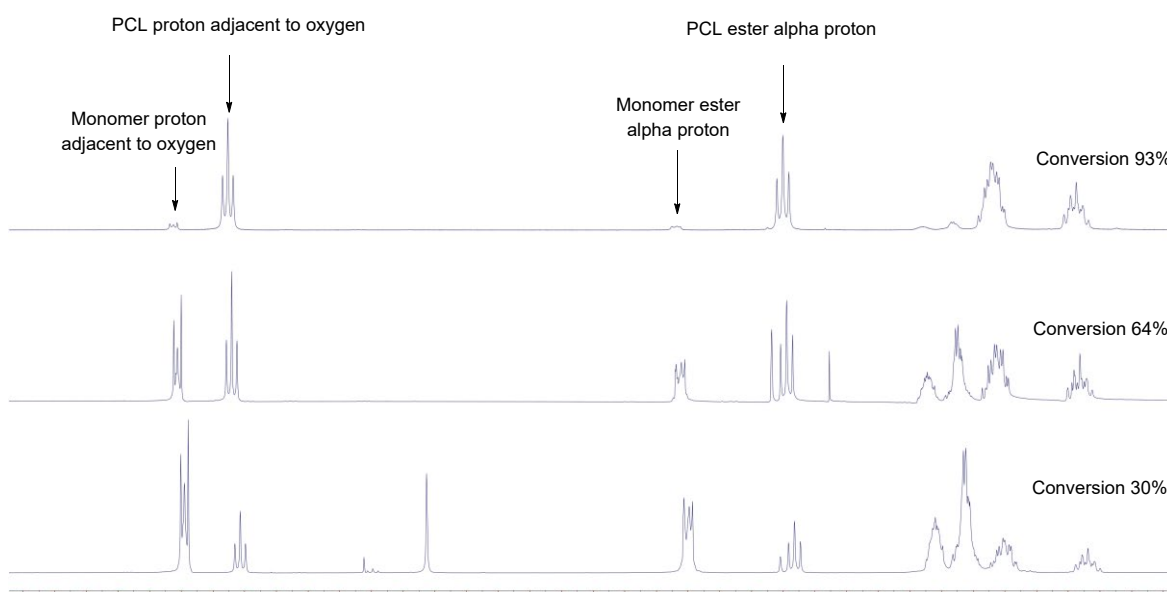


Figure 5.3: Stacked 1H NMR spectra (400MHz, $CDCl_3$, 293 K) of polymers with different conversions

As the figure suggested, obvious depletion of the monomer's proton signals can be observed when conversion goes up. The PCL and monomer peaks are far away from each other; thus no overlapping issue would occur. The conversion is therefore calculated by:

$$\text{Conversion} = \frac{\text{integration of PCL ester alpha proton}}{\text{integration of PCL and } \epsilon\text{-CL ester alpha proton}}$$

Equally, integrations of oxygen-adjacent protons can be used in the same way for conversion calculation.

The M_n and M_w values of PCL samples were obtained from GPC analyses, and the polydispersity indices (\mathcal{D}) were calculated according to the formula:

$$\mathcal{D} = M_w / M_n$$

In which M_w is weight average molecular weight and M_n is number average molecular weight.

For the polymers which were successful in MALDI-ToF analysis, the M_w , M_n and \mathcal{D} are also determined and compared with GPC results.

5.2.3. ϵ -caprolactone polymerization results

The reactant stoichiometry, temperature, reaction time, M_n , M_w , \mathcal{D} and conversion are recorded for each entry and presented in tables in this section.

5.2.3.1. Scoping Reaction Conditions

Each catalyst will operate within a different set of reaction conditions, and whilst the most desirable situation is when the boundaries of acceptable reaction conditions are broad (thereby giving a versatile catalyst system), the reality may be less ideal. It is therefore of the utmost importance to determine the optimum and the range of reaction conditions for a new catalyst; parameters to consider include stoichiometry, reaction time, temperature, and co-catalyst. To achieve optimization, several polymerization reactions were undertaken, and the results summarized in Table 5.2. Conversions are rounded to the nearest integer to compensate for the possible inaccurate integrations of NMR spectra. Equivalentents are calculated by molar ratio per metal centre, thus 1 equivalent of complex **1** is consider as 2 equivalentents of metal centre, since complex **1** is a dimer.

Table 5.2: Optimization stage polymerization result

Entry	ϵ -CL:Cat:Co	Temp/°C	Time/h	Co-catalyst	Conversion/%
1	400:1:1	80	24	PPNCl	23
2	400:1:1	80	24	BnOH	100
3	400:1:0	80	24	N/A	100
4	400:1:1	60	24	BnOH	100
5	400:1:1	40	24	BnOH	100
6	400:1:1	20	24	BnOH	100
7	400:1:1	20	1	BnOH	30
8	400:1:0	20	1	N/A	12
9	400:1.2:1.2	20	1	BnOH	45

ϵ -CL: ϵ -caprolactone; Cat: catalyst; Co: co-catalyst

Initial studies were performed at 80 °C; elevated temperatures are routine for aluminium catalysts in ring-opening polymerization.^{22–24} From Table 5.2 we can see that complex **1** give superior performance in ϵ -caprolactone (ϵ -CL) polymerization when used in conjunction with BnOH co-catalyst, entry 1 vs. 2 and entry 7 vs. 8; conversely the addition of PPNCl actually reduces the catalytic performance. At 80°C, use of PPNCl leads to sharp fall of conversion from 100% to 23% (Entries 1 and 3). Secondly, the reaction does not require any heating to proceed (Entries 2, 4, 5 vs. 6), it is spontaneous at room temperature, with relatively high speed, giving 45% conversion after 1 hour at 20°C with BnOH co-catalyst. These findings illustrate that **1** is a highly active catalyst for ϵ -CL ROP. According to past literature reports, many of the aluminium complexes require heating for efficient catalysis, the temperature standards are usually around 50-100°C. For example, Sarazin *et al.* developed a series of Al-salen catalysts, which operate at 50, 70 or 90°C for ROP of lactides,²⁴ whilst Li *et al.* reported a series of Al-ketiminato complexes that run at 80°C for ROP of ϵ -CL and lactides²² (structures illustrated in Figure 5.4). Similarly, Jones and co-workers reported several Al-salalen complexes which catalyze the ROP of lactides and ϵ -CL at 80°C,²³ and Bolley and co-workers reported chloro- ϵ -CL polymerization with aluminium complexes at 90°C.²⁵ Generally, room

temperature-operatable aluminium-based catalysts are not commonly seen for ROP. As for other metal complex catalysts such as lanthanide complexes, the ϵ -CL ROP could be a lot quicker, as stated in section 3.1.

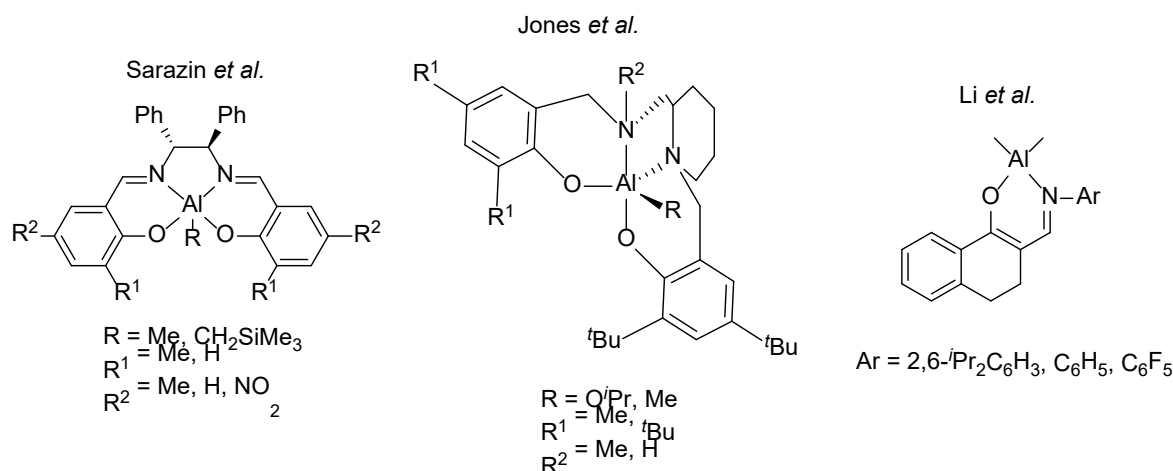


Figure 5.4: Structure of previously reported Al catalysts

These preliminary scoping studies indicate that $[(\text{CpHO})_2\text{Al}_2\text{Me}_4]$ (**1**) is highly active for ϵ -caprolactone polymerization, that 20°C is the most appropriate temperature for further studies, and that BnOH should be used to enhance its catalytic performance.

Having established the most appropriate operating parameters for the catalytic system, the ring-opening polymerization reaction was monitored over time to obtain greater insight into the catalytic performance. Polymerization data showing monomer conversion vs. time are summarized in Table 5.3 and Figure 5.5. This set of data is a trial of the catalysis with complex **1**, and as the conversions calculated from proton NMR deviates upon repeating the same entry, the most sensible set of data has been picked and illustrated in Table 5.3.

Table 5.3: ϵ -CL ROP catalysis results

Entry	1	2	3	4	5
Time/min	60	80	120	166	180
Conversion/%	30	60	64	72	93

Reaction conditions: 20°C, BnOH as co-catalyst, ϵ -CL:catalyst:co-catalyst=400:1:1.

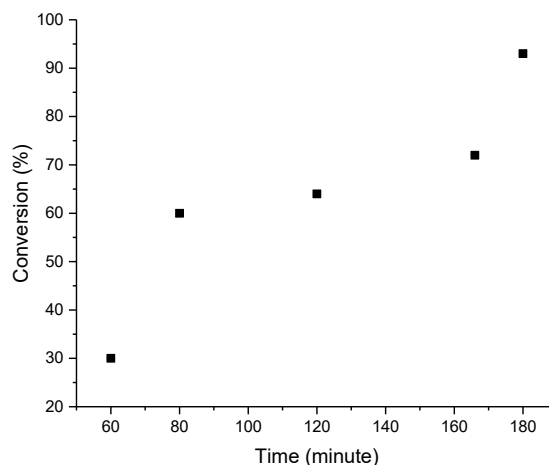


Figure 5.5: Conversion vs. Time plot, 1 equivalent of complex 1

The data points showed a general increasing trend, but the data points fluctuate too much that no solid conclusion can be drawn about the kinetics. Since the plot of conversion vs. time is not a straight line, which means the reaction is not 0th order with respect to monomer concentration, a semi-logarithmic plot (Figure 5.6) was then drawn to investigate if the reaction is first order with respect to monomer concentration. As conversion is the percentage of monomer that has polymerized, (1-conversion) is the percentage of free monomers, if the reaction is first order, its logarithmic plot will follow the equation:

$$\ln([M_0]/[M_t]) = kt$$

Where $[M_0]$ is the starting concentration of monomer, $[M_t]$ is the concentration of monomer at time t , t is time, k is rate constant. $[M_0]/[M_t] = 1/(1-\text{conversion})$

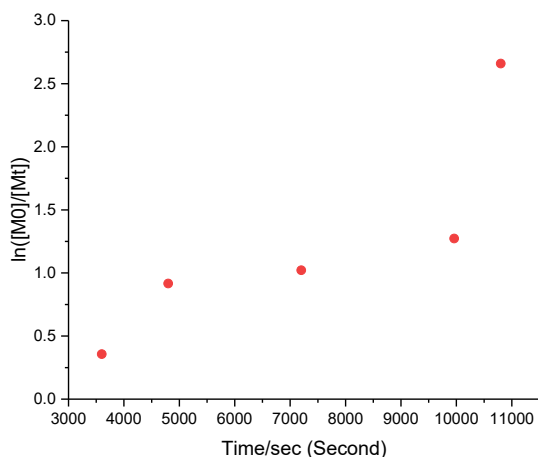


Figure 5.6: Semi-logarithmic plot of $\ln([M_0]/[M_t])$ vs. time

The overall pattern of the data point distribution does not fit into a straight line. However, without any other data, this could be an induction period at the beginning which is low first order, followed by three first order points and the 5th point is anomalous. Also, from the past literatures, ROP of lactides and caprolactones are expected to be first order (more about this later in this chapter). Since the semi-logarithmic plot is not informative enough, the data were then put to test with a second order plot to check whether the reaction is second order.

For a second order reaction, the reaction rate law will be:

$$1/[M_t] = 1/[M_0] + kt$$

Where $1/[M_t] = 1/[M_0](1 - \text{conv.})$. It can therefore be rearranged to be:

$$1/[M_t] - 1/[M_0] = kt$$

The resultant plot of $1/[M_t] - 1/[M_0]$ vs. time is provided in Figure 5.7.

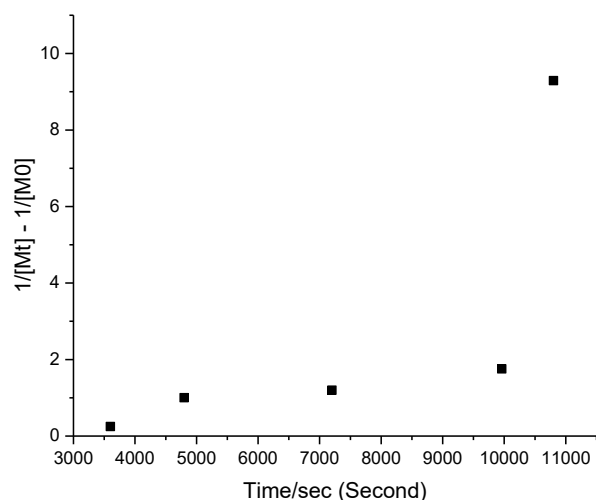


Figure 5.7: Plot of $1/[M_t] - 1/[M_0]$ vs. time

Again, no plausible straight line can be fitted into the plot. Thus, at this stage the reaction order is undetermined.

Repeating the above experiments led to a significant variation in results, which bringing into question the validity of the data and analysis of the reaction kinetics. However, when stoichiometric ratio [complex 1] : [BnOH] : [ϵ -CL] = 1.2 : 1.2 : 400 was used, much more reliable data were obtained. Thereafter repeating experiments with the increased quantities all showed consistent results. Possible reasons for this observation could be traces of water in the ϵ -CL which still persists after drying; if this were the case the water would react with the catalyst thus causing inconsistent performance. The additional 0.2 equivalent of catalyst may just be enough to compensate for the water-degraded amount hence giving reliable results. In light of this, a new series of reactions were undertaken. Reaction conditions were 20°C, BnOH as co-catalyst, 1.2 equivalent of both catalyst and co-catalyst. The Gel-Permeation Chromatography (GPC) data which will be discussed in detail in the next section is included in Table 5.4. Theoretical M_n is calculated by the formula:

$$\text{Theoretical } M_n = \text{Conversion} \times 400 \times 114.14 / [\text{equivalent of Al metal ion}] + 108.14$$

114.14 is the relative molecular weight of ϵ -caprolactone, 108.14 is the relative molecular weight of BnOH (as the co-catalyst, BnOH will be attached at the end of the polymer chain, thus involved in the molecular weight calculation).

Table 5.4: PCL catalysis results

Entry	1	2	3	4	5	6	7	8
Time/min	15	30	45	60	75	90	105	120
Conversion/%	8	15	31	45	58	80	86	93
M_n /Da	24767	13730	N/A	40412	54880	31312	43726	27818
\bar{D}	3.02	6.98	N/A	1.07	1.67	1.91	2.12	1.87
Theoretical M_n	3152	5815	11903	17229	22175	30545	32828	35492

20°C, BnOH as co-catalyst, ϵ -CL:catalyst:[Al]=400:1.2:1.2. N/A: cannot be obtained.

The conversion vs. time plot was drawn according to the data in Table 5.4, as shown in Figure 5.8.

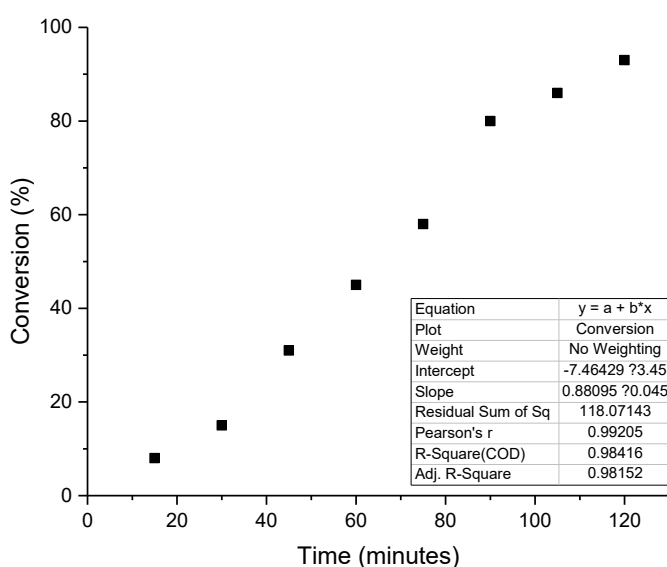


Figure 5.8: Conversion vs. Time plot, 1.2 equivalent of complex 1

Figure 5.8 illustrated that the conversion of ϵ -caprolactone monomer showed a general increasing trend with reaction time, but there is no good straight line of fitting. If a linear fitting is done with the data points, the slope will be 0.881 and R^2 is 0.984.

The $[\epsilon\text{-CL}]$ vs. time plot, $\ln[M_0/M_t]$ vs. time plot and $1/[M_t] - 1/[M_0]$ vs. time plot were then drawn as in Figure 5.9, 5.10 and 5.11 for comparison. The rate law expressions and calculations are the same as before.

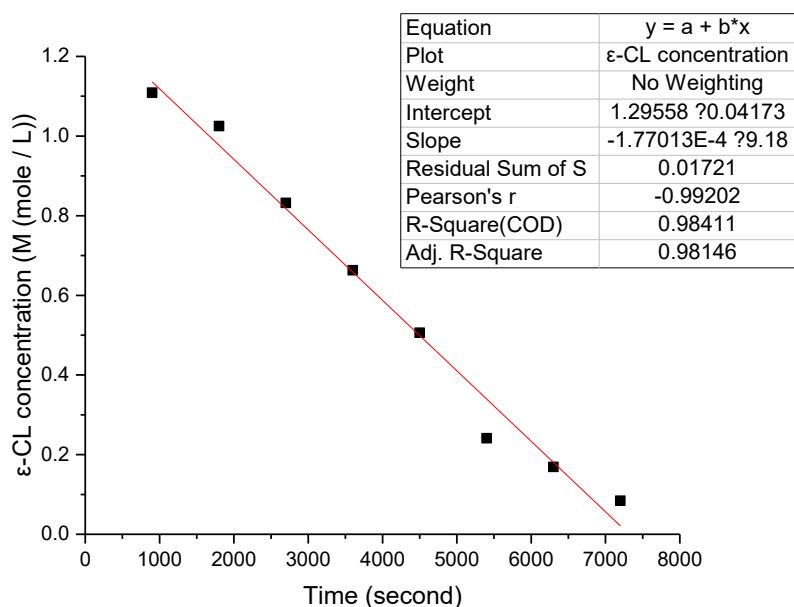


Figure 5.9: $[\epsilon\text{-CL}]$ vs. time plot for Table 5.4

If we assume the concentration of $\epsilon\text{-CL}$ showed a linear trend with time (which it should not), the rate constant can therefore be obtained by calculating the slope of the straight line according to the 0th order reaction rate law:

$$[M] = -kt$$

As the textbox in Figure 5.9 indicates, the slope for the straight line is -1.77×10^{-4} , thus the rate constant $k = 1.77 \times 10^{-4}$ M/s, with a coefficient of determination $R^2 = 0.984$.

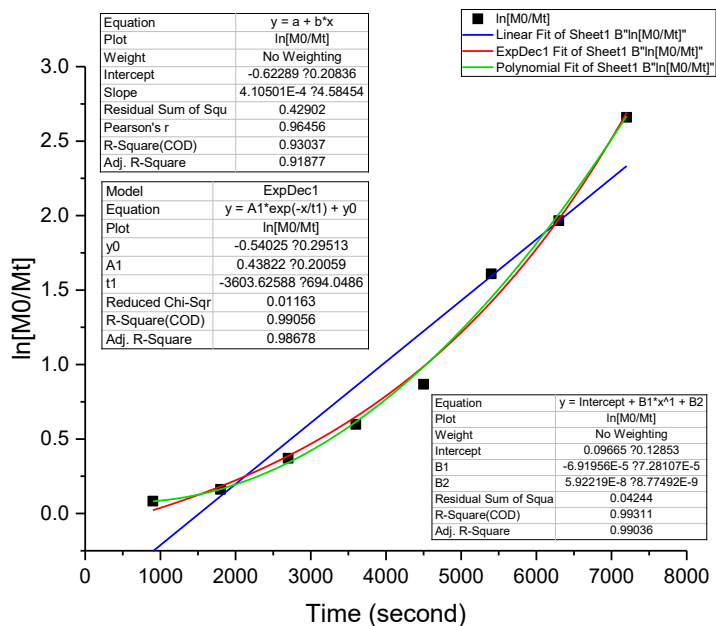


Figure 5.10: $\ln[M_0/M_t]$ vs. time plot for Table 5.4

This plot of $\ln[M_0/M_t]$ vs. time (Figure 5.10) is worth a deeper look into for further interpretation. As we can see from Figure 5.10, the blue linear fitting line has many data points sitting far away from it, leading to $R^2 = 0.93$, which is not satisfactory. The green polynomial fitting curve showed much better correspondence to the distribution of data points, giving $R^2 = 0.99$. The red exponential fitting also showed better correspondence to the data point distribution, with $R^2 = 0.99$ (slightly lower than that of polynomial fitting). The interesting semi-logarithmic plot which can fit into both exponential / polynomial patterns probably indicating a much complicated mechanism for the formation of PCL. As we will be discussing in the MALDI-ToF data section, several unidentified end groups could potentially be another sign that complex mechanisms / side reactions might be happening.

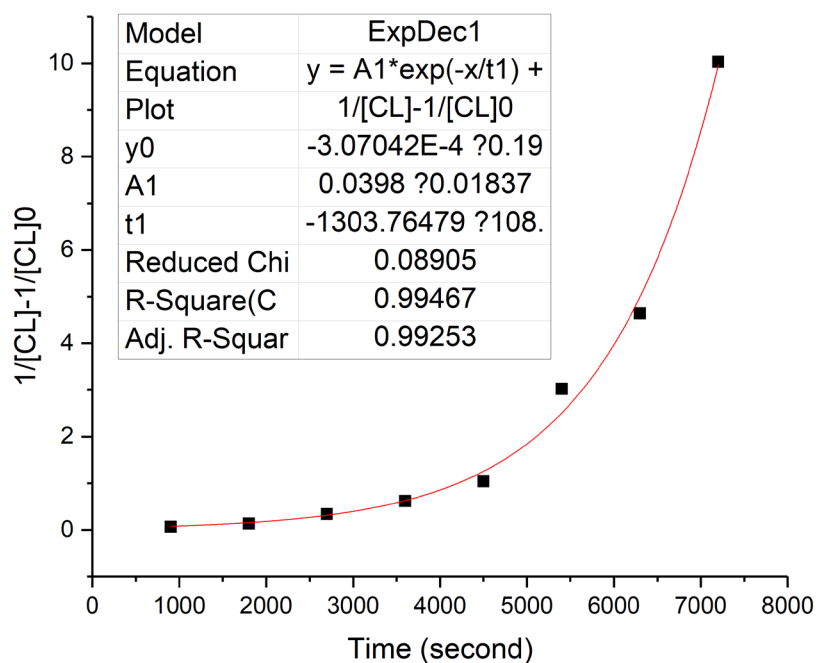
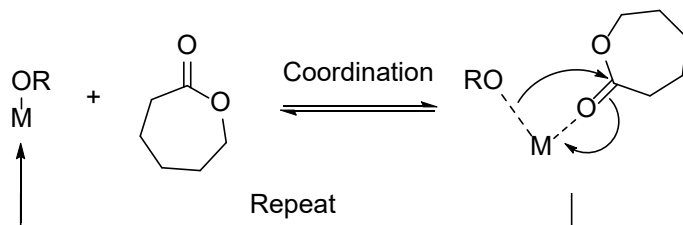


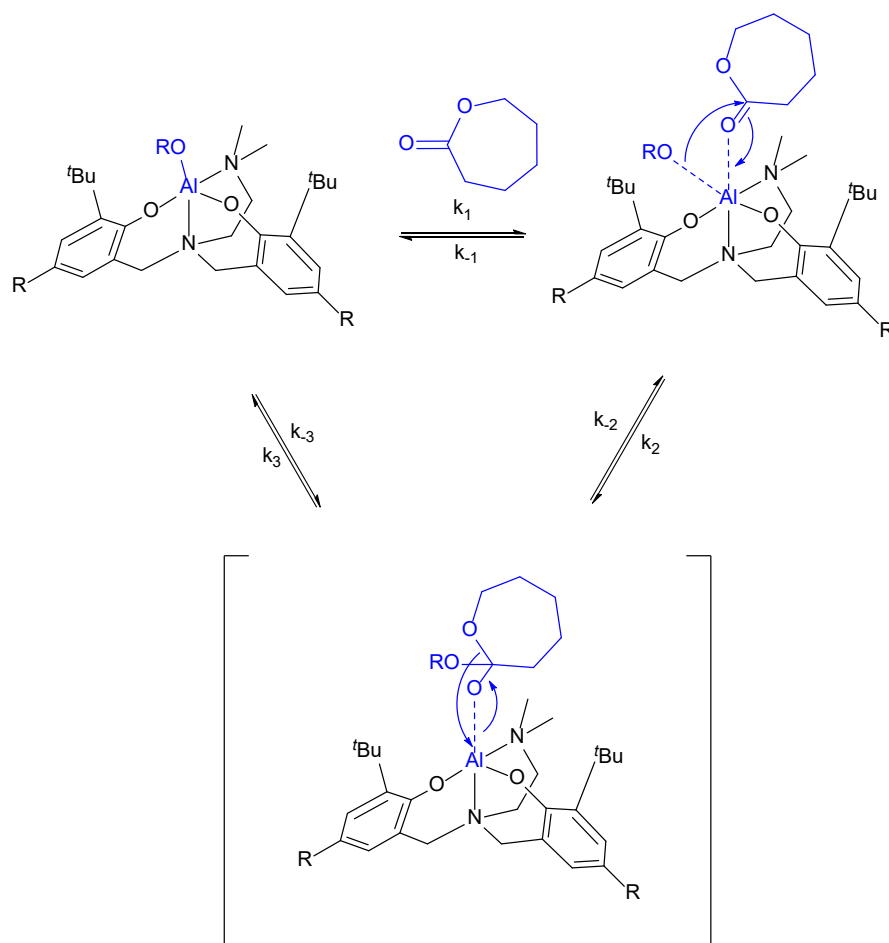
Figure 5.11: $1/[CL] - 1/[CL]_0$ vs. time plot from Table 5.4, $[CL]$ is the concentration of ϵ -caprolactone

This plot of $1/[CL] - 1/[CL]_0$ vs. time (Figure 5.11) again failed to have a good linear fitting line, as can be easily interfered from the figure. However, a good exponential fitting with $R^2 = 0.99$ is observed. The exponential / polynomial fitting of semi-logarithmic plot and exponential fitting of $1/[CL] - 1/[CL]_0$ vs. time plot all have better R^2 (all above 0.99) compared to that of linear fitting of the concentration vs. time plot (0.98), the authenticity of the linear fitting is lower statistically, thus there is reason to believe that the actual reaction mechanisms for the PCL synthesis with **1** involve more than what we have proposed. Literature wise, ROP of cyclic esters catalyzed by alkoxide complexes was generally believed to proceed via the coordination-insertion mechanism,^{26–29} as shown in Scheme 5.2.



Scheme 5.2: General cyclic ester ROP mechanism with metal complex catalyst²⁶

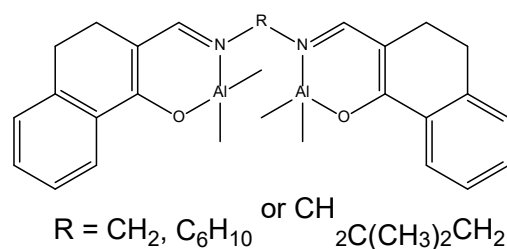
In-depth studies about kinetics of ϵ -CL with aluminium complex catalysts was reported by Tolman and co-workers in 2012²⁶ (Scheme 5.3). They proposed that for an Al-salen complex, the catalyzed ROP of ϵ -CL includes reversible binding of cyclic ester to the metal alkoxide (rate constant k_1 and k_{-1}); the subsequent attack of alkoxide on the activated carbonyl (rate constant k_2 and k_{-2}); and the ring-opening of the ϵ -CL to yield the new alkoxide. Tolman *et al.* also reported that the k_{-2}/k_2 and k_{-3}/k_3 steps are reversible.



Scheme 5.3: Proposed ϵ -CL ROP mechanism with Al-salen catalyst²⁶

Tolman *et al.* suggested that due to the enormous free energy loss during the ring-opening process,²⁶ the barrier for ring-opening (k_3) would be much lower than that of ring-closing (k_{-3}) and alkoxide de-insertion (k_{-2}). Also, based on the rapid collapse of the tetrahedral intermediate in the carboxylic acid derivative reactions, k_3 should be post-rate determining, as the k_3 step is too fast compared to k_{-3} and k_{-2} . Subsequently, with the assumptions that $[\epsilon\text{-CL}]$ is much larger than $[\text{catalyst}]$ and $k_{-1} \gg k_2$ (which means binding of $\epsilon\text{-CL}$ to catalyst is rapidly reversible), Tolman and co-workers then simplified the expression of the monomer binding equilibrium constant K to include k_1 and k_{-1} only, which is $K = k_1/k_{-1}$. During the computational studies of the experimental data, Tolman *et al.* found that the concentration data cannot be simply explained by first or second order rate laws, which is in agreement with our data as well. It was mentioned that they used polynomial fittings to fit the conversion vs. time data. Despite this catalyst model they used is a monometallic catalyst, the data and conclusions are of great scientific value. The journals regarding bimetallic polymerization kinetics, on the other hand, generally indicate first-order reactions. A paper from Huang *et al.* in 2016³⁰ reported a series of Al-salen binuclear complexes **5.1** (Figure 5.12) as catalysts for ROP of $\epsilon\text{-CL}$ /lactides. This series of catalysts exhibit first order when catalyzing the lactide ROP. Although no reaction kinetics about $\epsilon\text{-CL}$ was given, Huang and co-workers reported that the binuclear catalysts are far more active than their mononuclear analogies, ranging from 1.5 to 2.4-fold efficiency. They proposed the flexibility of the binuclear structure in solution allowed two metallic centres to approach and cooperate with each other for better catalytic performances. It was then deduced that the number of initiating groups on average in the bimetallic complexes is twice of that in the monometallic complex. The superior activity of **1** even under room temperature and its fast conversion could be the results of a bimetallic mechanism, which is more efficient comparing to traditional mononuclear ones. The fact that binuclear catalysts exhibit activity ranging from 1.4 to 2.5 compared to their mononuclear counterparts means in reality the 2 metal centres = 2-fold activity is not always true, as have suggested

by Huang and co-workers, there could be potential structural changes which may affect catalytic performances as well.



5.1
Huang *et al.*, 2016

Figure 5.12: Binuclear Al-salen type complex **5.1** by Huang *et al.*³⁰

Pang and co-workers reported a series of salen-type binuclear aluminium catalysts **5.2** in 2014 (Figure 5.13).³¹ This series of catalysts showed first order in monomers for both lactide ROP and ϵ -CL ROP. In addition, a plot of rate constant vs. catalyst concentration revealed that these two variables are linearly related. By comparing the rate constant for catalysts with different substituents, it was found that sterically demanding aromatic ring substituents reduce the ROP rate, which is reasonable since bulkier pendant groups hinder the approach of ϵ -CL monomers.

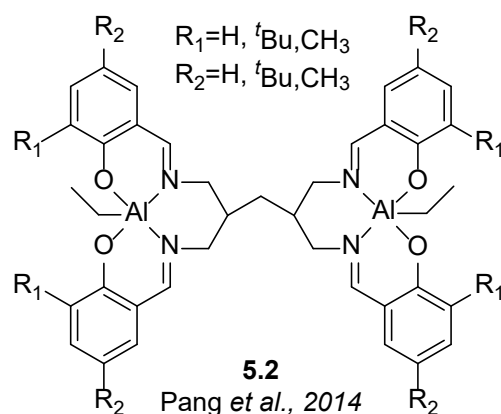


Figure 5.13: Binuclear Al-salen type complex **5.2** by Pang *et al.*³¹

From the past literature, it can be concluded that many bimetallic complexes exhibit first order kinetics in monomer concentration, and it is generally believed bimetallic is usually more efficient than monometallic catalysts. However, the different

observations by various researchers in terms of temperature requirements, reaction orders, activity, indicate that the specific ROP mechanisms with aluminium binuclear complexes could be largely affected by the identity of the ancillary ligand, the substituents of the ligand, electronic properties of the central aluminium, etc.

5.2.3.2. Poly(ϵ -caprolactone) Molecular Mass determination

Upon obtaining all the polymer samples, the samples were then tested by Gel Permeation Chromatography (GPC) to evaluate their molecular masses. The results are summarized in Table 5.4 in section 5.2.3.1.

Generally speaking, M_n and M_w values for polymer samples do not seem to follow any obvious trend. However, a general observation is that the M_n values are much higher than the theoretical M_n from 15 minutes to 75 minutes (entries 1 to 5). For entry 1, M_n is almost 8-fold of the theoretical value, entry 2 is about 2.3-fold, entry 4 is 2.3-fold, and entry 5 is 2.5-fold. This intriguing 2-fold relation leads to two possibilities. One being the rate of initiation is slower than the rate of propagation, the unbalanced initiation / propagation means fractions of catalyst does not enter the catalytic cycle, therefore there will be fewer propagating polymer chains thus each chain will be longer than calculated. Another possibility is that only one of the two aluminium centres is accessible for a growing polymer chain. Since the theoretical M_n values are calculated assuming both aluminium centres are accessible for propagating polymer chains, the ratio of ϵ -caprolactone is therefore calculated by monomer : aluminium centre = 400 : 1.2. However, if the maximum number of propagation chains on each catalyst molecule (which is a bimetallic catalyst) is 1 instead of the pre-assumed 2, the monomer : available aluminium centre will become 800 : 1.2, and the theoretical M_n at any given conversion will be approximately doubled (with the mass of the end group BnOH kept the same). The 1 polymer chain per metal complex theoretical M_n values were therefore calculated and presented in Table 5.5, the entry numbers are kept the same as in Table 5.4.

Table 5.5: GPC M_n and 1 chain per complex theoretical M_n for ϵ -CL ROP samples

Entry	1	2	3	4	5	6	7	8
GPC M_n	24767	13730	N/A	40412	54880	31312	43726	27818
Theo M_n	6196	11522	23698	34350	44242	60982	65548	70876
GPC/Theo	4.00	1.19	N/A	1.18	1.24	0.51	0.67	0.39

GPC/Theo: the ratio of (GPC M_n) / (Theo M_n).

As the values in the table suggested, if we adjust the theoretical M_n for 1 polymer chain per complex, entries 2, 4 and 5 will have their GPC M_n values close to the theoretical value, indicating a possibility for bimetallic mechanism, in which two metal centres cooperate for the propagation of a single polymer chain. More detailed elucidation for bimetallic mechanisms in section 3.3.

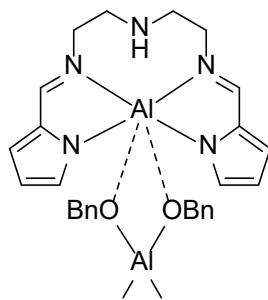
On the other hand, entry 6 and 8 seen M_n values only 86% and 66% of the theoretical M_n , and entry 7 is around 10% higher than theoretical value. The 2-fold relation is not maintained for entries following entry 5, which may be an adverse argument against the one polymer chain per catalyst molecule hypothesis. Polydispersity index (\bar{D}) wise, values as high as 3.02 and 6.98 are observed for the first half an hour of the reaction. The \bar{D} values then fall back to 1.07 at entry 4, rise back to 1.67 followed by fluctuations around 2.0. The poor \bar{D} control at the start of the reaction indicates potential complex initiation kinetics, which is also suggested by the observed M_n at the start of reaction as well. If we refer back to the literature samples of binuclear aluminium catalysts for ROP, we will find the following data as summarized in Table 5.6.

Table 5.6: Dispersity data from binuclear aluminium catalysts

Catalyst	Max. \bar{D}	Min. \bar{D}	M_n /Theo M_n
5.1 ³⁰	1.27	1.14	1.02 - 1.39
5.2 ³¹	1.25	1.08	0.94 – 1.10

Theo M_n : theoretical M_n . All values for ϵ -caprolactone ROP only.

These two examples of previously reported binuclear aluminium catalysts have good dispersity control, which holds true for the entire reaction time span. Catalyst **5.1** yielded M_n higher than theoretical values throughout the whole polymerization, while catalyst **5.2** showed PCL M_n increasing from lower than theoretical M_n to higher than theoretical M_n along with increasing reaction time. Having said that, $M_n / \text{Theo } M_n$ values for both **5.1** and **5.2** have never been close to 2.0, which is vastly different from the data for complex **1**. Also, for **5.2**, the good 1st order kinetics data, linear rate constant relation with catalyst concentration and linear relation between M_n and conversion all indicated that the ϵ -caprolactone ROP with it is under good control. The initiation / propagation should be following well-defined and stable kinetics in order to give these data. For **5.1**, it was found that the conversion will remain zero if no catalyst (*i*PrOH) was used. Subsequent NMR investigations conducted by Huang *et al.* revealed that Al-O^{*i*}Pr is the actual reactive species, and extra *i*PrOH is serving as chain-transfer agent. The overall ROP control by **5.1** catalyst, in terms of dispersity and $M_n / \text{Theo } M_n$ values, is a little bit weaker than **5.2**, but still quite good. Another report from Kong and co-workers³² about their binuclear aluminium catalyst **5.3** (Figure 5.14) for ϵ -caprolactone ROP showed a perfect match between Theo M_n and M_n when 1 : 1 aluminium centre : BnOH ratio is used, and the extra amount of BnOH would cause a decrease in M_n . Combining with the results from Pang *et al.*, it is evident that for their binuclear aluminium catalysts, both aluminium centres are able to provide polymer propagating sites. This conclusion from previous literature is not consistent with the data reported here, and the hypothesis of there being one polymer chain per catalyst molecule. Thus, the higher-than-expected M_n from the ROP experiments reported here is likely be due to the faster propagation than initiation rate, since only a relatively small number of catalyst molecules have initiated the polymerization, and the fast propagation leads to higher than expected number of monomers been added to each chain.



5.3

Kong *et al.*, 2014

Figure 5.14: Structure of binuclear aluminium complex **5.3** from Kong *et al.*³²

The apparently random M_n vs. conversion (Figure 5.15) from the ϵ -caprolactone ROP with **1** is a potential sign of complex initiation and / or reaction kinetics, which was also observed by Tolman and co-workers.²⁶ Despite Tolman's report being based on a mononuclear catalyst, it can be plausibly interpreted that if a bimetallic complex is having polynomial reaction kinetics on both of its metal centres, the resultant M_n vs. conversion will appear even more random than a mononuclear case.

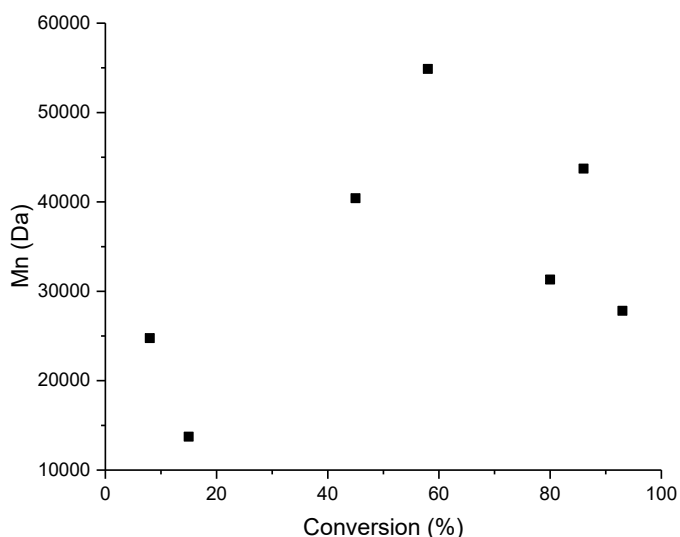


Figure 5.15: M_n vs. Conversion plot from Table 5.4

Matrix-Assisted Laser Desorption-Ionization Mass Spectrometry (MALDI-MS) was used to analyze the microstructure of the polymers. As a representative example, data for entry 3 (Table 5.4) are shown.

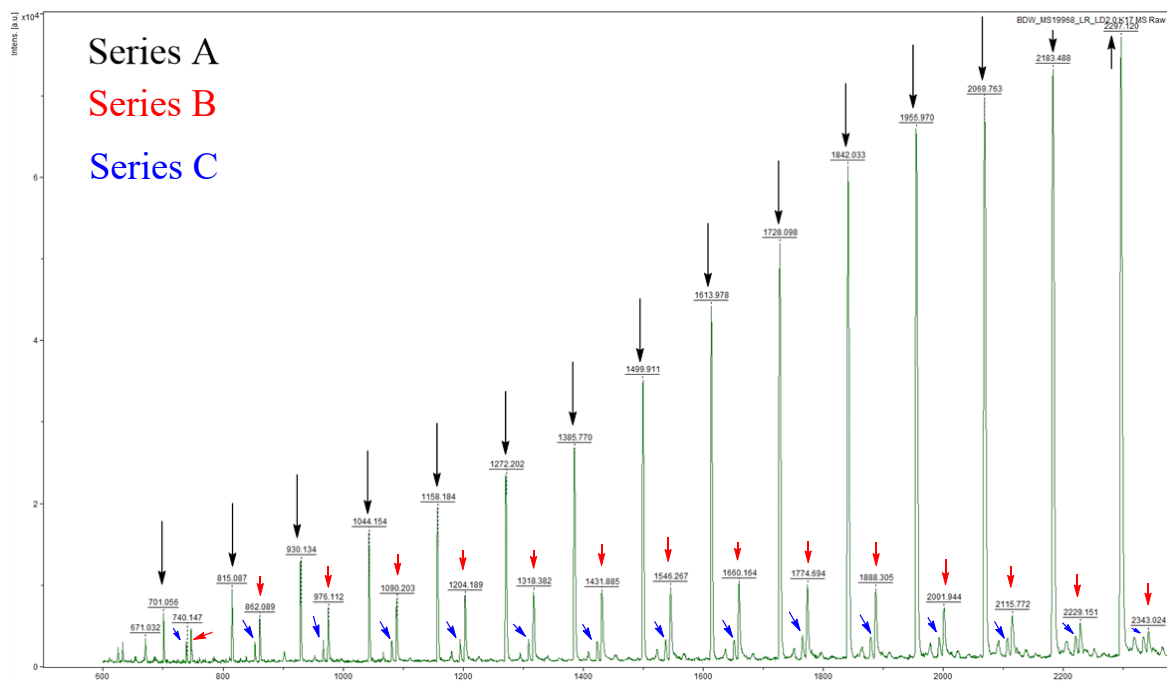


Figure 5.16: MALDI-MS spectrum of entry 3 (Table 5.4)

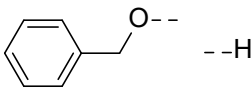
MALDI-MS revealed that 3 different polymer series exist in the sample, denoted Series A, B and C in Figure 5.16; all series have a spacing of 114.14 m/z (within the resolution of the instrument), which is evidence of the expected poly(ϵ -caprolactone) structure, since the repeating unit mass is the same as ϵ -caprolactone monomer mass (114.14 g / mol). The existence of three different series means there are three different types of end groups or else back-biting (the free end of the polymer chain reacted with the propagating end of the polymer chain) during polymerization. If the different series are caused by different end groups, the molecular masses of polymer samples can be calculated by the formula:

$$M_{\text{polymer}} = n \times M_{\text{monomer}} + M_{\text{Na}} + M_{\text{end groups}}$$

Where $M_{\text{species name}}$ represents the mass of the species. The inclusion of the sodium atomic mass is due to the use of sodium as the ion source. The end groups are the groups that initiated the polymerization and the hydrogen from reaction quenching, thus connected to the ends of the polymer chain after the polymerization is finished / quenched. In some rare cases, the catalyst will remain on one end of the chain as

well. With this formula, the end groups for series A, B and C can be obtained from the polymer mass, as summarized in Table 5.7.

Table 5.7: End groups for Entry 3

Series	Observed end group + Na mass (m / z)	Proposed end group mass (m / z)	Proposed end groups
A	130.137 ^a	107.1 + n × 114.14	 --H
B	62.116	39.1 + n × 114.14	undetermined
C	54.008	31.0 + n × 114.14	H ₃ C-O-- --H

^a: Observed end group + Na masses are obtained by averaging the differences between observed peak and integer multiples of 114.14 of all the peaks in the same series. Dashed bonds represent the bonds to the remaining polymer chain. Observed value is 15.977, since 15.977 is smaller than the relative atomic mass of Na (22.990), the actual end group mass should be at least 15.977 + 114.14 – 22.990 ≈ 107.1.

The end group mass for series A (the highest intensity peak series) is 107.1, and BnOH (benzyl alcohol) has a molecular mass of 108.14, thus BnO group has a mass of 107.13, a very close match to the observed 107.128 end group mass. This suggests that BnOH is a suitable co-catalyst for complex **1** in ϵ -caprolactone polymerization. Despite this, typical polymer chain will gain a proton at the opposite end (to the end group) of the polymer, which means if the proposed end group is BnO, the end group mass should be a total of 108. So far, we have no solid conclusion about the reason that caused the loss of one proton's mass in the end group mass. One possible explanation is the broad peaks in the spectrum causes peak-picking errors of 1, which is possible, given the broad peaks obtained with this instrument.

The end group mass for series B (the 2nd highest intensity peak series) is 39.1, no groups of matching mass can be found so far. Despite this, the 114 spacing in series B still justifies itself to be the ϵ -caprolactone polymer as expected.

The end group mass for series C (the lowest intensity peak series) is 31.019, and methanol (CH_3OH) has a molecular mass of 32.04, thus CH_3O group has a mass of 31.03, a close match to 31.0. This can be explained by the transesterification during quenching involved in the polymer synthetic route (procedure described in section 3.2). 0.5 mL of methanol was injected into the reaction mixture to quench the reaction, thus during the quenching, there is a chance that transesterification between methanol and polymer chain happened, so that CH_3O group is attached to the end of the resultant "chopped off" polymer chain and recognised as the end group during the MALDI test. Again, same as the case in series A, a proton's mass is missing from the end group mass due possible errors from the broad mass peaks during peak picking, same as series A's case.

Another fact about the MALDI peak series is that all three series showed a general decreasing trend in end group mass + Na with increasing length of polymer chain, with the end group mass value of the peak of lowest m/z about 2 to 3 higher than the end group mass value of the peak of highest m/z value, as shown in Figure 5.17. Although this trend could be a result of simple peak-picking errors due to peak broadness.

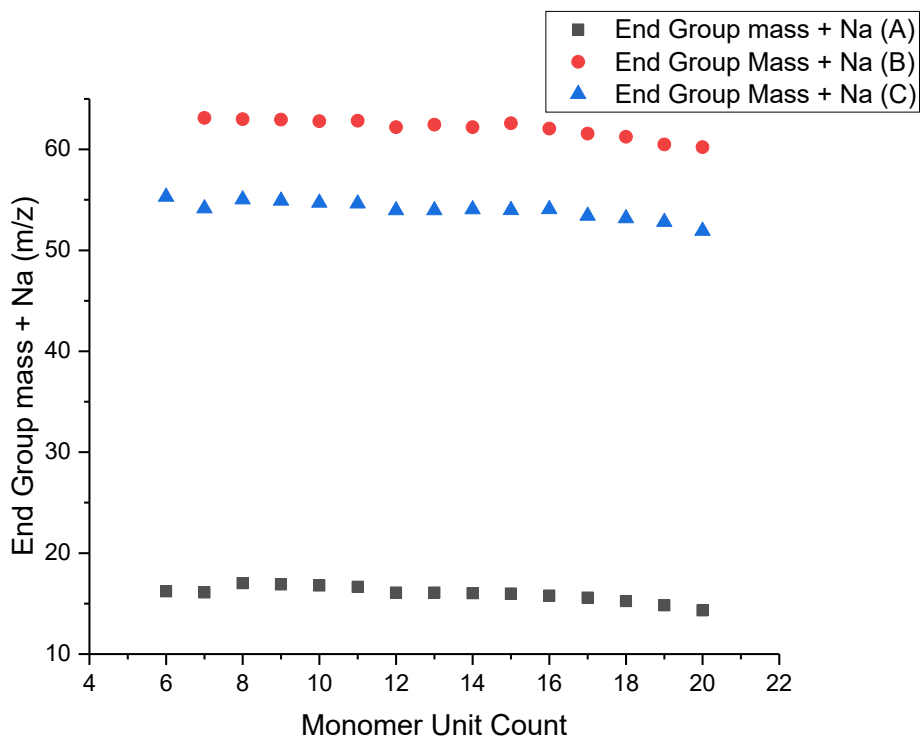
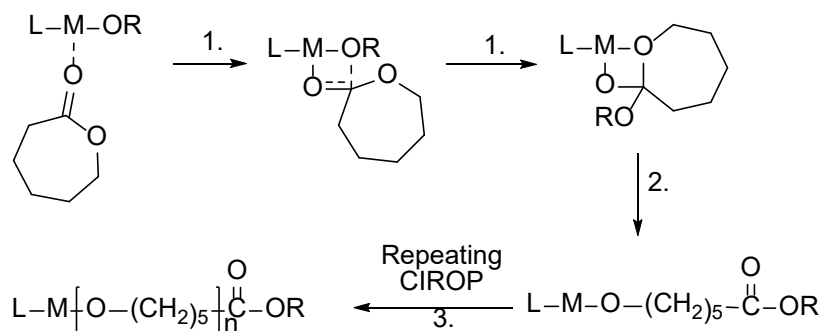


Figure 5.17: End Group Mass + Na variation

As the end group + Na mass has a difference of 2 to 3 between the highest and lowest ones, there is reason to believe that this could possibly give rise to a wrong mass of the end group, which deviates 1 mass unit from what it should be, as mentioned in discussion about series A and C. Thus, the end group masses from the spectrum will be indicative but not analytically precise.

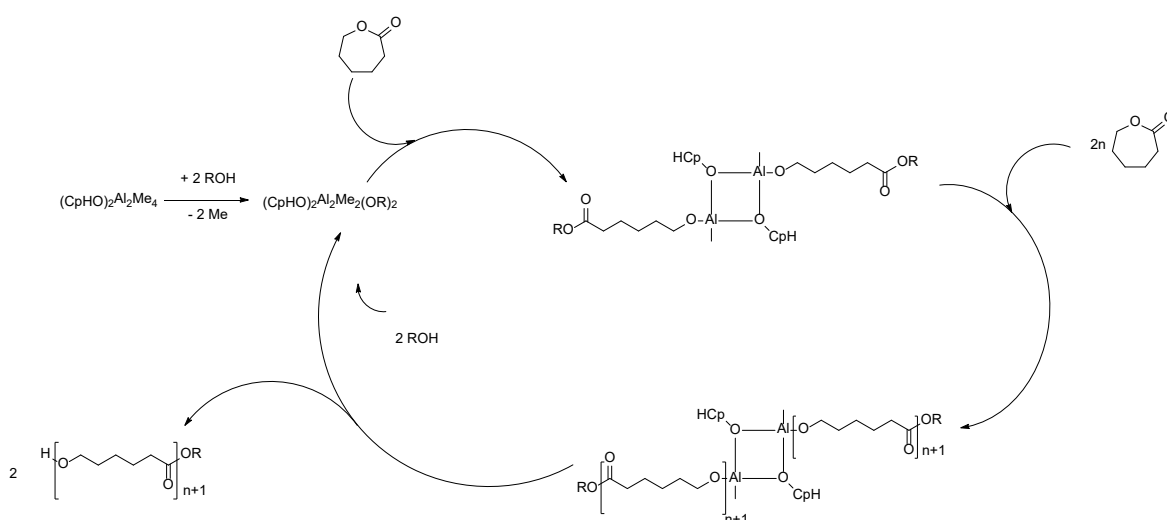
5.3. Mechanism and additional discussion

According to the research conducted by other researchers, the ring-opening polymerization of cyclic esters (including ϵ -CL) by alkoxide complexes is considered to proceed via coordination-insertion mechanism,^{29,33–35} as shown below.



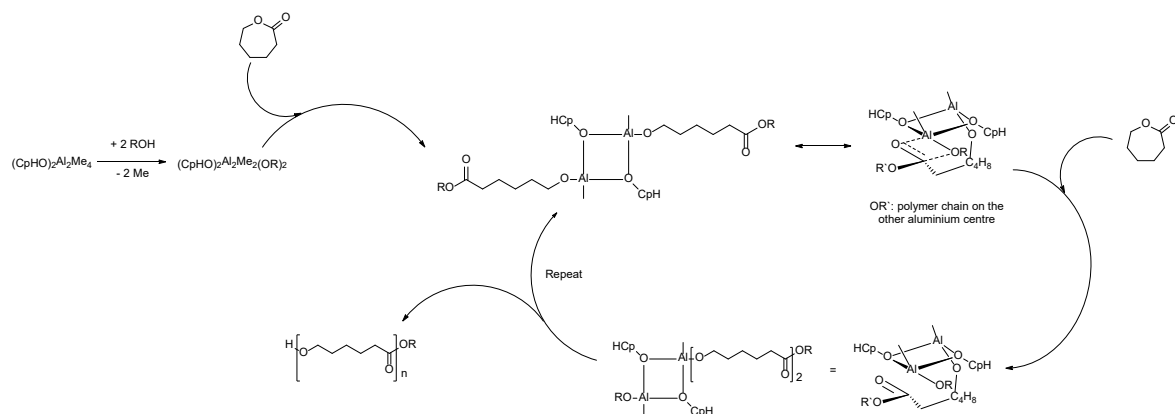
Scheme 5.4: Mechanism for ϵ -caprolactone coordination-insertion ROP

Based on the discussions and interpretations above, the general reaction mechanism for the polymerization of ϵ -caprolactone by $[(\text{CpHO})_2\text{Al}_2\text{Me}_4]$ (**1**) is proposed in Scheme 5.5. ROH represents co-catalyst BnOH.



Scheme 5.5: Proposed reaction mechanism for ϵ -CL homopolymerization catalyzed by complex **1** / BnOH

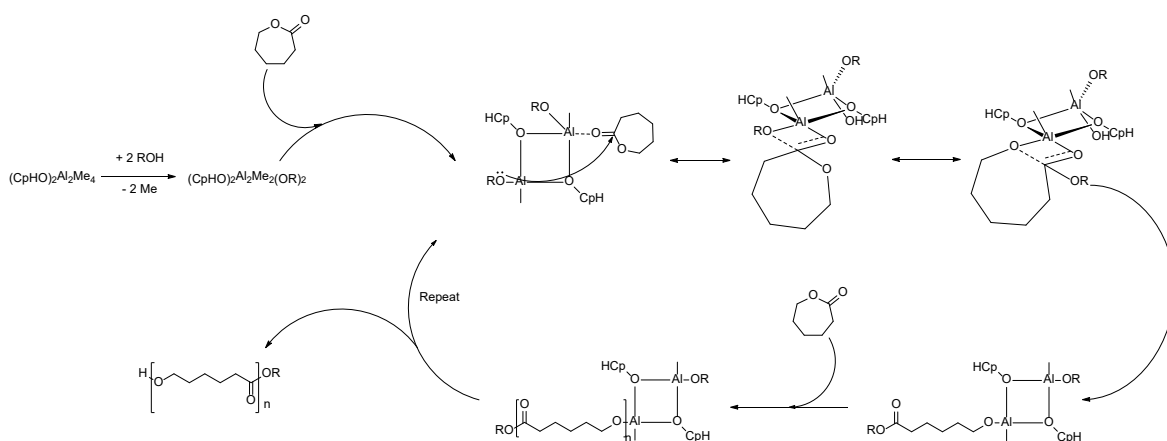
However, the complicated reaction kinetics we have encountered before suggesting that there could be more than one initiation mechanisms exist. For bimetallic complexes, one possibility might be the cooperation between two metal centres. Since both metal centres are Lewis acids, and a propagation polyester chain have multiple ester groups on it which are Lewis bases, we propose that a two-metal cooperating ROP could happen as in Scheme 5.6.



Scheme 5.6: First proposed bimetallic cooperation mechanism for **1**

In this proposed bimetallic cooperation mechanism, the alkoxide on one aluminium centre forms 4-membered transition state with the end of the polyester chain bound to the other aluminium centre in the same catalyst molecule. The transition state then goes through conventional coordination-insertion ROP to propagate. In this mechanism, the intramolecular CIROP could be faster than the normal CIROP which requires binding of a fresh caprolactone monomer. The ring strain upon forming the transition state should be negligible due to the flexibility of polymer chain. Despite little ring strain, it could still be hard to form the intramolecular transition state since the chain end will find it hard to reach all the way back to the activated catalyst. Similar bimetallic cooperation mechanisms have been proposed by other researchers, such as Sheng *et al.* regarding their Ln-Na complex,³⁶ and Isnard *et al.* regarding their binuclear aluminium complexes.

Surely, the transition state can be formed right after a caprolactone monomer binds to the catalyst as well. As shown in Scheme 5.7.



Scheme 5.7: Second proposed bimetallic cooperation mechanism for 1

The second proposed bimetallic cooperation requires every incoming monomer to go through the bimetallic cooperation and all monomers propagating on the same chain. The first proposed bimetallic cooperation mechanism, on the other hand, theoretically allows individual coordination insertion happens on both aluminium centres, then combine the two propagating chains later to produce a longer chain. In the actual reaction, a combination of several different initiation mechanism could result in complex initiation kinetics thus cannot be modelled by simple 0th, 1st or 2nd order curves. The real initiation could as well be a combination of all three, each with different probability, which results in complicated initiation kinetics. The random M_n vs. conversion plot (Figure 5.15) is another potential clue for the first proposed bimetallic cooperation, since the random combination of two polyester chains on the same catalyst will undoubtedly lead to random M_n distribution, especially at the start of the reaction. A plot of $M_n / \text{Theo } M_n$ vs. time is illustrated as Figure 5.18.

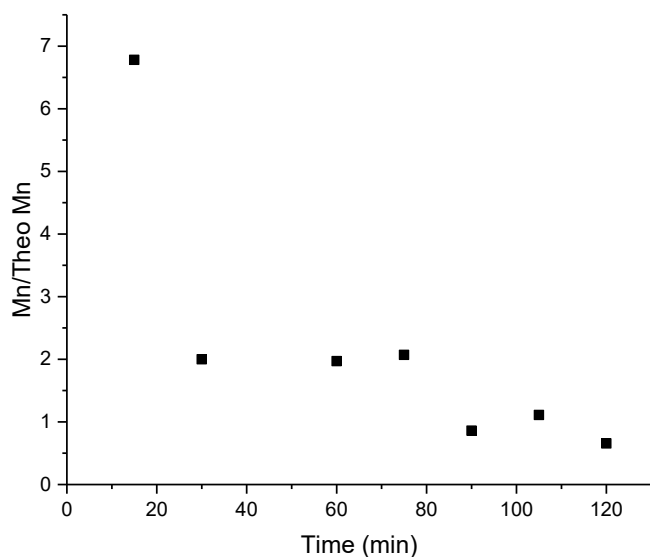


Figure 5.18: $M_n/\text{Theo } M_n$ vs. Time plot from Table 5.4

The distribution of data points indicates a higher-than-expected M_n at the start of the reaction, especially at 15 min. From 30 min to 75 min, the M_n is double the theoretical M_n . Finally, from 90 min to 120 min, the M_n falls to below 1.0. Possibly, at the start of reaction, the high activity of bimetallic catalyst (2nd bimetallic mechanism) which causes fast propagation combined with merging of chains (1st bimetallic mechanism) could result in a high M_n (15 min). Another possibility being poor initiation which causing less catalysts molecules to be active. From 30 min to 75 min, the 1st bimetallic mechanism dominates due to possible kinetic / thermodynamic advantages., therefore the combining of 2 polymer chains make the measure M_n quite close to 2-fold theoretical M_n . After 75 min, the general mechanism (Scheme 5.5) dominates, thus the $M_n / \text{Theo } M_n$ values approaches 1.0. The generally higher-than-expected M_n also indicates a slower initiation rate comparing to propagation rate, since fewer number of growing chains and high chain propagation speed result in high M_n .

Activity wise, we will again refer to **5.1**, **5.2** and **5.3** which we have mentioned before. Their key ϵ -caprolactone ROP results are summarized in Table 5.8.

Table 5.8: ϵ -CL ROP catalytic performance comparison of **1**, **5.1**, **5.2** and **5.3**

Catalyst	[Cat]:[CoC]:[CL]	Conversion/%	Time/min	Temp/°C	M _n	Dispersity	Theo M _n
1	1.2:1.2:400	8	15	20	24767	3.023	3652
1	1.2:1.2:400	45	60	20	40412	1.073	20545
1	1.2:1.2:400	93	120	20	27818	1.865	42460
5.1	1:2:200	89	6	80	10900	1.21	10200
5.1	1:2:400	91	12	80	23600	1.24	20800
5.1	1:2:600	93	15	80	33200	1.22	31900
5.2	1:2:200	98	150	40	11900	1.19	11200
5.2	1:2:400	95	275	40	20800	1.17	21700
5.2	1:2:600	92	390	40	29800	1.25	31600
5.3	1:0:200	92	5	35	17600	1.35	10700
5.3	1:0:400	85	9	35	22000	1.50	19500
5.3	1:0:600	98	25	35	35900	1.66	33700

[Cat]:[CoC]:[CL] = [Catalyst]:[Co-Catalyst]:[ϵ -CL], Theo M_n: Theoretical M_n

The fundamental difference between $[(\text{CpHO})_2\text{Al}_2\text{Me}_4]$ (**1**) and the three other catalysts is the temperature requirement. None of the other three binuclear aluminium catalyst is capable of catalysis at 20°C. In industrial applications, the extent of heating needed is critical, as large-scale heating would consume enormous amount of energy and fuel, which is not only non-ideal for environmental protection, but also poor for cost-control as well. The other difference is that generally **5.1**, **5.2** and **5.3** exhibit high dispersity control, but not by a large margin. **5.1** and **5.3** can convert 91% (12 minutes reaction time) and 85% (9 minutes reaction time) of 400 equivalents ϵ -caprolactone into polymer respectively, which is faster than complex **1** (93% conversion at 120 minutes reaction time), but again, the elevated reaction temperatures need to be considered. In most of the cases, sacrificing time for lower energy input, better ethical considerations and higher safety standard (large-scale heating always come with safety concerns) is acceptable. PCL is mainly used as large quantity commodity such as food packaging, so precise dispersity control is not always critical, which again makes **1** favoured for large-scale industrial applications.

5.4. Conclusions

In this chapter, in-depth investigation regarding efficacy of the $(\text{CpO})_2\text{Al}_2\text{Me}_4$ (**1**) towards ROP of ϵ -CL has been undertaken. Most previous bimetallic aluminium complexes have been reported to operate at elevated temperatures; but in the case of **1**, the high activity at room temperature has been seen, which makes it quite novel as an aluminium-based catalyst. The probing of different co-catalysts proved BnOH to be the best co-catalyst for **1**, which is common for metal complex catalysts. Through research and discussion of M_n , dispersity and conversion, it has been found that **1** has a complex ϵ -CL ROP initiation kinetics, which points to a complicated combination of several different initiation / propagation mechanisms. Generally, it has been seen that **1** can be utilized as a highly active bimetallic catalyst

for ϵ -CL ROP. Combining with its easy, low-cost synthetic route, **1** possesses good potential in the field of ϵ -CL ROP catalysis.

5.5. References

- 1 M. A. Woodruff and D. W. Hutmacher, *Progress in Polymer Science*, 2010, **35**, 1217–1256.
- 2 K. E. Uhrich, S. M. Cannizzaro, R. S. Langer and K. M. Shakesheff, *Chem. Rev.*, 1999, **99**, 3181–3198.
- 3 A. Khanna, Y. S. Sudha, S. Pillai and S. S. Rath, *J Mol Model*, 2008, **14**, 367–374.
- 4 M. Labet and W. Thielemans, *Chem. Soc. Rev.*, 2009, **38**, 3484.
- 5 L. Qin, Y. Zhang, J. Chao, J. Cheng and X. Chen, *Dalton Trans.*, 2019, **48**, 12315–12325.
- 6 A. Pilone, N. De Maio, K. Press, V. Venditto, D. Pappalardo, M. Mazzeo, C. Pellecchia, M. Kol and M. Lamberti, *Dalton Trans.*, 2015, **44**, 2157–2165.
- 7 K. Bakthavachalam, A. Rajagopal and N. Dastagiri Reddy, *Dalton Trans.*, 2014, **43**, 14816–14823.
- 8 Y. Wang, B. Liu, X. Wang, W. Zhao, D. Liu, X. Liu and D. Cui, *Polym. Chem.*, 2014, **5**, 4580–4588.
- 9 M.-Y. Shen, Y.-L. Peng, W.-C. Hung and C.-C. Lin, *Dalton Trans.*, 2009, 9906–9913.
- 10 H.-J. Fang, P.-S. Lai, J.-Y. Chen, S. C. N. Hsu, W.-D. Peng, S.-W. Ou, Y.-C. Lai, Y.-J. Chen, H. Chung, Y. Chen, T.-C. Huang, B.-S. Wu and H.-Y. Chen, *J. Polym. Sci. A Polym. Chem.*, 2012, **50**, 2697–2704.
- 11 S. Giese, T. Silva, D. L. H. Hughes, A. L. Rüdiger, E. de Sá, S. Zawadzki, J. Soares and G. Nunes, *J. Braz. Chem. Soc.*, 2017, **28**, 1440–1452.

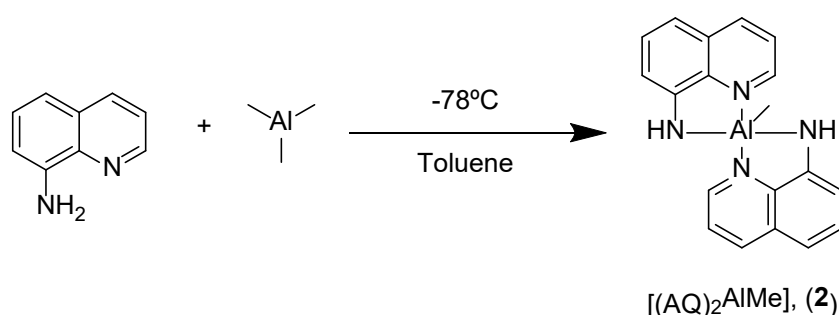
- 12 J. Cayuela, V. Bounor-Legaré, P. Cassagnau and A. Michel, *Macromolecules*, 2006, **39**, 1338–1346.
- 13 P. Cruz, Y. Pérez, I. del Hierro, R. Fernández-Galán and M. Fajardo, *RSC Adv.*, 2016, **6**, 19723–19733.
- 14 I. Palard, A. Soum and S. M. Guillaume, *Chem. Eur. J.*, 9.
- 15 X. Ni, W. Zhu and Z. Shen, *Chinese Journal of Catalysis*, 2010, **31**, 965–971.
- 16 L. Zhang, Y. Niu, Y. Wang, P. Wang and L. Shen, *Journal of Molecular Catalysis A: Chemical*, 2008, **287**, 1–4.
- 17 T.-L. Huang and C.-T. Chen, *Dalton Transactions*, 2013, 8.
- 18 Z. Zhong, M. J. K. Ankoné, P. J. Dijkstra, C. Birg, M. Westerhausen and J. Feijen, *Polymer Bulletin*, 2001, **46**, 51–57.
- 19 J. H. Khan, F. Schue and G. A. George, *Polym. Int.*, 2010, **59**, 1506–1513.
- 20 M.-H. Thibault and F.-G. Fontaine, *Dalton Trans.*, 2010, **39**, 5688.
- 21 C. Nakonkhet, T. Nanok, W. Wattanathana, P. Chuawong and P. Hormnirun, *Dalton Trans.*, 2017, **46**, 11013–11030.
- 22 Y. Liu, W.-S. Dong, J.-Y. Liu and Y.-S. Li, *Dalton Transactions*, 2014, 8.
- 23 P. McKeown, M. G. Davidson, G. Kociok-Köhn and M. D. Jones, *Chem. Commun.*, 2016, **52**, 10431–10434.
- 24 N. Maudoux, T. Roisnel, V. Dorcet, J.-F. Carpentier and Y. Sarazin, *Chem. Eur. J.*, 2014, **20**, 6131–6147.
- 25 A. Bolley, S. Mameri and S. Dagorne, *Journal of Polymer Science*, 2020, **58**, 1197–1206.

- 26 K. Ding, M. O. Miranda, B. Moscato-Goodpaster, N. Ajellal, L. E. Breyfogle, E. D. Hermes, C. P. Schaller, S. E. Roe, C. J. Cramer, M. A. Hillmyer and W. B. Tolman, *Macromolecules*, 2012, **45**, 5387–5396.
- 27 M. H. Chisholm, J. C. Gallucci, K. T. Quisenberry and Z. Zhou, *Inorg. Chem.*, 2008, **47**, 2613–2624.
- 28 A. P. Dove, V. C. Gibson, E. L. Marshall, H. S. Rzepa, A. J. P. White and D. J. Williams, *J. Am. Chem. Soc.*, 2006, **128**, 9834–9843.
- 29 E. L. Marshall, V. C. Gibson and H. S. Rzepa, *J. Am. Chem. Soc.*, 2005, **127**, 6048–6051.
- 30 H.-C. Huang, B. Wang, Y.-P. Zhang and Y.-S. Li, *Polym. Chem.*, 2016, **7**, 5819–5827.
- 31 X. Pang, R. Duan, X. Li, Z. Sun, H. Zhang, X. Wang and X. Chen, *RSC Adv.*, 2014, **4**, 57210–57217.
- 32 W.-L. Kong and Z.-X. Wang, *Dalton Trans.*, 2014, **43**, 9126.
- 33 L. Piao, M. Deng, X. Chen, L. Jiang and X. Jing, *Polymer*, 2003, **44**, 2331–2336.
- 34 A. Arbaoui and C. Redshaw, *Polym. Chem.*, 2010, **1**, 801.
- 35 J. Liu, J. Ling, X. Li and Z. Shen, *Journal of Molecular Catalysis A: Chemical*, 2009, **300**, 59–64.
- 36 H.-T. Sheng, J.-M. Li, Y. Zhang, Y.-M. Yao and Q. Shen, *Polyhedron*, 2008, **27**, 1665–1672.

Chapter 6: Synthesis, characterization, X-Ray crystal structure of aminoquinoline-aluminium complexes and the ROCOP performance of the complexes

6.1. Introduction

During the course of investigation of suitable metal complexes which may serve as catalysts for polymerization, researchers around the world have developed various different ligands. Among these ligands, salen-type and porphyrin-type seemed to be the most effective ligand types capable of catalysing ring-opening co-polymerizations (ROCOP), as have mentioned in Chapter 1. However, there are not many reports about ligands based on aminoquinoline-type structure, and none that have been employed in ring-opening co-polymerization catalysis. To verify whether aminoquinoline structure-related ligands can form metal complexes that can be utilized as ROCOP catalysts, we proposed a synthetic route which would yield a planar amido-quinoline complex, as shown in Scheme 6.1.



Scheme 6.1: Proposed aminoquinoline complex synthetic route

Most of the conventional ligand systems for ROCOP have planar, 4-donor structures (e.g., salen-type, porphyrin-type, salan-type), and there are also 4 donors in **2**, but the donors are two pairs on two aminoquinoline. Therefore, **2** may serve as a close imitation of those planar 4-donor ligand systems but with the two halves disconnected from each other, which means a higher tolerance towards non-planar structures for intermediates and transition states is attributed. Moreover, this complex can be facily synthesized in large scales with two commercially available precursors just in one step. To add up to this, tuning of the electronic / steric properties of the complex can be achieved through modifications of the NH moiety with only one extra step, as shown later in this chapter. Therefore, various ROCOP tests with complex **2** were undertaken.

Subsequently, two modified versions $[(AQ)_2AlCl]$ (**3**) and $[(AQMe)_2AlCl]$ (**4**) of **2** were synthesized and tested for ROCOP. The structures of **3** and **4** are provided in Figure 6.1.

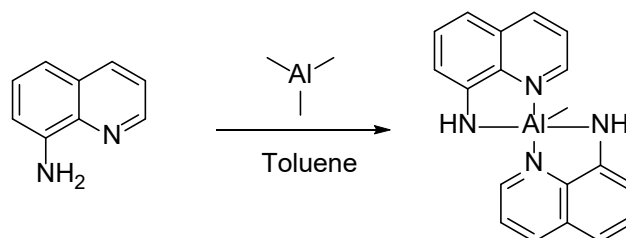


Figure 6.1: Structures of $[(AQ)_2AlCl]$ (**3**) and $[(AQMe)_2AlCl]$ (**4**)

6.2. Synthesis and characterization of complexes

6.2.1. Synthesis and characterization of $[(AQ)_2AlMe]$ (**2**)

The methyl aluminium complex $[(AQ)_2AlMe]$ (**2**) was prepared via the reaction of trimethylaluminium with two equivalents of 8-aminoquinoline in toluene at room temperature (Scheme 6.2). After workup, complex **2** was obtained as a brown powder.



Scheme 6.2: Synthesis route of **2**

Single crystals of $[(\text{AQ})_2\text{AlMe}]$ (**2**) were prepared by dissolving **2** in toluene, followed by filtration and cooling to -40°C . Single crystal X-ray diffraction analysis of **2** revealed its structure as in Figure 6.2. Principle bond lengths and angles are listed in Table 6.1 and Table 6.2.

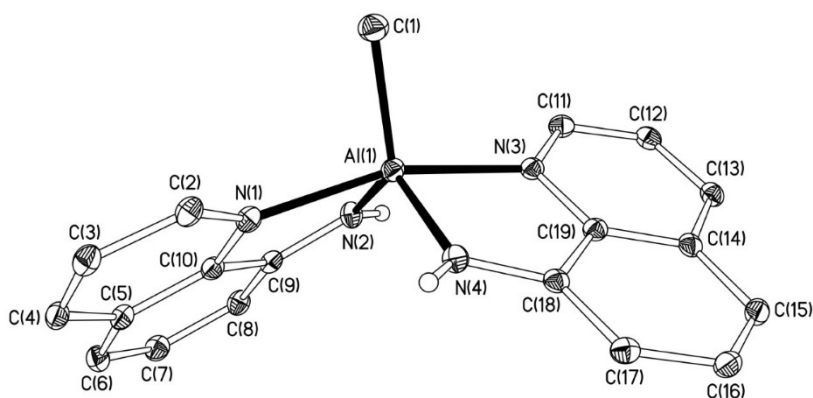


Figure 6.2: Molecular structure of $[(\text{AQ})_2\text{AlMe}]$ (**2**), ellipsoids drawn at 30% probability and hydrogen atoms (except hydrogens on N(2) and N(4)) omitted for clarity

Table 6.1: Principal bond lengths in **2**

Bond	Bond length / Å
Al(1)-N(1)	2.1034 (18)
Al(1)-N(2)	1.8767 (17)
Al(1)-N(3)	2.1019 (17)
Al(1)-N(4)	1.8691 (18)
Al(1)-C(1)	1.976 (2)
N(2)-C(9)	1.359 (2)
N(4)-C(18)	1.360 (2)

Table 6.2: Principal bond angles of in **2**

Bonds	Bond angle / °
N(4)-Al(1)-N(1)	91.46 (7)
N(2)-Al(1)-N(3)	89.28 (7)
N(2)-Al(1)-N(1)	80.44 (7)
N(4)-Al(1)-N(3)	80.76 (7)
N(4)-Al(1)-C(1)	117.99 (9)
N(3)-Al(1)-C(1)	102.04 (8)
N(2)-Al(1)-C(1)	121.52 (9)
N(1)-Al(1)-C(1)	96.18 (8)
N(4)-Al(1)-N(2)	120.44 (8)
N(3)-Al(1)-N(1)	161.77 (7)
Al(1)-N(3)-C(11)	130.65 (13)
Al(1)-N(3)-C(19)	110.62 (12)
Al(1)-N(4)-C(18)	118.98 (13)
Al(1)-N(1)-C(2)	130.91 (13)
Al(1)-N(1)-C(10)	110.57 (13)
Al(1)-N(2)-C(9)	118.63 (13)

Complex **2** crystallizes in the space group $P2_12_12_1$. The aluminium formed a distorted trigonal bipyramidal geometry with the aluminium ligated by four nitrogens and one carbon. From the bond angles, it can be interpreted that the N(1) and N(3) donors are on the axial position, with a bond angle $N(3)-Al(1)-N(1) = 161.77^\circ$ due to the distortion. C(1), N(2) and N(4) are on the equatorial positions since their bond angles with each other are close to 120° . The bond lengths around central aluminium ion and the data retrieved from CSD⁷ (Cambridge Structural Database) are summarized in Table 6.3. The Al-Cl data is also included for the comparison with molecular structures of complex **3**.

Table 6.3: Principal bond lengths similar structures of [(AQ)₂AlMe] from CSD

Bond	Min. length/Å	Max. length/Å	Mean length/Å	Number of complexes
Al-{N _{py} }	1.804	2.388	2.033	562
Al-{N _{amide} }	1.75	2.246	1.920	1218
Al-C	1.629	2.458	1.993	5191
Al-Cl	1.978	2.681	2.151	1562

For Al-{N_{py}}, the bond lengths of **2** (2.1019 and 2.1034 Å) are above average, possibly indicating weaker bond strengths but could also indicate a more constrained bond length imposed by the inclusion of a neighbouring amide. For Al-{N_{amide}}, the bond lengths of **2** (1.8691 and 1.8767 Å) are below average, whilst for Al-C, the bond length of **2** (1.976 Å) is comparable to the average; in all cases the observed bond lengths are within the range of values reported in the CSD.

From Table 6.2, it can be spotted that the methyl group on the aluminium does not sit perfectly between the two ancillary ligands. The angles of hetero ring nitrogen-aluminium-methyl carbon and amide nitrogen-aluminium-methyl carbon are different from their counterparts on the other aminoquinoline, which should be a result of the distorted trigonal bipyramidal structure **2** adopts. N(4)-Al(1)-C(1) is 117.99° (9), a 3.53° difference is seen comparing to N(2)-Al(1)-C(1) angle, which is 121.52° (9). N(3)-Al(1)-C(1) is 102.04° (8), a 5.86° difference is seen comparing to N(1)-Al(1)-C(1), which is 96.18° (8). Numbers in the bracket following the angles are the standard uncertainties.

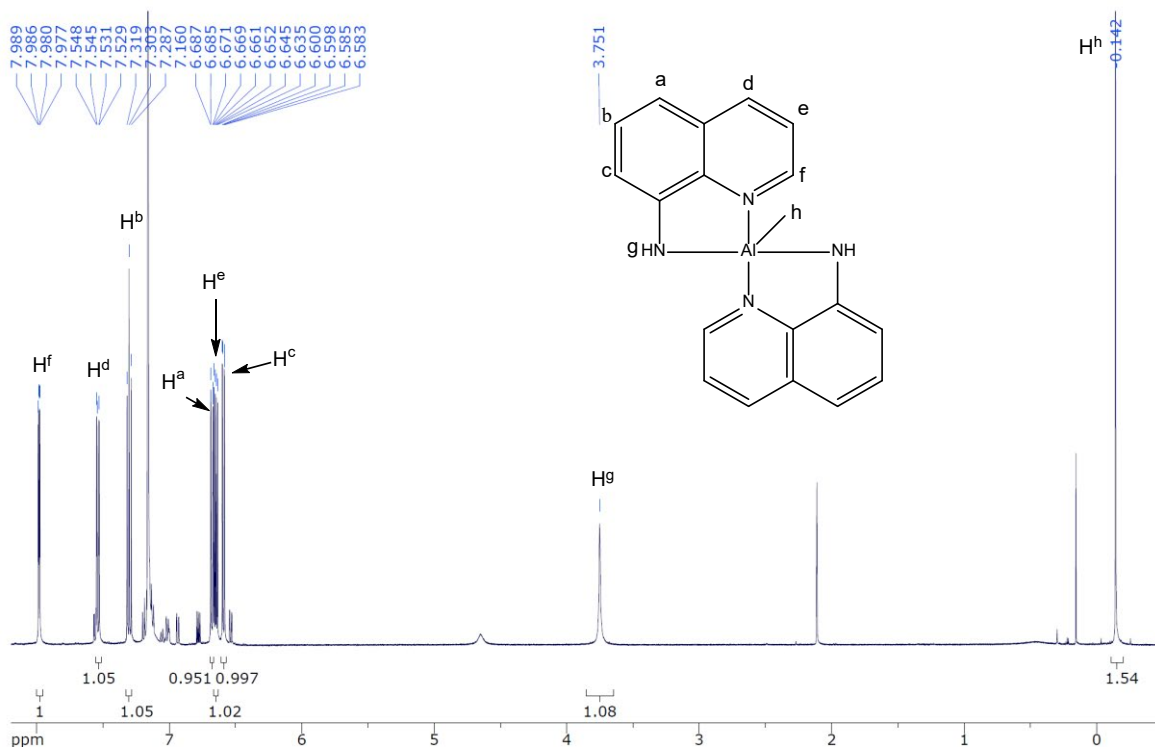


Figure 6.3: ¹H NMR spectrum (500 MHz, C₆D₆, 293 K) of [(AQ)₂AlMe] (**2**)

The ¹H NMR spectrum of complex **2** is shown in Figure 6.3. The ¹H NMR spectrum of **2** showed only one chemical environment for the aminoquinoline ligand, therefore the two ligands of **2** should be rotationally symmetrical about the central aluminium ion, which is consistent with the single crystal data. Same as complex **1**, the minor signals cannot be eliminated by multiple times of recrystallization and purification, or repetition of synthesis, and these signals appeared at basically same chemical shifts and in similar pattern. The minor peaks in the spectrum should therefore come from aggregation in solution (see section 6.2.3 for more detail about this); or from rearrangement of ligand in solution (one possible rearranged form in Figure 6.4). VT-NMR (variable temperature NMR) and the Van't Hoff plot obtained from it should be able to show that complexes are interchanging with each other, but Covid-19 outbreak prevented this, as stated in Chapter 2 (Covid-19 issue applies to complex **3** and **4** as well, and will not be mentioned after to prevent duplication). All proton counts are thus double the value of the integrations in the spectrum.

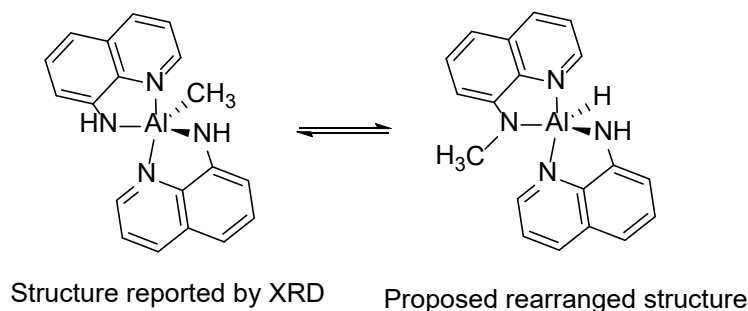
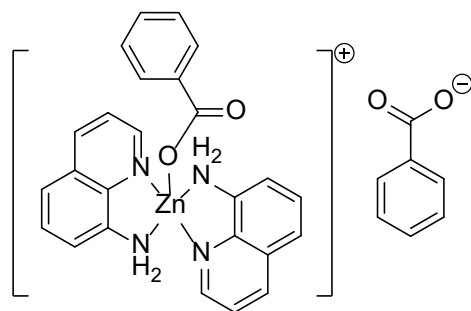


Figure 6.4: Proposed complex rearrangement

The singlet at -0.14 ppm integrates to 3H and is assigned to H^h; this chemical shift is comparable to the region where Al-Me signals are typically seen, for example, Imhoff and co-workers¹ reported Al-Me protons at -0.37 ppm, Armitage and co-workers reported Al-Me protons at -0.25 ppm,² Slaughter *et al.* reported Al-Me protons at -0.47 ppm.³ The singlet at 3.75 ppm integrates to 2H and is assigned to H^g; this chemical shift is comparable to the common chemical shift of aromatic NH₂ protons between 3.5 – 4.5 ppm. The double doublet at 6.60 ppm with ³J = 7.5 Hz and ⁴J = 1 Hz which integrates to 2H and is assigned to H^c; This chemical shift is comparable to the chemical shift of the same aminoquinoline proton on bis-(8-aminoquinoline) monobenzoato zinc(II) benzoate (**6.1**, Figure 6.5) reported by Baruah and co-workers, which is 6.62 – 6.74 ppm.⁴ The multiplet at 6.66 ppm integrates to 2H and is assigned to H^e; this chemical shift is comparable to that of same aminoquinoline protons in **6.1**, which is 6.62 – 6.74 ppm. The double doublet at 6.69 ppm with ³J = 8 Hz and ⁴J = 1 Hz integrates to 2H and is assigned to H^a; this chemical shift is comparable to that of same aminoquinoline protons in **6.1** which is 7.04 – 7.12 ppm. The app. triplet at 7.30 ppm with app. ³J = 8 Hz integrates to 2H and is assigned to H^b; this chemical shift is comparable to that of same aminoquinoline protons in **6.1**, which is 7.45 ppm. The double doublet at 7.55 ppm with ³J = 8.5 Hz and ⁴J = 1.5 Hz integrates to 2H and is assigned to H^d; this chemical shift is comparable to that of same aminoquinoline protons in **6.1** which is 7.82 ppm. The double doublet at 8.00 ppm with ³J = 4.5 Hz and ⁴J = 1.5 Hz integrates to 2H and is assigned to H^f; this chemical shift is comparable to that of same

aminoquinoline protons in **6.1** which is 8.20 ppm. All chemical shifts of protons in **6.1** are reported in C₆D₆.



6.1
Baruah *et al.*

Figure 6.5: Structure of bis-(8-aminoquinoline) monobenzoato zinc(II) benzoate (**6.1**) reported by Baruah and co-workers⁴

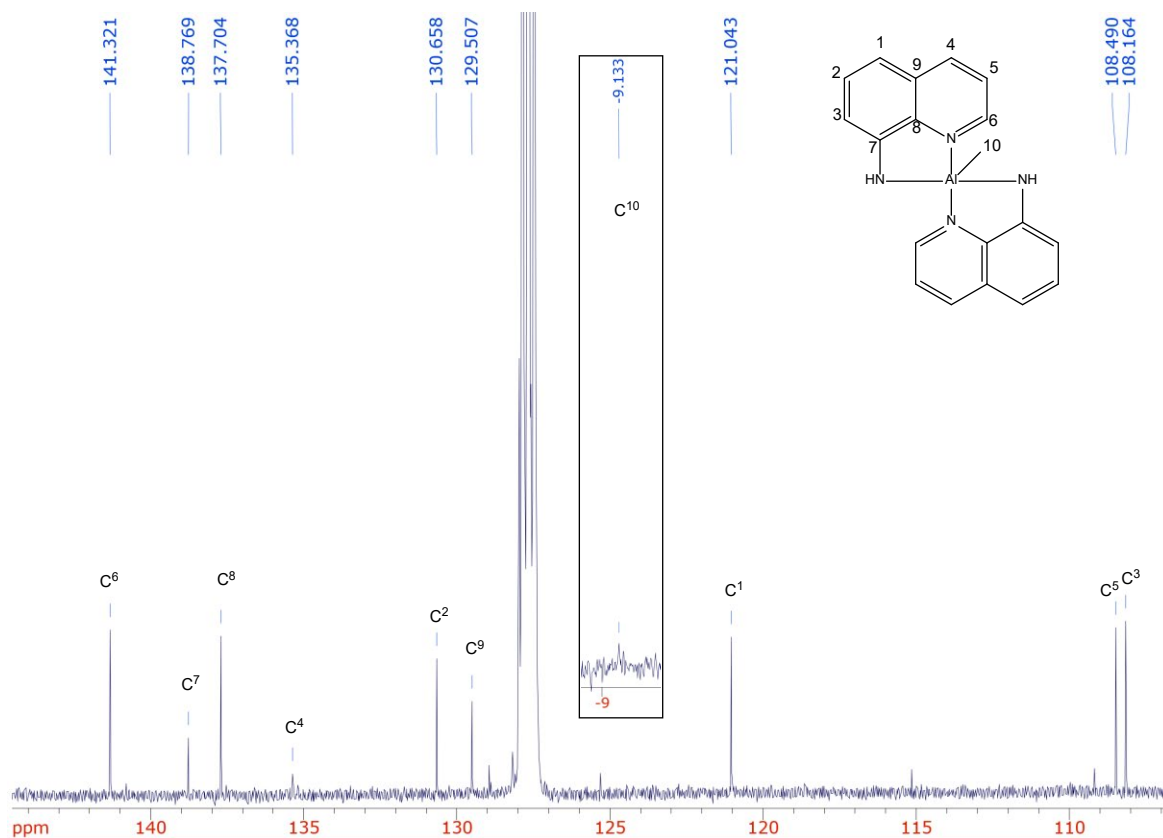


Figure 6.6: ¹³C NMR spectrum (125 MHz, C₆D₆, 293 K) of [(AQ)₂AlMe] (**2**); inset: C¹⁰ peak

Similar to ^1H spectrum, chemical shifts of protons on one aminoquinoline ligand are the same as their counterparts on the other side. The signal at -9.1 ppm is assigned to the aluminium-bound methyl, C^{10} ; this chemical shift is comparable to the typical Al-Me chemical shifts reported by Tritto *et al.*,⁵ which is -8.0 ppm. All the chemical shifts of the aromatic carbons are assigned by HSQC (heteronuclear single quantum coherence) 2D spectrum and have a comparable pattern to the ^{13}C chemical shifts of aminoquinoline pro-ligand reported in CDCl_3 .⁶ The signal at 108.2 ppm is assigned to C^3 . The signal at 121.5 ppm is assigned to C^1 . The signal at 129.5 ppm is assigned to C^9 . The signal at 130.7 ppm is assigned to C^2 . The signal at 135.4 ppm is assigned to C^4 . The signal at 137.7 ppm is assigned to C^8 . The signal at 138.8 ppm is assigned to C^7 . The signal at 141.3 ppm is assigned to C^6 .

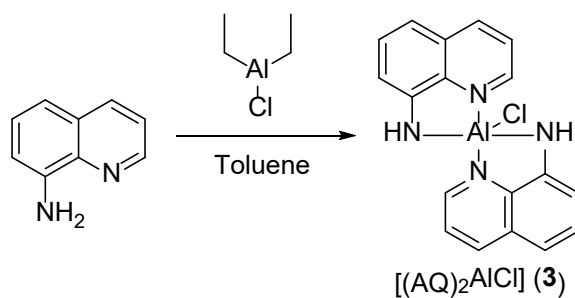
A minor component was evident in the NMR spectra of complexes **2** and **3**. NMR spectra were recorded on samples that had been recrystallized in the same way as used to obtain the single crystals. The minor component could not be removed regardless of recrystallization method, and the minor component does not correspond to pro-ligand. For most complexes of this general type, involving salen ligands contain sterically demanding $t\text{Bu}$ groups (which my ligand does not have), a degree of aggregation in solution is more than possible and would be consistent with the labile coordination chemistry of aluminium. No other species could be detected using mass spectrometry, which is again consistent with a solution state equilibrium. An example of aggregated aminoquinoline-Al complex is given in section 6.2.3.

6.2.2. Synthesis and characterization of $[(\text{AQ})_2\text{AlCl}]$ (**3**)

The results from ROCOP tests with complex **2** (details in section 6.3) indicated that it does not act as an outstanding epoxide / anhydride ROCOP catalyst. This, and the consideration that most ROCOP pre-catalysts tend to be chloride complexes, leads to the thought that changing methyl ligand to chloride may improve its catalytic performance. Generally, methyl group has a tendency to initiate epoxide

polymerization as it is quite nucleophilic, while chloride serves better as a softer initiator thus better for ROCOP. With this idea, $[(AQ)_2AlCl]$ (**3**) was synthesized.

The chloride aluminium complex $[(AQ)_2AlCl]$ (**3**) via the reaction of 1 equivalent of diethyl aluminium chloride with 2 equivalents of aminoquinoline in toluene at room temperature (Scheme 6.3). After workup, complex **3** was obtained as a light brown powder.



Scheme 6.3: Synthetic route of $[(AQ)_2AlCl]$ (**3**)

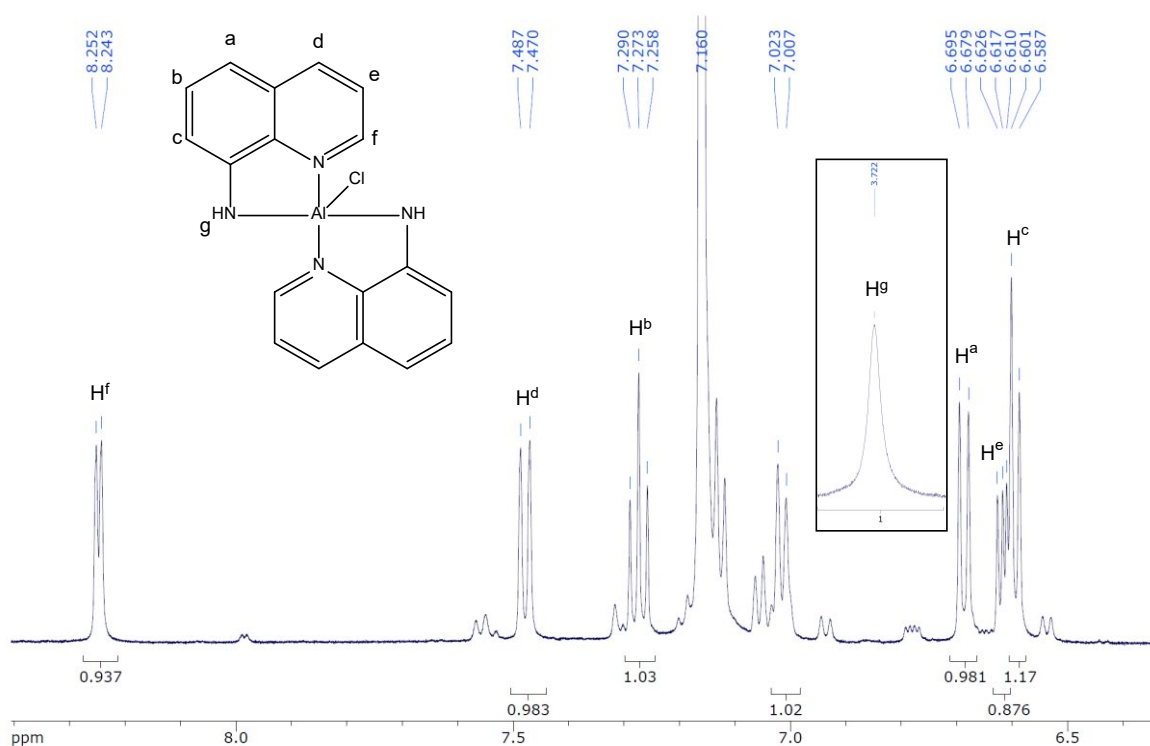


Figure 6.7: 1H NMR spectrum (500 MHz, C_6D_6 , 293 K) of $[(AQ)_2AlCl]$ (**3**); inset: H^g peak

The ^1H NMR spectrum of complex **3** is shown in Figure 6.7. As seen for complex **2**, only one environment for the two aminoquinoline ligands was observed, indicating that they are symmetrical with respect to the central aluminium ion, thus each proton on one ligand should have the same chemical shift and coupling pattern as its counterpart on the other side (although they are still expected to be magnetically inequivalent), and the proton counts should be double the integrations in the ^1H NMR spectrum. Same as complex 1 and 2, the minor signals persisted after careful recrystallizations and repetition of preparation steps, meaning high possibility of aggregated / rearranged complex existence. The singlet at 3.72 ppm integrates to 2H and is assigned to H^g ; this chemical shift is comparable to the common chemical shift of aromatic NH_2 protons between 3.5 – 4.5 ppm. All the aromatic protons are comparable to the chemicals shifts reported by Baruah and co-workers for **6.1**⁴ (which are similar to **2**), and have coupling patterns similar to the reported ^1H NMR spectrum of aminoquinoline in CDCl_3 .⁸ The app. doublet at 6.60 ppm with app. $^3J = 7$ Hz integrates to 2H and is assigned to H^c . The multiplet at 6.62 ppm integrates to 2H and is assigned to H^e . The doublet at 6.70 ppm with $^3J = 8$ Hz integrates to 2H and is assigned to H^a . The app. triplet (apparent triplet) at 7.27 ppm with app. $^3J = 8.5$ Hz (apparent coupling constant) integrates to 2H and is assigned to H^b . The doublet at 7.49 ppm with $^3J = 8.5$ Hz integrates to 2H and is assigned to H^d . The doublet at 8.25 ppm with $^3J = 4.5$ Hz integrates to 2H and is assigned to H^f .

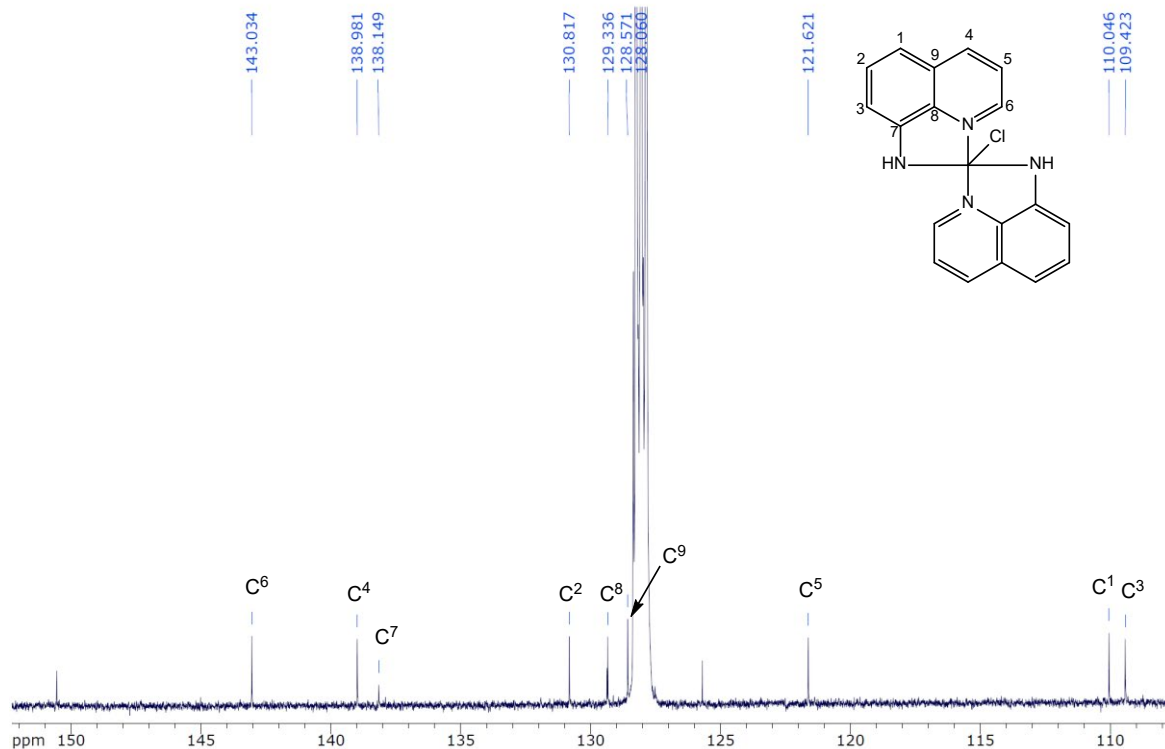


Figure 6.8: ^{13}C NMR spectrum (125 MHz, C_6D_6 , 293 K) of $[(\text{AQ})_2\text{AlCl}]$ (**3**)

The signals in the ^{13}C spectrum are assigned with the aid of a HSQC experiment. The signal at 109.4 ppm is assigned to C^3 . The signal at 110.0 ppm is assigned to C^1 . The signal at 121.6 ppm is assigned to C^5 . The signal at 128.6 ppm is assigned to C^9 . The signal at 129.3 ppm is assigned to C^8 . The signal at 130.3 ppm is assigned to C^2 . The signal at 138.7 ppm is assigned to C^7 . The signal at 139.0 ppm is assigned to C^4 . The signal at 143.0 ppm is assigned to C^6 .

Single crystals of complex **3** were grown from a toluene solution at -40°C . It was found that complex **3** has two polymorphs, of which one (polymorph A) closely resembles to the one previously reported by Engelhardt *et al.*,⁹ whilst another one (polymorph B) crystallize in a different space group, and with slightly different bond angles and bond lengths.

Polymorph A of complex **3** obtained from XRD investigation has a similar structure to that observed for complex **2**, but with slightly different bond angles and bond lengths. The obtained crystal structure is as illustrated in Figure 6.7. Same as the trigonal bipyramidal structure for **2**, in **3**, pyridine nitrogens N(1) and N(3) are at axial

positions (bond angle 167.25°), while the other two nitrogen and chloride are at equatorial positions, with their bond angles with each other close to 120° .

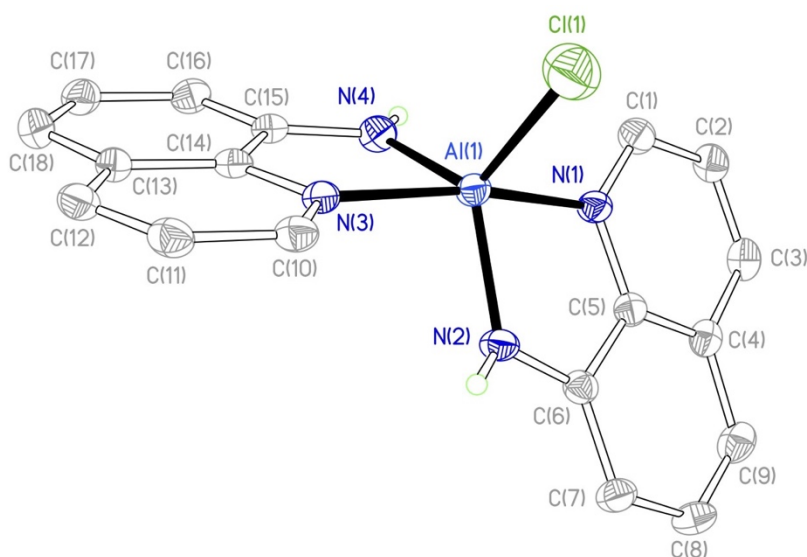


Figure 6.7: Molecular structure of complex **3** (polymorph A), ellipsoids drawn at 30% probability and hydrogen atoms (except hydrogen on N(2) and N(4)) omitted for clarity.

Principal bond lengths and bond angles for polymorph A of complex **3** are listed in Table 6.4 and Table 6.5 respectively.

Table 6.4: Principal bond lengths of complex **3**, polymorph A

Bond	Bond length / Å
Al(1)-N(1)	2.077 (4)
Al(1)-N(2)	1.867 (4)
Al(1)-N(3)	2.062 (4)
Al(1)-N(4)	1.868 (4)
Al(1)-Cl(1)	2.130 (2)
N(2)-C(6)	1.352 (6)
N(4)-C(15)	1.352 (6)

Table 6.5: Principal bond angles of complex **3**, polymorph A

Adjacent bonds	Bond angle / °
N(4)-Al(1)-N(1)	92.72 (17)
N(2)-Al(1)-N(3)	92.43 (16)
N(2)-Al(1)-N(1)	81.34 (16)
N(4)-Al(1)-N(3)	81.26 (17)
N(4)-Al(1)-Cl(1)	119.51 (15)
N(3)-Al(1)-Cl(1)	97.72 (13)
N(2)-Al(1)-Cl(1)	117.69 (16)
N(1)-Al(1)-Cl(1)	95.03 (14)
N(4)-Al(1)-N(2)	122.78 (19)
N(3)-Al(1)-N(1)	167.25 (17)
Al(1)-N(3)-C(10)	129.9 (3)
Al(1)-N(3)-C(14)	111.3 (3)
Al(1)-N(4)-C(15)	118.3 (3)
Al(1)-N(1)-C(1)	130.4 (3)
Al(1)-N(1)-C(5)	111.2 (3)
Al(1)-N(2)-C(6)	118.4 (3)

Polymorph A of Complex **3** crystallizes in the space group $P2_1/c$, different from that of complex **2**, which is $P2_12_12_1$. Compared to the single crystal structure of complex **2**, complex **3** saw a more symmetrical bond angles around the central metal site. Complex **2** showed bond angles of 117.99° and 121.52° for methyl – Al – N_{amide}, differed 3.83° away from each other. While for complex **3**, bond angles for Cl – Al – N_{amide} are 119.51° and 117.69° , differed by 1.82° , only 47.5% of the bond angle gap comparing to their counterparts in complex **2**. If the average bond angles were to be calculated, they are: 119.755 for complex **2**; 118.6 for complex **3**; 1.155° difference. Similarly, the methyl – Al – N_{py} bond angles are 102.04° and 96.18° in complex **2**, 5.86° angle difference. In complex **3**, the Cl – Al – N_{py} bond angles are 97.72° and 95.03° , giving 2.69° angle difference, approximately 45.9% of the angle difference of the counterpart in complex **2**. The average bond angles were

calculated to be: 99.11° for complex **2**; 96.375° for complex **3**; 2.375° difference. From the two pairs of average bond angles that related to the central aluminium ion, it can be concluded that complex **2** has the two aminoquinoline ligands bend further away from the methyl, resulting in larger bond angles comparing to complex **3**. Possible reason could be that CH₃ is more sterically demanding than Cl, causing the ligands at both sides of it bend away from it more. Overall, the structures of complex **2** and **3** are similar to each other, although not exactly identical.

For **3**, Al-{N_{py}} and Al-{N_{amide}} bonds have shorter bond lengths than CSD average, indicating higher bond strengths. On the other hand, the Al-Cl bond in **3** is longer than CSD average, indicating a weaker bond strength.

This molecular structure of [(AQ)₂AlCl] (**3**) is in the same space group as the one that has been previously reported by Engelhardt and co-workers in 1996,⁹ which is also the only existing report regarding this specific structure.

For Cl – Al – N_{amide} bond angles, reported data showed an average of 117.25°, with 1.3° difference between two angles. For Cl – Al – N_{py} bond angles, reported data showed an average of 95.3°, with 1.6° difference between two angles. The average bond angles around central aluminium ion are close to that of complex **3**, but all about 1° smaller than what we have obtained for complex **3**. The Al – N bond lengths reported by Engelhardt *et al.* (1.844, 1.840, 2.059, 2.069 in Å) are shorter than what we have obtained for complex **3** (1.867, 1.868, 2.077, 2.062 in Å), by about 0.01 – 0.02 Å. The reported Al – Cl bond length from Engelhardt *et al.*, however, is 2.184 Å, bigger than what we have measure from our crystal structure (2.130 Å) by 0.54 Å. The space group of [(AQ)₂AlCl] from Engelhardt *et al.* is P2₁/c, which is the same as the complex **3** crystal in this thesis. Overall, complex **3** resembles the reported crystal structure of [(AQ)₂AlCl] with tiny differences.

Polymorph B of **3** which is in the different space group has its details listed below.

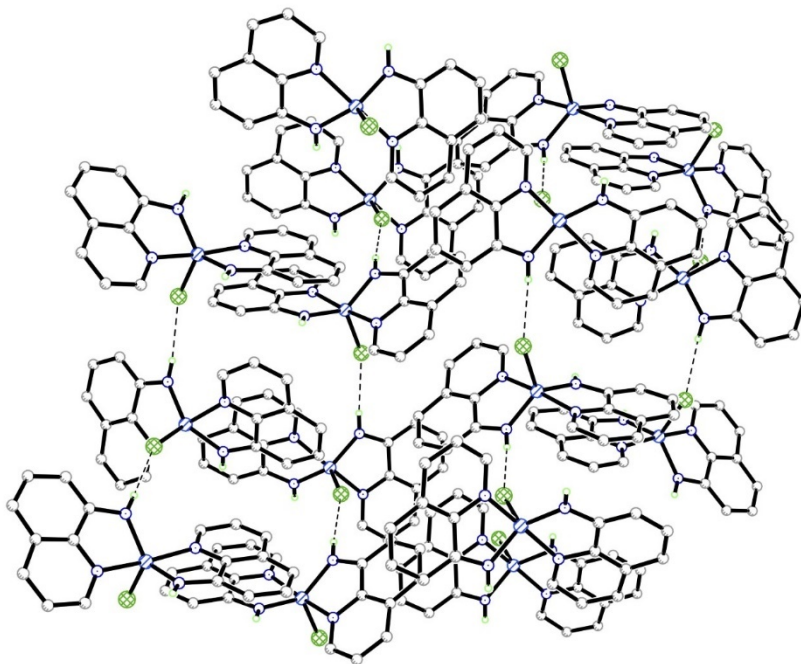


Figure 6.8: Crystal structure of $[(AQ)_2AlCl]$ (**3**), polymorph B, ellipsoids drawn at 30% probability and hydrogen atoms (except hydrogen on N(2) and N(4)) omitted for clarity

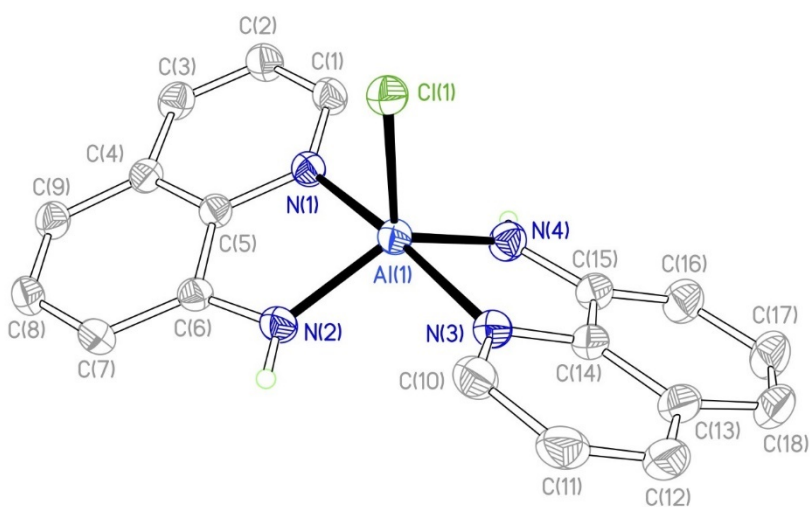


Figure 6.9: Molecular structure of $[(AQ)_2AlCl]$ (**3**), polymorph B, ellipsoids drawn at 30% probability and hydrogen atoms (except hydrogen on N(2) and N(4)) omitted for clarity

Table 6.6: Principal bond lengths of complex **3**, polymorph B

Bond	Bond length / Å
Al(1)-N(1)	2.038 (2)
Al(1)-N(2)	1.852 (2)
Al(1)-N(3)	2.033 (2)
Al(1)-N(4)	1.856 (2)
Al(1)-Cl(1)	2.2086 (9)
N(2)-C(6)	1.366 (3)
N(4)-C(15)	1.371 (3)

Table 6.7: Principal bond angles of complex **3**, polymorph B

Adjacent bonds	Bond angle / °
N(4)-Al(1)-N(1)	93.47 (9)
N(2)-Al(1)-N(3)	94.83 (9)
N(2)-Al(1)-N(1)	82.57 (8)
N(4)-Al(1)-N(3)	82.35 (9)
N(4)-Al(1)-Cl(1)	115.85 (8)
N(3)-Al(1)-Cl(1)	94.25 (7)
N(2)-Al(1)-Cl(1)	112.31 (7)
N(1)-Al(1)-Cl(1)	94.05 (6)
N(4)-Al(1)-N(2)	131.84 (10)
N(3)-Al(1)-N(1)	171.69 (9)
Al(1)-N(3)-C(10)	129.73 (17)
Al(1)-N(3)-C(14)	117.15 (18)
Al(1)-N(4)-C(15)	110.95 (17)
Al(1)-N(1)-C(1)	130.15 (16)
Al(1)-N(1)-C(5)	110.45 (15)
Al(1)-N(2)-C(6)	116.74 (16)

This polymorph crystallized in the space group *Pbca*, different from *P2₁/c* of the previous molecular structure. In Figure 6.8 it is also confirmed that hydrogen bonds

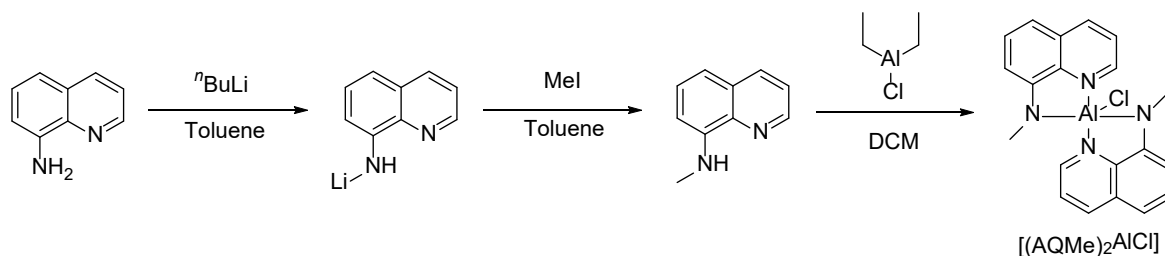
exist between the amide hydrogens and chlorides, this allowed molecules of **3** to be connected into a macromolecular assembly, which opens up the possibility for higher order aggregations. Same as the previous structure, N(3) and N(1) are on the axial positions of the trigonal bipyramid, but with an angle 171.69° (9), which is closer to the undistorted 180° comparing to polymorph B (167.25°). For the equatorial angles, polymorph B showed bigger deviations from the undistorted 120° , recording angles at 115.85° (8), 112.31° (7) and 131.84 (10). The bond lengths are also slightly different from polymorph A, but not as prominent as the bond angles. Bond lengths wise, Al-N_{py} is higher than the CSD average by a tiny amount (0.0003 Å), Al-N_{amide} is shorter than the CSD average, but all Al-N bond lengths are within the CSD recorded range. The Al-Cl bond is longer than the CSD average, possibly due to the repulsion with the aminoquinoline ligands.

Despite being documented already, [(AQ)₂AlCl] has not been put to catalytic tests in any existing papers, and the study of this complex in ROCOP is therefore an exciting prospect.

6.2.3. Synthesis and characterization of [(AQMe)₂AlCl] (**4**)

With the success in epoxide / anhydride ROCOP with complex **3**, attempts have been made to replace the amide hydrogen with other groups to see how they can affect the catalytic performance. The first replacement group attempted was methyl.

[(AQMe)₂AlCl] (**4**) was synthesized by reacting aminoquinoline with ⁿBuLi and MeI first to obtain AQMe, followed by reaction with diethyl aluminium chloride at room temperature. [(AQMe)₂AlCl] was obtained as a reddish-brown powder. The synthetic route of [(AQMe)₂AlCl] (**4**) is shown in Scheme 6.4.



Scheme 6.4: Synthesis of [(AQMe)₂AlCl] (**4**)

The ¹H NMR spectrum of complex **4** is shown in Figure 6.10.

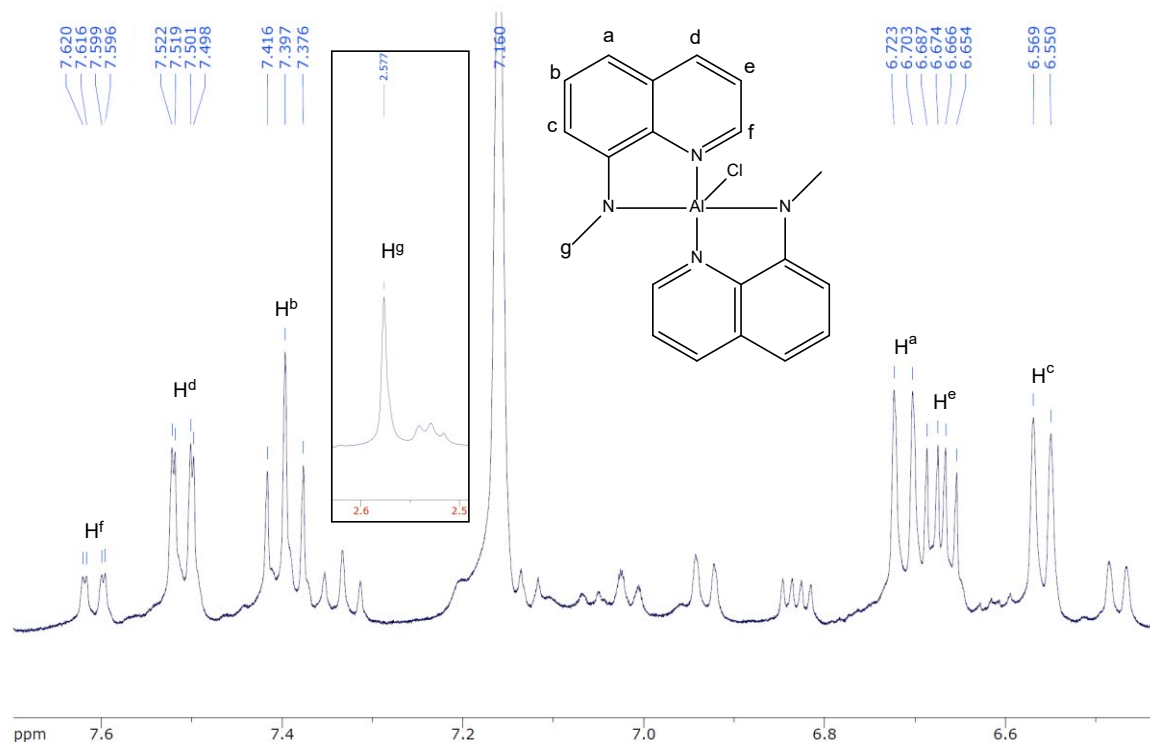


Figure 6.10: ¹H NMR spectrum (400 MHz, C₆D₆, 293 K) of [(AQMe)₂AlCl] (**4**);

inset: H_g peak

Good quality ¹H NMR cannot be obtained for [(AQMe)₂AlCl] (**4**) in any commonly used NMR solvent as it was found to be of very low solubility, which caused the signal to noise ratio to be quite low. This situation has also been reported by Engelhardt *et al.*,⁹ who are the first (and only) researchers reporting the [(AQ)AlCl] (**3**) complex before. They proposed that due to poor solubility of **3**, no meaningful NMR spectrum can be obtained, which does not happen to complex **3** but happened to complex **4**. Repetition of synthesis and recrystallization cannot eliminate the

minor peaks, and these minor peaks were at the same chemical shifts and in the same pattern for every spectrum recorded. Moreover, the discussed aggregation / rearrangement of complex in solution is highly likely to be affecting complex **4**, which is proved by the capturing of a tetrameric complex via single crystal X-ray diffraction (as will be discussed in this section). As can be seen from the ^1H NMR in Figure 6.10, the signals are low in intensity, and do not integrate to any reasonable values for some peaks. Due to the solubility issue, the impurity peaks could be higher in terms of integration than they actual proportion in the sample. Nonetheless, the aromatic protons seemed to follow the same coupling patterns and showed comparable NMR shifts to that of complex **2** and **3**, and hereby assigned as below.

The singlet at 2.58 ppm is assigned to the NMe protons H^g . The doublet at 6.57 ppm with $^3J = 7.6$ Hz is assigned to aromatic proton H^c . The multiplet at 6.69 ppm is assigned to aromatic proton H^e . The doublet at 6.72 ppm with $^3J = 8$ Hz is assigned to aromatic proton H^a . The app. triplet with app. $^3J = 7.6$ Hz at 7.40 ppm is assigned to aromatic proton H^b . The double doublet at 7.52 ppm with $^3J = 8.4$ Hz and $^4J = 1.2$ Hz is assigned to aromatic proton H^d . The double doublet at 7.62 ppm with $^3J = 8.4$ Hz and $^4J = 1.6$ Hz is assigned to aromatic proton H^f . The minor peaks do not correspond to aminoquinoline pro-ligand, thus there is no unreacted aminoquinoline left from previous synthesis steps (Figure 6.11).

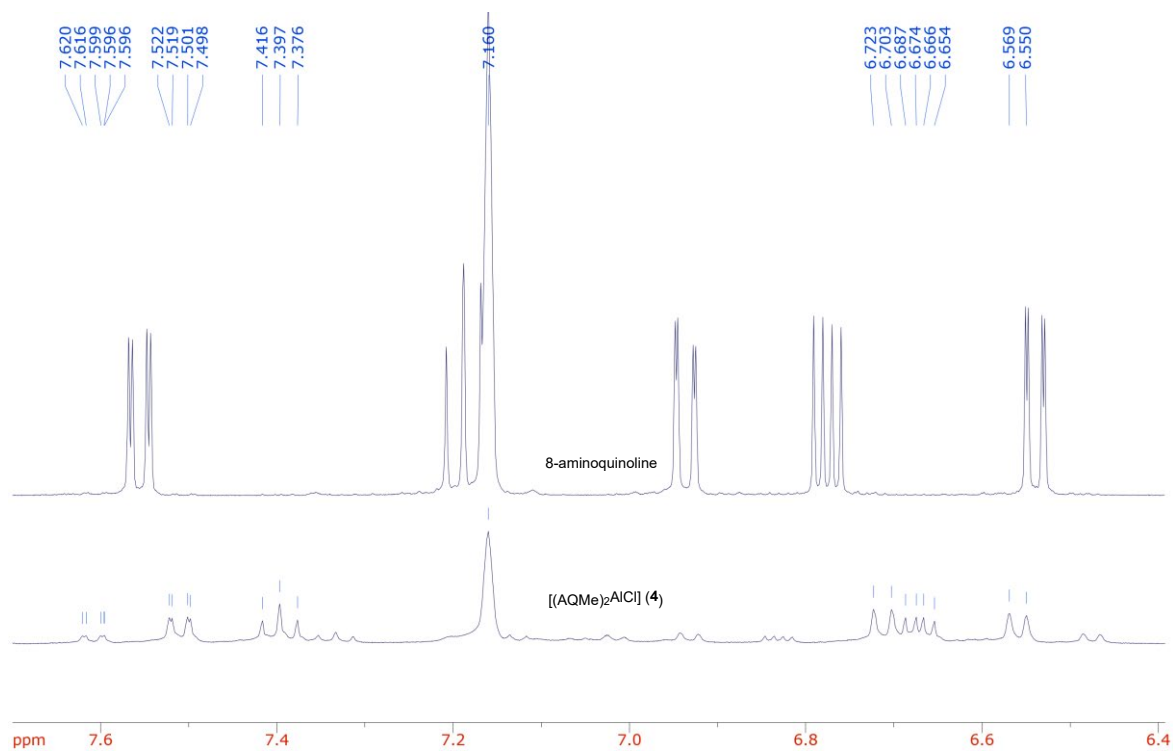


Figure 6.11: ^1H NMR (400 MHz, C_6D_6 , 293 K) comparison of pro-ligand aminoquinoline and complex **4**

As have discussed before, the minor peaks cannot be removed even after recrystallization, due to possible aggregation, rearrangement and magnetic inequivalence in the NMR solution. Previously in BDW group, it was found that 5-coordinate aluminium complexes can aggregate to form minor complex, which has been discussed in section 2.3.2, Figure 2.13). Also, in complex **4**, the NMe moieties could sterically clash with the opposite AQ ligand, resulting in one or more minor aggregated / rearranged complexes that appear as minor peaks in the NMR spectrum. The concept that the aminoquinoline complexes could aggregate in solution is supported by a serendipitous result when attempting to prepare $[(\text{AQMe})_2\text{AlCl}]$ (**4**) *in-situ* by reaction of aminoquinoline with $n\text{BuLi}$, followed by MeI, before adding AlEt_2Cl . An undetermined side reaction occurred during the reaction with the addition of MeI and as a consequence the tetrameric μ -imido aluminium complex $[(\text{AQ})\text{AlMe}]_4$ (**5**) was obtained, verified by the advantageous formation of single crystals. The molecular structure of $[(\text{AQ})\text{AlMe}]_4$ (**5**) is shown in Figure 6.12. Whilst the result could not be reproduced and therefore not discussed further

regarding its catalytic results in this thesis, and there is no indication that the minor components in the spectra of complexes **2** and **3** are this imido complex, the formation of complex **5** nevertheless demonstrates that such sterically undemanding ligands such as the aminoquinoline can easily form higher order aggregates.

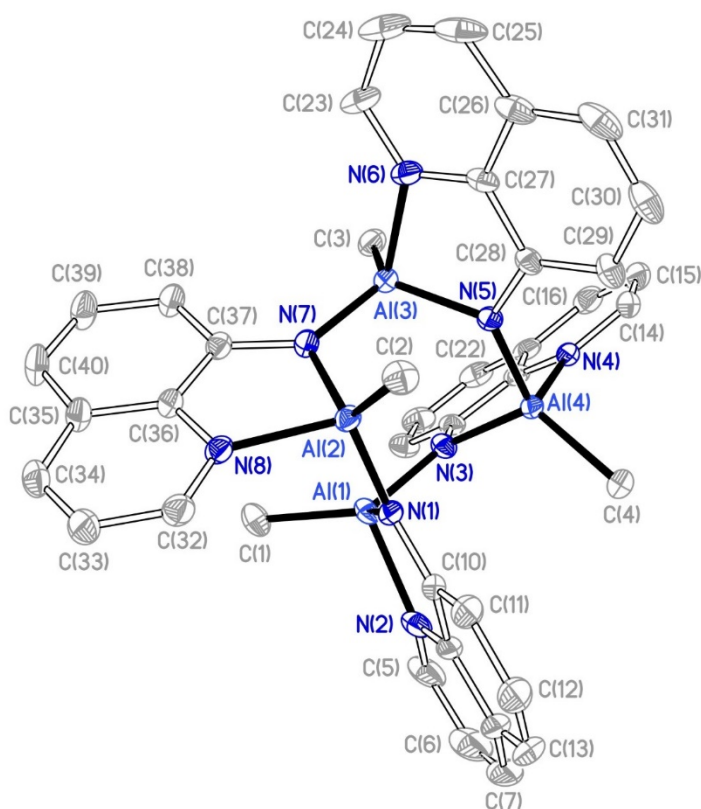


Figure 6.12: Structure of tetrameric $[(AQ)AlMe]_4$ (**5**), ellipsoids drawn at 30% probability and hydrogen atoms omitted for clarity.

Table 6.8: Principal bond lengths of $[(AQ)AlMe]_4$ (**5**)

Bond	Bond length / Å
Al(1)-N(1)	1.8651 (18)
Al(1)-N(2)	1.991 (2)
Al(1)-N(3)	1.8222 (19)
Al(1)-C(1)	1.961 (2)
N(1)-C(10)	1.361 (3)

Table 6.9: Principal bond angles of [(AQ)AlMe]₄ (**5**)

Adjacent bonds	Bond angle / °
N(3)-Al(1)-N(1)	106.21 (8)
N(2)-Al(1)-N(3)	104.37 (8)
N(2)-Al(1)-N(1)	86.23 (8)
N(3)-Al(1)-C(1)	122.66 (10)
N(2)-Al(1)-C(1)	107.40 (10)
N(1)-Al(1)-C(1)	122.19 (10)
Al(1)-N(1)-Al(2)	115.59 (5)

The bond lengths and bond angles around every aluminium ion are basically identical, thus only bond lengths and bond angles around Al(1) are included.

Generally, all the bond lengths are within the typical ranges as they should be from CSD data, and all slighter shorter than the average bond lengths, indicating overall stronger bonds. The geometry around each Al ion is a distorted tetrahedral, distortion mainly caused by the constraint to the N(2)-Al(1)-N(1) angle due to the structural limitation of aminoquinoline ligand itself.

Single crystals of complex **4** could not be obtained but the structure of the complex is assumed to be comparable to complex **3**, on the basis of mass spectrometry and NMR spectroscopic data. The parent ion was observed in the EI mass spectrum, which gave a peak at 376.1, as calculated for [(AQMe)₂AlCl]⁺.

6.3. ROCOP of anhydrides / epoxides with aminoquinoline – aluminium complexes as catalysts

Whilst the chloride complex [(AQ)₂AlCl] (**3**) has been reported previously, none of the aminoquinoline complexes have been studied for their efficacy in ROCOP. Therefore, such studies were undertaken to see if a new class of ROCOP catalysts could be developed.

6.3.1. ROCOP of anhydrides / epoxides with [(AQ)₂AlMe] (2) as catalyst

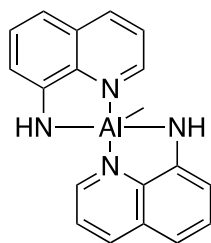


Figure 6.13: Structure of [(AQ)₂AlMe] (2)

To gain an initial indication of the effectiveness of [(AQ)₂AlMe] (2) (Figure 6.13) in catalyzing ROCOP reactions, several feasibility tests were undertaken.

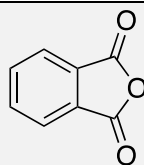
The general experimental procedures are as stated below.

In the glove box, the designated amount of complex **2** was added into an oven-dried screw-cap vial together with designated amount of PPNCI as co-catalyst. Calculated amount of epoxide and anhydride were then added, the vial then sealed, stirred and heated outside the glove box for a specific amount of time. Upon finishing, methanol was added to quench the reaction.

The epoxide and anhydride monomers used for these tests are listed below in Table 6.10 and Table 6.11.

Table 6.10: Epoxide monomers used for complex **2** catalysis tests

Propylene oxide (PO)	Cyclohexene oxide (CHO)	Epichlorohydrin (ECH)

Table 6.11: Anhydride monomers used for complex **2** catalysis tests

Phthalic anhydride (PA)

The epoxide / anhydride monomer choices are made based on the same reasons that have been discussed in Chapter 3.

The ROCOP results with these monomers and complex **2** as catalyst are summarized in Table 6.12, as shown below.

Table 6.12: ROCOP catalysis results of complex **2**

Entry	Epoxide/equiv.	Anhydride/equiv.	Time/minute	Selectivity/%	Conversion/%
1	PO/2000	PA/400	240	70	90
2	CHO/2000	PA/400	70	15	18
3	ECH/2000	PA/400	240	40	63

All reactions were at 100°C, with 1 equivalent of **2** as catalyst and 1 equivalent of PPNCI as co-catalyst.

From the table it can be seen that **2** is capable of catalyzing epoxide / anhydride ROCOP, but as shown by the results, at 100°C, the selectivities are not ideal for the chosen monomer combinations. One reason being the high reaction temperature causing more epoxide monomers to proceed through epoxide homopolymerization route rather than ROCOP route, another reason could be that complex **2** does not provide an energetically favoured reaction path for ROCOP to be predominant. Also, the methyl group on the complex could possibly initiate epoxide homopolymerization, as seen for the [(CpHO)₂Al₂Me₄], which catalyzed epoxide homopolymerization too well and therefore gave low selectivities for most of the ROCOP reactions. Conversion wise, 100°C should give quick ROCOP reactions, but in fact the highest conversion achieved in the three reactions was 90% (with a mere 70% selectivity),

other conversion at poor 18% and 63%. This fact means thermodynamically dissatisfying reaction pathways were provided by **2** for the ROCOP, thus reaction is rather slow. As have discussed in Chapter 1, an optimal catalyst for ROCOP usually requires a good leaving group for the whole reaction to be energetically favoured thus increase not only the selectivity but also the reaction rate. To prove that better leaving group on the catalyst leads to better selectivity and conversion, we then attempted to synthesize $[(AQ)_2AlCl]$ (**3**), which has a similar structure to complex **2**, but with the methyl group replaced by chloride. Since Cl^- is reported by many previous literatures to be a good initiating group for ROCOP,^{10,11} complex **3** therefore theoretically possesses a better initiating group, hence possibly provides better reaction pathways for ROCOP reactions. However, the methyl groups tend to de-coordinate from the complex and initiate the ring-opening polymerization of epoxide, while chlorides are more likely to de-coordinate from the complex after the ring-opening. Thus, it is best to initiate the epoxide using external chlorides, which exemplifies the importance of adding $PPNCl$ as a co-catalyst.

6.3.2. ROCOP of anhydrides / epoxides with $[(AQ)_2AlCl]$ (**3**) and $[(AQMe)_2AlCl]$ (**4**) as catalysts

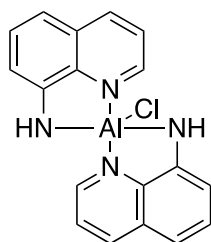


Figure 6.14: Structure of $[(AQ)_2AlCl]$ (**3**)

To verify the effect of replacing a methyl ligand for a chloride would bring into ROCOP catalysis, several ROCOP of epoxides / anhydrides were done with **3** as catalyst.

The general experimental procedures are as follows:

In glove box, the designated amount of complex **3** was added into an oven-dried screw-cap vial together with designated amount of PPNCI as co-catalyst. Calculated amount of epoxide and anhydride were then added, the vial then sealed, stirred and heated outside the glovebox for a specific amount of time. Upon finishing, methanol was added to quench the reaction.

The epoxide and anhydride monomers used for these tests are listed below in Table 6.13 and Table 6.14.

Table 6.13: Epoxides used for complex **3** ROCOP tests

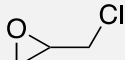
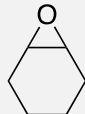
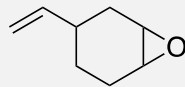
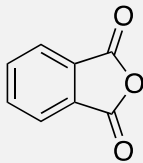
			
PO	ECH	CHO	VCHO

Table 6.14: Anhydrides used for complex **3** ROCOP tests


Phthalic anhydride (PA)

The ROCOP catalysis results for different combinations of the above monomers were summarized in Table 6.15 as below.

Table 6.15: ROCOP results of epoxide / anhydride with complex **3** as catalyst

Entry	Epoxide/Ratio	Anhydride/Ratio	Co-catalyst/Ratio	Temperature/°C	Time/min	Selectivity/%	Conversion/%
1	ECH/2000	PA/400	N/A	100	240	71	98
2	ECH/2000	PA/400	PPNCI/1	100	240	63	100
3	ECH/2000	PA/400	PPNCI/1	100	180	65	100
4	ECH/2000	PA/400	PPNCI/1	100	120	66	100
5	ECH/2000	PA/400	PPNCI/1	100	80	92	100
6	PO/2000	PA/400	PPNCI/1	100	180	66	100
7	PO/2000	PA/400	PPNCI/1	100	120	80	100
8	PO/2000	PA/400	PPNCI/1	100	60	89	98
9	PO/2000	PA/400	PPNCI/1	70	225	93	100
10	VCHO/2000	PA/400	PPNCI/1	70	245	99	87
11	CHO/2000	PA/400	PPNCI/1	70	180	100	100
12	CHO/2000	PA/400	PPNCI/2	70	180	100	100

All reactions were carried out with 1 equivalent of **3** as catalyst.

Entry 1 (Table 6.15) indicates that even without co-catalyst PPNCl, complex **3** still performed much better than complex **2** (98% conversion vs. 63% conversion), which justified the importance of including chloride in the complex for better ROCOP initiation. Due to the use of excess epoxide as solvent, even if the reaction mechanism is energetically much favoured for ROCOP than epoxide homopolymerization, once anhydride is depleted, the epoxide homopolymerization will take place nonetheless, which would lead to drop of selectivity if the reaction was left on beyond the time needed for full consumption of anhydride monomers. Subsequent reactions (Entry 2, 3, 4, 5) proved this hypothesis. As shown in the table, while keeping all the other reaction conditions the same, shortening the reaction time caused the selectivity to increase. Decreasing the reaction time from 240 min to 80 min causes the selectivity to increase from 63% to 92%, consistent with the hypothesis that after total consumption of anhydride, the catalyst will continue to catalyze the epoxide homopolymerization, which has a very low chance to happen when free anhydride monomers co-exist with epoxide. The mechanistic elucidation for this is as followed: After formation of the metal-alkoxide intermediate, the intermediate can react with either epoxide to afford an ether linkage, or an anhydride to afford an ester linkage. To proceed via epoxide homopolymerization, the alkoxide intermediate needs to form a 4-membered ring transition state with the incoming epoxide monomer, which is high in energy due to the ring stress (Scheme 6.5). In contrast, during ROCOP, the carboxylate afforded by opening an anhydride de-coordinates from the metal site before attacking a coordinated epoxide (Step 4 to 7, Scheme 6.6), which in many cases is much lower in energy compared to the 4-membering ring transition state of the epoxide homopolymerization. In Chapter 3 and Chapter 4, $[(\text{CpHO})_2\text{Al}_2\text{Me}_4]$ (**1**) was proved to provide a comparable or even lower energy reaction mechanism for epoxide homopolymerization compared to the epoxide / anhydride ROCOP, which is possibly caused by the bimetallic mechanism since **1** contains two aluminium ions. However, for complex **3**, it is demonstrated by experimental data that it catalyzes ROCOP preferably over epoxide

homopolymerization energy barrier. Under this scenario, the kinetic control of reaction becomes imperfect, thus leading to the existence of polyether in the yielded polymer. Based on this theory, lowering the reaction temperature would give better kinetic control thus higher selectivity, as shown in Entry 9, 70°C reaction temperature gave 93% selectivity together with 100% conversion. However, further decreasing reaction temperature did not give any better selectivity (not included in Table 6.15), which means complex **3** does not give perfect selectivity for this specific epoxide / anhydride combination. Entry 10 demonstrates that 70°C is a good reaction temperature that leads to 99% selectivity for PA / VCHO, the conversion rate can be increased to 100% by adjusting the reaction time. Similarly, for PA / CHO, 70°C gives 100% selectivity, and at 3 hours` reaction time, 100% conversion as well. Comparison between Entry 11 and 12 leads to the interpretation that the use of different equivalents of co-catalyst PPNCI (above 1 equivalent) does not affect the selectivity nor the conversion. Thus, to keep the lowest possible usage of PPNCI (which could be critical for cost control in industrial applications), 1 equivalent PPNCI is used for all the other ROCOP reactions with complex **3** and **4**.

With the conclusion that complex **3** worked well as a catalyst for epoxide / anhydride ROCOP, complex **4** was proposed and synthesized to compare the performance differences made by changing the amine hydrogen with methyl group. The structure of complex **4** is illustrated in Figure 6.15.

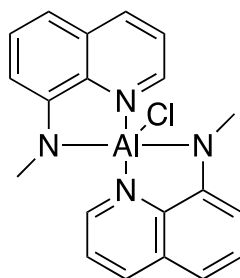


Figure 6.15: Structure of complex **4**

The trial reactions for complex **4** are generally the same as those for complex **3** and yielded similar trends. Several reactions regarding reaction times and reaction

temperatures were undertaken for both complex **3** and **4** to optimize the reaction conditions so that highest possible selectivity and conversion can be achieved. The finalized ROCOP results are listed in Table 6.18, and used epoxides and anhydrides are listed in Table 6.16 and 6.17.

General reaction and polymer purification procedures are described as followed:

In the glove box under nitrogen atmosphere, pre-weighted complex **3** or **4** (1 equivalent) was added into an oven-dried screw-cap vial. Chosen anhydride monomer (400 equivalents) was then added into the vial. Subsequently, excess epoxide monomer (2000 equivalents) which also works as solvent was added. The vial was then sealed, taken out of the glove box and put onto a pre-heated aluminium heating block. The reaction mixture then stirred under designated temperature for a certain amount of time. Upon finishing, methanol was injected into the reaction mixture to quench the reaction. A small aliquot of reaction mixture was taken and dissolved in CDCl_3 for NMR tests.

Reaction mixture then washed into a beaker with methanol, precipitate (polymer) was filtered out and dried under reduced pressure.

Table 6.16: Epoxides used for finalized complex **3** and **4** ROCOP reactions

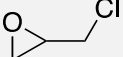
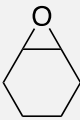
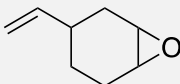
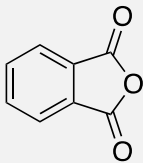
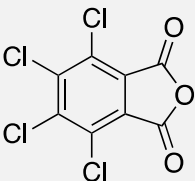
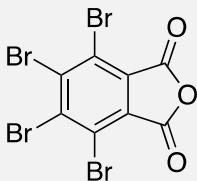
			
PO	ECH	CHO	VCHO

Table 6.17: Anhydrides used for finalized complex **3** and **4** ROCOP reactions

		
Phthalic anhydride (PA)	Tetrachlorophthalic anhydride (TCPA)	Tetrabromophthalic anhydride (TBPA)

All reactions in Table 6.18 contained 1 equivalent of PPNCI as co-catalyst.

Selectivity is calculated by the percentage of polyester in the polymer produced from ROCOP reaction, same as described in Chapter 3. The selectivity was calculated by the formula:

$$\text{Selectivity} = \frac{\text{Integration of polyester proton } ^1\text{H signal}}{(\text{Integration of polyether proton } ^1\text{H signal} + \text{Integration of polyester proton } ^1\text{H signal})}$$

Where proton signal is the proton signal of (a) specific iconic proton(s) on epoxide unit, which has different chemical shift in polyether and polyester, thus can be used as a handle for determining selectivity.

Conversion is calculated by the formula below, same as in Chapter 3:

$$\text{Conversion} = \frac{[\text{integration of PA aromatic protons in copolymer}]}{[\text{sum of integration of PA aromatic protons in copolymer and monomer}]}$$

As the rate-determining step for ROCOP is the step which epoxide adds to the polymer chain via ring-opening (step 6 to 7 in Scheme 6.6), the identity of the anhydride should not significantly affect the reaction rate, thus for a specific epoxide, any anhydride should yield the same conversion after the same time. Based on this approximation, the conversions of entries involve TCPA and TBPA are assumed to be the same as PA, since TCPA and TBPA have no trackable proton to be identified in their ^1H NMR spectra. Examples of spectra for selectivity and conversion calculations are provided in section 3.3, Chapter 3 and are not repeated here.

Unlike most of the polymer samples which are hard to separate from the reaction mixture or too little in weight after being separated in Chapters 3 and 4 (which make yield calculations almost without any scientific importance), many of the polymer

samples have decent weights after separation, therefore yield was included for all the entries in Table 6.18.

The yield was calculated by the formula:

$$\text{Yield} = \text{Weight of obtained polymer} / \text{theoretical total weight of polymer}$$

Where weight of obtained polymer is the weight of polymer obtained by the procedure described in the polymer purification procedures above in this section. However, mass losses definitely occurred during the polymer condensation, separation and drying process, and some of the polymers went through filter paper as well thus cannot be separated, so the yield is for reference only.

Table 6.18: Finalized ROCOP reaction results with complex **3** and **4** as catalysts

Entry	Monomer A/Ratio	Monomer B/Ratio	Catalyst	Temperature/°C	Time/min	Selectivity/%	Conversion/%	Yield/%
1	PA/400	ECH/2000	Complex 3	70	210	100	99	58
2	TCPA/400	ECH/2000	Complex 3	70	210	100	99	82
3	TBPA/400	ECH/2000	Complex 3	70	210	100	99	60
4	PA/400	ECH/2000	Complex 4	70	175	100	99	23
5	TCPA/400	ECH/2000	Complex 4	70	175	96	99	34
6	TBPA/400	ECH/2000	Complex 4	70	175	97	99	6
7	PA/400	CHO/2000	Complex 3	70	180	100	100	58
8	TCPA/400	CHO/2000	Complex 3	70	180	100	100	69
9	TBPA/400	CHO/2000	Complex 3	70	180	98	100	66
10	PA/400	CHO/2000	Complex 4	70	150	96	98	88
11	TCPA/400	CHO/2000	Complex 4	70	150	95	98	91
12	TBPA/400	CHO/2000	Complex 4	70	150	95	98	78
13	PA/400	PO/2000	Complex 3	70	225	93	100	50
14	TCPA/400	PO/2000	Complex 3	70	225	93	100	83
15	TBPA/400	PO/2000	Complex 3	70	225	93	100	76
16	PA/400	PO/2000	Complex 4	70	185	99	56	N/A*

17	PA/400	PO/2000	Complex 4	70	190	98	70	N/A*
18	PA/400	PO/2000	Complex 4	70	200	79	75	N/A*
19	PA/400	PO/2000	Complex 4	70	200	80	59	N/A*
20	PA/400	VCHO/2000	Complex 3	70	300	100	100	80
21	TCPA/400	VCHO/2000	Complex 3	70	300	100	100	96
22	TBPA/400	VCHO/2000	Complex 3	70	300	100	100	85
23	PA/400	VCHO/2000	Complex 4	70	240	100	100	80
24	TCPA/400	VCHO/2000	Complex 4	70	240	100	100	90
25	TBPA/400	VCHO/2000	Complex 4	70	240	100	100	80

* : Not measured due to inconsistency of repeating experiments. All reactions were done with 1 equivalent of catalyst and 1 equivalent of co-catalyst.

When using complex **4** as a catalyst for PO reactions (Entry 16 – 19, Table 6.18), the conversion showed significant fluctuation; ROCOP reactions involving PO are known in the Ward research group to be amongst the most problematic, since the low boiling point of PO renders it possible for some of the PO to occupy the vial headspace and reduce the conversions – an observation that can make conversions less reproducible than other epoxides.

For all other reactions the selectivity is generally excellent, with the lowest being 93% (Entry 13 to 15). Combining the facts that Entries 13 to 15 all involve PO and complex **4** does not operate nicely with PO in ROCOP, it is possible that these series of aminoquinoline-based catalysts have side reactions that are more significant with PO, and which affects complex **4** more than complex **3**. Despite this, 93% selectivity is still acceptable. For other epoxide / anhydride combinations, selectivities are all above 95%, indicating excellent control over the polymer microstructure. Conversions of >99% were achieved in reaction times from less than 3 hours to 5 hours, depending on epoxide / anhydride combinations, which can be regarded as outstanding compared to many catalyst systems in the literature. All the data in Table 6.18 combined together, we can conclude that complex **3** and **4** are efficient catalysts for ROCOP reactions of epoxide / anhydride. An intriguing finding is that for **4**, reaction time needed for ~ 99% conversion is always around 80% of that for **3**

This set of data suggest that by swapping the amide proton with methyl group, the catalytic activity is increased, and the magnitude of this increase is virtually the same for all PA monomer combinations. From the electronic aspect, a methyl group is more electron-donating than the hydrogen. Therefore, the aluminium central ion is made more electron-rich by the electron-donating methyl group. This ROCOP catalytic performance enhancement brought by more electron-donating ligands has been previous reported by Liu *et al.*,¹² Lu *et al.*¹³ and Darensbourg *et al.*¹⁴ They proposed that enhanced conversion and selectivity can be brought to epoxide / CO₂ ROCOP by catalysts with more electron-donating ligand. Lu *et al.* proposed that

stronger electron-donating ability of CH₃-N comparing to nitrogen results in increased catalytic activity (Figure 6.16).

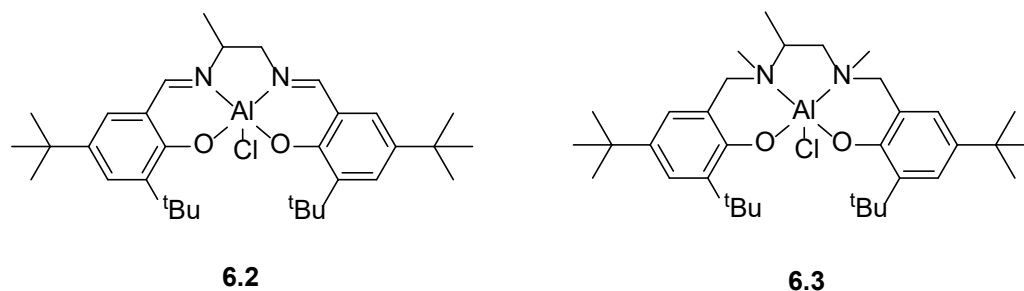


Figure 6.16: Structures of catalysts by Lu *et al.*¹³

As shown in Figure 6.16, **6.3** has methyl groups on the nitrogen instead of double bond in **6.2**, thus making **6.3** more electron-donating towards the central aluminium. This leads to increases of selectivity from 85% to 92% and turnover frequency (epoxide that have been translated into polymer) from 9% to 79% for epoxide / CO₂ ROCOP. Moreover, Lu *et al.* proposed that increase in ligand's steric hinderance would also increase the catalytic activity of the resultant metal complexes. By adding the methyl group onto the nitrogen, both are achieved at once, thus further increasing the activity of the catalyst.

6.3.3. MALDI-MS data of polymer samples

The polymer samples obtained from the experiments described in Table 6.18 were probed by Matrix-Assisted Laser Desorption-Ionization Mass Spectroscopy (MALDI-MS). MALDI-MS measures the mass numbers of the polymer samples, M_n and M_w can also be calculated from the MALDI-MS measured data for polymer property evaluation.

The MALDI-MS samples were prepared by the general procedure as described below:

Saturated sodium carbonate solution was made by adding excess sodium carbonate into High Performance Liquid Chromatography (HPLC) grade

tetrahydrofuran (THF), 30 minutes` stirring then gravitational filtration. 10 mg mL⁻¹ trans-2-[3-(4-tert-Butylphenyl)-2-methyl-2-propenylidene]malononitrile (DCTB) solution was prepared with HPLC grade THF as well. Measured weight of polymer sample was added into a vial, followed by the addition of HPLC grade THF to make 1 mg mL⁻¹ concentration solution. 10 µL of the polymer THF solution was extracted and transferred into a new vial, followed by the addition of 1 µL of sodium carbonate THF solution which works as the ion source, and 1 µL of DCTB solution which serves as the matrix. The mixture was then mixed properly to make a homogeneous solution, and 1 µL of the resultant solution was dropped onto the MALDI-MS sample plate and left in the fumehood overnight for solvent evaporation. After full evaporation of solvent, the MALDI-MS sample plate was put into the MALDI-MS instrument for testing.

However, as MALDI-MS is a method that does not work for every polymer sample, especially when a general sample preparation method was used for all the polymers, not all the polymer samples from Table 6.18 were successfully run by MALDI-MS. For those that gave proper polymer mass spectra, their results are summarized in Table 6.19. The entry numbers in Table 6.19 are the same as the one in Table 6.18 for easier recognition.

The theoretical M_n is calculated by the formula:

$$\text{Theoretical } M_n = 36.5 + \{ \text{Conversion} \times 400 \times (\text{sum of molecular masses of monomers}) / \text{equivalent of chloride} \}$$

Equivalent of chloride = equivalent of chloride on catalyst + equivalent of PPNCI = 2 (number of chlorides equals to the number of active chains in the reaction); 36.5 is the mass of H + Cl, which are the end groups of the polymer chain. All Theoretical M_n are rounded to the nearest integers.

Theoretical repeating unit mass is calculated by the formula:

$$\text{Theoretical repeating unit mass} = M_r (\text{epoxide monomer}) + M_r (\text{anhydride monomer})$$

Table 6.19: MALDI-MS results for polymer samples

Entry (Cat.) ^a	Monomers	M _n (LP)/Da	Đ (LP)	M _n (RP)/Da	Đ (RP)	Repeating unit mass/Da	Theoretical repeating unit mass/Da	Theoretical M _n /Da
1 (3)	PA/ECH	3481.66	1.01	3995.77	1.00	206.0	240.62	47679
2 (3)	TCPA/ECH	8022.12	1.00	N/A	N/A	378.7	378.42	74964
3 (3)	TBPA/ECH	N/A	N/A	6211.08	1.07	557.6	556.22	110168
4 (4)	PA/ECH	1263.81	1.11	N/A	N/A	241.8	240.62	47679
5 (4)	TCPA/ECH	501.484	1.02	N/A	N/A	219.0	378.42	74964
6 (4)	TBPA/ECH	N/A	N/A	N/A	N/A	N/A	556.22	110168
7 (3)	PA/CHO	5585.81	1.02	5485.29	1.02	246.1	246.243	49285
8 (3)	TCPA/CHO	N/A	N/A	N/A	N/A	N/A	384.043	76845
9 (3)	TBPA/CHO	N/A	N/A	N/A	N/A	N/A	561.843	112405
10 (4)	PA/CHO	6297.15	1.01	6232.55	1.02	246.2	246.243	48300
11 (4)	TCPA/CHO	N/A	N/A	N/A	N/A	N/A	384.043	75308
12 (4)	TBPA/CHO	N/A	N/A	5170.66	1.04	562.2	561.843	110157
13 (3)	PA/PO	N/A	N/A	N/A	N/A	N/A	206.18	41273
14 (3)	TCPA/PO	N/A	N/A	N/A	N/A	N/A	343.98	68833
15 (3)	TBPA/PO	N/A	N/A	N/A	N/A	N/A	521.78	104393

20 (3)	PA/VCHO	5498.29	1.05	5376.89	1.05	272.0	272.28	54493
21 (3)	TCPA/VCHO	4947.05	1.04	5037.29	1.03	272.1	410.08	82053
22 (4)	TBPA/VCHO	5491.96	1.02	5409.15	1.07	588.8	587.88	117613
23 (4)	PA/VCHO	5422.31	1.05	5343.68	1.07	272.1	272.28	54493
24 (4)	TCPA/VCHO	5104.37	1.05	5000.08	1.05	272.2	410.08	82053
25 (4)	TBPA/VCHO	N/A	N/A	5693.46	1.13	587.2	587.08	117613

LP represents Linear Positive mode measurements from the MALDI instrument, while RP stands for Reflector Positive mode measurements. In LP mode, an ion travel down a linear path, and the m/z (mass / charge) ratio is determined by the time it takes for the ion to reach the detector. In RP mode, at the end of an ion's traveling path, there is an ion mirror that reflects the ion at a small angle towards the detector. Usually, when both methods work, the RP mode will have better accuracy. All M_n and M_w reported are from the series of peaks with highest intensity in the spectra, with reasonable repeating unit masses. \bar{D} is determined by the Polytools software (by Bruker). N/A means the software could not identify appropriate average molecular weight information from the data. Repeating units are essentially the same for LP mode and RP mode (which theoretically should be), if both methods worked. If only one of the two modes is working, the repeating unit in the table is from the mode that works for the specific polymer sample.

Details about the N/A cells will be given later in the form of MALDI-MS spectra.

In Table 6.19, the first thing worth noticing is that all of the polymer samples showed excellent \bar{D} control, with the highest at 1.13 (entry 25, Table 6.19), and second highest at 1.11 (entry 4), all other \bar{D} values lower than 1.10 and many of them close to 1.0. This indicates that the ROCOP is performed in a controlled and stable manner when catalyzed by **3** and **4**. Second thing is that none of them has M_n value fall in vicinities of the theoretical M_n values. Possibilities that lead to this phenomenon could be back-biting, the scenario in which the end of the polymer reacted with the head of the polymer that is on the catalyst, resulting in early termination of the chain growth before the free anhydride monomer runs out. Liu's group¹² and Kerton *et al.*¹⁵ have proposed that stronger electron-donating ability of the amino donor causes reduced Lewis acidity of the central metal ion, leading to a weaker interaction with the growing anionic polymer chain, thereafter results in higher propensity of back-biting since some of the dissociated polymer chains will attack themselves (e.g. back-biting). This trend is observed for ECH-containing reactions (entries 1, 2 and 4, 5), as **4** (more electron-rich aluminium) results in much

lower M_n / M_w comparing to 3 (less electron-rich aluminium). However, for CHO and VCHO reactions, this trend is not observed. Entry 7 vs. 10, the CHO / PA polymer saw a molecular weight increase when 4 is used compared to 3. For VCHO / PA and VCHO / TCPA ROCOP, entries 20, 21 vs. 23, 24 also showed similar trends, that using 4 as catalyst results in higher polymer molecular weights than when 3 is used. A possible explanation could be that ECH is spatially smaller than CHO and VCHO, thus the folding and intramolecular attack of the dissociated anionic polymer chain onto itself is easier. However, back-biting could still be happening to all the entries, just to different extents, which would still result in lower-than-expected chain lengths. Also, the repeating unit mass, which is the separation between peaks in the same peak series (details about peak series and separation are discussed later in this chapter), either fit well with the theoretical repeating unit mass, or deviates by a big value from the theoretical value. For samples like entries 2, 3, 7, 10, 23, measured repeating unit masses fits almost perfectly into the theoretical values, while for Entry 1, 5, 21, 24, the experimental values differed by quite an amount from what they should be. The exact reason for this phenomenon is still unknown. Despite this, none of the samples gave two different repeating unit (e.g., one corresponds to epoxide monomer and another one corresponds to anhydride), all the entries with reasonable repeating units have their repeating unit mass = epoxide + anhydride. This is consistent with the hypothesis that the ring-opening of epoxide is significantly slower than the anhydride opening, thus the polymer ended with epoxide is not observed, and the MALDI-MS spectra generally gave “pseudo homopolymer” pattern. In a pseudo homopolymer pattern, mass units of copolymers can only be observed as the sum of co-monomers, and no specific single monomer mass unit can be observed.

For the software to recognize the mass peak series and analyze them properly, the MALDI-MS spectrum of a sample usually needs to be clear and sharp without too much baseline noise or peaks from other possible impurities (i.e., secondary mass

series that lie close to the main series). Representative MALDI-MS spectra are shown as below.

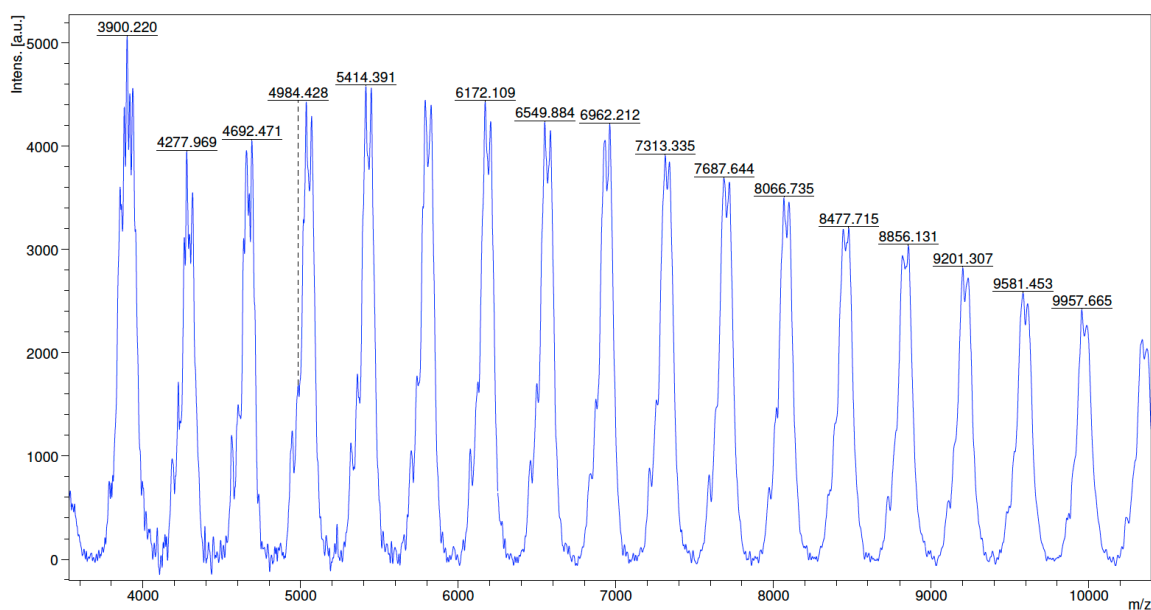
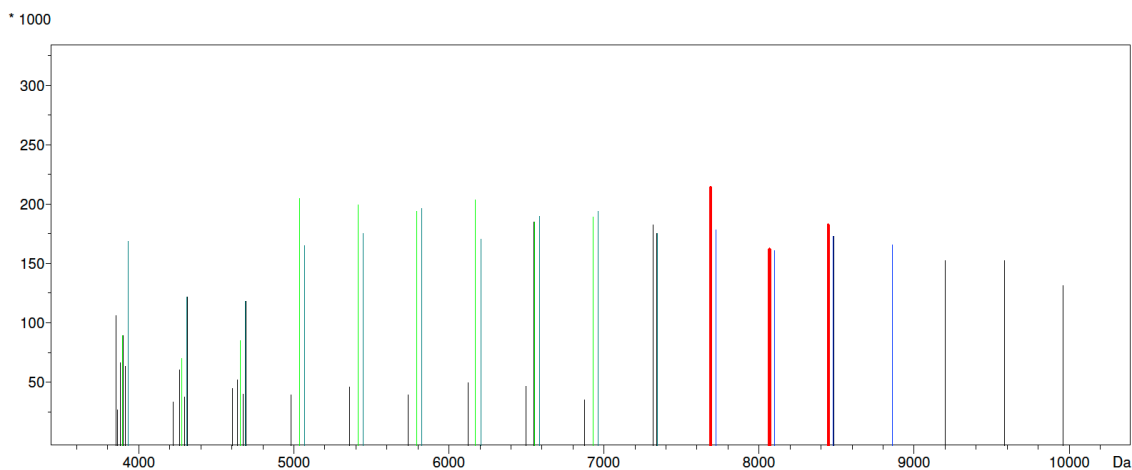


Figure 6.17: MALDI-MS spectrum (LP) for Entry 2 (TCPA/ECH, Table 6.19)

As we can see from Figure 6.17, a typical MS spectrum consists of several peak series, which should all have the same separation (if they are from the same monomer combination). Their different residual mass values are due to the different end groups attached to the polymer chains, which is the fundamental difference between individual polymer mass peak series. To achieve both visual clarity and analytical simplicity, the peaks can be reduced to straight line (eliminating their broadness), as shown in Figure 6.18.



n	ser.	rep.unit	resid.	end1	end2	cation	Mn	Mw	pd	DP	% I.	cnt
1	1	378.743	89.3741			Na	8022.12	8034.69	1.00157	21.1809	6	3
2	2	378.743	122.088			Na	8257.89	8279.85	1.00266	21.8034	7.4	4
3	3	378.743	89.0530			Na	5643.77	5781.55	1.02441	14.9013	15.5	9
4	4	378.743	122.950			Na	5720.91	5922.14	1.03517	15.1050	18.3	10

Figure 6.18: Line-peaks and peak lists (LP) for Entry 2 (TCPA/ECH, Table 6.19)

The colour of the lines correspond to the colour annotation in the n column of the peak list table; ser. stands for series; rep. unit stands for repeating unit mass value; resid. stands for the difference between measured polymer molecular mass and the closest integer multiple of repeating unit mass; cation stands for the cation source that have been used for sample preparation, which is sodium for the MALDI-MS samples in this chapter; M_n and M_w are number average molecular weight and weight average molecular weight for the polymer sample; pd is polymer dispersity index, which is calculated by the formula:

$$D = M_w / M_n$$

DP is degree of polymerization, which is the number of monomeric units in a polymer.^{16,17} In the case of alternating polymer we have in this chapter, monomeric unit is one epoxide monomer + one anhydride monomer. % I. is the percentage intensity of the peak series, and cnt is number of peaks in the peak series. These definitions stay the same for all the MALDI-MS peak lists in this chapter.

As we can see from Figure 6.18, all four series have the same repeating unit mass, which is only 0.283 Da away from the theoretical value. This fact serves as a great evidence that the polymer is a (almost) perfect alternating polymer, in agreement with the ^1H NMR analysis. Also, the residual mass for series 1/3 and series 2/4 are close to each other, with decimal place difference. This means they're highly likely to be actually the same series, which have been classified as different series because of inaccuracy arising from line broadness in the spectra. Theoretically, the identification of the end group can be addressed from the end group mass. However, efforts in finding end groups with good mass match and relevant structure gave no reasonable results for this peak list.

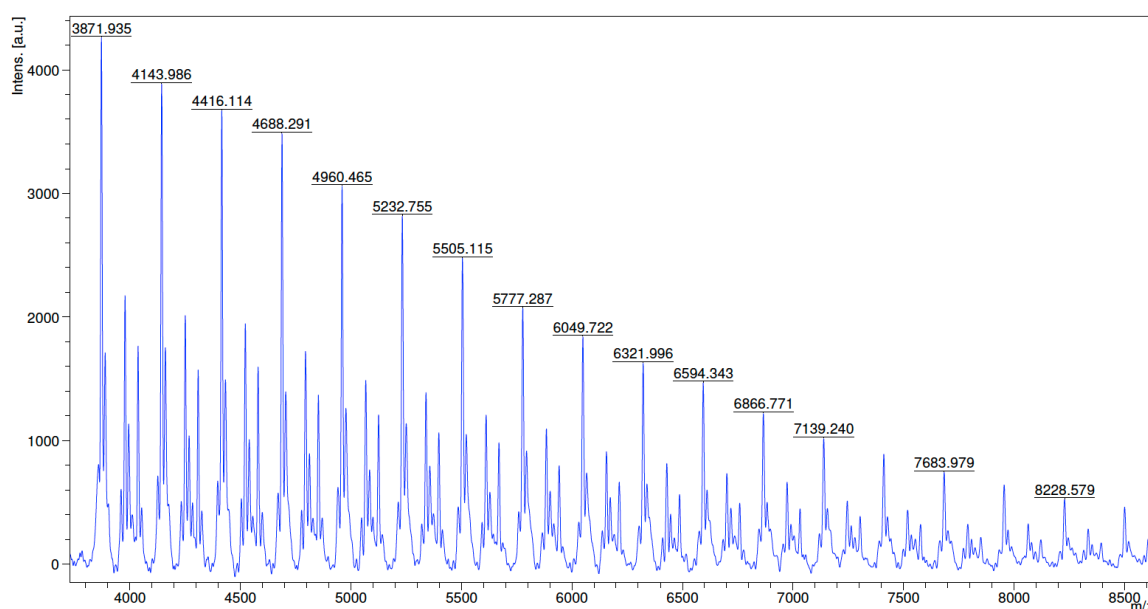
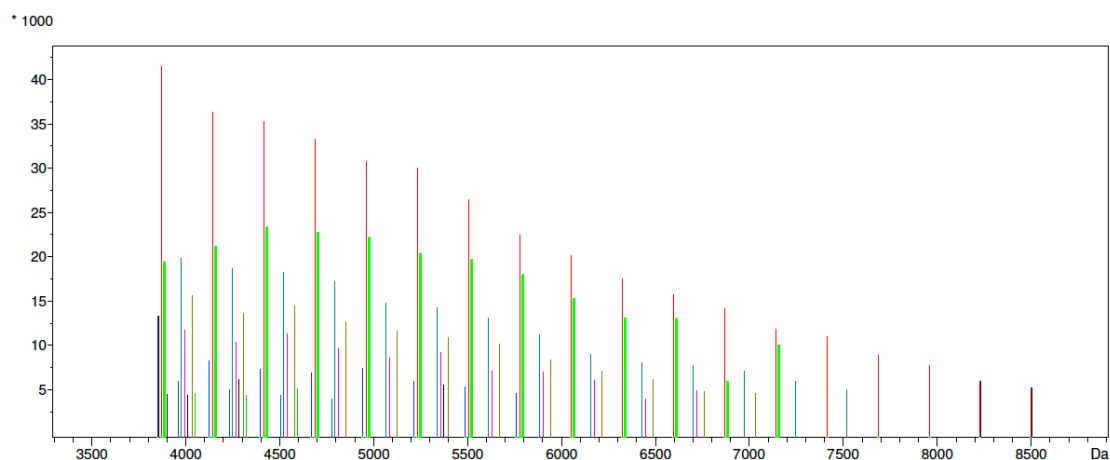


Figure 6.19: MALDI-MS spectrum (LP) for Entry 23 (VCHO/PA, Table 6.19)

LP spectrum of Entry 23 (Table 6.19) is another good example of typical polymer MS spectrum. Several series of peaks with same repeating unit but different residues, and the sharp peaks (narrower peak width) make this spectrum an even better example of a spectrum from a sample that is suitable for the specific MALDI-MS preparation method. Different sample preparation method can affect the outcome to a high extent, and there is no solid factor that determines what

preparation method can be used. The method used in this thesis is a general method that works for many but not every reported polymer samples synthesized.



n	ser.	rep.unit	resid.	end1	end2	cation	Mn	Mw	pd	DP	% I.	cnt
1	1	272.144	39.8038			Na	5422.31	5706.27	1.05237	19.9244	32.1	18
2	2	272.144	21.2941			Na	4611.79	4696.24	1.01831	16.9461	5.2	8
3	3	272.144	56.4245			Na	5239.90	5406.12	1.03172	19.2542	19.2	13
4	4	272.144	146.355			Na	5302.21	5499.24	1.03716	19.4831	14.8	14
5	5	272.144	204.318			Na	5188.25	5336.28	1.02853	19.0643	10.5	12
6	6	272.144	163.536			Na	5099.96	5232.46	1.02598	18.7399	7.9	11
7	7	272.144	220.798			Na	4311.98	4323.84	1.00275	15.8445	1.3	3
8	8	272.288	125.498			Na	4303.62	4325.00	1.00497	15.8054	1.7	4

Figure 6.20: Line-peaks and peak lists (LP) for Entry 23 (VCHO/PA, Table 6.19)

Same as the spectrum for entry 2 (Table 6.19), entry 23 also has a measured repeating unit mass (272.144) fitting almost perfectly into the theoretical value (PA + VCHO = 148.1 + 124.18 = 272.28), indicating the existence of 100% selectivity alternating polymer, consistent with the ^1H NMR data. However, 8 different series means there are at least 8 different end groups in this reaction, which means the termination step could be complicated. \bar{M}_w/\bar{M}_n wise, the control over polymer weight distribution is good, with \bar{M}_w/\bar{M}_n for all series close to 1.0.

For some other polymers which came out with poor MALDI-MS spectra, the software may refuse to analyze the spectra, but useful information can still be extracted from the spectra, below are some examples of poor MALDI-MS spectra from Table 6.19.

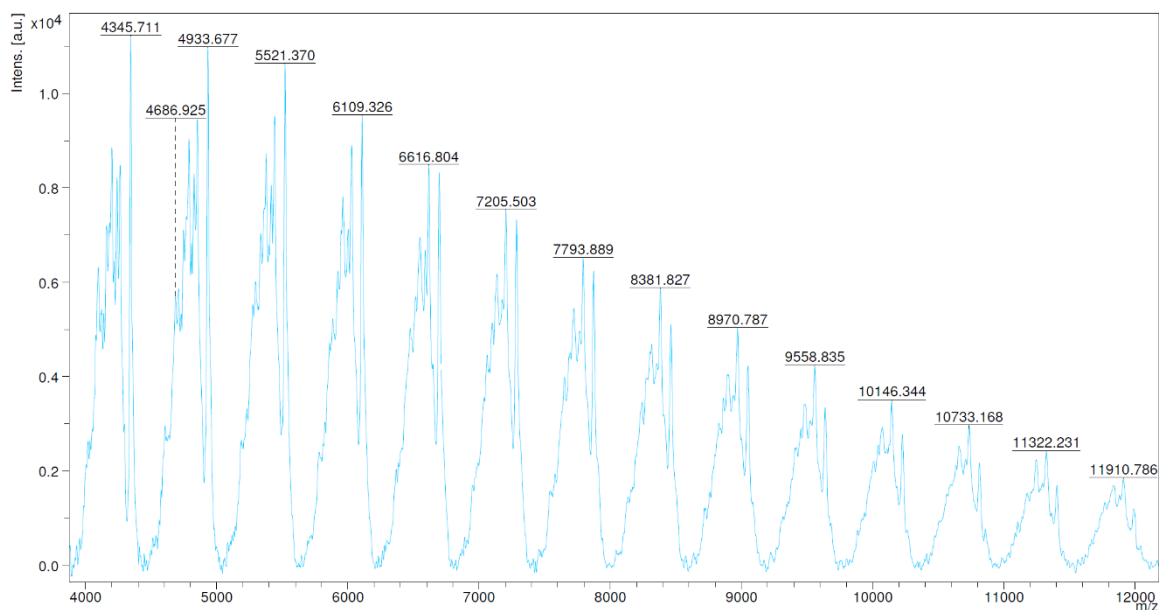


Figure 6.21: MALDI-MS spectrum (LP) for Entry 25 (VCHO/TBPA, Table 6.19)

As can be seen in the spectrum corresponding to Entry 25 (Table 6.19), the LP mode data are broad, and each big peak consists of a number of small peaks. This kind of spectrum means the polymer samples are not fully compatible with the MALDI sample preparation method. Despite this, it can still be seen that the sharpest peaks' series (4345.711, 4933.677, 5521.370) has a repeating unit about 587.8, which is consistent with the RP mode results and the theoretical repeating unit value. However, the LP mode result for Entry 25 is not accepted by Polytool, which means detailed data cannot be obtained by computational analysis. The factor that makes it incompatible with the Polytools software is probably its poor peak sharpness.

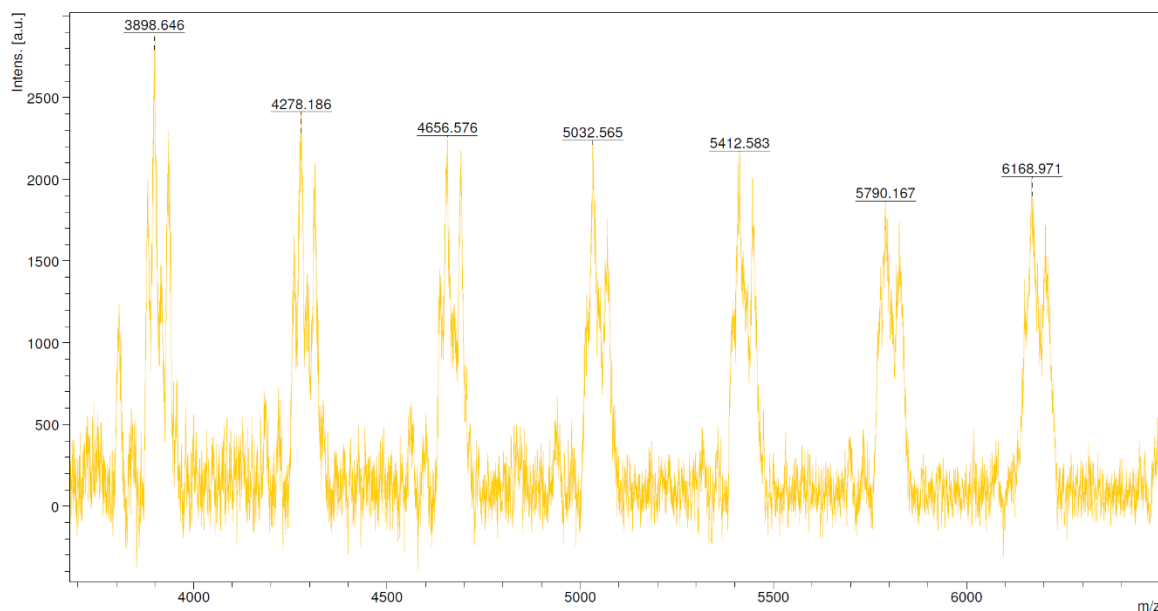


Figure 6.22: MALDI-MS spectrum (RP) for Entry 2 (ECH/TCPA, Table 6.19)

As can be seen in Figure 6.22, the RP MALDI spectrum for Entry 2 has broad peaks and high baseline noise. A high base noise level leads to low signal-to-noise ratio, thus poor spectrum quality. The sharpest peaks in the spectrum (3898.646, 4278.186, 4656.576, 5032.565, ...) showed a repeating unit mass around 378, in agreement with the LP and theoretical repeating unit value.

To demonstrate the trends in M_n / M_w changes regarding different catalysts used and different monomers used, several plots were prepared, as shown below.

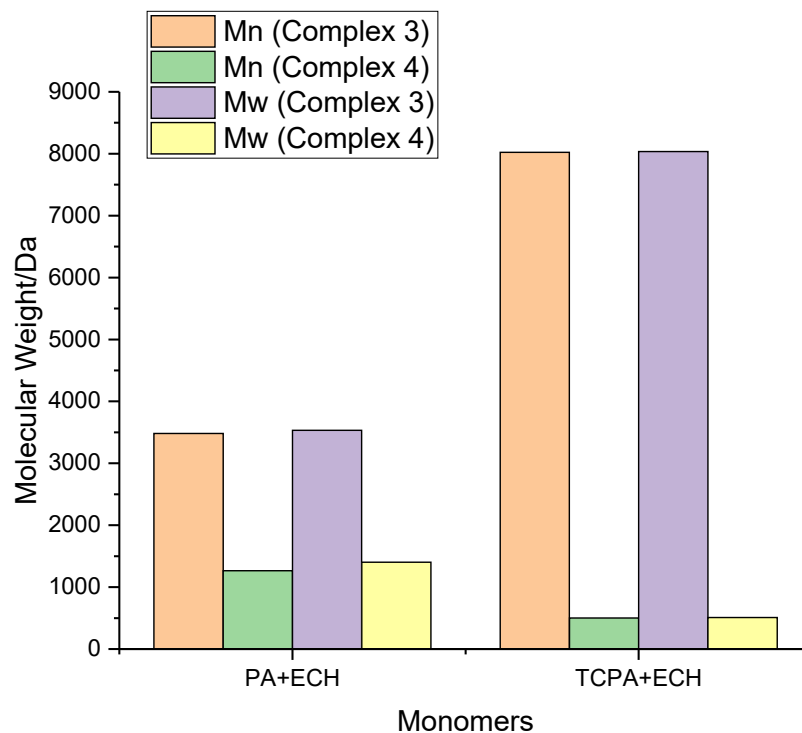


Figure 6.23: M_n / M_w comparison for ROCOP with ECH catalyzed by complexes **3** and **4**

For ECH ROCOP samples, complex **3** yielded much higher M_n and M_w compared to complex **4**. Although as a catalyst, complex **4** required a shorter reaction time to reach 100% conversion, it possibly induces more side reactions (such as back-biting) which may cause the polymer chains to terminate earlier than seen for complex **3**.

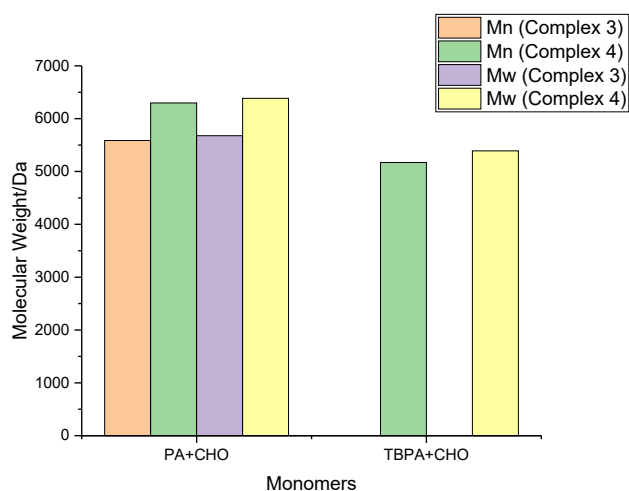


Figure 6.24: M_n / M_w comparison for ROCOP with CHO catalyzed by complexes **3** and **4**

For PA+CHO, complex **4** catalyzed sample is higher in both M_n and M_w , indicating a more stable chain growth process.

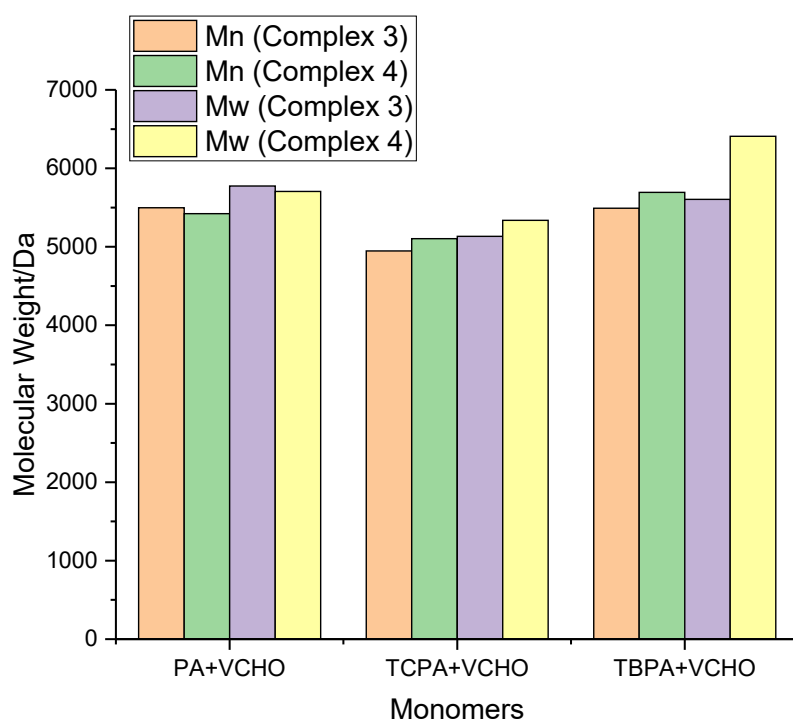


Figure 6.25: M_n / M_w comparison for ROCOP with VCHO catalyzed by complexes **3** and **4**

As the set with most software-recognizable data, VCHO seemed to be the epoxide monomer that produces best quality ROCOP polyesters in terms of MALDI-MS (which means these samples are most compatible with the sample preparation method used for MALDI-MS, but as mentioned before in the discussions of Figure 6.19, there is no certain criterium that can be relied on to determine which method is suitable for which type of polymer). For every monomer combination, complex **3** and **4** gave polymers with comparable M_n and M_w (with M_w for TBPA+VCHO showing a 1071.57 difference). In this scenario, the methyl group on complex **4** seemed to be accelerating the reaction comparing to hydrogen on complex **3**, without affecting the chain growth too much.

6.3.4. Gel-Permeation Chromatography (GPC) data of polymer sample

Whilst the MALDI analyses gave definitive evidence for the alternating polymer microstructure, the method is not reliable enough to rely on the molecular weight averages, since not all samples were seen to give equal quality data. Therefore, following the MALDI-MS tests, polymers samples were analyzed by Gel-Permeation Chromatography (GPC) to obtain another set of molecular weight data for comparison. The results are summarized in Table 6.20 as below. The entry numbers in Table 6.20 are kept the same as Table 6.18 and 6.19 for easy reference.

Table 6.20: GPC results for polymer samples

Entry	Cat.	Monomer	M _n	M _w	Đ	Theoretical M _n
1	3	ECH/PA	581 ^a	635 ^a	1.09	47679
2	3	ECH/TCPA	10850	16249	1.50	74964
3	3	ECH/TBPA	32067	49413	1.54	110168
4	4	ECH/PA	803 ^a	1282 ^a	1.60	47679
5	4	ECH/TCPA	138777	640465	4.62	74964
6	4	ECH/TBPA	5183 (657828) ^b	22021 (1188220) ^b	4.25 (1.81) ^b	110168
7	3	CHO/PA	15384	17155	1.12	49285
8	3	CHO/TCPA	18197	26571	1.46	76845
9	3	CHO/TBPA	17348	27425	1.58	112405
10	4	CHO/PA	11456	12826	1.12	48300
11	4	CHO/TCPA	17702	28854	1.63	75308
12	4	CHO/TBPA	20409	36117	1.77	110157
13	3	PO/PA	3061	3812	1.25	41273
14	3	PO/TCPA	641 ^a	1206 ^a	1.88	68833
15	3	PO/TBPA	73590	117178	1.59	104393
16	4	PO/PA	9278	10234	1.10	41273
20	3	VCHO/PA	8795	12588	1.43	54493
21	3	VCHO/TCPA	29137	40506	1.39	82053
22	3	VCHO/TBPA	25588	43493	1.7	117613
23	4	VCHO/PA	7136	10979	1.54	54493
24	4	VCHO/TCPA	25500	36380	1.43	82053
25	4	VCHO/TBPA	28289	48156	1.70	117613

Cat.: catalyst. ^a: Possibly anomalous results. ^b: Measurements from another peak, but considered to be non-real, as the numbers are too high.

The data in Table 6.20 gives molecular weights that are much higher than the ones given by the MALDI-MS (except those that are labelled as anomalous, which are too low for polymer) in terms of both M_n and M_w. Still, the M_n from GPC tests are generally lower than the theoretical molecular weight (except Entry 5), the reasons

should be the same as have been discussed in section 6.3.3, since back-biting seems to be facile in ROCOP. As for entry 5, the higher-than-expected M_n could be a result of slow initiation, since a slow initiation would result in fewer propagating polymer chains, and each chain would have more monomer units on them comparing to the calculated number, thus higher M_n . Dispersity wise, comparing to MALDI-MS data, GPC dispersities are much higher, with some values even above 4.0. A poor dispersity control possibly means complex reaction kinetics, frequent back-biting, etc.

To compare the effects on the molecular weight by the structural difference between complexes **3** and **4**, and the choice of monomers, the ROCOP reaction entries with similar monomer combination but different catalysts were selected, and plots are drawn for better visual illustration.

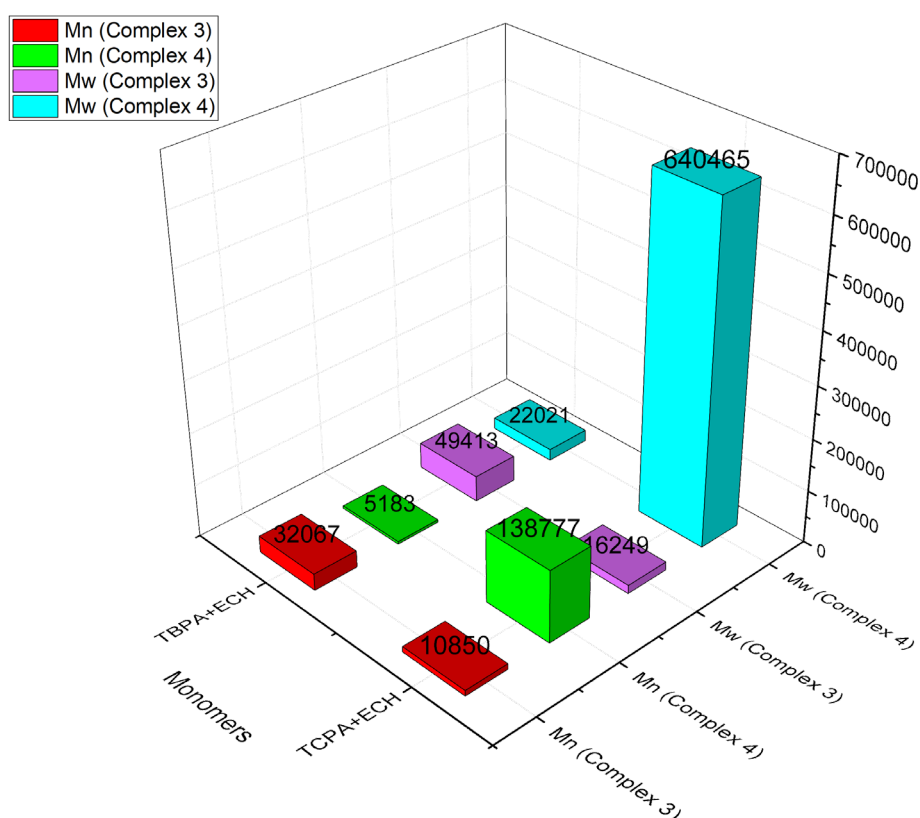


Figure 6.26: M_n / M_w comparison for ROCOP with ECH catalyzed by complexes **3** and **4**

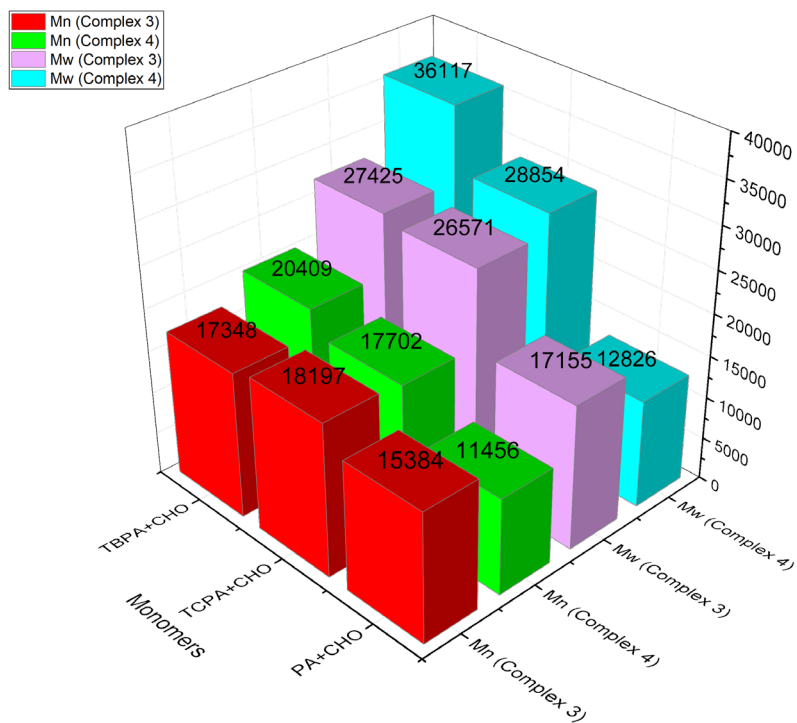


Figure 6.27: M_n / M_w comparison for ROCOP with CHO catalyzed by complexes **3** and **4**

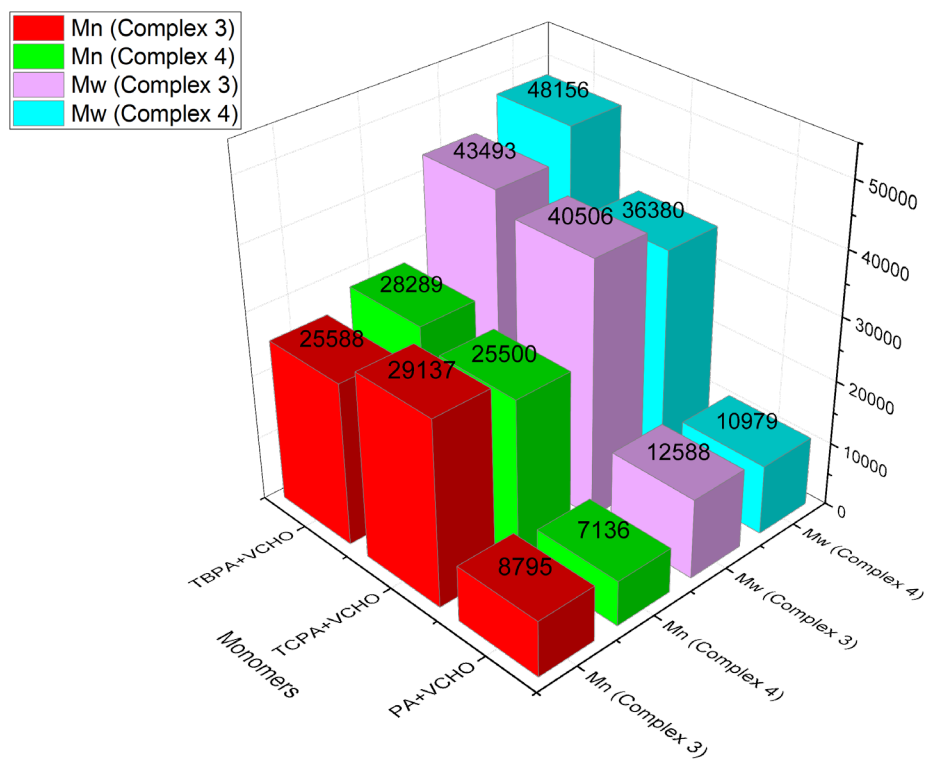


Figure 6.28: M_n / M_w comparison for ROCOP with VCHO catalyzed by complexes **3** and **4**

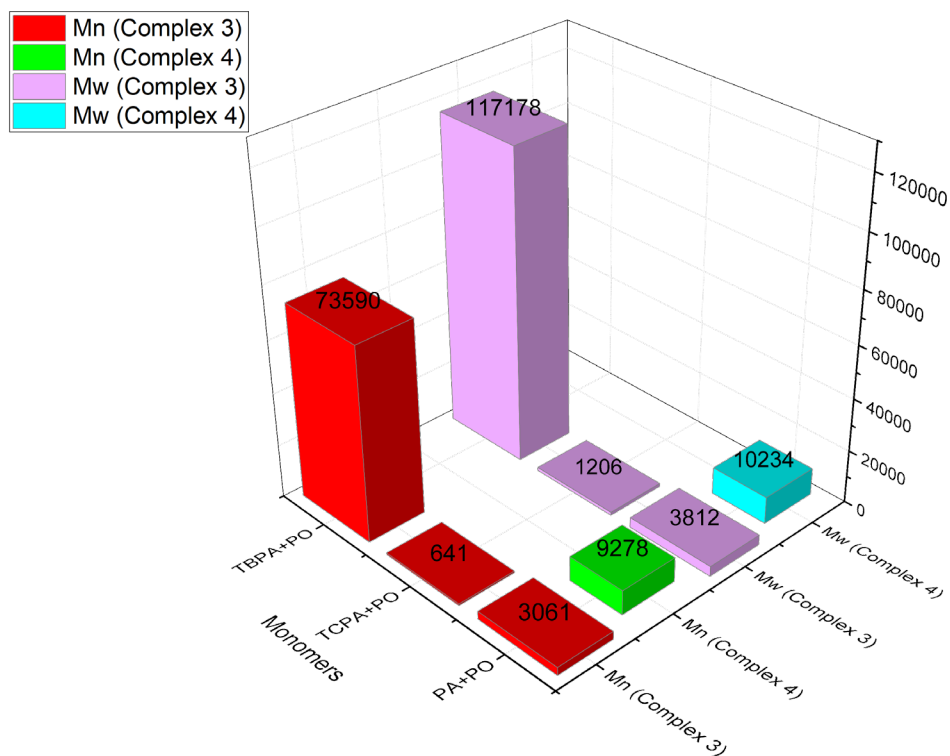


Figure 6.29: M_n / M_w comparison for ROCOP with PO catalyzed by complexes **3** and **4** (dubious data, for reference only)

As seen in Figures 6.27 and 6.28, for complex **3**, generally speaking, ROCOP with TCPA (tetrachlorophthalic anhydride) as monomer gave the highest M_n, PA (phthalic anhydride) gave the lowest, with TBPA (tetrabromophthalic anhydride) lying between the two, but closer to TCPA. On the other hand, complex **4** gave the highest M_n and M_w when TBPA was used, followed by the TCPA as the second highest, and PA being the lowest. The M_w trend for complex **3** is the same as complex **4**. Surely, the use of different monomers makes the theoretical molecular weights intrinsically different; with this being said, TBPA still generally giving lower degree of polymerization (DP) compared to TCPA. In Figure 6.27 and 6.28, the PA / TCPA included ROCOP samples have lower M_n and M_w when complex **4** is used as catalyst compared to complex **3**; while for TBPA reactions, complex **4** gave high M_n / M_w data than complex **3**. An interesting fact is in Figure 6.26, complex **4** ROCOP samples showed large M_w values that made the Đ to be more than 4.0, as in Entries 5 and 6 in Table 6.20. The exact reason for this is unknown, and Entry 5 (Table 6.19) gave a 1.08 Đ in MALDI-MS. Possible cause could be that some polymer series

cannot be picked up by MALDI, thus resulting in loss of data and inaccurate evaluation

In the report from Liu *et al.*,¹³ the catalytic results of **6.2** (more Lewis acidic Al) and **6.3** (less Lewis acidic Al) (structures in Figure 6.30, re-presented here for convenience) have been compared, which are listed in Table 6.21. Nozaki *et al.* (complex **6.4**),¹⁸ Darensbourg *et al.* (complex **6.5**)¹⁹ and Liu *et al.* (complex **6.6**)¹² also reported catalysts with similar structures, which are illustrated in Figure 6.31. Their catalytic activities are also included in Table 6.21.

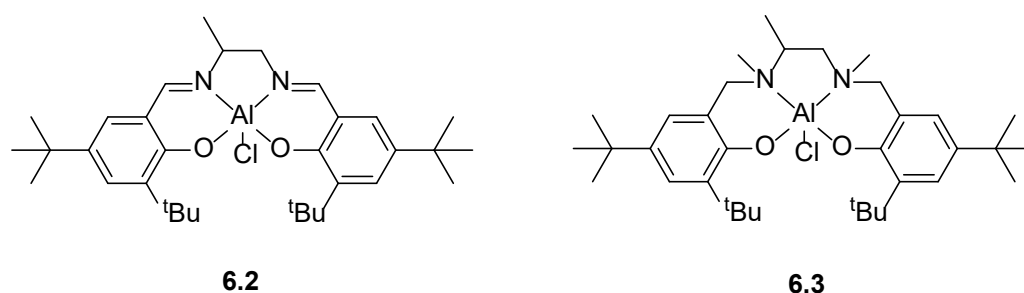


Figure 6.30: Structures of catalysts by Lu *et al.*¹³

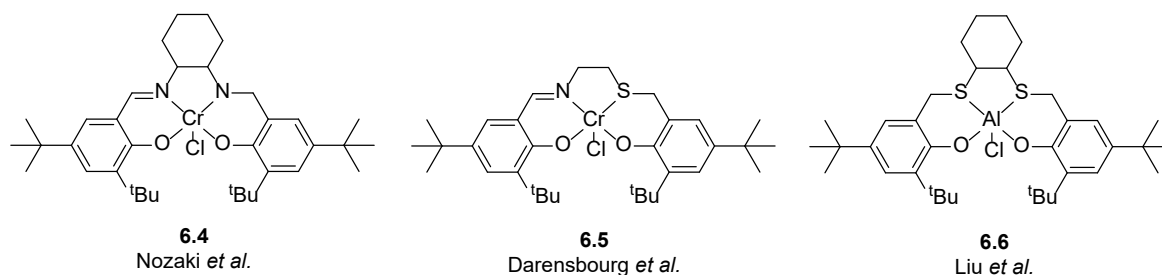


Figure 6.31: Structures of catalysts **6.4**,¹⁸ **6.5**¹⁹ and **6.6**¹²

Table 6.21: Representative catalytic performances of **3**, **4**, **6.2** and **6.3**

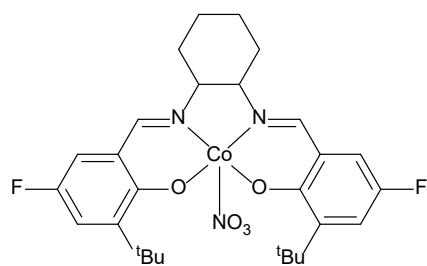
Catalyst	Monomer	Time/min	Select./%	M _n /Da	Đ	TOF/h ⁻¹
6.2 ^a	PO/CO ₂	1440	85	6300	1.28	9
6.3 ^a	PO/CO ₂	480	96	35400	1.22	60
6.4 ^b	CHO/CO ₂	120	>99	8800	1.14	210
6.5 ^c	CHO/CO ₂	360	69	7200	1.25	49
6.6 ^d	VCHO/C O ₂	360	44	6000	1.26	13
3	CHO/PA	180	100	15400	1.12	133
4	CHO/PA	150	96	11500	1.12	157
3	VCHO/P A	300	100	8800	1.43	80
4	VCHO/P A	240	100	7100	1.54	100

^a: 25°C, co-catalyst ⁿBu₄NNO₃, [catalyst]:[co-catalyst]:[PO] = 1:1:1000, 1.5 MPa CO₂ pressure. ^b: 70°C, co-catalyst PPnCl, [catalyst]:[co-catalyst]:[CHO] = 1:1:1000, 1.3 MPa CO₂ pressure. ^c: 90°C, co-catalyst PPnCl, [catalyst]:[co-catalyst]:[VCHO] = 1:2:1000, 3.0 MPa CO₂ pressure. TOF: turnover frequency, defined as number of epoxide-anhydride unit formed in polymer chain per unit time (per hour in Table 6.21). Select.: selectivity.

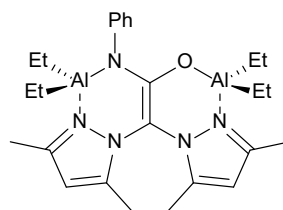
For **6.2** and **6.3**, reduced central metal Lewis acidity leads to 9% increase in selectivity, a dramatic increase in M_n and slightly better dispersity control, in line with Lu *et al.*'s elucidation that making central metal more electron-rich causes better activity. **6.5** has a more electron-rich central Cr ion compared to **6.4** since sulphur is better at electron-donating. In ROCOP catalysis, **6.4** achieved better selectivity, dispersity, much higher TOF as well as higher M_n compared to **6.5**. This indicates that a more electron-donating ligand possibly has an adverse effect on Cr complexes' ROCOP catalytic activity. **6.6** has a more electron-rich central Al comparing to **6.3**, and again adverse effects have been observed. Al³⁺ has a radius of 53 pm and Cr³⁺ has a radius of 62 pm,²⁰ therefore Cr³⁺ in **6.4** should be a softer Lewis acid than Al³⁺ in **6.2** (the ligand system of these two are comparable). If a

comparison was taken between **6.2** and **6.4**, we can see that **6.4** yielded higher M_n , higher TOF, better selectivity and lower dispersity. In this case lower Lewis acidity causes catalytic performance to rise. Overall, it can be seen that Lewis acidity of the central metal ion can exert either positive or negative effect towards the ROCOP catalysis performance. 6.2 vs. 6.4 and 6.2 vs. 6.3 showed that lower Lewis acidity = higher catalytic performance; while 6.4 vs. 6.5 and 6.3 vs. 6.6 indicated that lower Lewis acidity = lower catalytic performance. Therefore, a hypothesis is proposed that the “lower Lewis acidity = higher catalytic performance” effect of metal complexes has an optimal point, above which the reduction in Lewis acidity increases general catalytic performances, and if the Lewis acidity is too low for central metal ion, the general catalytic performance will be inhibited. For **3** and **4**, the electron-donating methyl groups on **4** which make central Al ions in **4** less Lewis acidic have undoubtedly enhanced the reaction rate and TOF, as the reaction time needed for full conversion is around 20% shorter if **4** is used instead of **3**. The M_n and dispersity control, on the contrary, are confusing since the MALDI-MS results and GPC results showed two trends that are opposite to each other. MALDI-MS indicates that lower Lewis acidity of Al leads to higher M_n and a tiny change in dispersity, while GPC shows that shorter chain lengths and poorer dispersity control are observed with lower Lewis acidity of the Al ions. However, same as discussed above, MALDI-MS may fail to pick some of the polymer series, making it a less stable method for measuring polymer masses. Based on GPC data, it is then proposed that the electronic effects on **3** and **4** are at the vicinity of the optimal point of the electronic effect, which lead to improvement of reaction speed but poorer dispersity control and shorter chain length.

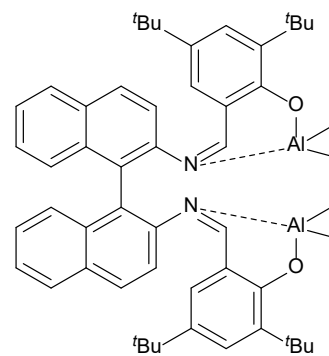
Some previously reported Al-based catalysts **6.7** (Coates *et al.*),²¹ **6.8** (Otero *et al.*)²² and **6.9** (Mazzeo *et al.*)²³ for epoxide / anhydride ROCOP with their performances are summarized in Table 6.22 for comparison with **3** and **4**. The structures of the previously reported Al-based catalysts are illustrated in Figure 6.32.



6.7
Coates *et al.*



6.8
Otero *et al.*



6.9
Mazzeo *et al.*

Figure 6.32: Structures of examples of previously reported Al-based ROCOP catalysts

Table 6.22: ROCOP catalytic performances of some Al complexes

Cat.	Monomer	Co-cat.	Ratio	T/°C	t/min	Conv./%	Select./%	M _n /Da	Đ	TOF/h ⁻¹
6.7	PO/PA	PPNNO ₃	1:1:800:400	30	210	70	>99	19100	1.16	80
6.7	ECH/PA	PPNNO ₃	1:0:400:400	30	150	80	>99	21000	1.13	128
6.8	CHO/PA	TBAB	1:1:200:200	80	960	100	95	3600	1.11	13
6.9	CHO/PA	PPNCl	1:4:100:100	110	420	75	81	9600	1.30	14
3	PO/PA	PPNCl	1:1:2000:400	70	225	98	96	3.060	1.25	107
3	ECH/PA	PPNCl	1:1:2000:400	70	210	99	100	4000	1.00	114
3	CHO/PA	PPNCl	1:1:2000:400	70	180	100	100	1540	1.12	133
3	VCHO/PA	PPNCl	1:1:2000:400	70	300	100	100	8800	1.43	80
4	ECH/PA	PPNCl	1:1:2000:400	70	175	99	100	1200	1.11	136
4	CHO/PA	PPNCl	1:1:2000:400	70	150	98	96	1150	1.12	157
4	VCHO/PA	PPNCl	1:1:2000:400	70	240	100	100	7130	1.54	100

Cat.: catalyst; Co-cat.: co-catalyst; T: reaction temperature; t: reaction time; Conv.: conversion; Select.: selectivity; Đ: polymer dispersity. PPNNO₃: bis(triphenylphosphine)iminium nitrate; TBAB: tetrabutylammonium bromide; PPNCl: bis(triphenylphosphine)iminium chloride. TOF: turnover frequency, defined as equivalent of epoxide converted to polymer per hour.

From the table it can be seen that for CHO/PA reactions, **3** and **4** out-performed **6.8** and **6.9** in terms of lower reaction temperature, significantly shorter reaction time, higher (or comparable) conversion and selectivity. Moreover, the equivalent of anhydride used for **3** and **4** is 400 while **6.8** and **6.9** are 200 and 100 respectively, again exemplify the high catalytic performance of **3** and **4**. However, the M_n values of CHO/PA samples catalyzed by **3** and **4** are noticeably lower than that of **6.8** and **6.9**. For ECH/PA reactions, **3** and **4** gave better conversion, comparable selectivity but requires higher reaction temperature and longer reaction time comparing to **6.7**. For the PO/PA reactions, **3** gave higher conversion, lower M_n , comparable selectivity but requires higher temperature comparing to **6.7**. For all reactions, the TOF are generally excellent. For CHO/PA and PO/PA, both **3** and **4** showed much higher TOF than the selected example catalysts. CHO/PA reactions only showed TOF = 13 h⁻¹ and 14 h⁻¹ for **6.8** and **6.9**, while **3** and **4** showed TOF of 133 h⁻¹ and 157 h⁻¹ respectively, suggesting the high activity of them as ROCOP catalysts. For PO/PA reaction, **3** gave 107 h⁻¹ TOF comparing to the 80 h⁻¹ of **6.7**, again higher by a fair margin. For the ECH/PA reaction, **3** gave a TOF value of 114 h⁻¹, lower than 128 h⁻¹ of **6.7**. But after the reduction of central ion Lewis acidity by adding methyl group, **4** again out-compete **6.7** in terms of TOF, yielding a value of 136 h⁻¹. Generally, both **3** and **4** exhibit higher than average TOF values.

Overall, complex **3** and **4** can be regarded as efficient catalyst for ROCOP of epoxide / anhydride that gave excellent conversion and selectivity, while operating at moderate temperature and relatively short reaction time.

6.3.5. Density Functional Theory (DFT) calculations and mechanistic interpretations

Following the experimental data I have obtained, density function theory (DFT) calculations were then deployed for in-depth mechanistic explanations of ROCOP with complex **3** and **4**.

A plausible mechanism for the ring-opening co-polymerization of succinic anhydride (SA) and ethylene oxide (EO), as models for the substrates described in this chapter, was investigated using density functional theory. Calculations were performed by Dr. Benjamin Ward using the Gaussian 09 program. The M06-2X functional was used, employing the triple zeta basis set. The calculated energy profile is shown in Figure 6.33. The initial complex used in the calculations was the hypothetical species $[(AQ)_2Al(OAc)_2]$, with acetate representing a carboxylate-terminated polymer chain.

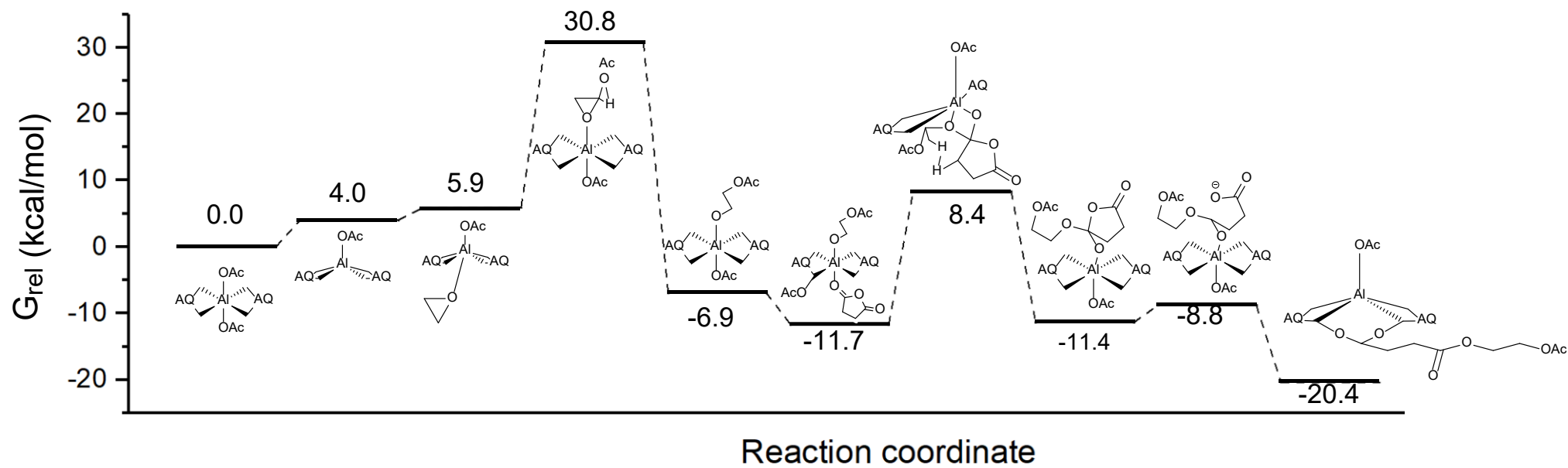


Figure 6.33: Calculated free energy profile for the copolymerization of succinic anhydride and ethylene oxide by $[(AQ)_2Al(OAc)_2]$

The mechanisms, structures of transition states and intermediates are constructed based on the work by Coates *et al.*¹⁰ Initially, the initiation process ring opens two epoxide, forming aluminium bis(alkoxide). Due to the rapid ring-opening of anhydride which quickly forms aluminium bis(carboxylate), the aluminium bis(carboxylate) is modelled as the primary state of the catalyst. The bis(carboxylate) is approximated by biacetate, which represents the growing polymer chain. The first step of the reaction is the de-coordination of the acetate from the aluminium centre, which leaves an available site for epoxide to coordinate. This step is moderately endergonic (+4.0 kcal/mol); the decoordinated acetate can H-bond to the amide on the aminoquinoline, which lies at +3.5 kcal/mol.

Subsequently, EO monomer coordinates to the aluminium centre, causing a small energy rise to 5.9 kcal/mol. If the decoordinated acetate H-bonds to the amide then the energy rises to +6.5 kcal/mol, which is not significantly different, so the H-bonded acetate and 'free' acetate are likely to be in equilibrium. This equilibrium could be critical to the mechanism since the H-bonded acetate (polymer chain) is held in close proximity to the aluminium and is therefore preorganized to attack a coordinated epoxide. The dissociated polymer chain will then attack the coordinated epoxide. The attack of acetate onto the epoxide happens externally to the coordination sphere; Natural bonding orbital (NBO) analysis suggests that this transition state can be described as the attack of an sp^3 hybridized lone pair of an acetate oxygen to an empty p orbital on the epoxide carbon (Figure 6.35). The attacked p orbital on the epoxide carbon is part of the breaking bond of the 3-membered epoxide hetero-ring, which is best described as a p-p end-on interaction (Figure 6.34). This transition state is the highest energy point of the whole potential energy surface (30.8 kcal/mol), which is consistent with previous report by Coates *et al.*¹⁰ and suggests that an elevated temperature should be required for the reaction to proceed, as seen experimentally. The energy drops to -6.9 kcal/mol following epoxide ring-opening.

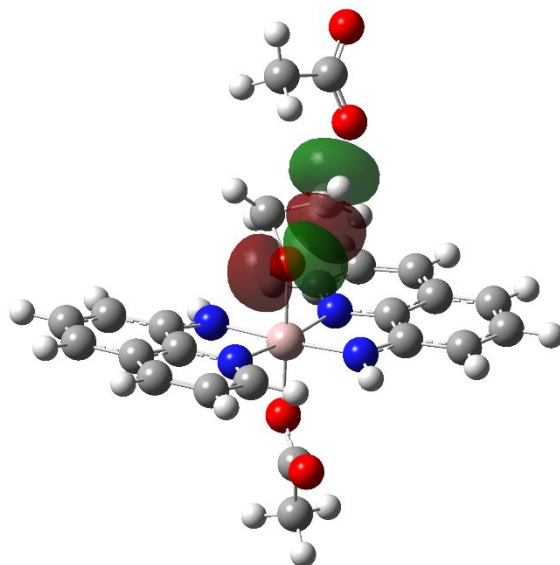


Figure 6.34: NBO-derived bond breaking orbitals of acetate and epoxide

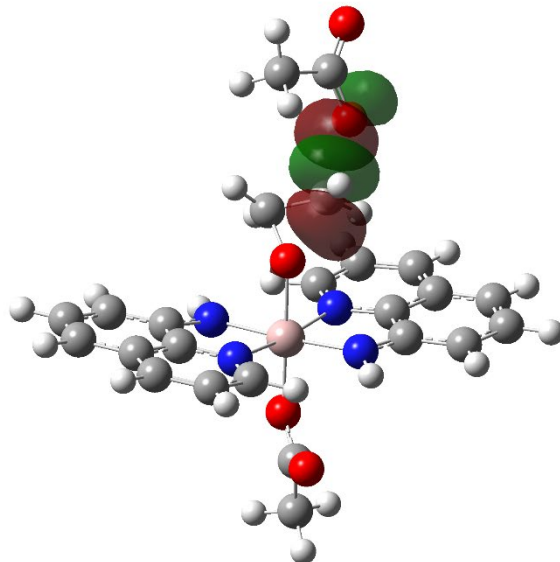


Figure 6.35: NBO-derived bond forming orbitals of acetate and epoxide

The next step is the coordination of the anhydride. The calculated most stable conformation of this step is where the anhydride displaces a polymer chain. This

conformation brings down the free energy to -11.7 kcal/mol. The displaced polymer chain H-bonds to the amide of the aminoquinoline. Then, one of the aromatic nitrogens of aminoquinoline dissociates from the aluminium to provide vacancy for the attack of epoxide oxygen onto the aluminium.

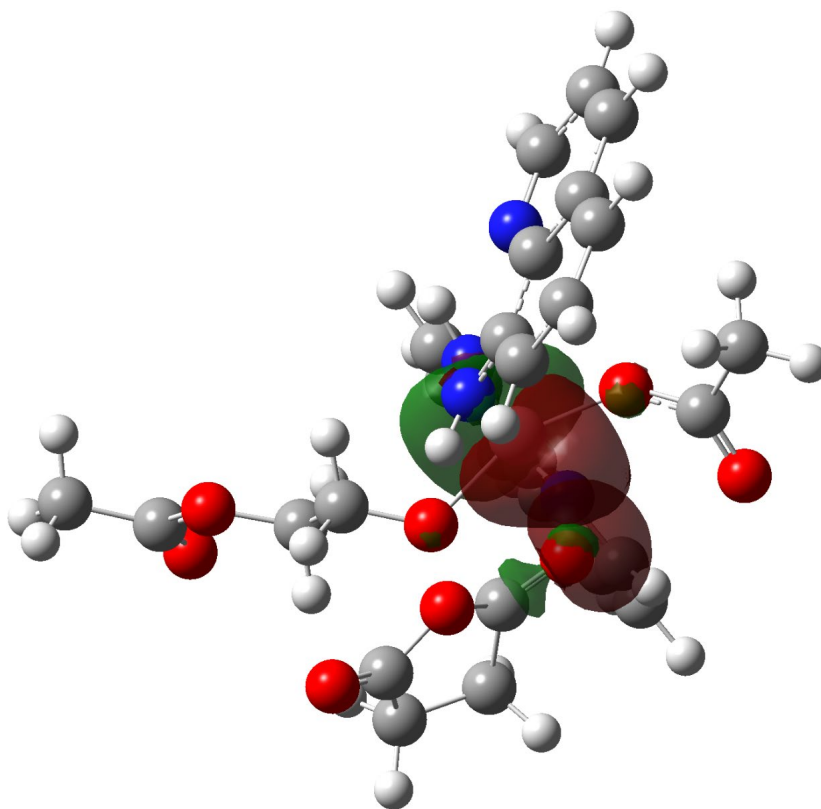


Figure 6.36: NBO-derived orbitals involved in the coordination of anhydride to aluminium

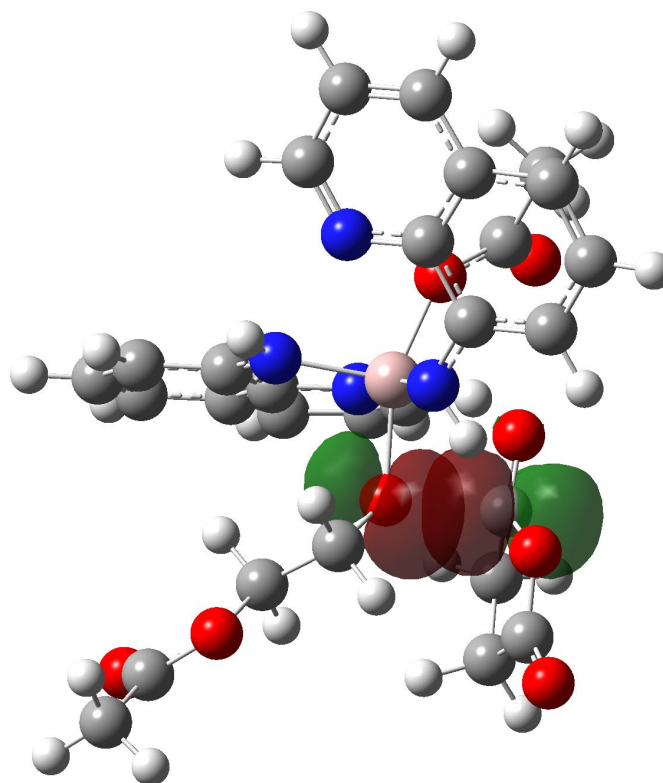


Figure 6.37: NBO-derived orbitals involved in the insertion of alkoxide onto the anhydride carbonyl group

The aromatic nitrogen will then coordinate back onto the aluminium, and the anhydride thus becomes part of the polymer chain. Subsequently, the anhydride will ring-open, to form an acetate. The breaking bond can be described as an end-on p-p overlap (NBO analysis, Figure 6.38). Overall, the reaction with anhydride closely resembles the insertion-opening mechanism typically seen for the ring-opening polymerization of cyclic esters. The transition states for involved in anhydride addition to the polymer chain are significantly lower than that for epoxide opening, consistent with this being a fast step, and thus consistent with literature precedent and the patterns observed with MALDI (ie only pseudo monomers seen in the repeat units).

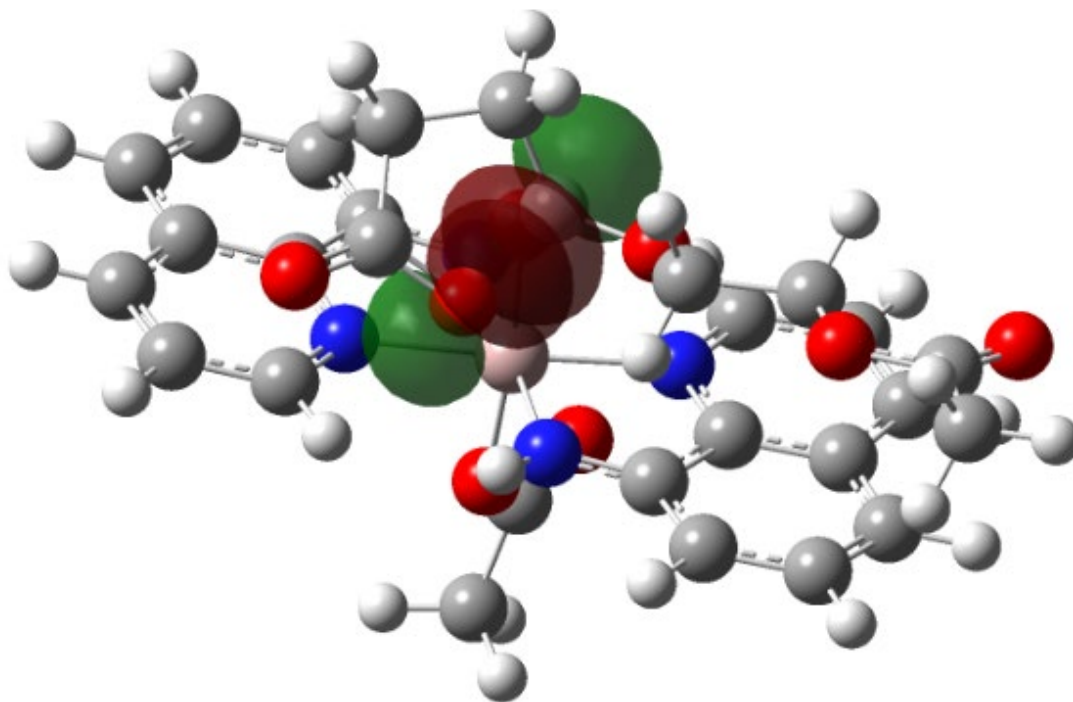


Figure 6.38: NBO-derived orbitals involved in anhydride ring-opening

Finally, the newly formed acetate (polymer chain) will dissociate from the aluminium and H-bond to the aminoquinoline ligand, leaving aluminium centre vacant for the next round of catalysis.

6.4. Conclusion

In this chapter, three different epoxide / anhydride ROCOP catalysts have been reported, which are based on aminoquinoline and its derivatives. Among these three catalysts, [(AQ)₂AlCl] (**3**) and [(AQMe)₂AlCl] (**4**) have shown outstanding catalytic performance for epoxide / anhydride ROCOP. By comparing their performances, it was proposed that the electron-donating group on the amide will improve the performance of the catalyst. Moreover, detailed DFT calculations has been done to provide comprehensive mechanistic insights for the ROCOP catalyzed by aminoquinoline-Al type complexes. This chapter also revealed that to improve the catalytic performance, more different pendant groups on the amide moiety of the

aminoquinoline should be tried, and the electron-donating / electron-withdrawing abilities shall be further investigated. As of now, electron-donating groups poses positive effect on reaction rate and sometimes on M_n and polymer dispersity. To conclude, this new series of aminoquinoline-based catalysts have proven themselves to be competent for ROCOP catalysis under mild conditions, thus worth further future study and probing.

6.5. References

- 1 D. W. Imhoff, L. S. Simeral, S. A. Sangokoya and J. H. Peel, *Organometallics*, 1998, **17**, 1941–1945.
- 2 A. Armitage, O. Boyron, Y. Champouret, M. Patel, K. Singh and G. Solan, *Catalysts*, 2015, **5**, 1425–1444.
- 3 J. Slaughter, A. J. Peel and A. E. H. Wheatley, *Chem. Eur. J.*, 2017, **23**, 167–175.
- 4 A. M. Baruah, R. Sarma and J. B. Baruah, *Inorganic Chemistry Communications*, 2008, **11**, 121–124.
- 5 I. Tritto, M. C. Sacchi, P. Locatelli and S. X. Li, *Macromol. Chem. Phys.*, 1996, **197**, 1537–1544.
- 6 8-Aminoquinoline(578-66-5) 13C NMR,
https://www.chemicalbook.com/SpectrumEN_578-66-5_13CNMR.htm,
(accessed 12 March 2021).
- 7 C. R. Groom, I. J. Bruno, M. P. Lightfoot and S. C. Ward, *Acta Crystallogr B Struct Sci Cryst Eng Mater*, 2016, **72**, 171–179.
- 8 8-Aminoquinoline(578-66-5) 1H NMR,
https://www.chemicalbook.com/SpectrumEN_578-66-5_1HNMR.htm,
(accessed 13 March 2021).
- 9 L. M. Engelhardt, M. G. Gardiner, C. Jones, P. C. Junk, C. L. Raston and A. H. White, *J. Chem. SOC. Dalton Trans.*, 1996, 3053-3057.
- 10 M. E. Fieser, M. J. Sanford, L. A. Mitchell, C. R. Dunbar, M. Mandal, N. J. Van Zee, D. M. Urness, C. J. Cramer, G. W. Coates and W. B. Tolman, *J. Am. Chem. Soc.*, 2017, **139**, 15222–15231.

- 11 B. A. Abel, C. A. L. Lidston and G. W. Coates, *J. Am. Chem. Soc.*, 2019, **141**, 12760–12769.
- 12 G. Si, L. Zhang, B. Han, H. Zhang, X. Li and B. Liu, *RSC Adv.*, 2016, **6**, 22821–22826.
- 13 B. Li, G.-P. Wu, W.-M. Ren, Y.-M. Wang, D.-Y. Rao and X.-B. Lu, *J. Polym. Sci. A Polym. Chem.*, 2008, **46**, 6102–6113.
- 14 D. J. Darensbourg, M. Ulusoy, O. Karroonnirum, R. R. Poland, J. H. Reibenspies and B. Çetinkaya, *Macromolecules*, 2009, **42**, 6992–6998.
- 15 H. Plommer, L. Stein, J. N. Murphy, N. Ikpo, N. Mora-Diez and F. M. Kerton, *Dalton Trans.*, 2020, **49**, 6884–6895.
- 16 A. D. MacNaught and A. Wilkinson, in *Compendium of chemical terminology: IUPAC recommendations*, Blackwell Science, Oxford, 2. ed., 1997.
- 17 J. M. G. Cowie, in *Polymers: chemistry and physics of modern materials*, Blackie, Glasgow, 2. ed., 1991.
- 18 K. Nakano, M. Nakamura and K. Nozaki, *Macromolecules*, 2009, **42**, 6972–6980.
- 19 B. Han, L. Zhang, S. J. Kyran, B. Liu, Z. Duan and D. J. Darensbourg, *J. Polym. Sci. Part A: Polym. Chem.*, 2016, **54**, 1938–1944.
- 20 Metallic, Covalent and Ionic Radii(r)*, <http://www.wiredchemist.com/chemistry/data/metallic-radii>, (accessed 15 March 2021).
- 21 A. M. DiCiccio, J. M. Longo, G. G. Rodríguez-Calero and G. W. Coates, *J. Am. Chem. Soc.*, 2016, **138**, 7107–7113.

- 22 M. Martínez de Sarasa Buchaca, F. de la Cruz-Martínez, J. Martínez, C. Alonso-Moreno, J. Fernández-Baeza, J. Tejeda, E. Niza, J. A. Castro-Osma, A. Otero and A. Lara-Sánchez, *ACS Omega*, 2018, **3**, 17581–17589.
- 23 F. Santulli, I. D’Auria, L. Boggioni, S. Losio, M. Proverbio, C. Costabile and M. Mazzeo, *Organometallics* 2020, **39**, 1213–1220.

Chapter 7: Experimental

7.1. General Methods and Instrumentation

All experimental manipulations related to syntheses / purification of air sensitive chemicals, assembling of polymerization reactions and preparation of air sensitive samples for characterization were conducted with standard Schlenk line or glove box techniques under argon or nitrogen atmosphere. Solvents were dried over activated 4 Å molecular sieves and refluxed over potassium (tetrahydrofuran, benzene) or sodium / benzophenone (diethyl ether) under nitrogen atmosphere and collected by distillation prior to use. Other solvents (toluene, pentane and hexane) were collected from a MBraun SPS-800 solvent purification system which dries solvents over activated alumina. Dried solvents were stored over potassium mirrors (except dichloromethane and tetrahydrofuran). Deuterated solvents were dried over potassium (deuterated benzene) or calcium hydride (deuterated chloroform), underwent freeze-pump-thaw degassing and trap to trap distillation, then stored in a glove box under a nitrogen atmosphere.

Epoxides (propylene oxide, cyclohexene oxide, styrene oxide, epichlorohydrin) and ϵ -caprolactone were dried over freshly ground calcium hydride with vigorous stirring for at least 48 hours, degassed by freeze-pump-thaw method, distilled by trap to trap distillation and stored in screw-cap vials in glove box under nitrogen atmosphere. All anhydrides for ring-opening copolymerization (ROCOP) were purified by recrystallization via cooling of hot saturated chloroform solution, followed by sublimation under reduced pressure. All other chemicals were purchased from commercial suppliers and used directly unless stated specifically.

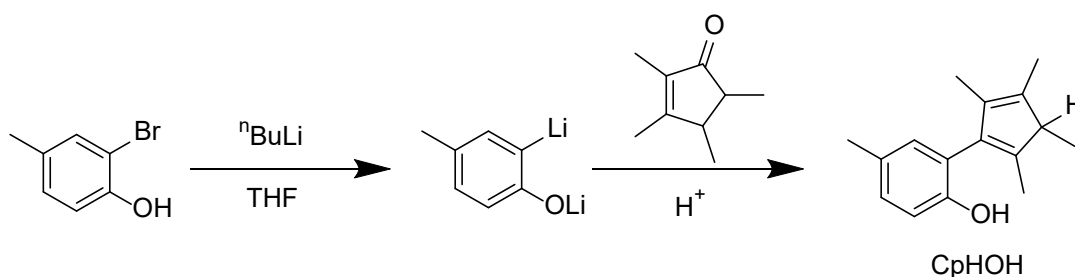
NMR samples of air / moisture sensitive compounds were prepared in the glove box under nitrogen atmosphere in 5 mm Wilmad 507-PP NMR tubes with J. Young Teflon valves. ^1H and $^{13}\text{C}\{-^1\text{H}\}$ NMR spectra were recorded on Bruker Fourier 300, Bruker DPX 400 and Bruker Avance 500 spectrometers. ^1H and ^{13}C assignments were

confirmed where necessary with the use of two-dimensional ^1H - ^1H and ^{13}C - ^1H NMR experiments. ^1H and ^{13}C spectra were referenced internally to residual deuterated solvent (^1H) or solvent (^{13}C) resonances and reported relative to tetramethylsilane ($\delta = 0$ ppm). Chemical shifts are quoted in δ (ppm) and coupling constants in Hertz (Hz). Infrared spectra were recorded on SHIMADZU IR AFFINITY-1S. Infrared data are quoted in wavenumbers (cm^{-1}). Infrared samples of air / moisture sensitive compounds were prepared as potassium bromide pellets in a glove box.

Mass spectra were recorded at School of Chemistry, Cardiff University, Cardiff, UK. MALDI-ToF (Matrix-Assisted Laser Desorption-Ionization Time of Flight) spectra were obtained using a Waters MALDI-ToF micro mx mass spectrometer. GPC (Gel Permeation Chromatography) data were obtained using an Agilent 1260 Infinity II Multi-Detector GPC/SEC System. Elemental analyses were performed at the School of Human Sciences, London metropolitan University. X-Ray data for single-crystal analyses were measured by the UK National Crystallography Service, School of Chemistry, University of Southampton, Southampton, UK or at the School of Chemistry, Cardiff University, Cardiff, UK. The X-Ray structures were subsequently solved using SHELXT and refined using SHELXL-2014 by Dr. Benjamin Ward.

7.2. Ligand Synthesis

7.2.1. Synthesis of CpHOH ligand



Scheme 7.1: Synthetic procedure of CpHOH

The synthetic procedure of 2-(tetramethylcyclopentadienyl)-4-methylphenol (CpHOH) ligand was adapted from journal by Chen and co-workers.¹ Scheme 7.1 is the schematic illustration of the synthetic procedure.

2-bromo-4-methylphenol (26.5 mmol, 3.2 mL, 1 equivalent) was dissolved in THF (25 mL) under argon. The mixture was stirred and cooled to 0°C in an ice / water bath, followed by addition of ⁿBuLi solution (6 mmol, 24 mL, 2.26 equivalents, 2.5 M solution in hexanes), dropwise over 30 minutes at 0°C. A white precipitate formed. The resulting mixture was then allowed to warm to room temperature and stirred for another 2 hours. The mixture was then cooled to -78°C in dry ice / acetone bath, and 2,3,4,5-tetramethyl-2-cyclopentenone (4 mL, 26.7 mmol) was added dropwise over 30 minutes at -78°C. The mixture was stirred overnight at room temperature. After overnight stirring, the mixture appeared yellow-brown. Water (2 mL) was then added to the mixture, followed by addition of concentrated hydrochloric acid (12 mL). The organic layer was separated and washed 3 times with concentrated hydrochloric acid (5 mL). Volatiles were removed by rotary evaporation, leaving a yellow-brown oily residue. The residue was distilled under 1.04 x 10⁻¹ mbar pressure and 44°C, obtaining CpHOH as a yellow crystalline solid. Weight of CpHOH: 2.98 g. Yield: 49%.

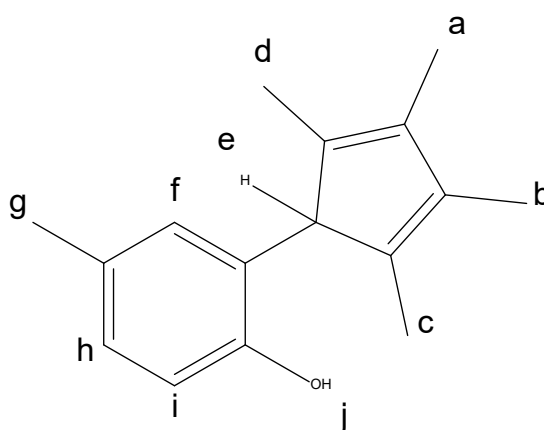


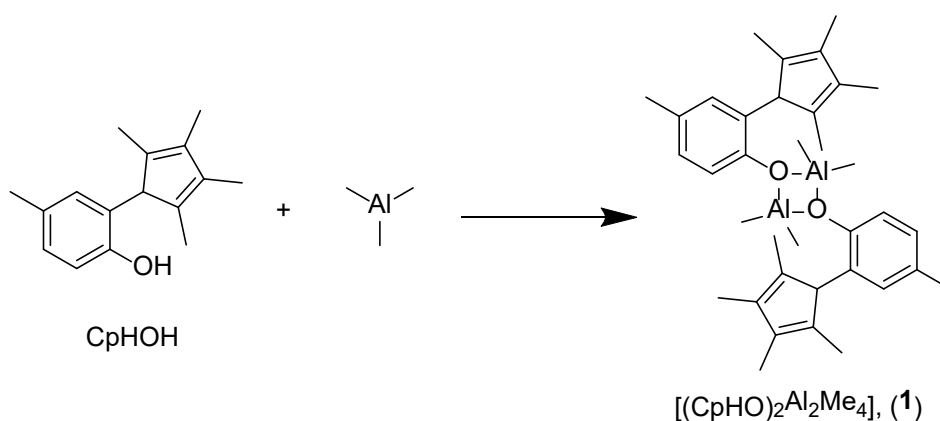
Figure 7.1: Proton labels for ¹H NMR data of CpHOH

¹H NMR (400 MHz, CDCl₃, 293 K): δ 6.97 (app. s, H^f, 1H); δ 6.91 (app. d, app. ³J = 8.0 Hz, Hⁱ, 1H); δ 6.62 (app. d, app. ³J = 8.0 Hz, H^h, 1H); δ 3.14 (s, H^j, 1H); δ 2.63

(app. q, $^3J = 6.4$ Hz, H^e, 1H); δ 2.27 (app. s, H^g, 1H); δ 1.57 (s, H^d and H^b, 6H); δ 1.22 (d, $^3J = 7.2$ Hz, H^a, 3H).

7.3. Metal complex synthesis

7.3.1. Synthesis of [(CpHO)₂Al₂Me₄], (**1**)



Scheme 7.2: Synthesis of [(CpHO)₂Al₂Me₄], (**1**)

In the glove box, CpHOH (1 g, 4.38 mmol) was dissolved in toluene (50 mL) in a Schlenk flask. The mixture was stirred at room temperature for 15 minutes to allow CpHOH to completely dissolve. AlMe₃ solution (4.38 mmol, 2.19 mL, 2.0 M solution in hexanes) was then added to the solution dropwise over 20 minutes at room temperature. Upon completion of addition, the mixture was allowed to stir for another 15 minutes. The Schlenk flask was then taken out of glove box and the volatiles in the mixture were evaporated under reduced pressure on the Schlenk line. [(CpHO)₂Al₂Me₄] (**1**) was obtained as a cream-coloured powder. Weight of **1**: 1.07g. Yield: 86%.

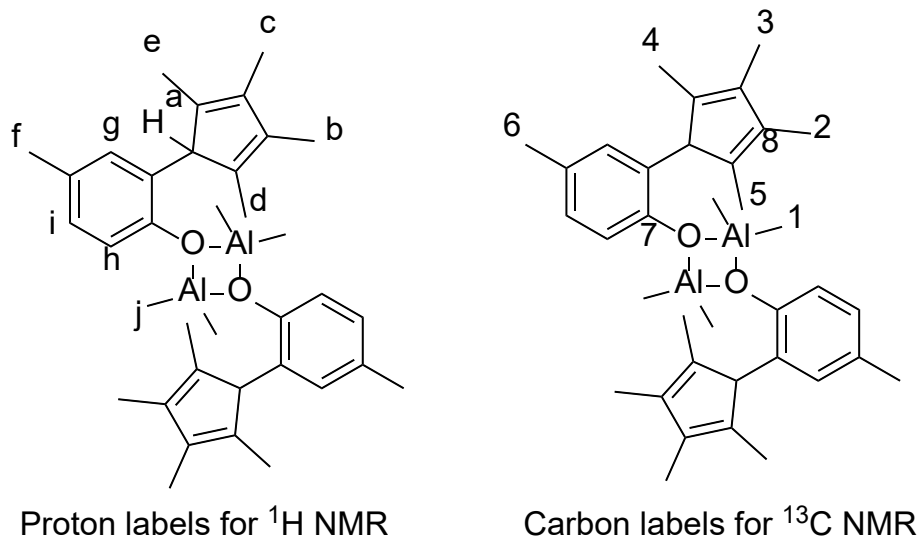


Figure 7.2: Atom labels for NMR spectra of $[(\text{CpHO})_2\text{Al}_2\text{Me}_4]$ (**1**)

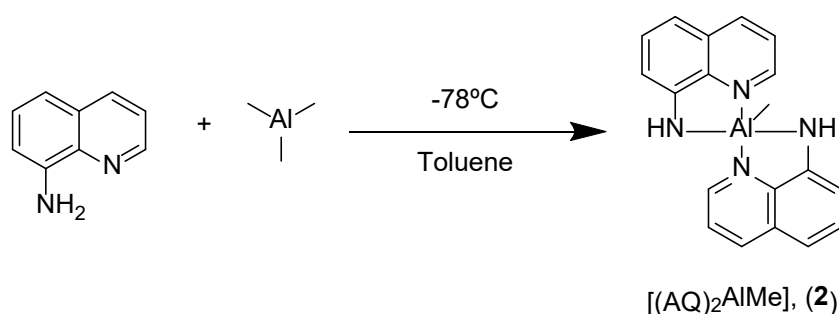
^1H NMR (500 MHz, CDCl_3 , 293 K): δ 7.20 (app. d, app. $^3J = 8.5$ Hz, H^{h} , 2H); δ 6.76 (app. dd, app. $^3J = 8.5$ Hz, app. $^4J = 2.5$ Hz, H^{i} , 2H); δ 6.59 (app. d, app. $^4J = 2.5$ Hz, H^{g} , 2H); δ 2.11 (m, H^{a} , 2H); δ 1.92 (app. s, H^{f} , 6H); δ 1.86 (m, H^{c} and H^{d} , 12H); δ 1.78 (m, H^{e} and H^{b} , 12H); δ -0.18 (s, H^{j} , 12H).

^{13}C NMR (125 MHz, C_6D_6 , 293 K): δ 148.3 (C^7); δ 138.7, 136.9, 134.6, 131.0, 129.1 (aromatic carbons except C^7); δ 122.6, 125.5, 128.2, 128.4 (Cp carbons except C^8); δ 56.1 (C^8); δ 21.3 (C^2); δ 20.4 (C^4); δ 12.5 (C^5); δ 11.3 (C^3); δ -8.6 (C^1).

Anal. Calcd. for $[(\text{CpHO})_2\text{Al}_2\text{Me}_4]$ ($\text{C}_{35}\text{H}_{50}\text{Al}_2\text{O}_2$): C, 76.02%; H, 8.86%. Found : C, 69.42%; H, 6.84%.

m/z (%) (EI): 568.36, $[(\text{CpHO})_2\text{Al}_2\text{Me}_4]^+$, 100%.

7.3.2. Synthesis of [(AQ)₂AlMe], (2)



Scheme 7.3: Synthesis of [(AQ)₂AlMe], (2)

In a Schlenk flask, 8-aminoquinoline (6.94 mmol, 1 g) was dissolved in toluene (50 mL) with stirring under argon atmosphere and room temperature. The mixture was then cooled to -78°C in dry ice / acetone bath, followed by addition of 1.39 mL of AlMe₃ solution (3.47 mmol, 1.39 mL, 2.5 M solution in hexanes) dropwise over 10 minutes. The mixture was allowed to stir at -78°C for another 30 minutes, then volatiles were removed under reduced pressure on the Schlenk line. [(AQ)₂AlMe] (2) was obtained as a light brown powder. Weight of **2**: 0.94 g. Yield: 82%.

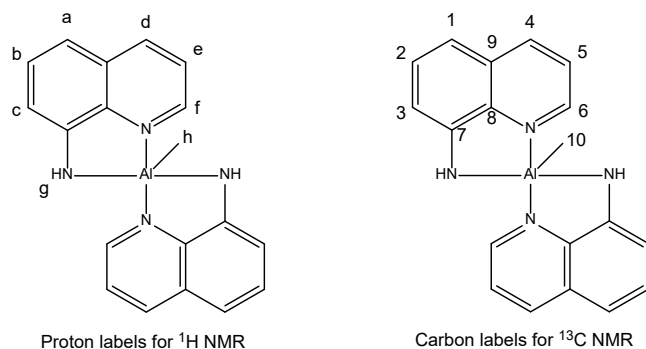


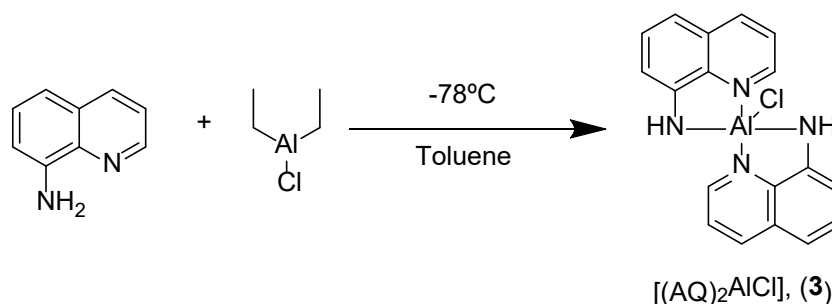
Figure 7.3: Atom labels for NMR spectra of [(AQ)₂AlMe], (2)

¹H NMR (500 MHz, C₆D₆, 293 K): δ 8.00 (app. dd, app. ³J = 4.5 Hz, ⁴J = 1.5 Hz, H^f, 2H); δ 7.55 (app. dd, app. ³J = 8.5 Hz, ⁴J = 1.5 Hz, H^d, 2H); δ 7.30 (app. t, app. ³J = 8 Hz, H^b, 2H); δ 6.69 (app. dd, app. ³J = 8 Hz, ⁴J = 1 Hz, H^a, 2H); δ 6.66 (m, H^e, 2H); δ 6.60 (app. dd, app. ³J = 7.5 Hz, ⁴J = 1 Hz, H^c, 2H); δ 3.75 (s, H^g, 2H); δ -0.14 (s, H^h, 3H).

^{13}C NMR (125 MHz, C_6D_6 , 293 K): δ 141.3 (C^6); δ 138.8 (C^7); δ 137.7 (C^8); δ 135.4 (C^4); δ 130.7 (C^2); δ 129.5 (C^9); δ 121.5 (C^1); 108.5 (C^5); 108.2 (C^3); -9.1 (C^{10}).

Anal. Calcd. for $[(\text{AQ})_2\text{AlMe}]$ ($\text{C}_{19}\text{H}_{17}\text{AlN}_4$): C, 69.50%; H, 5.22%; N, 17.06%. Found: C, 69.32%; H, 5.42%; N, 16.86%.

7.3.3. Synthesis of $[(\text{AQ})_2\text{AlCl}]$, (**3**)



Scheme 7.4: Synthesis of $[(\text{AQ})_2\text{AlCl}]$, (**3**)

In a Schlenk flask, 8-aminoquinoline (1 g, 6.94 mmol) was dissolved in toluene (50 mL) with stirring under argon atmosphere and room temperature. The mixture was then cooled to -78°C in dry ice / acetone bath, followed by addition of AlEt_2Cl solution (3.47 mL, 3.47 mmol, 1.0 M solution in toluene) dropwise over 10 minutes. The mixture was allowed to stir at -78°C for another 30 minutes, then volatiles were removed under reduced pressure on the Schlenk line. $[(\text{AQ})_2\text{AlCl}]$ (**3**) was obtained as a brown powder. Weight of **3**: 0.94 g. Yield: 82%.

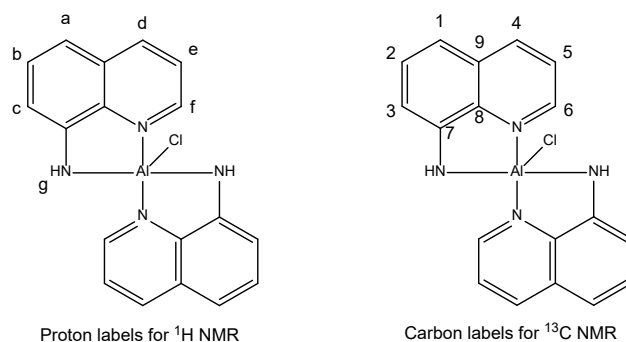


Figure 7.4: Atom labels for NMR spectra of $[(\text{AQ})_2\text{AlCl}]$ (**3**)

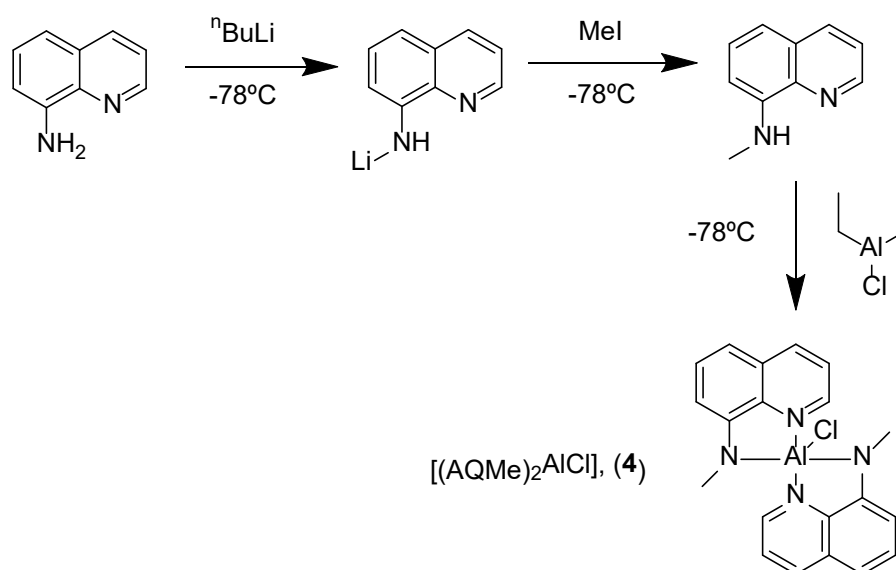
^1H NMR (500 MHz, C_6D_6 , 293 K): δ 8.25 (d, $^3J = 4.5$ Hz, H^f , 2H); δ 7.49 (d, $^3J = 8.5$ Hz, H^d , 2H); δ 7.27 (app. t, app. $^3J = 8.5$ Hz, H^b , 2H); 6.70 (d, $^3J = 8$ Hz, H^a , 2H); 6.62 (m, H^e , 2H); 6.60 (d, $^3J = 7$ Hz, H^c , 2H); 3.72 (s, H^g , 2H).

^{13}C NMR (125 MHz, C_6D_6 , 293 K): δ 143.0 (C^6); δ 139.0 (C^4); δ 138.1 (C^7); δ 130.3 (C^2); δ 129.3 (C^8); δ 128.6 (C^9); δ 121.6 (C^5); δ 110.7 (C^1); 109.4 (C^3).

Anal. Calcd. for $[(\text{AQ})_2\text{AlCl}]$ ($\text{C}_{18}\text{H}_{14}\text{AlClN}_4$): C, 61.99%; H, 4.05%; N, 16.06%. Found: C, 54.13%; H, 5.52%; N, 13.02%. Despite submitting single crystals of the sample that were used to confirm the identity of **3**, satisfactory CHN analyses could not be obtained.

m/z (%) (EI): 348.07, $[(\text{AQ})_2\text{AlCl}]^+$, 100%.

7.3.4. Synthesis of $[(\text{AQMe})_2\text{AlCl}]$, (**4**)



Scheme 7.5: Synthesis of $[(\text{AQMe})_2\text{AlCl}]$, (**4**)

In a Schlenk flask, 8-aminoquinoline (1 g, 6.94 mmol) was dissolved in toluene (50 mL) with stirring under argon atmosphere and room temperature. The mixture was then cooled to -78°C in dry ice / acetone bath, followed by the addition of $n\text{BuLi}$ solution (6.94 mmol, 2.78 mL, 2.5 M solution in hexanes), dropwise over 5 minutes

with vigorous stirring. MeI (6.94 mmol, 0.43 mL) was then added into the reaction mixture with stirring at -78°C . The mixture then allowed to warm up to room temperature and stirred overnight. The volatiles in the mixture were then removed under reduced pressure on the Schlenk line followed by the addition of DCM. The mixture was then stirred for 15 minutes to allow complete dissolving of desired product in DCM. A cannula filter was then prepared by wrapping a filter paper which was oven dried for 2 hours onto the metal cylinder end of the cannula using Teflon tape. The solution then underwent cannula filtration under argon atmosphere into another Schlenk flask. Volatiles then removed under vacuum on the Schlenk line, leaving $[(\text{AQMe})_2\text{AlCl}]$ (**4**) as a red-purple powder. Weight of **4**: 0.89 g. Yield: 68%.

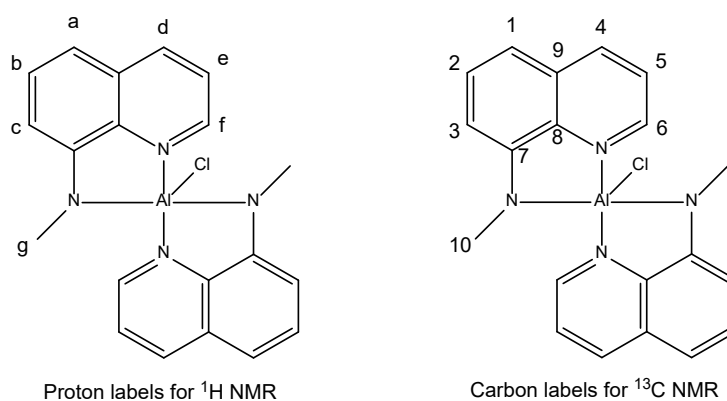


Figure 7.5: Atom labels for $[(\text{AQMe})_2\text{AlCl}]$, (**4**)

^1H NMR (400 MHz, C_6D_6 , 298 K): δ 7.62 (dd, $^3J = 8.4$ Hz, $^4J = 1.2$ Hz, H^f); δ 7.52 (dd, $^3J = 8.4$ Hz, $^4J = 1.2$ Hz, H^d); δ 7.40 (app. t, app. $^3J = 7.6$ Hz, H^b); δ 6.72 (d, $^3J = 8$ Hz, H^a); δ 6.69 (m, H^e , 2H); δ 6.57 (d, $^3J = 7.6$ Hz, H^c); δ 2.58 (s, H^g). The low solubility of **4** made NMR spectrum not satisfactory enough for precise integration.

Informative ^{13}C NMR and 2D NMR cannot be obtained due to possible solubility issue reported by Engelhardt *et al.*²

Despite submitting sample from the same recrystallized batch that was used to confirm the identity of **4**, satisfactory CHN analyses could not be obtained, possibly due to incomplete combustion or sample degradation.

m/z (%) (EI): 376.10, [(AQMe)₂AlCl]⁺, 100%.

7.4. Syntheses and isolation of polymers

7.4.1. Syntheses of polyethers with chosen metal complexes as catalysts

The syntheses of polyethers with chosen metal complexes as catalysts all follow the same reaction protocols described as below.

In the glove box, the desired weight of catalyst was measured out and transferred into a screw-cap vial equipped with stirrer bar. The epoxide monomer was then measured out with variable volume pipette and transferred into the screw-cap vial. The vial was then closed tightly, taken out of the glove box and quickly accommodated into a slotted aluminium heating block which had been pre-heated to the designated temperature. The reaction mixture then allowed to stir for a certain time under the designated temperature. Upon reaching the planned reaction time, the screw-cap vial was opened, and methanol (0.5 mL) was added to quench the reaction.

7.4.2. Syntheses of polyesters via ring-opening copolymerization of anhydrides and epoxides with chosen catalysts

The syntheses of polyesters via ring-opening copolymerization of anhydrides and epoxides with chose catalysts generally follow two different kinds of synthetic protocols: 1. Solvent method; 2. Solvent-free method, where an excess of epoxide (liquid) serves as both solvent and reagent.

7.4.2.1. Solvent method

In the glove box, the desired weight of chosen catalyst and co-catalyst (if needed) were measured out and transferred into a 7 mL screw-cap vial equipped with a stirrer bar. Then, the desired weight of anhydride (solid) was measured out and transferred

into the 7 mL screw-cap vial. The epoxide (liquid) was then measured out using a variable volume pipette, transferred into the same vial, followed by quick addition of the chosen solvent to make the mixture's volume 7 mL. The vial then closed tightly and taken out of glove box, accommodated into the slot of a slotted aluminium heating block which has been pre-heated to the designated temperature. The reaction mixture then allowed to stir for a certain time under designated temperature. Upon reaching the planned reaction time, the screw-cap vial was opened, and 0.5 mL of methanol was added to quench the reaction.

7.4.2.2. Solvent-free method

In the glove box, the desired weight of chosen catalyst and co-catalyst (if needed) were measured out and transferred into a 7 mL screw-cap vial equipped with a stirrer bar. Then, the desired weight of anhydride (solid) was measured out and transferred into the 7 mL screw-cap vial as well. The epoxide (liquid, in excess) was then measured out using a variable volume pipette, transferred into the same vial. The vial then closed tightly and taken out of the glove box, accommodated into the slot of a slotted aluminium heating block which had been pre-heated to the designated temperature. The reaction mixture then allowed to stir for a certain time under designated temperature. Upon reaching the planned reaction time, the screw-cap vial was opened, and 0.5 mL of methanol was added to quench the reaction.

7.4.3. Syntheses of poly-caprolactones via ring-opening polymerization with [(CpHO)₂Al₂Me₄] (1) as catalyst

Syntheses of poly-caprolactones via ring-opening polymerization with **1** as catalyst all follow the same reaction protocol described as below.

To a 7 mL vial equipped with a stirrer bar, the chosen amount of catalyst **1** was weighted out and added. ϵ -caprolactone was measured out by variable volume pipette then transferred into the same vial, and toluene was added as solvent to make the total volume of reaction mixture to 7 mL. The vial was then closed tightly,

taken out of the glove box and either put into slot of a slotted aluminium heating block which had been pre-heated to a certain temperature; or put directly onto a stirring plate (for reactions at room temperature). The reaction mixture then allowed to stir and react for a certain time period. After the designated time, the vial was opened, and 0.5 mL of methanol was injected to quench the reaction.

7.4.4. Isolation of polymers from reaction mixture

All the synthesized polymers are isolated from the reaction mixture with the same procedure described as below.

Due to the non-polar nature of the polymers (polyester, poly-caprolactone, polyether) synthesized, if polar solvent was added, the polymers will precipitate out because of the decrease in solubility. As such, methanol is an ideal choice as the anti-solvent to precipitate out the resultant polymers. Meanwhile, the monomers can still be dissolved in methanol, hence the isolated precipitate will be pure polymer after drying.

At the end of the reaction, quenching of catalyst and preparation of NMR samples, the reaction mixture in the vial was poured into a 250 mL beaker. The vial was then washed thoroughly with methanol, all the precipitate formed is scraped or flushed into the same beaker (with methanol) containing the reaction mixture. Subsequently, 150 mL of methanol was added into the beaker and the mixture was stirred for 30 minutes. The mixture was then filtered with gravitational filtration, the residue was air-dried in the fumehood for one hour and transferred into a 50 mL round-bottom flask, dried on the rotary evaporator until appears to be free-flowing powder.

7.5. References

- 1 Y.-X. Chen, P.-F. Fu, C. L. Stern and T. J. Marks, *Organometallics*, 1997, **16**, 5958–5963.
- 2 L. M. Engelhardt, M. G. Gardiner, C. Jones, P. C. Junk, C. L. Raston and A. H. White, *J. Chem. Soc. Dalton Trans.*, 1996, 3053–3057.

Chapter 8: Conclusions

In this thesis, four different aluminium-based complexes have been reported. [(CpHO)₂Al₂Me₄] (**1**) was synthesized and had its structure characterized by NMR spectroscopy, mass spectrometry and single crystal X-ray diffraction. Its catalytic performances (for epoxide / anhydride ring-opening copolymerization, ε-caprolactone ring-opening polymerization and epoxide ring-opening polymerization) have been investigated. **1** proved itself to be an efficient and effective catalyst for ε-caprolactone and epoxide ring-opening polymerization at room temperature. Kinetic studies (of ε-caprolactone and epoxide) have been undertaken and found that epoxide polymerization catalyzed by **1** lead to a first order with respect to monomer, as expected. Extensive discussions of reaction mechanisms, reaction kinetics and catalytic performances are also included. [(AQ)₂AlMe] (**2**, AQ = 8-amidoquinoline) was synthesized and had its structure characterized by NMR spectroscopy, mass spectrometry and single crystal X-ray diffraction. During the catalysis probing, it was found complex **2** is not particularly effective. However, **2** served as a keystone for the developing of two highly efficient epoxide / anhydride ROCOP catalysts, [(AQ)₂AlCl] (**3**) and [(AQMe)₂AlCl] (**4**). **3** has been previously reported, but its activity in catalysis has yet to be investigated before. A new polymorph of **3** has also been found and reported in this thesis. Both complexes were synthesized, characterized and exhibit high catalytic activity towards epoxide / anhydride ROCOP reactions. **3** and **4** possess high catalytic activity, low synthetic cost and difficulty, thus are potent candidate for industrial catalysis. Comprehensive discussions were included regarding catalytic activity, activity differences brought by change in electronic properties, structural differences, etc. Density functional theory calculations have been undertaken to provide detailed mechanistic insight of the ROCOP catalyzed by **3** and **4**.

Overall, **1**, **2** and **4** are novel aluminium complexes, of which **1** and **4** exhibit excellent catalytic performances. **3** has been reported previously, but this thesis

contains the first report of its use in catalytic studies. Generally, this thesis provides study results of two new ligand systems, and their aluminium complexes were found to be highly effective catalysts, although not across all reactions probed. In particular, complex **1** was found to be particularly effective towards epoxide and ϵ -caprolactone ROP, thus opening the way to probing new low-coordinate alkoxide aluminium complexes. The successful development of highly active catalysts with simple ligand system (**3** and **4**) provides useful information for the development of catalysts using “out of the bottle”; multi-functional ligand systems are not the only way to develop good catalysts. Through all the work covered and reported in this thesis, I hope to give some new directions for the developing and designing of metal complex catalysts, which may serve as stimulants for the future studies in this field.

Appendices: X-ray crystal structure data

Table 1: Crystal data and structure refinement for [(CpHO)₂Al₂Me₄] (1)

Identification code	fz3
Empirical formula	C ₃₆ H ₅₀ Al ₂ O ₂
Formula weight	568.72
Temperature	100(2) K
Wavelength	1.54178 Å
Crystal system	Monoclinic
Space group	P2 ₁ /n
Unit cell dimensions	$a = 8.20240(10) \text{ \AA}$ $\alpha = 90^\circ$ $b = 14.88810(10) \text{ \AA}$ $\beta = 97.7730(10)^\circ$ $c = 13.9433(2) \text{ \AA}$ $\gamma = 90^\circ$
Volume	1687.08(3) Å ³
Z	2
Density (calculated)	1.120 Mg/m ³
Absorption coefficient	0.986 mm ⁻¹
F(000)	616
Crystal size	0.200 × 0.100 × 0.050 mm ³
θ range for data collection	4.366 to 68.235 °
Index ranges	-9 ≤ h ≤ 9, -17 ≤ k ≤ 17, -16 ≤ l ≤ 16
Reflections collected	30063

Independent reflections	3092 [R(int) = 0.0424]
Completeness to $\theta = 67.679^\circ$	100.0%
Absorption correction	Semi-empirical from equivalents
Max. and min. transmission	1.00000 and 0.74579
Refinement method	Full-matrix least-squares on F^2
Data / restraints / parameters	3092 / 0 / 188
Goodness-of-fit on F^2	1.076
Final R indices [$I > 2\sigma(I)$]	$R_1 = 0.0350$, $wR_2 = 0.0977$
R indices (all data)	$R_1 = 0.0366$, $wR_2 = 0.0990$
Extinction coefficient	n/a
Largest diff. peak and hole	0.251 and -0.267 e. \AA^{-3}

Table 2: Crystal data and structure refinement for [(AQ)₂AlMe] (2)

Identification code	fz2	
Empirical formula	C ₁₉ H ₁₇ Al N ₄	
Formula weight	328.35	
Temperature	100(2) K	
Wavelength	1.54178 Å	
Crystal system	Orthorhombic	
Space group	P2 ₁ 2 ₁ 2 ₁	
Unit cell dimensions	$a = 7.87590(10) \text{ \AA}$	$\alpha = 90^\circ$
	$b = 11.35150(10) \text{ \AA}$	$\beta = 90^\circ$
	$c = 17.99840(10) \text{ \AA}$	$\gamma = 90^\circ$
Volume	1609.12(3) Å ³	
Z	4	
Density (calculated)	1.355 Mg/m ³	
Absorption coefficient	1.151 mm ⁻¹	
F(000)	688	
Crystal size	0.100 × 0.050 × 0.020 mm ³	
θ range for data collection	4.605 to 68.195 °	
Index ranges	-8 ≤ h ≤ 9, -13 ≤ k ≤ 13, -21 ≤ l ≤ 21	
Reflections collected	29957	
Independent reflections	2953 [R(int) = 0.0345]	
Completeness to θ = 67.679 °	100.0%	

Absorption correction	Semi-empirical from equivalents
Max. and min. transmission	1.00000 and 0.62945
Refinement method	Full-matrix least-squares on F^2
Data / restraints / parameters	2953 / 2 / 224
Goodness-of-fit on F^2	1.071
Final R indices [$I > 2\sigma(I)$]	$R_1 = 0.0236$, $wR_2 = 0.0651$
R indices (all data)	$R_1 = 0.0242$, $wR_2 = 0.0655$
Absolute structure parameter	-0.016(10)
Extinction coefficient	n/a
Largest diff. peak and hole	0.147 and -0.193 e.Å ⁻³

Table 3: Crystal data and structure refinement for [(AQ)₂AlCl] (**3**), polymorph A

Identification code	fz6	
Empirical formula	C ₁₈ H ₁₄ AlClN ₄	
Formula weight	348.76	
Temperature	180(2) K	
Wavelength	1.54178 Å	
Crystal system	Monoclinic	
Space group	P2 ₁ /c	
Unit cell dimensions	a = 13.5866(8) Å	α = 90 °
	b = 10.6671(5) Å	β = 94.496(7) °
	c = 11.0733(7) Å	γ = 90 °
Volume	1599.91(16) Å ³	
Z	4	
Density (calculated)	1.448 Mg/m ³	
Absorption coefficient	2.695 mm ⁻¹	
F(000)	720	
Crystal size	0.173 × 0.118 × 0.056 mm ³	
θ range for data collection	5.278 to 72.759 °	
Index ranges	-16 ≤ h ≤ 12, -8 ≤ k ≤ 13, -10 ≤ l ≤ 13	
Reflections collected	5529	
Independent reflections	2816 [R(int) = 0.0405]	
Completeness to θ = 25.000 °	87.5%	

Absorption correction	Gaussian
Max. and min. transmission	1.000 and 0.745
Refinement method	Full-matrix least-squares on F^2
Data / restraints / parameters	2816 / 2 / 223
Goodness-of-fit on F^2	1.184
Final R indices [$I > 2\sigma(I)$]	$R_1 = 0.0899$, $wR_2 = 0.2660$
R indices (all data)	$R_1 = 0.1093$, $wR_2 = 0.2911$
Extinction coefficient	n/a
Largest diff. peak and hole	0.633 and -1.355 e.Å ⁻³

Table 4: Crystal data and structure refinement for [(AQ)₂AlCl] (**3**), polymorph B

Identification code	fz7	
Empirical formula	C ₁₈ H ₁₄ AlClN ₄	
Formula weight	348.76	
Temperature	180(2) K	
Wavelength	1.54178 Å	
Crystal system	Orthorhombic	
Space group	Pbca	
Unit cell dimensions	$a = 11.0859(4) \text{ \AA}$	$\alpha = 90^\circ$
	$b = 11.3788(3) \text{ \AA}$	$\beta = 90^\circ$
	$c = 25.8690(7) \text{ \AA}$	$\gamma = 90^\circ$
Volume	3263.23(17) Å ³	
Z	8	
Density (calculated)	1.420 Mg/m ³	
Absorption coefficient	2.643 mm ⁻¹	
F(000)	1440	
Crystal size	0.102 × 0.061 × 0.027 mm ³	
θ range for data collection	5.255 to 72.829 °	
Index ranges	-13 ≤ h ≤ 13, -13 ≤ k ≤ 13, -32 ≤ l ≤ 17	
Reflections collected	12703	
Independent reflections	3206 [R(int) = 0.0399]	
Completeness to θ = 67.679 °	99.9%	

Absorption correction	Gaussian
Max. and min. transmission	1.000 and 0.890
Refinement method	Full-matrix least-squares on F^2
Data / restraints / parameters	3206 / 2 / 223
Goodness-of-fit on F^2	1.019
Final R indices [$I > 2\sigma(I)$]	$R_1 = 0.0418$, $wR_2 = 0.1044$
R indices (all data)	$R_1 = 0.0572$, $wR_2 = 0.1138$
Extinction coefficient	n/a
Largest diff. peak and hole	0.274 and $-0.275 \text{ e.}\text{\AA}^{-3}$

Table 5: Crystal data and structure refinement for [(AQ)AlMe]₄ (**5**)

Identification code	fz5	
Empirical formula	C ₄₇ H ₄₄ Al ₄ N ₈	
Formula weight	828.82	
Temperature	100(2) K	
Wavelength	1.54178 Å	
Crystal system	Triclinic	
Space group	P $\bar{1}$	
Unit cell dimensions	$a = 13.0084(2)$ Å	$\alpha = 83.5690(10)$ °
	$b = 15.6615(2)$ Å	$\beta = 85.2240(10)$ °
	$c = 21.5706(2)$ Å	$\gamma = 87.9580(10)$ °
Volume	4350.25(10) Å ³	
Z	4	
Density (calculated)	1.265 Mg/m ³	
Absorption coefficient	1.335 mm ⁻¹	
F(000)	1736	
Crystal size	0.100 × 0.050 × 0.020 mm ³	
θ range for data collection	2.068 to 67.066 °	
Index ranges	-15 ≤ h ≤ 15, -17 ≤ k ≤ 18, -25 ≤ l ≤ 25	
Reflections collected	74744	
Independent reflections	15455 [R(int) = 0.0557]	
Completeness to $\theta = 67.066$ °	99.5%	

Absorption correction	Semi-empirical from equivalents
Max. and min. transmission	1.00000 and 0.76130
Refinement method	Full-matrix least-squares on F^2
Data / restraints / parameters	15455 / 126 / 1073
Goodness-of-fit on F^2	1.057
Final R indices [$I > 2\sigma(I)$]	$R_1 = 0.0458$, $wR_2 = 0.1153$
R indices (all data)	$R_1 = 0.0569$, $wR_2 = 0.1208$
Extinction coefficient	n/a
Largest diff. peak and hole	0.630 and -0.414 e.Å ⁻³